

Dynamic Simulation of Water Quality in Surface Water Systems
Utilizing a Lagrangian Reference Frame

By

HARIDARSHAN LAL RAJBHANDARI

B.Tech., Civil Engineering (Indian Institute of Technology, Kanpur) 1980

M.S., Civil Engineering (University of California, Davis) 1989

DISSERTATION

Submitted in partial satisfaction of the requirements for the degree of

DOCTOR OF PHILOSOPHY

in

Engineering

in the

OFFICE OF GRADUATE STUDIES

of the

UNIVERSITY OF CALIFORNIA

DAVIS

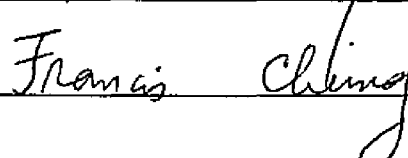
Approved:



(G.T. Orlob)



(I.P. King)



(F.I. Chung)

Committee in Charge

1995

UMI Number: 9617972

UMI Microform 9617972
Copyright 1996, by UMI Company. All rights reserved.

**This microform edition is protected against unauthorized
copying under Title 17, United States Code.**

UMI
300 North Zeeb Road
Ann Arbor, MI 48103

ABSTRACT

The quality of water in the nation's rivers, lakes and estuaries is increasingly threatened due to anthropogenic causes. To effectively evaluate impacts on water quality of water management plans or natural causes, and to design protective measures to mitigate possible adverse effects, it is first necessary to characterize the spatial and temporal distribution of water quality variables.

Mathematical models are useful and even necessary tools for water quality planning programs. This dissertation examines numerical problems encountered in application of these models and remedial measures required to control them. It documents inferences drawn from model experiments, and describes the development and application of a new mathematical model, DSM2-QUAL, designed to cope with numerical problems. The model simulates the dynamics of primary production including such variables as dissolved oxygen, phytoplankton, nutrients and temperature. In order to minimize the numerical difficulties of models set in an Eulerian framework, DSM2-QUAL utilizes a Lagrangian reference frame, adopting the basic one-dimensional transport algorithm of the BLTM (Branched Lagrangian Transport Model).

Using a dynamic flow field obtained from a hydrodynamic model, the water quality model performs advective and diffusive steps of mass transport. New routines are incorporated for computation of decay,

growth and interactions among water quality parameters. A suitable numerical scheme is employed to update constituent concentrations at each time step. Reaction kinetics incorporated in DSM2-QUAL are verified by applying it to a hypothetical test problem and comparing simulated results with those from QUAL2E, a popular water quality model based on steady-state hydraulics.

The new model is applied to the Sacramento-San Joaquin Delta, a complex estuarine system in Northern California, first for calibration and verification on a reach of San Joaquin River near the City of Stockton. Results demonstrate the capability of DSM2-QUAL to describe accurately the traditional variables of concern to water quality managers. Tests show the model's utility in evaluating alternatives in terms of incremental changes in water quality. Additional data requirements for improved understanding of complex processes affecting water quality in the estuarine systems, including future applications and extensions of the model, are discussed.

ACKNOWLEDGEMENTS

I wish I am an expert in writing, at least just for today, so that I can make an attempt in expressing my deep appreciation for the chairman of my dissertation committee Professor Gerald T. Orlob for his guidance in this research, constant support, patience and endless generosity with time. He has always been there, when I needed him, both in a professional and personal level. The memory of this association with him, as a great advisor and friend, will remain fresh in my mind for years to come. I would like to thank Professor Ian King for serving in my dissertation committee, for thoroughly reviewing this manuscript, and providing me with many valuable suggestions. Many of the issues related to numerical problems discussed in this research were first introduced to me in the classes taught by him. I also wish to express my sincere appreciation to Dr. Francis Chung of the California Department of Water Resources for serving in my dissertation committee, carefully reviewing this manuscript, and providing me with many useful suggestions. His keen interest in this research, for its potentially useful role in water resources management, was very encouraging.

This dissertation would not have been in this shape without the unflinching dedication, love and support of my family. I thank my wife Vidya dearly for her endless patience and encouragement even during the demanding periods of this research. Her word processing of much of the text of this manuscript was a welcome help indeed. My children, Sangi and Sunay, have too been wonderful inspiration; they were very understanding of my time constraints. I am indebted to

my parents for their love and support and their unfailing encouragement in the pursuit of my education. Books written by my dad some years ago, as I remembered, added inspiration to me, easing the stresses of writing this dissertation. My thanks are also to my sister and brothers for their love and understanding.

Ramdarshan has especially been inspiring, exchanging books and thoughts with me on issues such as insight, clarity and wisdom.

Warmest thanks to my friends and colleagues Tara Smith, Andy Bale, Gabriela Meyer, Camilla Saviz, Nimi Mahadevan, Kamyar Guivetchi, Jamie Anderson and many others at the Dept. of Civil and Environmental Engineering at UC Davis and the Modeling Support Branch of the DWR for their encouragement, interactions and help. This certainly made my graduate study enjoyable and memorable. I would like to thank Dr. Paul Hutton for his encouragement and assistance. I appreciate Dr. Parviz Nader's readiness to help and many useful tips in computer program debugging.

My appreciation also to the Chief of the Modeling Support Branch Mr. George Barnes and Dr. Ali Ghorbanzadeh for their support and assistance. I am grateful to the administrative staff of the Dept. of Civil and Environmental Engineering at UC Davis for their splendid cooperation throughout my graduate study. Thanks are also to Janaki Pradhan and my friends at Davis for their moral support. Finally, my heart-felt appreciations to Professor Ray Krone and Dr. Johannes DeVries for their guidance, moral support and friendship throughout the period of my graduate study at UC Davis.

Dedicated to:

all those people who
through writing or other means
are working
to bring peace and harmony in the world.

Table of Contents

ABSTRACT	i i
ACKNOWLEDGEMENTS	i v
DEDICATION	v i
LIST OF TABLES	x
LIST OF FIGURES	x i
1. INTRODUCTION	2
1.1 Background.....	2
1.2 Objectives and Scope of Study.....	4
1.3 Organization of the Report.....	6
2. THEORY AND LITERATURE REVIEW	10
2.1 Mixing and Longitudinal Dispersion.....	10
2.1.1 Advection-Diffusion Equation.....	12
2.1.2 Longitudinal Dispersion.....	14
2.2 Numerical Methods of Solution.....	18
2.2.1 Eulerian Methods.....	18
2.2.2 Lagrangian Methods and Method of Characteristics.....	27
2.3 Review of Applied Water Quality Models.....	34
3. RESEARCH METHODOLOGY: MODEL EXPERIMENTS	42
3.1 Effect of Grid Resolution on Model Results: A Numerical Experiment:.....	42
3.2 Lagrangian Approach to Modeling.....	48
3.3 Solution Algorithm of BLTM.....	53
3.3.1 Governing Equations.....	53
3.3.2 Need for Further Development.....	57
3.4 Tests with BLTM: Modeling Newport Bay.....	58
3.4.1 Description of Newport Bay Estuary.....	58
3.4.2 Hydrodynamics and Model Input.....	59
3.4.3 Objectives.....	64

3.4.4	Model Application.....	65
3.4.5	Discussion of Simulation Results.....	66
3.4.6	Investigation of Time Required to Reach Dynamic Equilibrium.....	68
3.4.8	Comparison with the Link-Node Model Results.....	81
4.	MODEL DEVELOPMENT PHASE 1: FORMULATION.....	86
4.1	Introduction.....	86
4.2	Water Quality.....	89
4.2.1	Formulation of Water Quality Equations.....	91
4.2.2	Water Quality Parameters and Related Processes.....	94
4.3	Numerical Scheme for Updating Kinetic Interactions.....	103
4.4	Case Study: Sacramento-San Joaquin Delta.....	112
4.4.1	Ecosystem.....	112
4.4.2	Water Quality.....	114
4.4.3	Modeling Need.....	117
4.4.4	Spatial Discretization.....	118
4.4.5	Hydrodynamics Model.....	118
4.4.6	Special Features for Simulation of Water Quality in the Delta.....	121
4.5	Description of New Subroutines.....	125
4.6	Additional Comments.....	127
4.7	Test Case for Verifying the Reaction Kinetics in the New Model.....	134
4.8	Summary.....	141
5.	MODEL DEVELOPMENT PHASE 2: APPLICATION, PERFORMANCE AND ANALYSIS.....	143
5.1	Conditions for Model Evaluation.....	143
5.2	Model Input.....	146
5.3	Scenario 1: Calibration of the Model.....	161
5.4	Scenario 2: Verification of the Model.....	174
5.5	Diurnal Variation in Water Quality.....	182
5.6	Sensitivity Analysis.....	185

6. CONCLUSIONS AND RECOMMENDATIONS	207
6.1 Summary and Conclusions.....	207
6.2 Recommendations and Future Directions.....	211
REFERENCES	220
APPENDIX A	234
A.1 Governing Equations For Water Quality Parameters.....	234
A.2 Components of Heat Exchange at the Air-Water Interface.....	243
APPENDIX B: DISPERSION FACTOR	249
APPENDIX C: USER'S MANUAL	251
C.1 Transport Input File (BLTM.IN).....	251
C.2 Kinetic Rate Coefficients File (QUALITY.IN).....	256
C.3 Meteorological Data Input File (MET.IN).....	264

List of Tables

Table 3.1	Comparison of field Data and Model Results Salinity (parts per thousand).....	79
Table 4.1	Initial Conditions and Water Quality at the Upstream Boundary for the Test Problem.....	137
Table 4.2	Reaction Coefficients for the Test Problem.....	138
Table 4.2	(contd.) Reaction Coefficients for the Test Problem.....	139
Table 4.3	Climatologic Coefficients used in the Test Problem.....	139
Table 5.1	Hydrology used in Model Calibration and Verification.....	147
Table 5.2	Water Quality (Field Data) at the Model Boundary September 1988 Simulation.....	149
Table 5.3	Water Quality (Field Data) at the Model Boundary October 1988 Simulation.....	150
Table 5.4	Water Quality (Field Data) at Selected Delta Locations, September 1988 Simulation.....	151
Table 5.5	Water Quality (Field Data) at Selected Delta Locations, October 1988 Simulation.....	152
Table 5.6	Typical Ranges and Assigned or Calibrated Values for Reaction Coefficients.....	166
Table 5.6	(contd.) Typical Ranges and Assigned or Calibrated Values for Reaction Coefficients.....	167
Table 5.7	Climatologic Coefficients used in Temperature Calibration.....	168
Table A.1	Temperature Coefficients for Reaction Rate.....	243
Table A.2	Unit Conversion Related to Heat Equations.....	248

List of Figures

Figure 2.1	Numerical Experiment for Mass Transport Shown after 16 Time Steps.....	25
Figure 2.2	Interpolation in an Eulerian Reference Frame.....	31
Figure 2.3	Lagrangian Reference Frame	33
Figure 3.1	Modified Part of the Delta Network. Nodes added in the Grid are Shown by Solid Circles.....	43
Figure 3.1	(Contd.) Modified Part of the Delta Network. Nodes added in the Grid are Shown by Solid Circles.....	44
Figure 3.2	Computed Daily Average Electrical Conductivities (July 1988).....	47
Figure 3.3	Definition Sketch: Nodal Continuity.....	51
Figure 3.4	Schematic Showing Interparcel Flows.....	55
Figure 3.5	Newport Bay, California.....	60
Figure 3.6	Link-Node Network, Newport Bay.....	61
Figure 3.7	Branch-Junction Network, Newport Bay	62
Figure 3.8	Tide at Newport Bay Boundary (March, 1978).....	63
Figure 3.9	Computed Hourly Variation of Salinity at Branch 28 (near Lower Boundary).....	69
Figure 3.10	Computed Hourly Variation of Salinity at Branch 26	70
Figure 3.11	Computed Hourly Variation of Salinity at Branch 22	71
Figure 3.12	Computed Hourly Variation of Salinity at Branch 10	72
Figure 3.13	Computed Salinity at Three Locations of Newport Bay Estuary ($D_f=0.2$).....	73

Figure 3.14	32-Day Salinity History (Computed) of Branch 28 (near Lower Boundary)	75
Figure 3.15	32-Day Salinity History (Computed) of Branch 26.....	76
Figure 3.16	32-Day Salinity History (Computed) of Branch 22.....	77
Figure 3.17	32-Day Salinity History (Computed) of Branch 10.....	78
Figure 3.18	Salinity at Branch 28 (near Lower Boundary) using BLTM and Link-Node Models	83
Figure 3.19	Salinity at Branch 26 using BLTM and Link-Node Models.....	84
Figure 3.20	Salinity at Branch 22 using BLTM and Link-Node Models.....	85
Figure 4.1	Flowchart for the Dynamic Simulation of Water Quality in an Aquatic System.....	87
Figure 4.2	Interaction among Water Quality Constituents in the Model.....	93
Figure 4.3	Numerical Scheme used in Subroutine KINETICS.....	106
Figure 4.4	Flowchart for Subroutine KINETICS.....	107
Figure 4.4	(Contd.) Flowchart for Subroutine KINETICS.....	108
Figure 4.5	Flowchart for Subroutine CALSCSK	110
Figure 4.6	Sacramento-San Joaquin Delta	113
Figure 4.7	DWRDSM Delta Model Grid.....	120
Figure 4.8	Node with Agricultural Drainage and Diversion.....	124
Figure 4.9	An Example of Open Water Area (Reservoir).....	124
Figure 4.10	Flowchart for Subroutine CALDO.....	128
Figure 4.11	Flowchart for Subroutine CALALG (Algae).....	129
Figure 4.12	Flowchart for Subroutine CALTEMP	130
Figure 4.13	Flowchart for Subroutines HEAT and MET	131

Figure 4.14	Computed Chlorophyll-a after 24 Hours	140
Figure 4.15	Computed Dissolved Oxygen after 24 Hours.....	140
Figure 4.16	Computed Temperature after 24 Hours	141
Figure 5.1	Monitoring Stations in the San Joaquin River near Stockton	145
Figure 5.2	Selected Monitoring Stations in the Sacramento- San Joaquin Delta.....	148
Figure 5.3	Dissolved Oxygen at Martinez (Sept. 23 to Oct. 15, 1988)	154
Figure 5.4	Dissolved Oxygen in the San Joaquin River at Mossdale (Sept. 15 to Oct. 15, 1988).....	154
Figure 5.5	Total Dissolved Solids at Martinez (Sept. 15 to Oct. 15, 1988).....	155
Figure 5.6	Total Dissolved Solids in the San Joaquin River at Mossdale (Sept. 15 to Oct. 15, 1988).....	155
Figure 5.7	Temperature at Martinez (Sept. 15 to Oct. 15, 1988).....	156
Figure 5.8	Temperature in the San Joaquin River at Mossdale (Sept. 15 to Oct. 15, 1988)	156
Figure 5.9	Dissolved Oxygen in the San Joaquin River at Stockton (Sept. 15 to Oct. 15, 1988).....	157
Figure 5.10	Temperature in the San Joaquin River at Stockton (Sept. 15 to Oct. 15, 1988)	157
Figure 5.11	Total Dissolved Solids in the San Joaquin River at Stockton (Sept. 15 to Oct. 15, 1988).....	158
Figure 5.12	Weather Data, Sacramento (Sept. 20, 1988).....	160
Figure 5.13	Cloud and Pressure Data, Sacramento (Sept. 20, 1988).....	160
Figure 5.14	Tide at Martinez (Sept. 20, 1988).....	161

Figure 5.15	Comparison of Stage for Calibration Period (Sept. 20, 1988) San Joaquin River near Stockton.....	162
Figure 5.16	Tidal Day Average of Computed Flows (San Joaquin River).....	163
Figure 5.17	Variation of Channel Widths in the San Joaquin River.....	164
Figure 5.18	Variation of Channel Depths in the San Joaquin River.....	164
Figure 5.19	Calibration of Temperature.....	168
Figure 5.20	Calibration of Dissolved Oxygen.....	171
Figure 5.21	Observed and Simulated Nitrate-N (Sept. 1988).....	172
Figure 5.22	Observed and Simulated Chlorophyll-a (Sept. 1988).....	175
Figure 5.23	Observed and Simulated Ortho-phosphate (Sept. 1988).....	175
Figure 5.24	Tide at Martinez (Oct. 12, 1988).....	176
Figure 5.25	Comparison of Stage for Verification Period San Joaquin River near Stockton.....	177
Figure 5.26	Verification of Temperature.....	178
Figure 5.27	Verification of Dissolved Oxygen.....	179
Figure 5.28	Observed and Simulated Nitrate-Nitrogen (Oct. 1988).....	180
Figure 5.29	Observed and Simulated Chlorophyll-a (Oct. 1988).....	181
Figure 5.30	Observed and Simulated Ortho-phosphate (Oct. 1988).....	181
Figure 5.31	Computed Hourly Variation of Chlorophyll-a (Channel 17).....	183

Figure 5.32	Computed Hourly Variation of Dissolved Oxygen (Channel 17).....	183
Figure 5.33	Computed Hourly Variation of Ammonia-N (Channel 17).....	184
Figure 5.34	Computed Hourly Variation of Nitrate-N (Channel 17).....	184
Figure 5.35	Computed Hourly Variation of Ortho-phosphate (Channel 17).....	186
Figure 5.36	Computed Hourly Variation of Organic Nitrogen (Channel 17).....	186
Figure 5.37	Computed Hourly Variation of Temperature (Channel 17).....	187
Figure 5.38	Computed Solar and Atmospheric Radiation (based on Sacramento weather data Sept. 20, 1988).....	187
Figure 5.39	Weather Data, Sacramento, July 1988 (Monthly Average)	189
Figure 5.40	Cloud and Pressure Data, Sacramento, July 1988 (Monthly Average)	190
Figure 5.41	Computed Solar and Atmospheric Radiation based on Sacramento Data, July (average) 1988	191
Figure 5.42	Response of River DO to Change in Climate and to Increase in Effluent Loading	192
Figure 5.43	Response of River Temperature to Change in Climate and to Increase in Effluent Loading.....	194
Figure 5.44	Response of River Chlorophyll-a to Change in Climate and to Increase in Effluent Loading.....	194
Figure 5.45	Computed Diurnal Temperature (Channel 17) Two Climate Conditions.....	195
Figure 5.46	Computed Diurnal Chlorophyll-a (Channel 17) Two Climate Conditions.....	197

Figure 5.47	Computed Diurnal DO (Channel 17) Two Climate Conditions.....	197
Figure 5.48	Computed Diurnal Nitrate-N (Channel 17) Two Climate Conditions.....	199
Figure 5.49	Computed Diurnal Ammonia-N (Channel 17) Two Climate Conditions.....	199
Figure 5.50	Simulated Dissolved Oxygen in the Delta (Sample Plot, Sept. 1988 Test Run).....	202
Figure 5.51	Simulated Temperature in the Delta (Sample Plot, Sept. 1988 Test Run)	203
Figure 5.52	Simulated Chlorophyll-a in the Delta (Sample Plot, Sept. 1988 Test Run).....	204
Figure 5.53	Simulated Nitrate-N in the Delta (Sample Plot, Sept. 1988 Test Run)	205
Figure 5.54	Simulated TDS in the Delta (Sample Plot, Sept. 1988 Test Run).....	206

**Dynamic Simulation of Water Quality in Surface
Water Systems Utilizing a Lagrangian
Reference Frame**

Haridarshan L. Rajbhandari

1995

1. INTRODUCTION

1.1 Background

There has been an increasing public concern for the maintenance of water quality in the nation's rivers, lakes and estuaries. Changes induced by anthropogenic factors often modify water quality characteristics, sometimes drastically, of aquatic systems. These characteristics include, but are not limited to, dissolved oxygen, temperature, toxic substances nutrients, and measures of primary production in the system. In turn, changes in these properties affect animal and plant life in the nation's water resources. An example in California is the continuing decline of Chinook salmon production in the Sacramento River which is the principal source of inflow to the Sacramento-San Joaquine Delta. Another is the apparent demise of striped bass in the Delta.

Mathematical models have the potential to play important roles in aiding the water resources managers in resolving such complex water quality issues. For example models can provide objective and quantifiable assessments for evaluating the effects of changes in the surrounding environment on water quality. Changes in water quality may be either due to natural causes or the consequences of projects development. Most of the investigative tools that are available to decision makers today are not adequate to describe the important dynamic variations in quality that occur in complex aquatic systems. Estuarine environments, like that of California's

Sacramento-San Joaquin Delta, are especially difficult to analyze. They deserve the special attention of modelers. A reliable tool can contribute greatly in the overall goal of Delta water management of finding an equitable balance among various, at times seemingly conflicting, needs of all those that share Delta waters. An introductory treatise on the Delta is given in Chapter 4.

The research described in this dissertation is an outgrowth of a perceived need for an "application-ready" water quality model that can be applied with confidence to hydrodynamically complex estuarine systems. Although a large body of literature exists today on numerical methods to describe mass transport processes in such systems, there have been relatively few studies concerning models that are capable of simulating the full range of dynamic processes that determine diurnal variations in water quality variables. In some models a sinusoidal variation in oxygen production, for example, is assumed based on limited field measurements (Lee et al., 1991). Among the few models that are actually capable of describing dynamic variations in water quality, most are unable to avoid an appreciable degree of numerical mixing which leads to uncertain results. Fewer still have been calibrated and verified against reliable field data. There is a need for a dependable, easily applied, model that can simulate the full range of dynamic, interrelated processes that govern oxygen balance in a estuarine environment.

1.2 Objectives and Scope of Study

The objective of this research is to develop a mathematical model that can describe the transport and distribution of important water quality variables in natural aquatic systems. The model should be able to describe the dynamic (including diurnal) variations in the distribution of important water quality variables, even in complex estuarine systems.

In order to minimize the common numerical difficulties faced by most practical models set in an Eulerian framework, a Lagrangian transport modeling framework is adopted as a base for the development of a new water quality model. This does away with the use of higher order schemes that are often more computationally intensive, and which have sometimes been adopted in Eulerian or Eulerian-Lagrangian frameworks to reduce numerical mixing problems. Also, it reduces the need for expertise in computational mathematics in order to ensure proper execution. The model developed in this study is relatively easy to understand, and to use. It also assumes that the system being modeled can be approximated spatially by a simple one-dimensional network of grids.

Kinetic interactions among variables in the new model are based on the relationships derived from the recent literature, and are pertinent in the present context, i.e. the Sacramento-San Joaquin Delta. Within constraints posed by data availability and model assumptions, accurate simulation of dissolved oxygen and related

variables in a complex estuary will be attempted. This requires actual data or time-varying estimates of phytoplankton, key nutrients and biochemical oxygen demand, as well as data on temporal and spatial distributions of actual dissolved oxygen concentrations. Temperature of water, which directly influences dissolved oxygen and other water quality variables, and is, by itself, a significant water quality parameter of interest, will also be simulated. Computation of net transfer of energy at the air-water interface will be a major factor in temperature predictions apart from the changes induced by the processes of advection and diffusion, that affect all variables. The model will also have capability to simulate an arbitrary non-conservative constituent or a conservative substance, such as total dissolved solids or chlorides.

A cost-effective numerical scheme will be employed to update constituent concentrations accounting for change due to decay, growth or kinetic interactions with other constituents within each time step.

The development of a model cannot be considered complete until it is actually applied to a real system and model coefficients are calibrated against field data. The model should then be validated by applying it to the same system, but for a different set of boundary conditions. Undesirable features may not appear until the model is tested in the rigorous contexts of realistic unsteady flows and complex geometry that commonly occur in prototype systems. Such tests may reveal some features of the model that

may need to be modified. This important part of development of the new model will be achieved in the present instance by applying it to the complex estuarine system of the Sacramento-San Joaquin Delta in California. Model credibility must be established before using it as a tool to support water quality management decisions that often involve expenditures of large amounts of money and commitments to courses of action that may be irrevocable. This process of establishing model credibility is accomplished in part through carefully performed model calibration and verification. In this study the processes of calibration and verification will focus primarily on a reach of the San Joaquin River near the City of Stockton, where there exist a body of water quality data that is uniquely superior in spatial and temporal coverage when compared to other regions of the Delta.

1.3 Organization of the Report

This report is organized as follows. Chapter 2 begins with a general treatise on the theory of mixing in transport processes. Next, a review of numerical schemes in solving these processes is provided. It is shown that despite the proliferation of numerical techniques many of them exhibit undesirable properties such as spurious oscillations, and numerical dispersion and diffusion. Techniques to remedy these difficulties are researched from the literature and are specifically addressed in this section. Finally, a review is provided of some of the widely applied water quality models for rivers and estuaries. Numerical difficulties that may affect the performance of these models are highlighted.

Chapter 3 describes the methodology followed in the course of the present research. In any modeling endeavor, the decisions concerning appropriate grid resolutions, both in space and time, are important factors. Design of the grid and selection of time step can guide the economic aspects and selection of a numerical scheme. Along this line, this chapter first presents a numerical test performed on a real prototype system to examine the effects of grid resolution on the performance of an existing water quality model. Based on the results of this test and a survey of the related literature, it was decided to adopt a Lagrangian approach for achieving the objective of this research. A possible choice of a suitable Lagrangian algorithm is described in the subsequent sections.

The last section in this chapter describes assessment of the Branched Lagrangian Transport Model (BLTM) (Jobson and Schoellhamer, 1992) by applying it in a test case to Newport Bay Estuary in Southern California. A series of tests performed on this system indicated that the BLTM is suitable to describe the basic transport part (advection and diffusion) of the proposed water quality model for a conservative substance. Some modifications were required in the computer code to increase computational efficiency. Routines describing reactions kinetics provided with the original BLTM package, however, were not sufficient for the purpose of the present study. Consequently, it was decided to develop a complete set of new routines representing reaction kinetics pertinent to this study.

Chapter 4 describes the main processes of model development in this research. It includes those that govern the formulation of water quality equations for the purpose of this model. The development of a numerical scheme for the purpose of updating changes in constituent mass due to kinetic interactions among constituents is also described. The Sacramento-San Joaquin Delta is presented as a case study to demonstrate the performance of the developed tool. The prototype system was discretized in the spatial domain and an existing hydrodynamic model was used to provide the necessary circulation information at the specified spatial grid for subsequent use by the water quality model. The next section presents the main features of the computer program developed in this study. Finally, a test case is presented verifying the consistency of reaction kinetics represented in the new model with those of QUAL2E.

Chapter 5 describes how the model was applied to the Sacramento-San Joaquin Delta and discusses results of calibration and verification, specific to the region near the San Joaquin River reach in the vicinity of the City of Stockton. Simulations are further performed to examine the response of the river quality to changes in climate and boundary conditions. Contour plots representing the distributions (simulated) of selected constituents in the Delta are also presented.

Chapter 6 summarizes water quality modeling efforts, conclusions derived from the first application of this new model (DSM2-QUAL) and recommendations for future work.

A list of equations governing reaction kinetics for each constituent represented in the model, including components of surface heat exchange, is included in Appendix A. The relationship between "dispersion factor" and the Peclet number is derived in Appendix B. A manual of instructions for preparation of input files for the users of DSM2-QUAL is included at the end of the report (Appendix C).

2. THEORY AND LITERATURE REVIEW

2.1 Mixing and Longitudinal Dispersion

Advection¹, diffusion and dispersion are the principal mechanisms of mass transfer in all aquatic systems. Diffusion and dispersion have often been used indiscriminately to describe natural mixing processes without really indicating the fundamental differences between the two physical processes.

Diffusion theory assumes that the motion of each fluid molecule is independent of the motion of its immediate neighbors, and states simply that the rate of mass transfer from a region of high concentration to a region of low concentration is proportional to the concentration gradient between the two regions. Dispersion, on the other hand, is a mechanism by which fluid particles undergo relative displacement solely by virtue of differences in mean velocities along adjacent stream lines (Water Resources Engineers, Inc., 1965).

In turbulent flow small-scale eddies continually erode the edges of a tracer cloud introduced into the flow field, increasing local concentration gradients which in turn allow molecular diffusion to occur faster. Turbulent eddies which may be randomly generated in the flow may transfer both momentum and mass. The combined effects of molecular diffusion and turbulent velocity fluctuations is called turbulent diffusion, a process considered analogous to

¹ Some authors use the term convection to describe this process.

molecular diffusion. In a natural turbulent regime, the effect of molecular diffusion is usually considered negligible (Orlob, 1959), hence, the effective diffusion process in natural surface water systems is almost always that of turbulent diffusion, also known as eddy diffusion (Bowden, 1984).

Our understanding of turbulent diffusion in rivers and estuaries is far from complete. Experiments conducted in the 1950's and 1960's such as those of Orlob (1959), Fischer (1968) and Sayre (1969) proved that Fickian analysis of diffusion can provide only a rough approximation of turbulent transport mechanisms. Much of the available knowledge on turbulent diffusion is based on empirical results and laboratory studies.

A significant contribution to the theory of turbulent diffusion was made by G. I. Taylor in 1921 when he derived the "Theory of diffusion by continuous movements." His analysis was based on turbulent properties of the flow and is considered to be more realistic than the Fickian approach which only considers properties of the fluid. Taylor's basic idea was that in a turbulent fluid, or in any continuous motion, a correlation exists between the state of a particle at a particular time and its state a short interval of time later. The degree of correlation is a function of the interval. As the time interval increases the correlation diminishes toward zero. Eventually, the variance of the tracer cloud, released into turbulent flow, increases linearly with time. This suggests that in a stationary homogenous field of turbulence (the case for which Taylor's approach was originally formulated) turbulent diffusion

can also be modeled using Fick's law provided sufficient time has elapsed since tracer injection. The interested reader may refer to Rutherford (1994) for the derivation of Fickian model for turbulent diffusion.

2.1.1 Advection-Diffusion Equation

In the region close to a non-steady point source (near-field mixing region), transport due to advection and mixing are usually important in all three coordinate directions and the full three-dimensional advection-diffusion equation is required to predict tracer concentrations. For a coordinate system aligned along the principal direction of flow, the equation can be written as:

$$\frac{\partial c}{\partial t} + u_x \frac{\partial c}{\partial x_j} = \frac{\partial}{\partial x_j} \left(E_j \frac{\partial c}{\partial x_j} \right) \quad (2.1)$$

where

c = tracer concentration,

u_x = $u_x(x,t)$, fluid velocity in the direction of flow,

E_j = $E_j(u,x,t)$, effective dispersion tensor.

In most cases of interest the transport equation can be simplified to the vertically or transversely averaged two-dimensional forms. For example, in most rivers, concentration becomes relatively uniform over the depth before complete lateral mixing has taken place (Elhadi et al., 1984). In such cases a depth averaged form of the two-dimensional equations can be used, i.e.,

$$\frac{\partial c}{\partial t} + u_x \frac{\partial c}{\partial x} = \frac{1}{h} \frac{\partial}{\partial x} \left(h E_x \frac{\partial c}{\partial x} \right) + \frac{1}{h} \frac{\partial}{\partial y} \left(h E_y \frac{\partial c}{\partial y} \right) \quad (2.2)$$

where

- c = depth-averaged tracer concentration,
- u_x = depth-averaged velocity in x direction,
- h = local depth,
- E_x = longitudinal dispersion coefficient,
- E_y = transverse dispersion coefficient.

The dispersion coefficients used should include the effects on mixing of vertical variations in velocity.

A tracer originating from a point source eventually mixes across the channel. In some circumstances, vertical and transverse concentration gradients in the far-field region may not be important ecologically (Rutherford, 1994). In such cases a second spatial averaging is performed resulting in the one-dimensional form of the transport equation. When lateral and vertical mixing are complete longitudinal dispersion can be treated basically like diffusion, i.e., as a random process, as shown in the following equation.

$$\frac{\partial c}{\partial t} + u_x \frac{\partial c}{\partial x} = \frac{1}{A} \frac{\partial}{\partial x} \left(A E_x \frac{\partial c}{\partial x} \right) \quad (2.3)$$

where

- c = cross-sectional averaged concentration,
- u_x = cross-sectional averaged velocity,
- A = cross-sectional area,

E_x = longitudinal dispersion coefficient.

It is important to note that the coefficient E_x above is not the same as E_x used in eq. (2.2), since it implicitly includes the effects of both lateral and vertical mixing.

2.1.2 Longitudinal Dispersion

The one-dimensional advection-diffusion equation (2.3), has been often used in modeling rivers and estuaries. The magnitude of the dispersion coefficient depends on the time and space scales of the processes being simulated. For shorter time scales higher resolution of simulated hydrodynamics is produced, hence water quality variations must be described in greater detail. Therefore, in high resolution models, more refined coefficients are needed than those which, for example, consider only average hydrodynamics over a tidal cycle.

The magnitude of the dispersion coefficient can also change depending on location, i.e., as a function of space. Since this term includes the effects of non-uniformity of velocities in the y and z directions, the greater will be the deviation between the actual and the cross-sectional averaged velocity, and the greater will be the effective dispersion coefficient.

Taylor's analysis, noted earlier, suggests that longitudinal dispersion obeys Fick's law if the turbulence is homogenous and stationary and a sufficiently long time has elapsed since the release of the tracer. In natural irregular channels turbulence will

certainly not be homogenous; nevertheless eq. (2.3) provides a useful approximation for longitudinal dispersion.

A number of investigators have attempted to express the value of the dispersion coefficient E_x in terms of geometric properties of the channel and other parameters of the flow in laboratory model studies or in natural rivers, with limited success.

Longitudinal dispersion arises essentially due to vertical exchange of momentum related to the velocity gradient, hence the longitudinal dispersion coefficient can be estimated from a knowledge of velocity distribution. This approach was first developed by Taylor (1953, 1954) who conducted his experiments in a rectilinear pipe and obtained the following equation for longitudinal dispersion

$$E_x = 10.1ru^* \quad (2.4)$$

where

r = radius of the pipe,

u^* = shear velocity, defined as $u^* = \sqrt{\frac{\tau_0}{\rho}}$

τ_0 = shear stress at the channel bottom.

$$= \frac{f\bar{u}^2}{8}$$

ρ = density of water,

f = Darcy-Weisbach friction factor,

\bar{u} = mean velocity.

Elder (1959) improved on Taylor's results by considering a logarithmic velocity distribution for the case of open channel flow and derived:

$$E_x = 5.93du^* \quad (2.5)$$

where

d = mean depth.

Fischer (1967) extended the work of Taylor and Elder to real streams and came up with the following expression for E_x :

$$E_x = \frac{I h^2 \overline{u'^2}}{e_t} \quad (2.6)$$

where

I = a dimensionless integral which quantifies the velocity variation over the cross-section,

≈ 0.07 for real streams (Fischer et al., 1979),

h = characteristic length $\approx 0.7W$,

W = channel width,

$\overline{u'^2}$ = expected square of the deviation of the depth-averaged velocity from the mean velocity

$\approx 0.2 \bar{u}^2$

\bar{u} = mean velocity,

e_t = transverse mixing coefficient $\approx 0.6du^*$,

d = channel depth.

Other variables are as defined previously.

Substitution of the above expressions leads finally to the following empirical expression for the longitudinal dispersion coefficient:

$$E_x = \frac{0.011\bar{u}^2 W^2}{du^*} \quad (2.7)$$

An alternative expression for eddy diffusion is based on Kolmogoroff's theory of similarity, verified later by Orlob (1959) in a laboratory experiment. It is expressed as

$$E_x = (\text{constant}) E^{1/3} L^{4/3} \quad (2.8)$$

where

E = rate of energy dissipation per unit mass,

L = characteristic length scale.

L may be taken as the mean size of the eddies participating in the diffusion process. E for steady uniform flow may be determined by

$$E_x = |\bar{u}| g S \quad (2.9)$$

where

S = slope of energy grade line,

g = acceleration due to gravity,

\bar{u} = cross-sectional mean velocity.

Adopting channel depth (d) as the mixing scale and making substitutions for E and L , Water Resources Engineers, Inc. (1965) derived the following simplified relationship for computation of eddy diffusion coefficient in Sacramento-San Joaquin Delta channels.

$$E_x = c |\bar{u}| d \quad (2.10)$$

where c is a function of channel roughness.

In broad natural channels the hydraulic radius is often used in place of mean channel depth.

A similar relationship is derived in the description of hydraulic components in QUAL2E manual (Brown and Barnwell, 1987) which is:

$$E_x = 3.82 kn \bar{u} d^{5/6} \quad (2.11)$$

where

- k = dispersion constant (dimensionless),
- n = Manning's roughness coefficient,
- \bar{u} = cross-sectional mean velocity, ft/s,
- d = mean depth, ft.

2.2 Numerical Methods of Solution

A review of various numerical schemes for solving mass transport equations is presented in this section. Since the model developed in this research is in one-dimensional form, examples are usually provided of one-dimensional equations. The general nature of difficulties applies as well to two- and three-dimensional models.

2.2.1 Eulerian Methods

In most Eulerian methods partial differential equations are discretized, and the resulting algebraic equations containing unknowns (concentrations in this case) are solved at a number of fixed grid points in the computational domain. The transformation of the original differential equations into the system of algebraic equations is usually achieved using either finite difference or finite element methods.

Finite difference methods are often easier to formulate than finite element methods, and sometimes require less computer memory. Also, preparation and input of data is usually easier for regular systems. Finite element methods on the other hand are often more suitable for handling complicated land boundaries and providing grid refinements in zones of interest.

Finite Difference Methods

Finite difference methods have been used in the solution of transport equations since the late 1950's (Noye, 1987A). These methods typically discretize the computational domain using an orthogonal grid. The differential transport equation over each space-time grid is replaced by an algebraic equation obtained by finite difference approximation of spatial and temporal derivatives. For example,

$$u \left(\frac{\partial c}{\partial x} \right)_i \equiv u_i \frac{c_{i+1} - c_{i-1}}{2\Delta x} ; D \left(\frac{\partial^2 c}{\partial x^2} \right)_i \equiv D_i \frac{c_{i+1} - 2c_i + c_{i-1}}{\Delta x^2} \quad (2.12)$$

where Δx represents the size of the spatial grid. The earliest finite difference techniques used forward differencing in time and central differencing in space to approximate both the advection and diffusion terms. These methods performed well in situations where dispersion dominates (lower Peclet Number¹, usually below 2); however, when advection dominates, as in the case of steep concentration gradients (higher Peclet Number), these methods

¹ Peclet Number (P_e) is defined as $\frac{U\Delta x}{E_x}$

suffered from spurious oscillations, including overshooting of peaks and undershooting of troughs, even resulting in unrealistic negative concentrations (see, for example, Roache, 1972, Sobey, 1984, Gresho and Lee, 1981).

In non-uniform flow fields where u_x and E_x (in eq. 2.3) may vary from point to point both in space and time, the transport equation may vary in character, being predominantly parabolic (diffusive) in some regions and predominantly hyperbolic (advective) in others (Neuman, 1981). It has proven difficult to find a single numerical method which adequately treats both aspects of the problem (Holly and Polatera, 1984). Price et al. (1966) recognized that the numerical difficulties result largely from spatial discretization. They showed that solution oscillations can be eliminated if the size of the spatial grid is made sufficiently small, i.e., such that $Pe < 2$. This is not always practical, since it could require unrealistic computation costs, when solving real systems.

In order to avoid spurious oscillations, more recently developed explicit finite differencing methods use centered finite-differences only for the diffusion terms, and replace the advective derivatives by upstream differences (i.e., backward in space, also called "upwind" methods). These one-sided differences are of first order accuracy, as shown below.

$$u \left(\frac{\partial c}{\partial x} \right)_i \equiv u_i \frac{c_i - c_{i-1}}{\Delta x} \quad \text{if } u_i > 0 \quad (2.13)$$

$$\text{or } u \left(\frac{\partial c}{\partial x} \right)_i \equiv u_i \frac{c_{i+1} - c_i}{\Delta x} \quad \text{if } u_i < 0 \quad (2.14)$$

Unfortunately, such a scheme introduces large truncation errors which are equivalent to a numerical dispersion term (see, for example, Chaudhari, 1971). The effect of these errors is to smear sharp concentration fronts.

Noye (1987B) compared the accuracy of various finite difference methods based on magnitudes of the truncation error terms (of the modified partial differential equations) and found that only upstream methods were always positive definite. These methods introduced large amount of numerical diffusion which spread the peak excessively as time passed.

It is extremely difficult to distinguish in the computed solution between the numerical dispersion introduced by the numerical algorithm and the physical process of longitudinal dispersion

$\frac{\partial}{\partial x} \left(E_x \frac{\partial c}{\partial x} \right)$. For transport in streams physical dispersion may

sometimes be small in comparison with numerical dispersion, and hence computed dispersion can be largely attributed to the latter.

In reversing estuarine flows, however, hydrodynamic dispersion may be the dominant physical process in determining average pollutant levels over a time cycle. Failure to correctly represent dispersion mechanisms may result in solutions which are seriously in error, as also noted by Sobey (1984).

In order to reduce numerical diffusion (or dispersion) sufficiently to prevent masking actual physical dispersion it may be necessary to use extremely small spatial and temporal increments, thereby

directly increasing computation costs (Neuman, 1981, Thomson et al., 1984). Then there is no advantage of using upstream differencing techniques (because solution oscillations are often minimal or eliminated in such cases, anyway).

Various methods have been adopted in order to reduce numerical dispersion in upstream differencing techniques. One way to reduce numerical dispersion in these schemes is to cancel part of the truncation error by using higher order approximations in space (Leonard, 1979A), or in time (Chaudhari, 1971, van Genuchten and Gray, 1978). Chaudhari used an explicit upstream differencing scheme and demonstrated that by adding a term to the dispersion coefficient smearing of the front could be reduced, while still retaining the non-oscillatory nature of the solutions. Leonard (1979A) developed an explicit third order (in space) difference method which was shown to be "highly accurate and free of wiggles (provided boundary conditions are treated properly)". However, the methods are limited in their ability to resolve sudden jumps in values within a small number of grid points. The scheme by van Genuchten and Gray (1978) will be discussed under finite element methods.

An alternative approach to prevent spurious oscillations in the solution is the flux-corrected transport (FCT) proposed by Boris and Book (1973). FCT algorithms, called SHASTA (Sharp and Smooth Transport Algorithm) by the authors, add a "flux-corrected" anti-diffusion term to correct the large truncation errors produced by the transport algorithm (see Book et al., 1975). The nice feature of

this procedure is that positive concentration is always guaranteed, while propagation of steep gradients is handled satisfactorily. The numerical results for an upstream differencing scheme combined with FCT are compared with a standard Galerkin finite element method, an upstream differencing scheme (UDS) and the exact solutions in Lam (1976). The finite element method produced accurate solutions for smooth concentration profiles, whereas steep gradients were simulated better with UDS+FCT.

Finite Element Methods

In the last two decades, or so, finite element techniques have been increasingly applied to transport problems. In the finite element method the spatial region is divided into elements of convenient shape and size, such as triangles or quadrilaterals. Within each element information is concentrated at nodes located at vertices and mid-sides. This information may be interpolated to any other point in the element using pre-selected interpolation functions. Using a weighted residual method, the original partial differential equation is then transformed into a system of ordinary differential equations in time. Solution of these equations gives the values of specific properties of the fluid at nodes.

When the weighting functions used are the same as the interpolation functions, the resulting finite elements are called "Galerkin finite elements" (Baptista et al., 1984). The classic linear Galerkin approach is equivalent to using centered difference in a finite difference method, and hence gives oscillatory solutions

when the advection terms are dominant. Approaches using higher order finite elements (van Genuchten, 1977) or higher order integration schemes in time (such as Smith, 1977), despite some improvement, have not removed the major numerical difficulties.

Earlier remedial measures included upwinding based on the technique of upstream weighting as used for finite difference methods. In a numerical experiment using quadratic upwinding of the form $w_q = 0.75(1+\zeta)(1-\zeta)$ for the weighting functions (Rajbhandari, 1990), solution oscillations were eliminated for a Peclet number of 19 and a transport Courant number of 1.9. However, the solution peak was grossly underpredicted due to excessive numerical dissipation introduced by the scheme as shown in Figure 2.1. This observation is consistent with those reported in the literature (see, for example, Heinrich and Zienkiewicz, 1979). These upwind finite elements (also called "Petrov-Galerkin finite elements") introduce numerical diffusion which may be comparable in magnitude to the actual physical diffusion being modeled.

There have been some criticisms of use of the upwinding approach (for example, see Gresho and Lee, 1981, Leonard, 1979B). Gresho and Lee argue that solution oscillations ("wiggles") that occur in advection-dominated transport problems signal that some important portion of the solution (i.e., physics of the process) is not being adequately modeled and that judicious refinement of the mesh may be necessary, depending upon the extent of oscillations. Algorithms specifically designed to smooth the oscillations on coarse grids are not acceptable, as the smoothed numerical

solutions may not represent solutions of the original partial differential equation. A variation of the upwind method can be found in Hughes and Brooks (1979) wherein an artificial diffusion term, equivalent to the one implicitly introduced in the upwind schemes, is computed and added to each element at each time step.

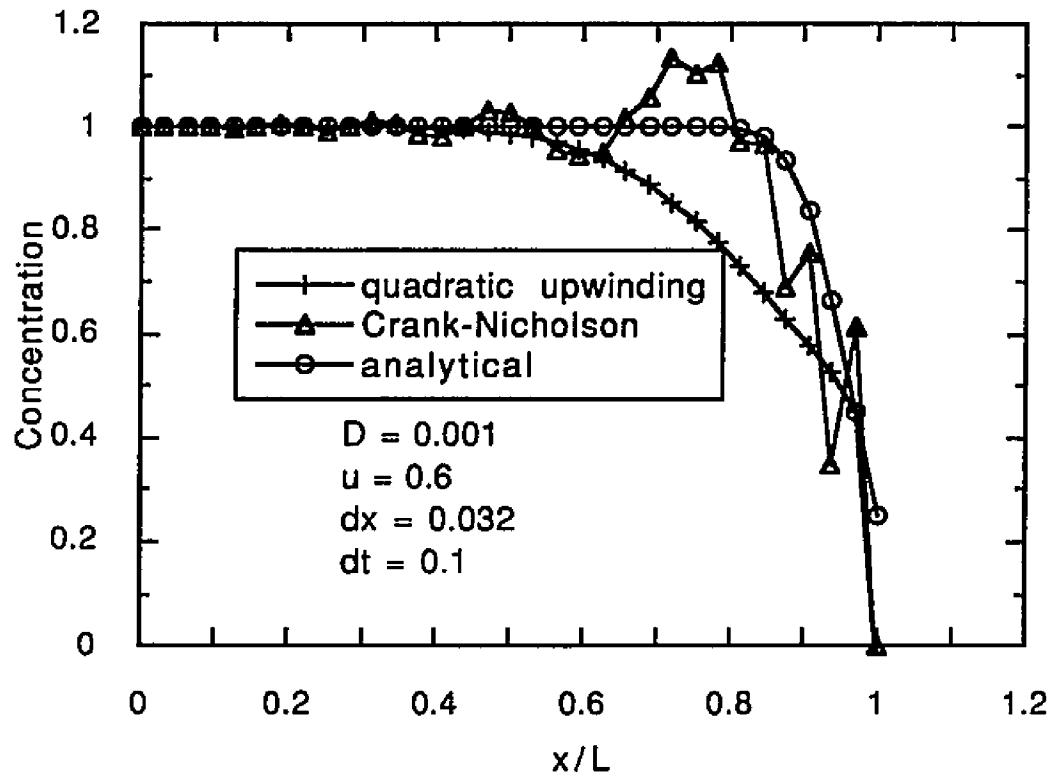


Figure 2.1 Numerical Experiment for Mass Transport
Shown after 16 Time Steps
(Reproduced from Rajbhandari, 1990)

van Genuchten and Gray (1978) presented a series of higher order finite difference and finite element schemes (up to fourth order) with consistent higher order approximations of the time derivative (through the introduction of appropriate dispersion corrections). Superior results were obtained with Hermitian schemes. Numerical

dispersion and solution oscillations were still observed, although small, over the parameter range presented.

Gray and Pinder (1976) examined the Fourier response characteristics of a number of finite difference and finite element schemes. They concluded that the right choice of a numerical scheme involves trade-offs between computational effort, accuracy, and mathematical abstraction. Hermitian elements were found to be superior, but using them added to the computational effort.

Sobey (1982) evaluated the Fourier response characteristics of a number of finite elements (that varied in element order and order of nodal continuity¹) over the parameter range of physical interest, and confirmed the fundamental importance of resolving the smaller wave lengths in spatial discretization. It was concluded that the performance of the complete first order Hermitian element, which has concentrations and their spatial and time derivatives as nodal parameters, was reasonably adequate. Sobey (1984) pointed out that such higher order nodal continuity is equally appropriate in the context of the finite difference method and the method of characteristics. There is no inherent advantage in choosing any one of these approaches in the Eulerian framework.

¹ See Chapter 3 for a definition sketch of nodal continuity.

2.2.2 Lagrangian Methods and Method of Characteristics

Since standard Eulerian methods are not numerically satisfactory and the relatively complicated formulations required to improve them may not be easily adaptable to complex systems, it is of interest to investigate the methods based on the Lagrangian approach. Lagrangian methods solve the transport equation on a grid that moves with the local velocity, thereby avoiding numerical treatment of the hyperbolic operators.

When considering pure advective transport, the Lagrangian equation and the Eulerian characteristic equation are identical (Sobey, 1984). Setting the right-hand side of equation (2.3) to zero, one obtains¹:

$$\frac{\partial c}{\partial t} + u \frac{\partial c}{\partial x} = 0 \quad (2.15)$$

which can be replaced by

$$\frac{DC}{Dt} = 0 \quad (2.15A)$$

in which $D/Dt = (\partial/\partial t) + u (\partial/\partial x)$ represents the total (or substantial) derivative along the trajectory defined by

$$\frac{dx}{dt} = u(x,t) \quad (2.16)$$

In physical terms, eq. (2.15) means that if the trajectory between a departure point "P" and an arrival point "A" (see Figure 2.2) is determined by integrating eq. (2.16), then eq. (2.15A) implies:

¹ Note that the subscript x in (u_x) is dropped for simplicity.

$$C_A = C_P \quad (2.17)$$

i.e., the concentration remains constant along the trajectory (Holly and Polatera, 1984). Numerical methods utilizing Lagrangian schemes, either in part or full, are reviewed here briefly.

Jensen and Finlayson (1980) utilized a scheme that transformed the one-dimensional advection-diffusion equation from an Eulerian coordinate system to a coordinate system that moves (as a rigid body) with the velocity of the front. The location of the boundary changes with time. When the velocity field is uniform, this scheme entails a shifting of the entire domain toward the front at a rate equal to the fluid velocity, resulting an equation free of the advection term. However, for a non-uniform velocity field the advection term is not removed, thus leaving some first-order residual derivatives. This shifting of the domain accounts for the advective component of transport, while the dispersive component is determined relative to the moving coordinate system (MCS). Using orthogonal collocation on finite elements in an example problem, the authors obtained results that showed no oscillations even at high Peclet numbers. They pointed out that improvement in MCS comes from an optimum location of nodes. Since the front remains fixed in a moving coordinate system, more grid points can be concentrated there, but fewer grid points can be used elsewhere. However, for application to very irregular geometries (as would be the case in natural systems), this form of a moving coordinate system is difficult to implement (Thomson et al., 1984).

Varoglu and Finn (1980) used space-time finite elements combined with the method of characteristics to overcome the numerical difficulties posed by the advection term. In this method characteristic curves of the hyperbolic operator ($E_x=0$) form the sides of the elements joining nodes at consecutive time levels. The effect is like creating a mesh that moves through space as time progresses, in a direction determined by the characteristics of the associated pure advection equation. The resulting finite elements become free of advection terms, resulting in a relatively well-behaved diffusion-type problem. The authors' test examples showed no solution oscillations and produced only a small amount of numerical dispersion in the case of pure advection. The down side of this method is that at each time step a new space-time mesh needs to be generated which may require substantial computational effort in solving large systems.

In order to avoid the numerical problems encountered when modeling a steep moving front, O'Neill (1981) utilized a moving, deforming coordinate system (MDCS) to generate nodal points in space which are functions of time. In contrast to the approach used by Jensen and Finlayson (1980), in which the entire numerical coordinate system moves with the fluid velocity, this method relies on reducing the relative size of the advection term locally (near the location of the front where it matters most) by selecting a mesh velocity that closely matches the fluid velocity around the front. Elsewhere, the finite element mesh is allowed to deform according

to the difference between the mesh and the fluid velocity. Thus the advection term is not fully removed.

It is apparent from the above discussions that most schemes that utilize Lagrangian methods do not seem to completely take advantage of the method. Fixed grids are often retained for the solution of associated dispersion calculations. Because of the hybrid nature of some of these methods and the method described below, they are sometimes called Eulerian-Lagrangian methods. In general, at every time step, these methods use the backward characteristic to find the location of the particle at the previous time. The difficulty of correctly solving the advective term reduces (or rather transforms) to a problem of approximately determining the concentration at this location by some kind of interpolation between the known concentration values in the uniform fixed grid. The following discussion further illustrates this point.

Referring to Figure 2.2 if P were to arrive at A at time $(n+1)\Delta t$, by interpolation the location of P is:

$$x(p) = i\Delta x - u\Delta t$$

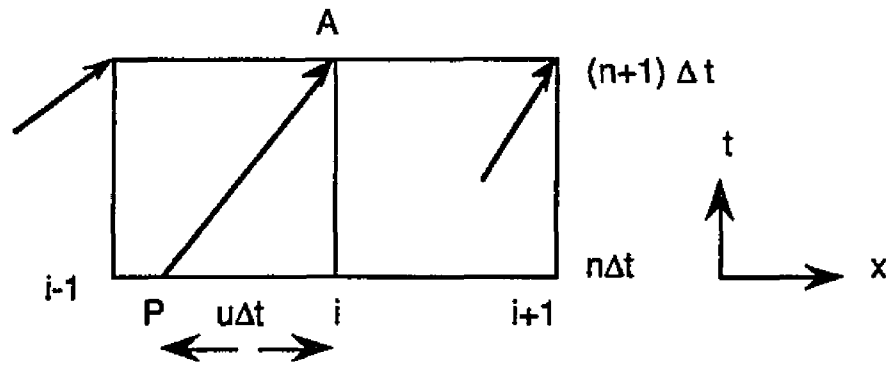


Figure 2.2 Interpolation in an Eulerian Reference Frame

The concentration can now be determined by interpolating from known values of concentrations at adjacent grids. If a linear interpolation is used, based on eq. (2.17), the new concentration (C_A) will be:

$$c_i^{n+1} = c_i^n - \frac{u\Delta t}{\Delta x} (c_i^n - c_{i-1}^n) \quad (2.18)$$

Note that this is identical to a finite difference method that is explicit, and is "upwind" in space (Roache, 1972). As discussed earlier, this scheme inevitably introduces artificial diffusion. Numerical difficulties of modeling the advective terms are removed, but problems of numerical damping are not quite removed. The damping can be eliminated to some extent by using higher order interpolation method such as quadratic interpolation over the grids $i-1$, i and $i+1$ proposed by Leith (1965).

The problem with using higher order interpolation (but retaining $C^{0,0}$ nodal continuity) is that it requires the use of additional surrounding nodes, thus using information which may be physically

too far from P . As an alternative approach, Holly and Preissmann (1977) constructed compact cubic and quintic interpolation polynomials using only two computational points, the required additional degrees of freedom being supplied by the first and second derivatives of the concentration fields at these two points. A higher order interpolation is thus obtained without using information outside the cell containing point P .

Although this method achieves higher accuracy, requirement of solving auxiliary advection equation for the first derivative of the concentration field adds substantially to the computation cost. A comparable degree of accuracy can be obtained using an appropriate cubic interpolation at the foot of the characteristic trajectory (Schohl and Holly, 1991). By constructing a fourth-order, cubic-spline interpolating polynomial over the computational domain at time n , these authors avoided the auxiliary problem and were able to achieve some reduction in computation time.

The full advantage of the Lagrangian method, or the method of characteristics, can only be realized if the computations are transferred completely to a moving coordinate system (see Figure 2.3). The convenience of interpreting concentrations at fixed

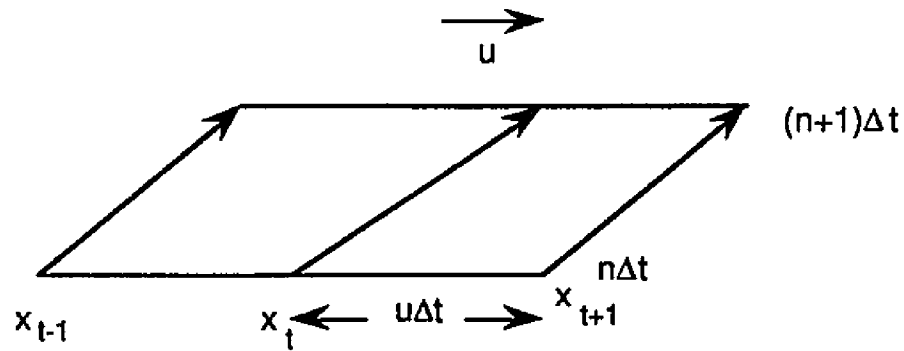


Figure 2.3 Lagrangian Reference Frame

locations is lost, but so is also the need of explicitly determining the advective transport term, thereby avoiding solution oscillations. The resulting grid is irregular and inconvenient for the associated dispersion computations (for example, see Sobey (1983) and McBride and Rutherford (1984)), but the gain in accuracy in solving advective transport conditions far outweighs the extra effort needed for dispersion calculations.

Sobey (1983) used a fractional step method, separating the transport equation into advection, diffusion and reaction stages. A local analytical solution is adopted for the reaction stage and the method of characteristics along a moving coordinate system for the advection stage. Both these stages are essentially exact, whereas the third stage, i.e., dispersion, is handled using an optimized finite difference step that also (by using an appropriate algorithm) specifically accounts for the non-uniform grid generated by the moving coordinate system adopted for the advection step. Examination of Fourier response characteristics and numerical experiments performed using parameter range appropriate for

estuarine flows showed almost complete elimination of solution oscillations and numerical dispersion. The LAMBDA (Lagrangian Approach to the Mass Balance of Dispersion and Advection) scheme developed by McBride and Rutherford (1984) is applicable only to steady-state flow cases.

Further discussions on Lagrangian schemes are presented in Chapter 3.

2.3 Review of Applied Water Quality Models

A major purpose of developing a water quality model is to actually apply it to a real system, and once its usefulness is proven, to use it as a tool in the management of water resources systems. While a careful review of different numerical schemes (described in Section 2.2) is essential in the selection of the most accurate and economically feasible numerical algorithms, it is equally important to test resulting models on real systems. Tests against analytical solutions for simplified problems are important and necessary, but they do not often reveal deficiencies that may be encountered in modeling real complex estuarine systems. Many undesirable features may not appear until a particular set of circumstances is modeled. It is therefore considered timely to present a brief review of the most widely used one-dimensional water quality models, and to include some comments on the numerical problems encountered in their applications.

LINK-NODE MODEL

The Link-Node water quality model is one of the earliest models, to have been applied to estuarine systems. Developed in the mid 1960's by Water Resources Engineers, Inc., this model, together with its companion hydrodynamic model, has undergone several modifications, and is available in various forms both for the steady-state (tidally averaged) and dynamic conditions. Link-Node models are formulated such that mass is conserved at each node, and the network (of 'links') mimics transport among a series of continuously stirred tank reactors (CSTR'S), the "nodes."

These models have been applied to estuarine systems in several locations of the United States and abroad (for example, see Chen and Orlob, 1975 and Orlob et al., 1991). An attractive feature of the model is its flexibility to adapt to different prototype geometries and its ability to simulate dynamic variations of a number of important water quality variables, including those involved in primary production and dissolved oxygen dynamics.

As with most Eulerian models, the Link-Node model tends to diffuse mass numerically, which may be comparable in magnitude to, or even greater than, actual physical diffusion. Numerical diffusion arises because concentrations cannot be represented except at grid points, and can be excessive in regions of steep concentration gradients. Because the front is translated in each time step to the next adjacent node it moves more rapidly than it should actually, resulting in a numerically dispersed front.

As discussed in Section 2.2, the magnitude of the numerical diffusion can be reduced by decreasing the size of the spatial grid. This theory is apparently supported by the results of a numerical experiment described in the beginning of Chapter 3. However, stability requirements of an explicit scheme make it necessary to reduce the time step as well, such that $u\Delta t < \Delta x$, which would result in many smaller time steps and increased computation costs.

These numerical characteristics were recognized during early uses of the model, hence, in some applications the physical dispersion terms in the model were dropped entirely to partially correct for the numerical effect. In order to reduce numerical mixing the so-called quarter-point technique was used, in which the concentration of the advected water is weighted at a ratio of three quarters to the concentration at the upstream grid point and at one quarter to the concentration at the downstream grid point (Orlob et al., 1967). A detailed description of the Link-Node model (DQUAL) is given in (Smith and Roig, 1986).

WASP4

The WASP4 (Water Quality Analysis Simulation Program Version 4), maintained by the US Environment Protection Agency, is perhaps the most comprehensive water quality model currently in use for estuarine water quality studies. The model represents the prototype geometry as a series of "segments." Using hydrodynamic information obtained from a companion model DYNHYD4 (a version of Link-Node hydrodynamic model), this model simulates conventional

water quality parameters such as dissolved oxygen, phytoplankton and nutrients, as well as processes involved in the fate of toxic chemicals, including ionization, hydrolysis, oxidation etc. (Ambrose et al., 1988).

When an upstream differencing scheme is used, the numerical dispersion in this model is given by

$$E_{\text{num}} = u/2(L-u\Delta t) \quad (2.19)$$

where

- u = velocity,
- L = segment length,
- Δt = time step.

For reducing the numerical error, a factor modifying the upstream weighting is used, as also described by Bella and Grenney (1970). These authors investigated convection errors associated with commonly used finite difference models that are also explicit. They derived the following relationship for the "pseudo-dispersion":

$$D_p = u/2 [(1-2\gamma)L-u\Delta t] \quad (2.20)$$

where

- γ = proportionality factor representing flux between adjacent cells (called 'advection factor' in Ambrose et al., 1988),
- L = distance between cells.

Note that

- $\gamma = 0$ represents an upstream difference scheme,
- $\gamma = 0.5$ represents a central difference scheme.

For a particular segment size and velocity, numerical dispersion can be reduced by increasing the time step (only up to a limit of L/u from stability considerations).

QUAL2E

QUAL2E (Brown and Barnwell, 1987) is one of the most commonly used water quality models for riverine systems, both in the US and abroad. This model, maintained and supported by EPA, uses steady-state hydraulics and, hence, has no capability to simulate tidal river or estuarine conditions. Nevertheless, a discussion of the model is included in this section because it is an excellent water quality package with many useful features. For example it is capable of simulating the dynamics of water quality over the diurnal cycle, e.g.,--- time varying boundary conditions for heat and light can be introduced to drive primary production. The model also requires some comment on the specific numerical problems it presents. The model developed in this dissertation utilizes many of the kinetic formulations and the heat budget routine described in the QUAL2E manual.

QUAL2E uses an implicit backward difference scheme to approximate advection, represented by

$$\frac{c_i^{n+1} - c_i^n}{\Delta t} + u \frac{c_i^{n+1} - c_{i-1}^{n+1}}{\Delta x} = 0 \quad (2.21)$$

where

n = integer denoting time level.

This scheme produces numerical dispersion of the form

$$E_{\text{num}} = u \Delta x / 2 (1 + u \Delta t / \Delta x) \quad (2.22)$$

(for example see Roache, 1972).

QUAL2E can be used for pulse loads with appropriate minor modifications to input routines (Walton and Webb, 1994). These authors showed that in simulation of pulse loads, the existing solution scheme produced excessive smearing. To overcome this problem they modified the QUAL2E difference scheme to an explicit formulation and found superior results with minimal smearing for simulation of the identical pulse loads. The modification may, however, require a much smaller time step to satisfy stability restrictions imposed by an explicit scheme.

It is noted from eq. (2.22) that E_{num} is always positive; so numerical dispersion always exists. The advantage of the implicit scheme is that it is unconditionally stable. Walton and Webb (1994) commented that under the most common scenarios for which QUAL2E is used, such as continuous loading of waste water discharges, the model, as it is, performs well.

Other Models

DWRDSM

DWRDSM model is used extensively by the California Department of Water Resources (DWR) for modeling of conservative constituents (see Hutton and Chung, 1992). It is a modified version of the original Fischer Delta Model (H. B. Fischer Inc., 1984), which was based on the Lagrangian box model approach, and that was adapted to the link-node configuration of grids developed by Resource Management Associates (Smith and Roig, 1986) for the Sacramento-San Joaquin Delta. This model uses information on tidal stage supplied by its hydrodynamic module and recomputes the flows based on these stages for advective transport. Unlike the Link-Node Model, which accepts trapezoidal approximations of the prototype cross-sections, this model requires rectangular approximation of the cross-sections.

The model in its present formulation can simulate only conservative substances. Because of the Lagrangian formulation, numerical dispersion associated with the advective term is largely eliminated. The model is tied to the hydrodynamic module which is based on the method of characteristics. Because continuity of flow is enforced at the junctions, and not strictly within channels, there is potential of flow "leakage" in channels. DWR recently modified the so-called "leak plug option" to overcome this deficiency, but it can be used only in quasi-steady state runs, in which the net change in stage over a tidal cycle is zero (DWR, 1992). Enforcing this

option can lead to stability problems, in which case the model must be re-run with a smaller time step. The reader may refer to DWR (1994B) for details. The leak-plug option cannot be used in the simulation of continuous (non-repeating) tides because the amount of leakage cannot be computed easily in such runs.

RMA4Q

RMA4Q is a recently developed water quality model (King and DeGeorge, 1994) based on one- and two-dimensional finite elements. It is capable of simulating both conservative and non-conservative constituents. Interactions among the constituents are based on QUAL2E. This model, derived from the finite element transport model RMA4 (King, 1990) depends on a companion/hydrodynamic model RMA2 (King, 1993) for a description of velocities and depths at all nodes within the water body.

An extended version of RMA4Q has recently been applied to model an accidental spill of metam sodium that occurred in Dunsmuir, California (Saviz et al., 1995). Examples of RMA4Q can also be found in the Australian Water and Coastal Studies (1995) and the New South Wales Department of Public Works and Services (1995). At the present time, sufficient number of references are not available to provide useful comments on the performance of RMA4Q. The model, being Eulerian-based, may be subject to some numerical difficulties (reviewed in Section 2.2) when applied to steep gradient scenarios.

3. RESEARCH METHODOLOGY: MODEL EXPERIMENTS

3.1 Effect of Grid Resolution on Model Results:

A Numerical Experiment

A numerical test was performed on a real prototype system to examine the effects of changing grid size on the performance of a water quality model. From the perspectives of practicality and robustness of the test, the complex estuarine system of the Sacramento-San Joaquin Delta in California was chosen for testing the model. A description of the Delta is given in Chapter 4. Because of its proven usefulness in estuarine water management applications, and also because numerical dispersion in the model is only partially controllable, the Link-Node Water Quality Model was used in this study. The general inferences that may be drawn from this study should be applicable to Eulerian transport models, that are explicit in time and are of similar numerical structure.

The Link-Node Hydrodynamic (RMA/DWR version) and RMA Dynamic Water Quality (DQUAL) models were used to simulate the effects of modifying channel element (link) size in the western part of the Delta (Figure 3.1). The area considered lies to the west of Rio Vista and south of Suisun Marsh. The maximum length of the channel elements in that region is 21,000 ft. (for the original grid network). Channel elements were modified such that elements longer than 13,000 ft. were halved and those longer than 18,000 ft. were divided into three links for purposes of achieving more uniform and shorter link sizes in that area. Consequently, channel lengths were

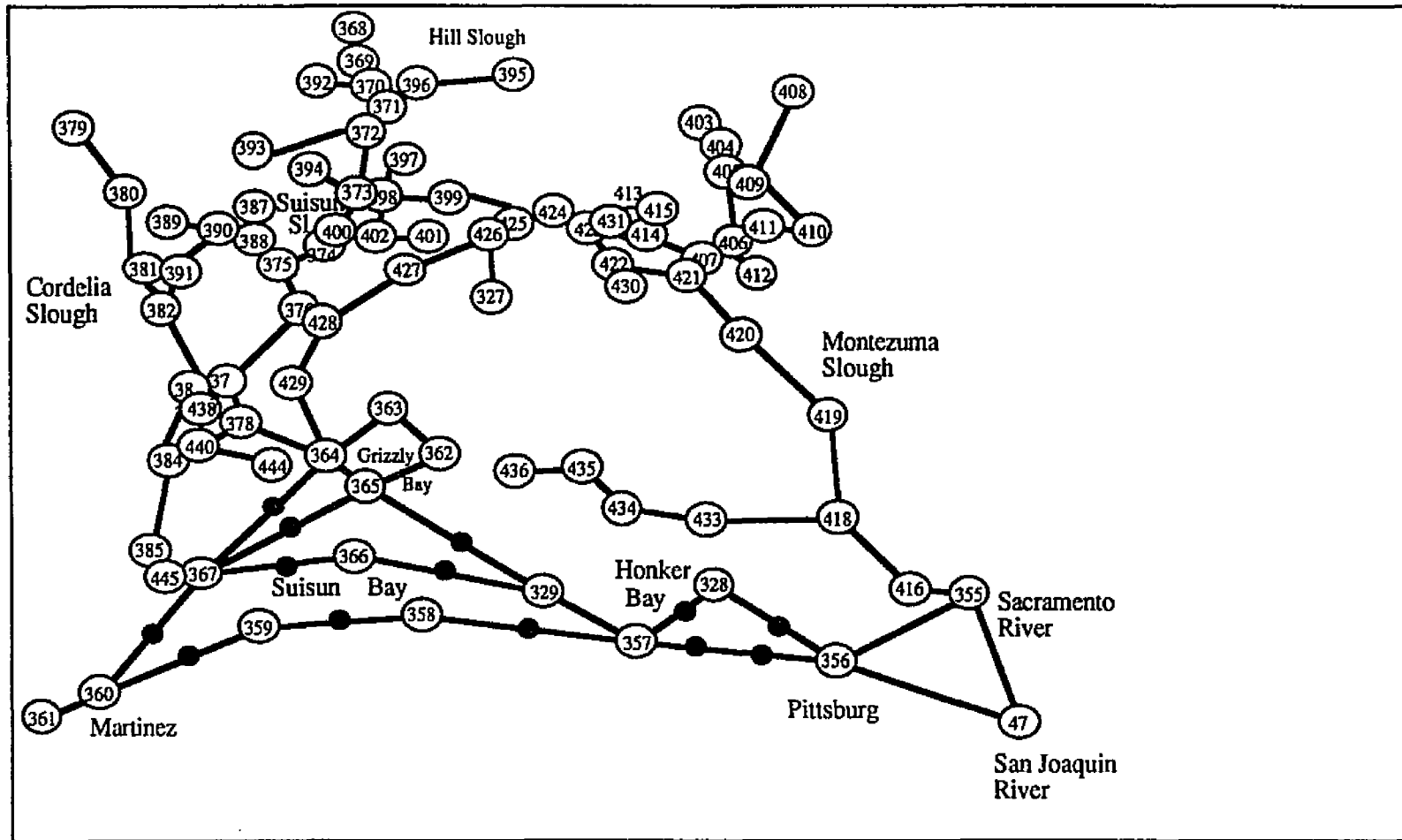


Figure 3.1 Modified Part of the Delta Network (continued to next page)

Nodes added in the grid are shown by solid circles.

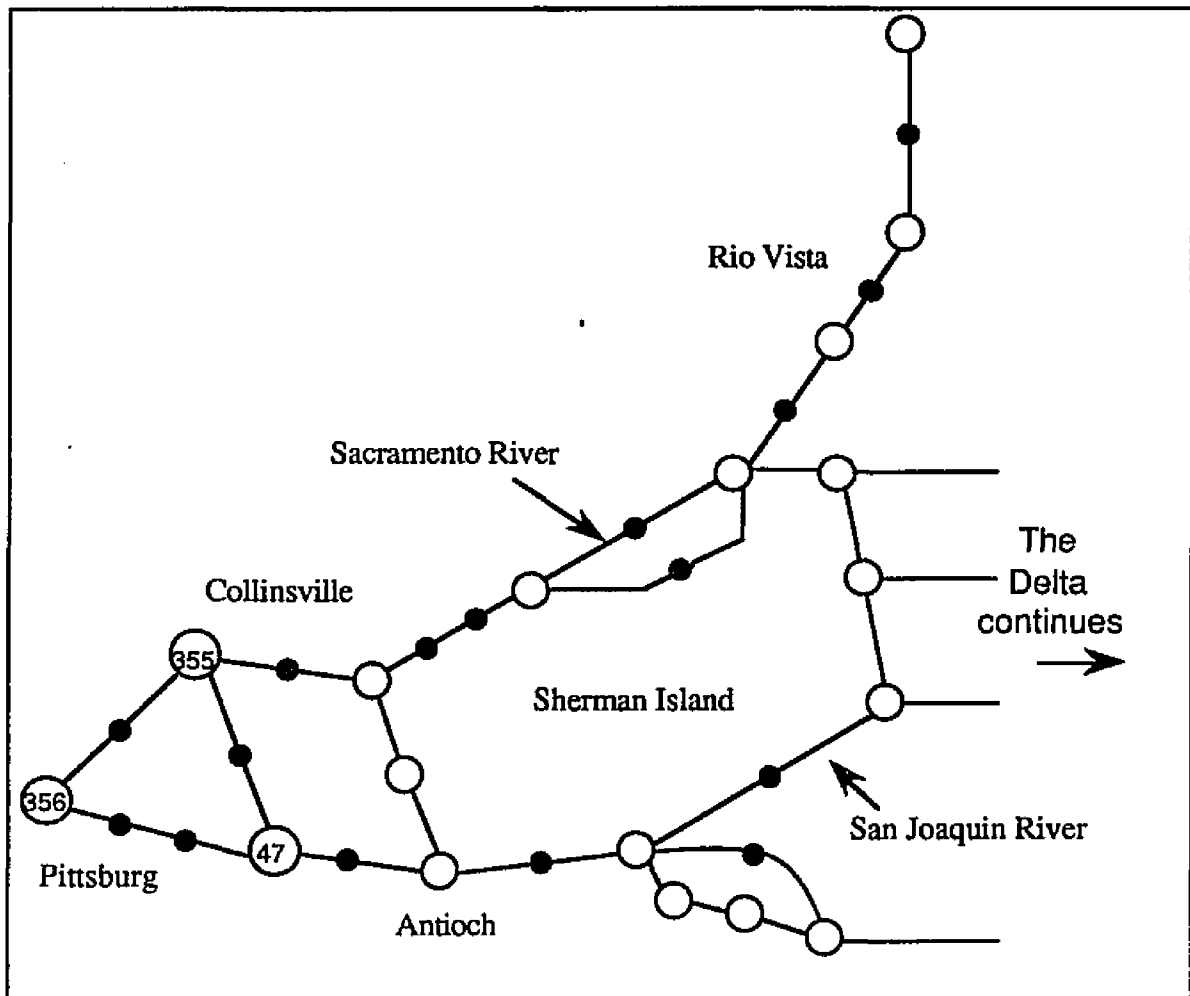


Figure 3.1 (contd.) Modified Part of the Delta Network
Nodes added in the grid are shown by solid circles.

less than 13,000 ft. for the modified grid. This modification resulted in an additional 29 nodes and 29 channel elements in the network, thus increasing the total number of channel segments in the Delta to 592 connected at 488 separate junctions.

The modified part of the link-node network is shown in Figure 3.1 where the nodes added in the grid are indicated as solid circles.

The geometric characteristics of the system required for the hydrodynamic model run were accordingly modified.

To determine the effect of grid resolution on numerical dispersion identical hydrodynamic and water quality runs were made for the Delta using first the RMA/DWR grid network and then the modified grid network. Tidal boundary conditions corresponded to the 19-year mean tide condition near Benicia. For each hydrodynamic run a "warm up" period of three tidal cycles was allowed for convergence on the cycle to be used as input to the quality model. A time step of 90 seconds was found to be satisfactory for hydrodynamic model stability.

DQUAL, the RMA Link-Node model, was driven by the outputs of the hydrodynamic model, repeated over several tidal cycles for both standard and modified link-node configurations. Boundary flows, i.e., the inflows of the Sacramento and San-Joaquin Rivers, were assigned at electrical conductivities of 162 and 793 micromhos/cm, respectively. The model was allowed to run to approximate steady state EC concentrations at western Delta locations.

In order to illustrate the effect of grid modification, computed EC values at different nodal locations along parts of Suisun Bay, San Joaquin River, and Middle River were plotted for both cases. Figure 3.2 shows these EC values for locations including Martinez near the seaward boundary and Union Island toward the southeast end of the Delta (for location, see Figure 4.7). Computed EC values

corresponding to the modified grid network are smaller, although by varying amounts at different locations in the Delta. These differences gradually decrease and become negligible at Node 52 which is located relatively far from the presently modified region and is subject more to the influence of San Joaquin River water quality. An apparent explanation for the lower EC values associated with the more detailed grid is that the intruding front's advance into the Delta was less accelerated by being restricted to transport through a succession of shorter "links", in each successive time step. With the less detailed grid given the same number of time steps, transport of downstream quality was accelerated.

This study is not entirely adequate to indicate just how much modification will be necessary ultimately to improve significantly the accuracy in simulation. It is not sufficient also to suggest that it would be feasible to achieve such modification for the complex channel configuration of the Delta. The investigation does show, however, that model results are sensitive to changes in grid size, although to varying degrees. The extent of this sensitivity depends on the specific locations of the areas where the grid is being modified and the regions of water quality investigation. Moreover, it suggests the need for an improved water quality simulator, one that minimizes numerical dispersive effects.

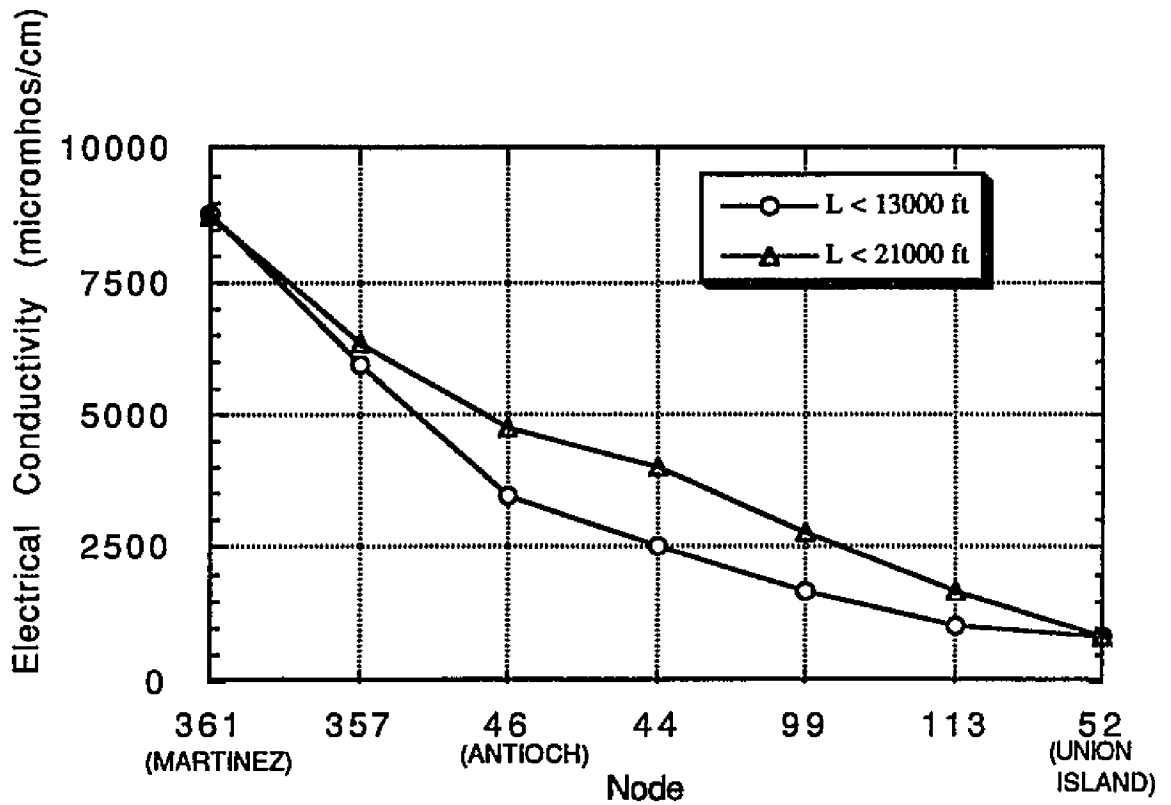


Figure 3.2 Computed Daily Average Electrical Conductivities
(July 1988)

3.2 Lagrangian Approach to Modeling

The review of different numerical schemes (Chapter 2) showed that when modeling steep concentration gradients Eulerian methods of solution suffer from numerical difficulties. Combined Eulerian-Lagrangian methods (ELM), recently developed in both one and two dimensions, provide somewhat improved solutions over those of Eulerian methods. However, higher order interpolation methods that are required increase computation cost.

In pure Lagrangian methods, however, dispersion between parcels is calculated directly as constituents are convected and tracked, thus avoiding the need of any interpolation to get their concentrations at fixed locations. Examples of such methods are given by Fischer (1972), Barrett and Malloney (1972), and Jobson and Schoellhamer (1992). These methods, also known as Lagrangian box models, solve the transport equation by keeping track of moving volumes (also, called boxes) of water. Each box or parcel of water has vertical end walls and is assumed to be uniformly mixed. Parcels of water are displaced in an upstream or downstream direction according to the nature of channel flow and geometry defined for an Eulerian grid. Dispersion is modeled using an appropriate exchange of flow between adjacent parcels.

The assumption of completely mixed parcels may cause interpolation errors when determining the concentration at a given point. The major reason for the improved accuracy of a Lagrangian model, in comparison to an Eulerian model, is that these

interpolations are done only when output is desired and the interpolated values are not used in further computations. In an Eulerian model, similar interpolation errors are made for every time step and grid point, but the interpolated values are used as the basis for all further computations (Jobson, 1987A).

Among these Lagrangian models, the transport algorithm provided in the Branched Lagrangian Transport Model (BLTM) (Jobson and Schoellhamer, 1992) is considered an appropriate choice to adopt as a base model for the present study. It has the following desirable attributes.

- The earlier versions of the Lagrangian Transport Model (LTM) (Jobson, 1981) have been applied to model nitrogen kinetics in natural rivers such as the Chattahoochee River (Jobson, 1985 and 1987B). The algorithm is capable of handling problems with large concentration gradients (Jobson, 1980) and highly unsteady flows (Jobson, 1985).
- The model is independent of hydrodynamic model drivers. In other words, it is not tied to any particular model (except for the basic assumption of one-dimensionality) to provide required information on the hydrodynamics of the system being modeled. The model, however, is best suited to cell-type hydrodynamic models i.e. those with flow defined over a cell. The information required on discharge, cross-sectional area and topwidth of the channel can be derived by using any of a number of existing one-dimensional unsteady hydrodynamic models

including the USGS Four Point Model (DeLong, 1995), the RMA Link-Node Model, the DWRDSM Model, and the BRANCH Model (Schaffranek et al., 1981). Of course, some changes in the code are inevitable to provide output in a format acceptable by BLTM.

- The model is easily available from the United States Geological survey (USGS) for review, numerical tests and further development.
- Although the model is not known to have been applied to very large and complex one-dimensional estuarine systems, it shows a potential to avoid shortcomings observed in application of other water quality models to such systems, particularly numerical mixing problems, as noted in the previous section and Chapter 2.

A somewhat comparable alternative to Lagrangian box models is the Lagrangian model with zero order continuity of concentration ($C^{0,0}$) of the kind as described by Sobey (1983) (see Section 2.2 for a brief description). The sketch shown in Figure 3.3b illustrates nodal continuity of concentration resulting with the zero order assumption.

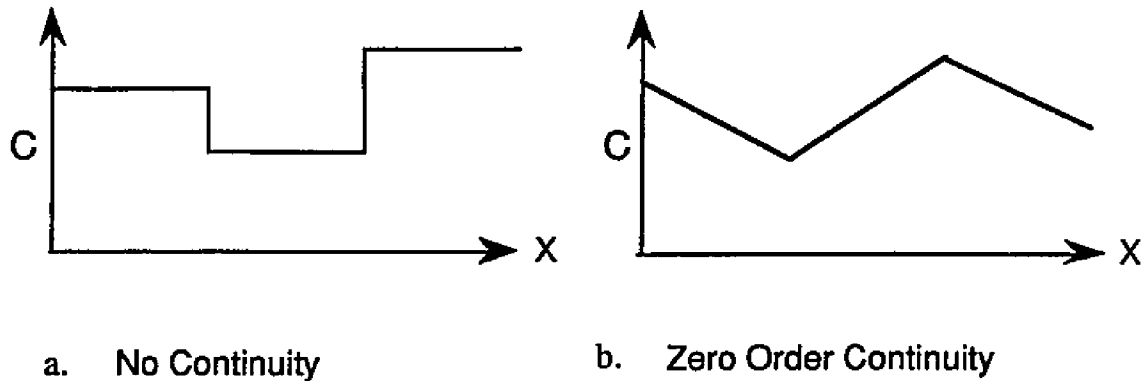


Figure 3.3 Definition Sketch: Nodal Continuity

In applications where simulation often involves those of effluent outfalls (point sources), thus producing sharp concentration fronts, a high degree of resolution is required of the flow field in both space and time. Otherwise, errors involved in the prediction of the characteristic path may be large enough to affect the results for mass transport, especially in the vicinity of the outfall. In such situations the Lagrangian approach with $C^{0,0}$ nodal continuity has some advantages over the box models, because numerical integration of an appropriate order (such as, those based on Runge-Kutta algorithms) can be used to integrate the unsteady equation

$$\frac{dx}{dt} = u(x,t) \quad (3.1)$$

the order depending upon the resolution of velocity available from the hydrodynamic calculations.

In box models, on the other hand, it is implicitly assumed that the flow field is constant over the local space and global time step.

This assumption is appropriate in situations where the velocity field is available at a sufficiently fine resolution of the space-time grid.

The disadvantage with Sobey's method is that it results in a non-uniform grid for associated dispersion calculations, which requires relatively complex algorithms to solve. This increases computation cost.

In a box model, such as LTM, parcels are uniformly mixed, which means that continuity of concentration is not enforced at parcel boundaries (see Figure 3.3a). Mass, however, is conserved in the system. Using Fourier analysis of results for a test case (where necessarily velocity u is held constant) with $Pe=50$, Schoellhamer (1985) showed that LTM did not show any phase error, an observation he noted to be consistent with previous applications of LTM that showed no oscillation errors. The author concluded that a Lagrangian box model such as LTM is "almost as accurate as the implicit $C^{0,0}$ Lagrangian model like the fractional step algorithm by Sobey (1983)", and is more cost effective.

Because of the assumption that segments of water are uniformly mixed, some numerical mixing is unavoidable, but this can be made small by having short segments (Barrett and Mollowney, 1972). In BLTM this can be enforced by using small time steps. The basic formulation of BLTM is described in the next section.

3.3 Solution Algorithm of Branched Lagrangian Transport Model (BLTM)

BLTM solves the advection-diffusion equation by using a Lagrangian reference frame in which the computational nodes move with the flow (Jobson and Schoellhamer, 1992). It is an updated version of the model, LTM, documented by Jobson (1981), Schoellhamer and Jobson (1986) and Schoellhamer (1988). While LTM is applicable only to one-dimensional unidirectional flows, such as in rivers, BLTM can be used in branched river systems and for reversing flows, such as occur in tidally affected rivers.

3.3.1 Governing Equations

In the Lagrangian reference frame the conservation of mass equation is written for a specific parcel of fluid, which is:

$$\frac{\partial C}{\partial t} = \frac{\partial}{\partial \xi} \left[E_x \frac{\partial C}{\partial \xi} \right] \pm k C + s \quad (3.2)$$

where

- C = constituent concentration,
- E_x = longitudinal dispersion coefficient,
- k = first order rate constant,
- s = sources and sinks which are often functions of other constituent concentrations,
- ξ = distance from the parcel, the Lagrangian distance coordinate.

$$\xi = x - x_0 - \int_{t_0}^t u \, dt \quad (3.3)$$

x_0 = location of the fluid parcel at time t_0 .

x = Eulerian distance coordinate

(Jobson (1987))

Advection

Transport by advection is handled in BLTM by moving discrete water parcels. The solution starts with a series of parcels spaced along the river at intervals of $u\Delta t$. Initial concentrations are assigned to each parcel, and at each location where water enters into the modeled system. Generally, one or more parcels are defined within each branch of the system. As new water enters the system (at boundaries) during a simulation, parcels are added that have a volume equal to the inflow volume during each time step. When a parcel passes the most downstream location, it is simply discarded.

Dispersion

Mixing is modeled on the basis of flow exchanged between parcels. The boundary between neighboring parcels is moved at the mean flow velocity, but because a velocity profile exists at the boundary, water near the bed and sides of channels is moving slower than the water near the surface. This is depicted schematically by the velocity profiles in Figure 3.4. Consequently, a parcel, K, moving with the average stream velocity must contribute some volume of water to, and receive an equivalent volume from, its adjacent

downstream parcel, $K+1$. An identical process applies at the boundary with the upstream parcel, $K-1$. This interparcel flow results in a transfer of constituent mass between parcels. The net effect is that parcels that have higher constituent concentrations

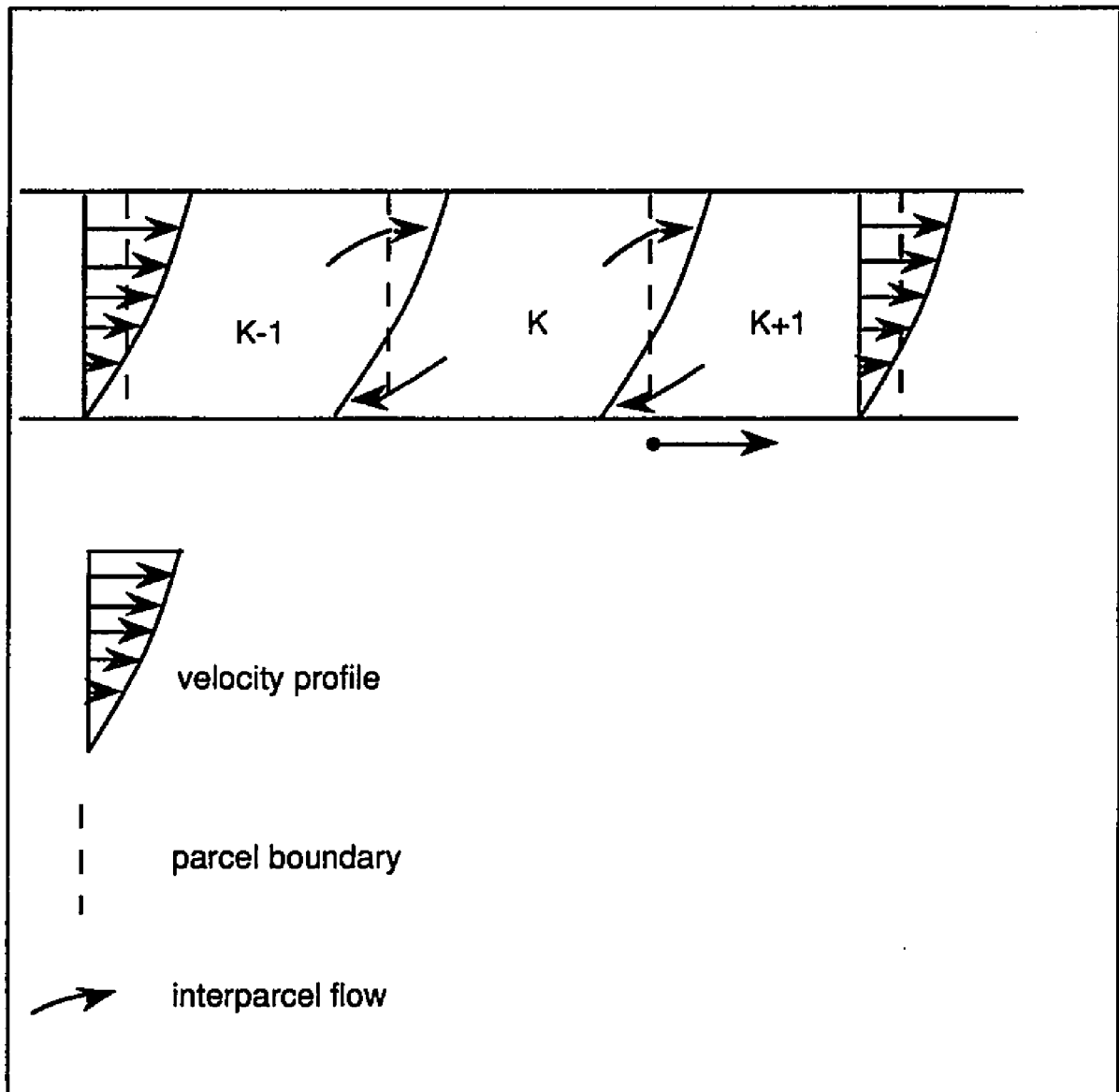


Figure 3.4 Schematic Showing Interparcel Flows

than their neighbors lose mass and those that have lower concentrations gain mass. This causes concentrations of constituents to spread longitudinally (Goodwin, 1991).

The dispersion formulation in the BLTM is based on the above concept of flow exchange. A user-defined fraction, called the dispersion factor (D_f), of the total channel discharge (Q) is used to represent the amount of water exchanged (DQ) at each parcel boundary at the same location, e.g.,

$$DQ = D_f Q \quad (3.4)$$

Using a simple explicit finite-difference scheme for the flow condition shown in Figure 3.4, Schoellhamer and Jobson (1986B) showed that D_f can also be expressed as

$$D_f = \frac{E_x}{u \Delta x} = \frac{1}{Pe} \quad (3.5)$$

in which E_x is the longitudinal dispersion coefficient and Pe is the Peclet number. This indicates that the assumed definition of D_f (eq. 3.4) is valid. See Appendix B for the derivation of eq. (3.5).

For steady flow, $\Delta x = u \Delta t$, so

$$D_f = \frac{E_x}{u^2 \Delta t} \quad (3.6)$$

Thus D_f is a function of E_x as well as the model time step.

Schoellhamer and Jobson (1986B) recommend D_f values to be in the range of 0.1 to 0.4 for the greatest model stability and accuracy.

Based on an estimate of the longitudinal dispersion coefficient and a representative velocity, users can select the model time step to assure a value of D_f in the optimal range.

In the BLTM all mass passing through a junction is mixed before entering the next river segment or branch. So numerical mixing may occur at junctions (Jobson and Schoellhamer, 1992).

3.3.2 Need for Further Development

BLTM has the capability to simulate up to ten non-conservative constituents. Jobson and Schoellhamer (1992) suggest that often users may find it necessary to write their own kinetics routines to suit their requirements.

During the investigative phase of this research, and while making tests with the BLTM as applied to the Newport Bay system described in the next section, it was determined that for the purpose of the present study a complete new set of water quality routines should be developed. The new routines, adapted to the basic transport framework of BLTM, should then be tested by applying it to a real estuary. Further discussions on the new model development are presented in Chapter 4.

3.4 Tests with BLTM: Modeling Newport Bay

To examine the applicability of the BLTM model, it was considered prudent first to solve a field problem at a small scale. Newport Bay in Southern California possesses a number of features which make it a good system on which to test the performance of a mathematical model. Estuarine conditions of Newport Bay provide a fairly severe test of solution algorithms, as flows in this system may vary from zero to very large values in either direction. A brief description of the Newport Bay system, its schematization for modeling, and the testing of BLTM is provided below.

3.4.1 Description of Newport Bay Estuary

Newport Bay is a small but complex estuarine system, located in Orange County, California (Figure 3.5). It is comprised of numerous shallow salt marshes and mud flats with a total surface area of about 1000 acres. The southern end of Upper Newport Bay receives drainage from San Diego Creek, the principal source of inflow. Runoff from a basin of about 1000 square miles carries sediments, dissolved substances, and organics into the estuary, which are finally transported to the Pacific Ocean. Profiles of sediments deposited in the estuary show that it has been remarkably altered by the transport and deposition of sediment from the surrounding highlands. Additional inflows into Upper Newport Bay are contributed through the East Costa Mesa, Santa Ana-Delhi, and Santa Isabella channels and by Big Canyon Creek. The southernmost end of the Bay is its only opening to the Pacific Ocean and the locale of

maximum salinity. The northern extremity receives fresh water inflows into the system and possesses the lowest salinity. Between these localities the water is brackish, varying in salinity gradually from that of fresh water at the upstream boundary to ocean salinity at its lower boundary depending on the effects of hydrologic inflow and tidal motion (Onyejekwe, 1983).

Figure 3.6 shows the link-node (element-junction) schematization of the system conceptualized as a continuum of elements and junctions in 2-D space. Each element is an approximation of a channel in the prototype, while each junction represents either a real intersection of channels or an imaginary junction introduced to provide more detail in the model, or to avoid numerical instability. The Newport Bay Estuary network was approximated by 33 channels (links) and 28 nodes. Correspondingly, the BLTM network (Figure 3.7) was characterized by 28 branches, 15 internal junctions and 8 external junctions. Note that each of the Branches 4, 12, 14, 17 and 24 represents two links corresponding to the link-node network. Lengths of the channel elements represented in the network range from approximately 1600 ft. to 6600 ft., with most channel lengths in the range between 2000 ft. to 3000 ft.

3.4.2 Hydrodynamics and Model Input

For hydrodynamics computation, nodes are characterized by surface area, depth, volume, and side slopes, and are interconnected by links, or elements. Elements are defined by width, length, depth, roughness, and cross sectional area. There is a one to one

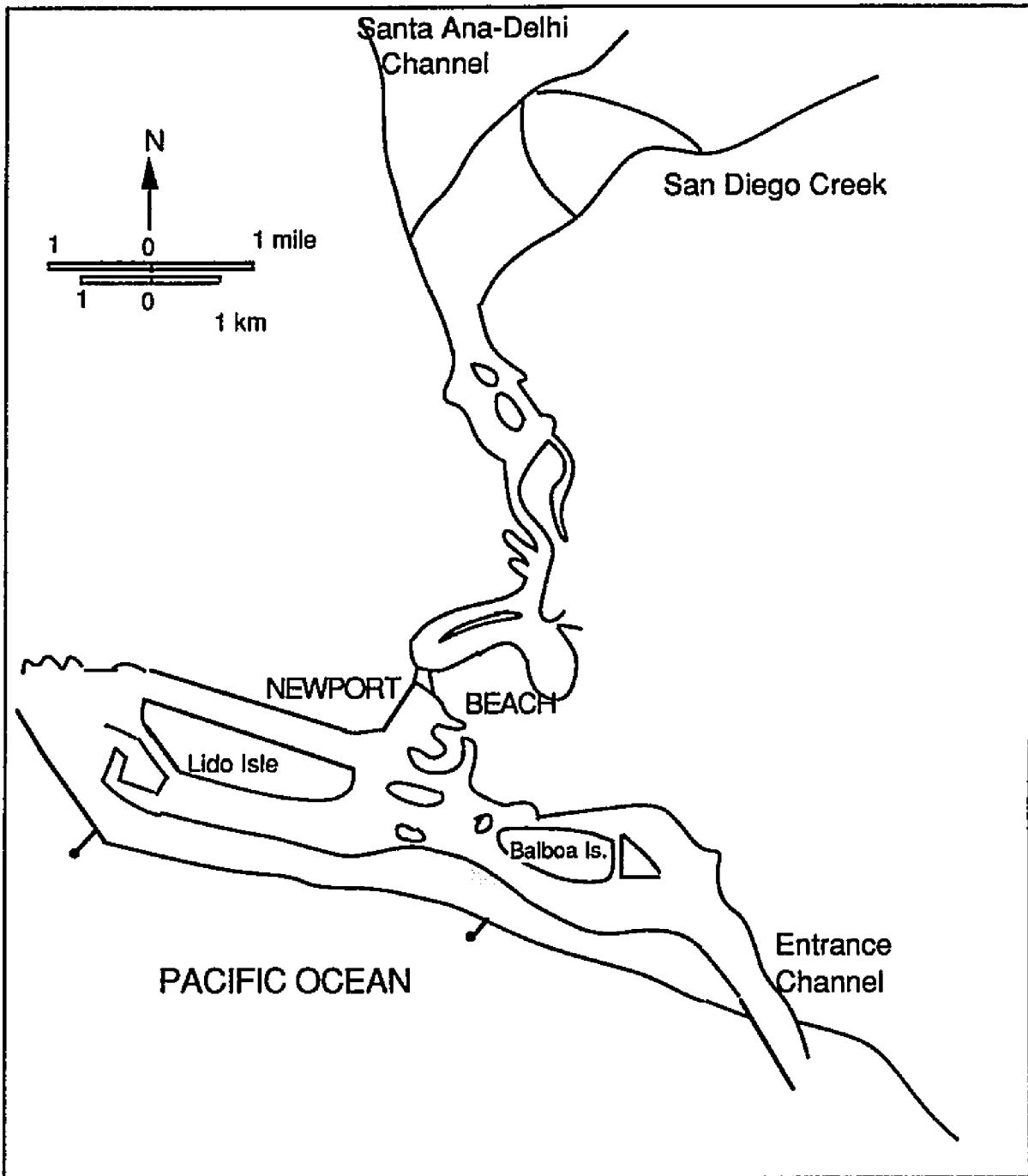


Figure 3.5 Newport Bay, California
(Adapted from Water Resources Engineers Inc., 1973)

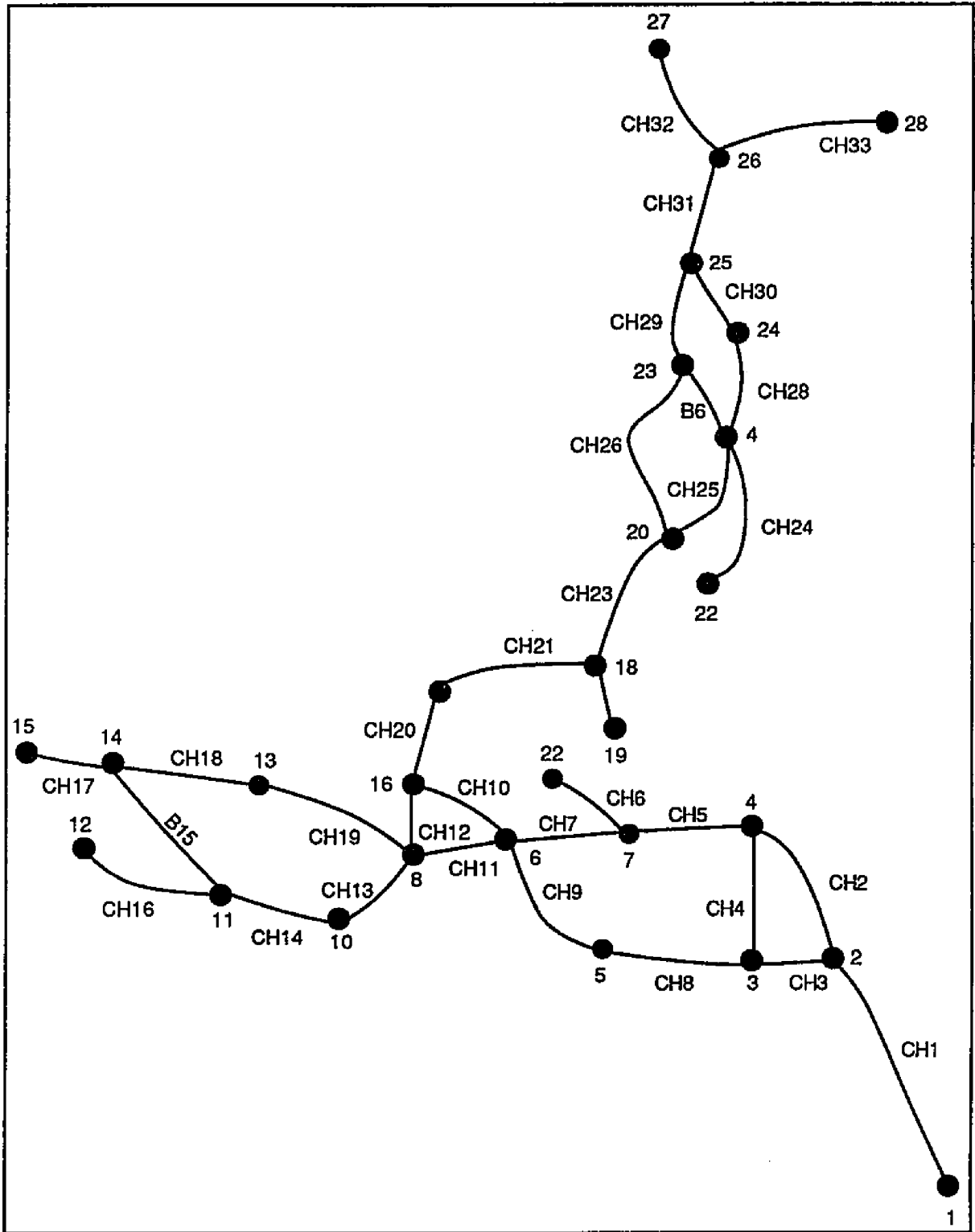


Figure 3.6 Link-Node Network, Newport Bay

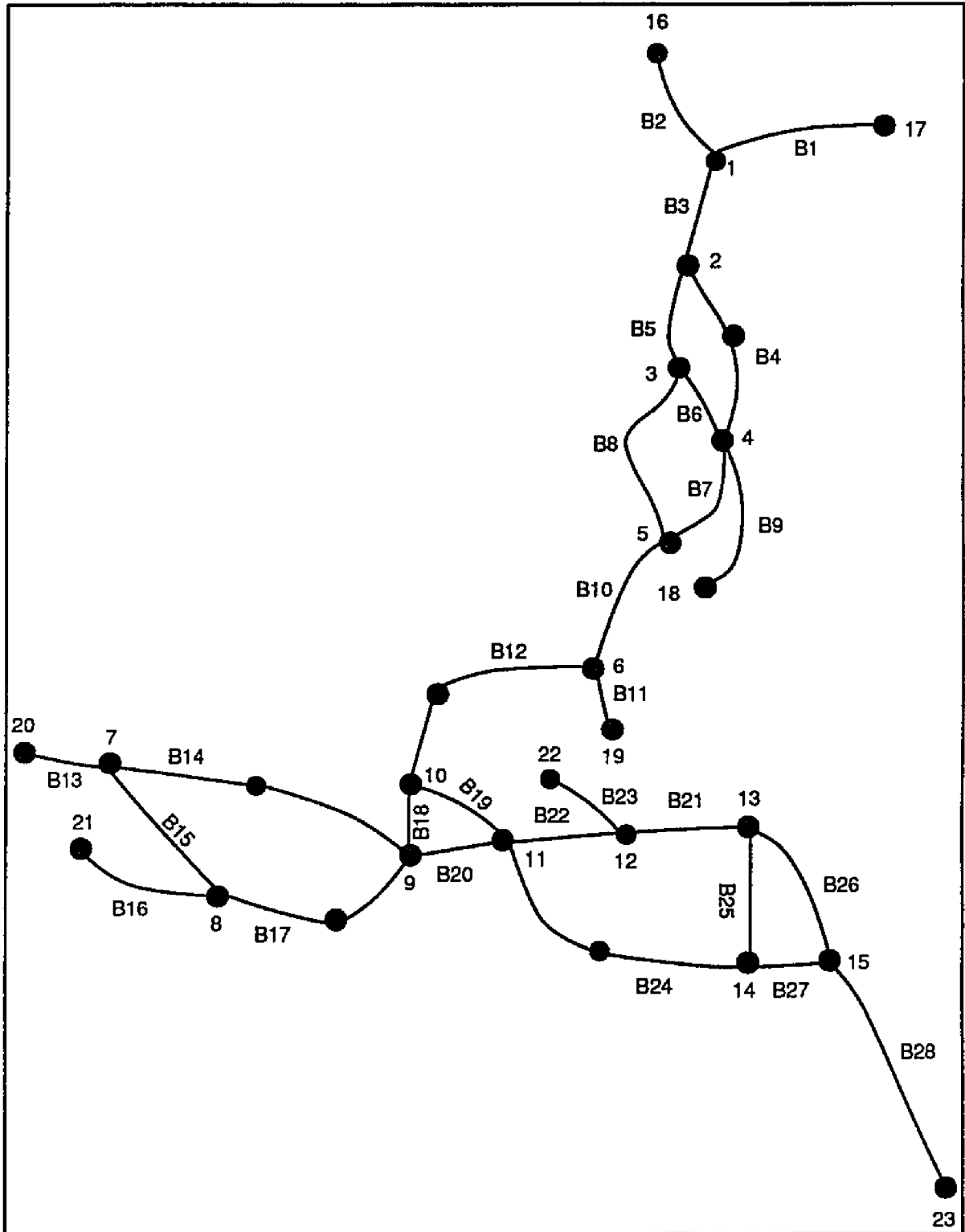


Figure 3.7 Branch-Junction Network, Newport Bay

correspondence between the Link-Node schematization used for hydrodynamics computation and the element-junction representation for quality computation for both BLTM and Link-Node water quality models. This scheme makes it possible for the same hydrodynamics information to be used easily in either water quality program.

The average total discharge for the two main tributaries into Upper Newport Bay, namely San Diego Creek and the Santa Ana Delhi Channel, was approximately 30 cfs on February 27, 1978. Using this flow as the freshwater input, and the available tide of March 1978 imposed at the seaward end (Figure 3.8), the Link-Node

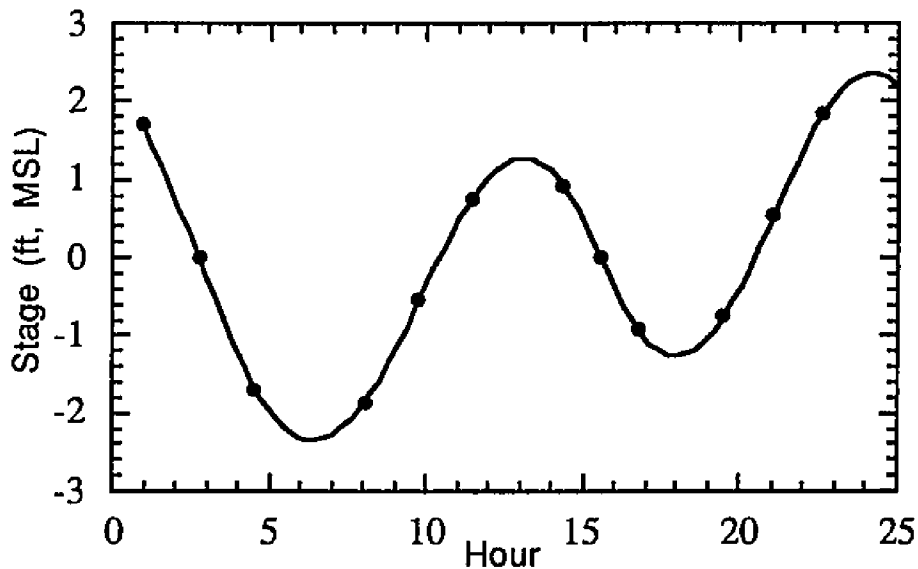


Figure 3.8 Tide at Newport Bay Boundary (March, 1978)

hydrodynamics program was run for five diurnal periods until a state of dynamic equilibrium was achieved. The output of the run consisted of temporal descriptions of flows, water surface elevations and channel velocities. All this information was stored in a file for subsequent use in the water quality programs. Before executing the hydrodynamic model, it was modified to create a flow file, containing the hydraulic information in a format required by the BLTM model. Initial and boundary concentrations were input to the water quality models and were run using information obtained from the hydrodynamics program. Time steps of 1 hour were used, as commonly assigned in Link-Node Water Quality Model applications.

3.4.3 Objectives

The tests reported here were performed to examine the ability of the BLTM model to replicate tidal dynamics of a small, but complex, estuarine system and to investigate the effects of dispersion in the performance of the model algorithm. A somewhat limited verification was achieved by comparison of model performance with field data reported in the literature. Results from these runs were also compared with those from the Link-Node water quality model with two objectives: (1) to test whether the model results follow a generally expected trend as shown by the Link-Node Model (because of its known capability in modeling estuarine water quality, as discussed in chapter 2), and (2) to evaluate the extent of numerical problems that are likely to be encountered using the Link-Node Water Quality Model because of its Eulerian formulation.

3.4.4 Model Application

As a first step, all water within the modeled channel system was arbitrarily assigned an initial concentration of zero, including water entering the system through the upstream boundaries. Water at the lower boundary near the entrance to the ocean was assigned a concentration of 34 parts per thousand (ppt). The specification of constant concentrations at the boundaries required that all of the fresh water ($c=0$) leaving the system would never enter again. In reality, however, water discharged from the channels to the ocean during ebb flow would mix with water outside the boundary of the physical system and a fraction of diluted discharge would certainly enter the system during the succeeding flood tides. Thus, the evaluation method would be expected to overestimate salt intrusion from the ocean in direct proportion to the fraction of channel water at a concentration of the previous ebb flow that enters again during flood flow. The results analyzed in this section correspond to the end of a period spanning eight tidal cycles (200 hours).

Initial Difficulty with Model Runs

Difficulties were experienced initially in making simulation runs with the BLTM. Investigation revealed that at periods when low flows occur, parcel sizes become very small (as expected). When this occurs, a special feature of the BLTM subdivides the time step (see Schoellhamer and Jobson, 1986B) to avoid numerical instability. Because of a large number of time step subdivisions, computation time for this system increased excessively, making the

run impractical. It was discovered that this behavior resulted because of an extremely small accuracy criterion (for deciding when to combine very small parcels) coded into the model. Apparently, this criterion was "hardwired" only in the earlier versions of the model (perhaps meant for very small channel network systems or for non-tidal flows). Once changes were made in the code to accommodate a more reasonable accuracy criteria, the number of time step subdivisions was reduced and the model performed satisfactorily.

In the later versions of the model (from USGS), this part of the code was already updated, although the problem it created was not identified. Currently, the user can select a criterion as input for the minimum flow of interest. This change is important since minimum flows of interest are certain to vary widely, depending upon the particular system modeled. There should not be a fixed criterion in the model.

3.4.5 Discussion of Simulation Results

The influence of dispersion factors on the salinity profile in Newport Bay is shown in Figure 3.9. Salinity plots are for runs using BLTM dispersion factors of 0.05, 0.20 and 0.45 for a parcel close to lower boundary. For low dispersion the model simulates advection dominated transport, which is why at the higher of the two low tide events the concentration level is very nearly the same as the boundary salinity. Computed concentrations corresponding to this scenario are virtually at zero level for the first seven hours of

ebb tide, then jump to 34 ppt as the flow reverses. For $D_f=0.20$ and 0.45 the influence of ebb flow is higher, as shown by lower concentration extremes. Salinity increases as the simulation continues over a number of tidal cycles because the effect of low initial concentrations (beginning at zero level) on computed results is slowly eliminated as tidal influences gradually dominate.

Figure 3.10 shows variations in salinity at the upstream end of Branch 26 over an 8-day period for values of D_f at 0.05, 0.20 and 0.45 (see Figure 3.7 for location). It is interesting to note that for $D_f=0.05$ salinity starts rising only after hour 13, whereas for higher values of D_f , it climbs up right after hour 11. Similarly, at low tides salinity returns to lower values for smaller D_f because of lower mixing at the tidal mouth. At high tides differences in salinity among runs with different D_f values are not as significant, although for such tides salinity tends to peak higher for lower dispersion factors.

Figure 3.11 shows similar plots for the upstream end of Branch 22 which is located approximately 2.5 miles upstream from the lower boundary at the estuary mouth. Salinity levels generally follow the trend shown previously for Branch 26, although at an overall lower level of concentrations because of its greater distance from the sea. The mean salinity at the end of eighth tidal cycle is approximately 18 ppt for simulation using a dispersion factor of 0.2. It is noted that the salinity fluctuation over a tidal cycle is highest for this location among the four locations examined, owing

to its location virtually equidistant from either boundary, in contrast to the others.

Salinity history of Branch 10 at its upstream end is shown in Figure 3.12. This junction is located at about 5.1 miles from the lower boundary. In general, the influence of D_f on salinity variation follows the pattern shown by concentration histories at the other locations. The gain in salinity level is slower because this branch is located closer to the upper (landward) boundary than to the seaward boundary, and thus is subject to more flushing from fresher water. At the end of the eighth tidal cycle the mean salt concentration reached about 10 ppt for the simulation based on D_f of 0.3. A plot comparing salinity history at three locations, one next to the lower boundary and the other two at the upstream ends of Branches 22 and 26, is presented in Figure 3.13 to provide an impression of the local salinity gradient. The D_f used was 0.2.

3.4.6 Investigation of Time Required to Reach Dynamic Equilibrium

The BLTM was run for a period of 32 tidal days to investigate its stability and computational efficiency, and to estimate the approximate time required to reach equilibrium concentrations for the conditions prescribed. This simulation required about 4.5 minutes of CPU time on a Sun SPARC-2 workstation running at 40MHZ. There was no indication of instability for the scenarios tested, an encouraging result since the test covered a wide range of dispersion factors.

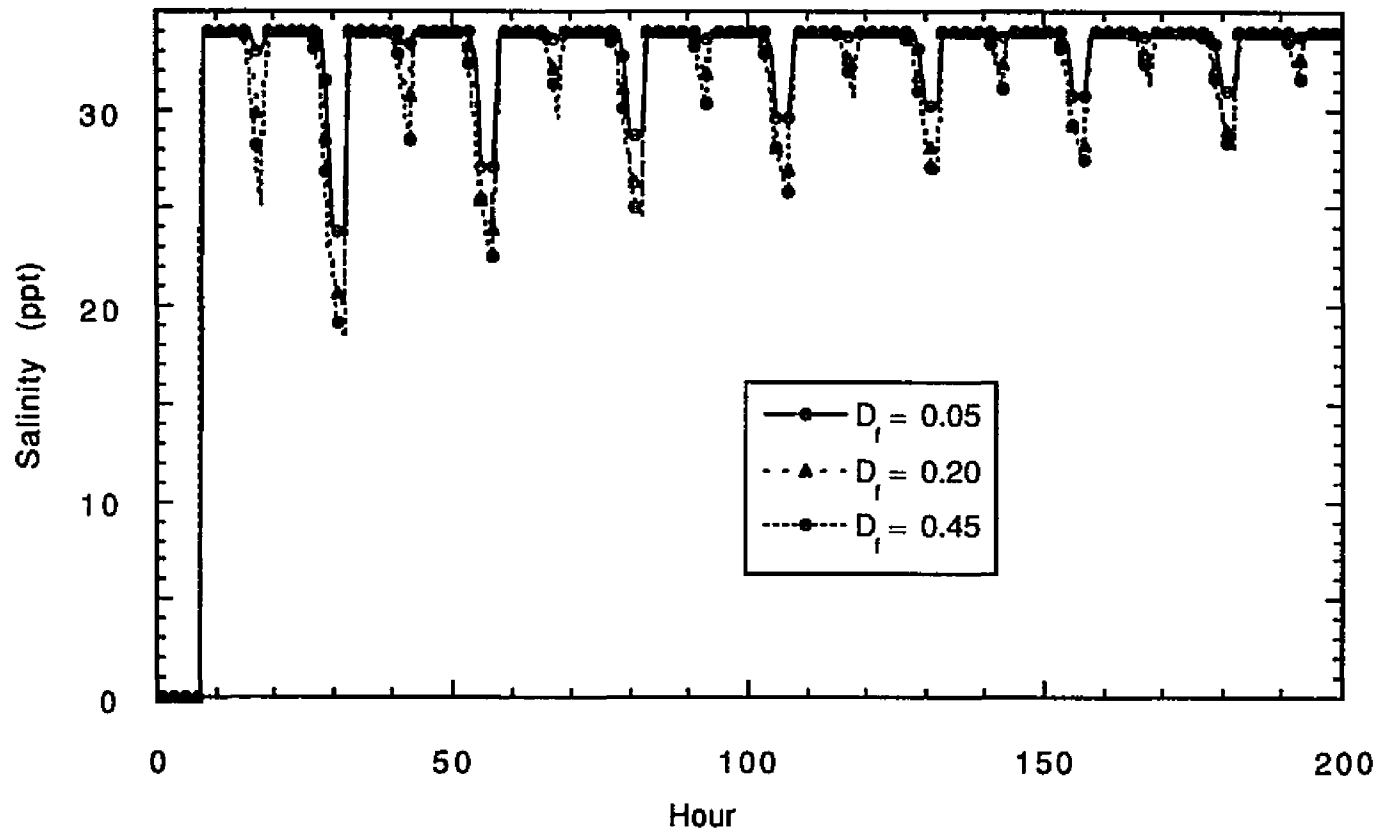


Figure 3.9 Computed Hourly Variation of Salinity at Branch 28 (near Lower Boundary)

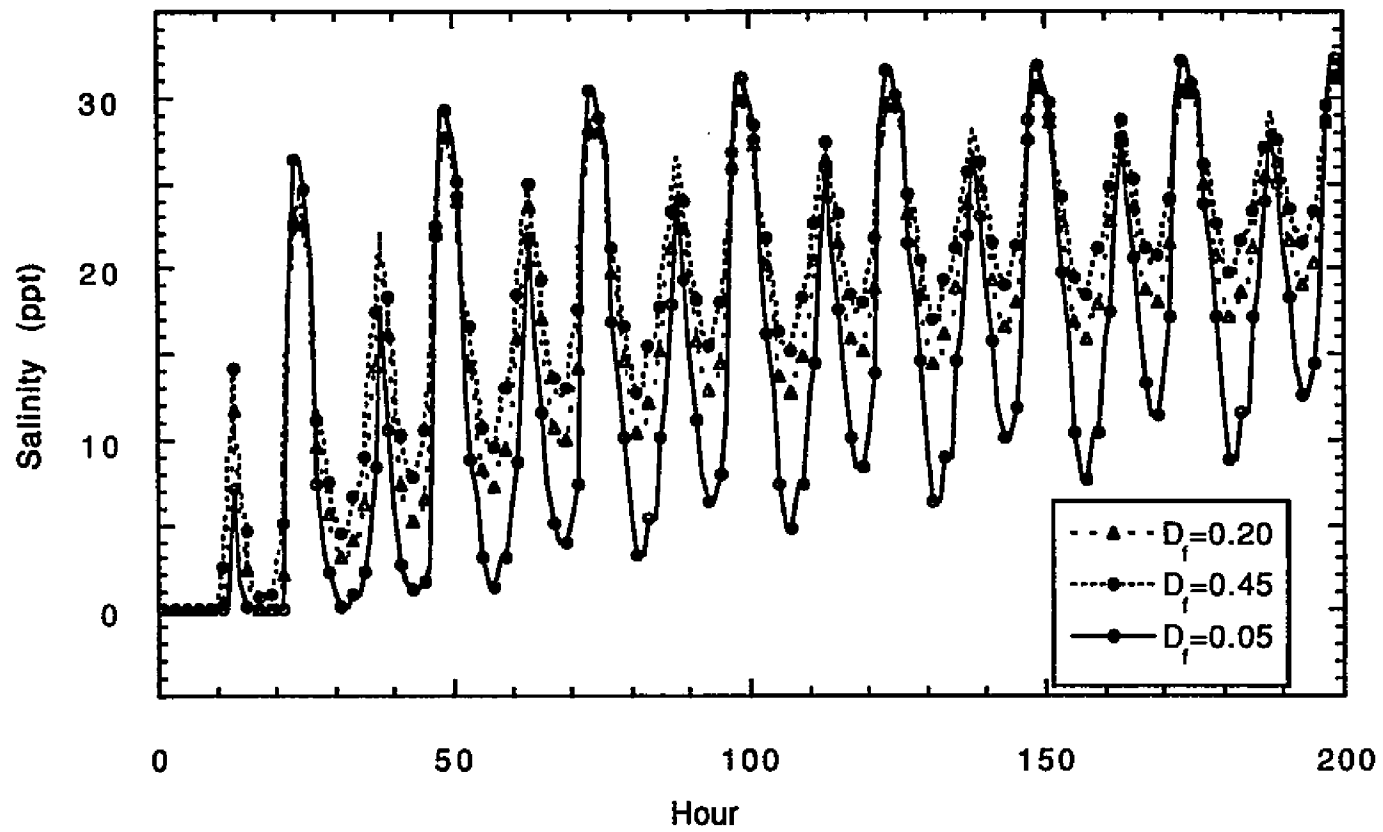


Figure 3.10 Computed Hourly Variation of Salinity at Branch 26

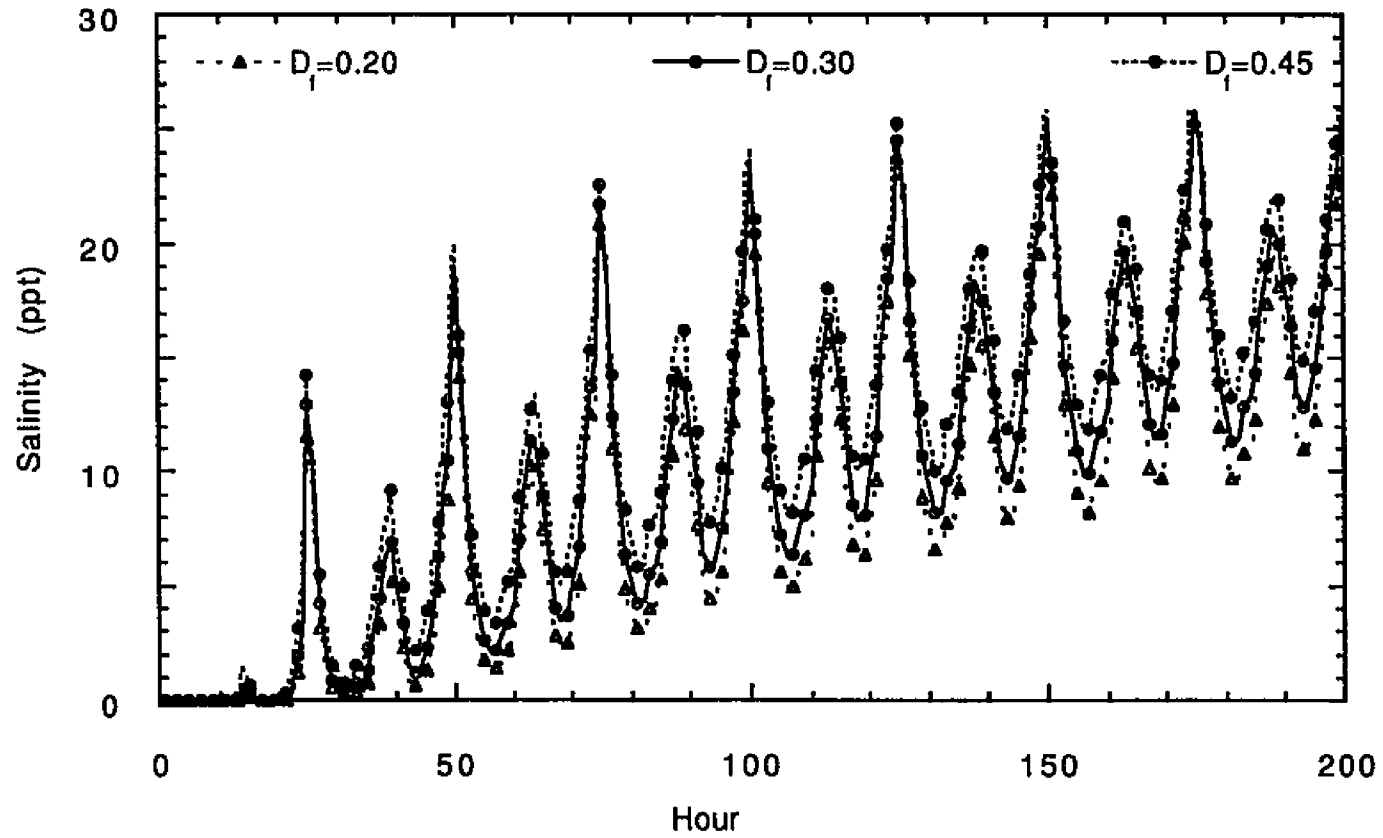


Figure 3.11 Computed Hourly Variation of Salinity at Branch 22

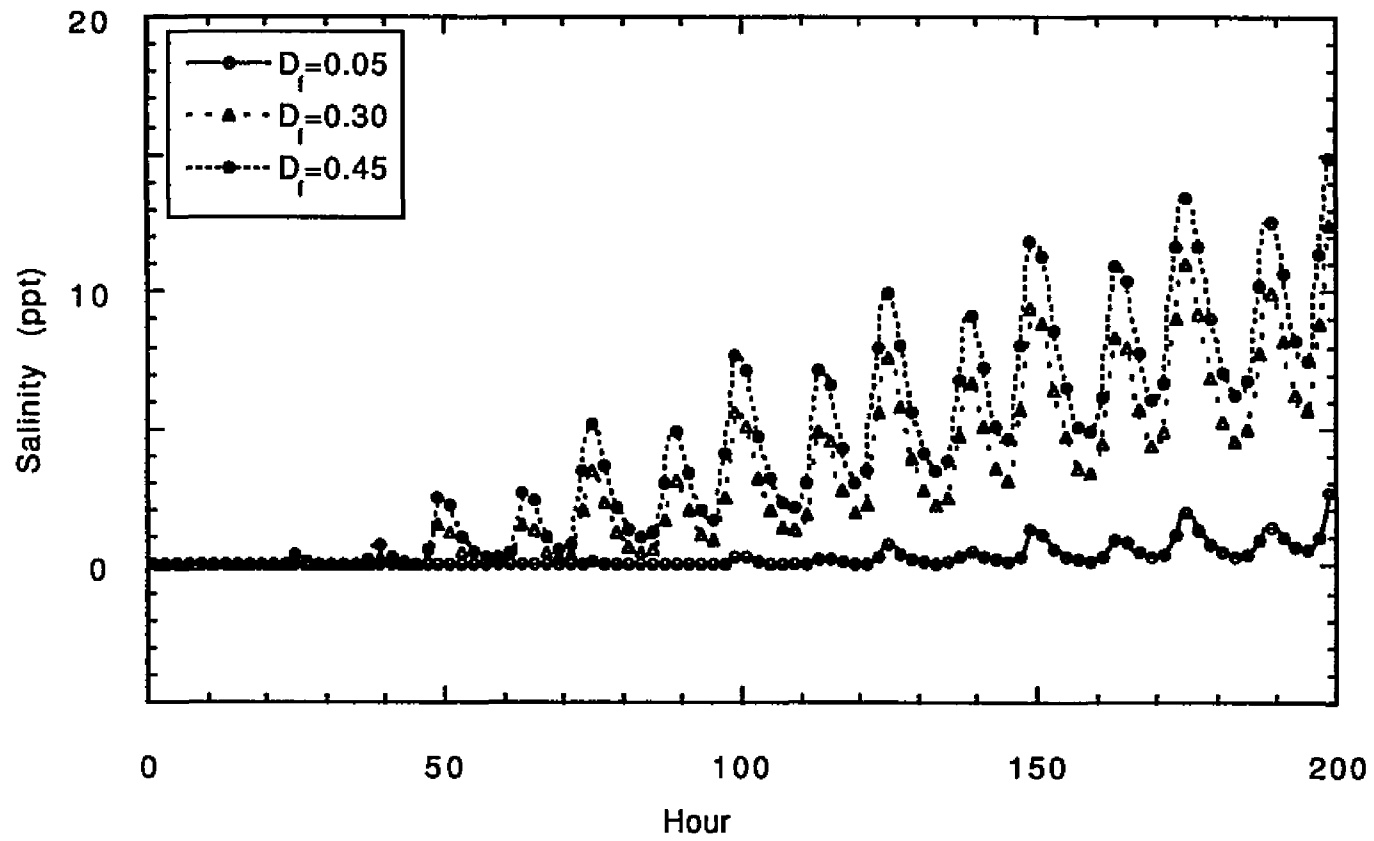


Figure 3.12 Computed Hourly Variation of Salinity at Branch 10

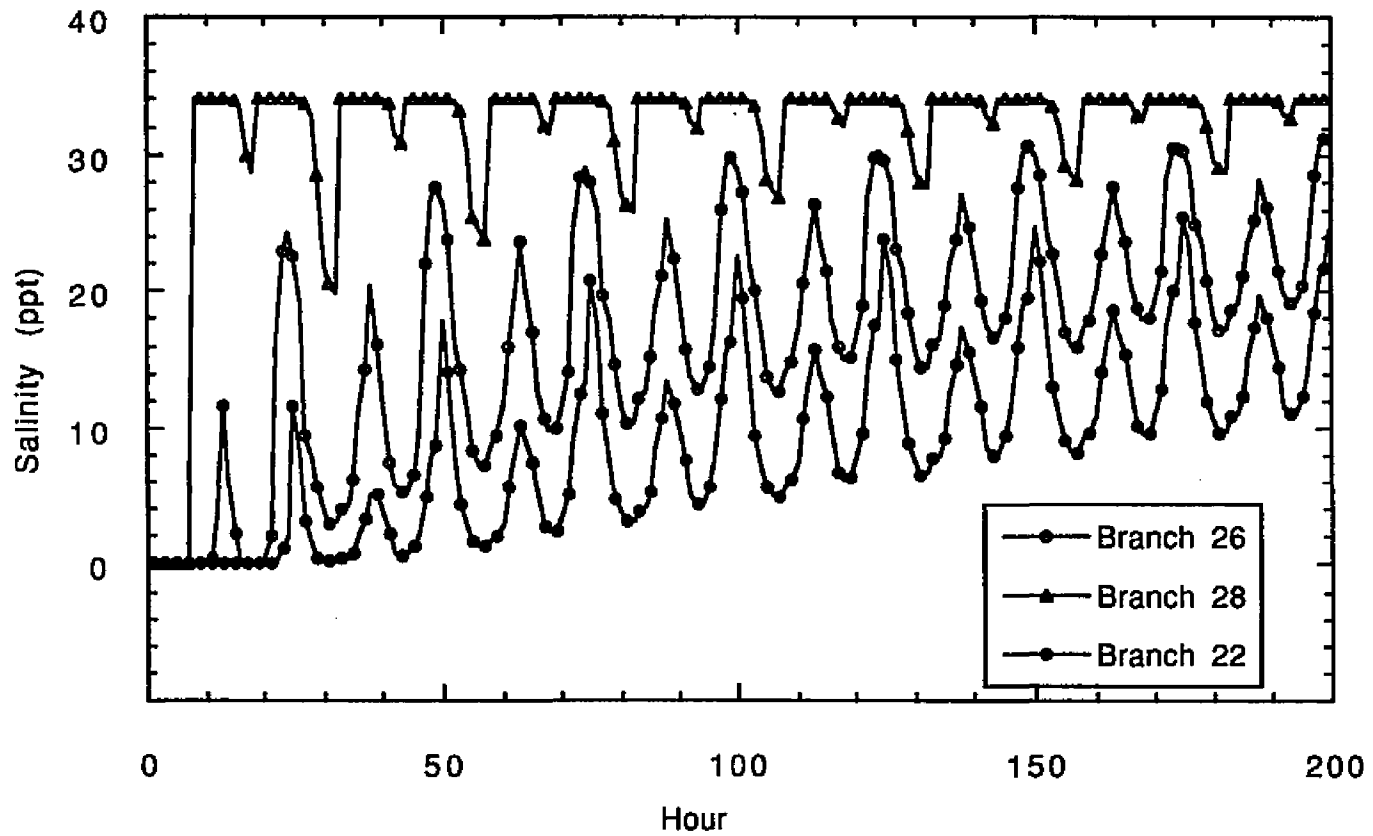


Figure 3.13 Computed Salinity at Three locations of Newport Bay Estuary ($D_f=0.2$) .

Figure 3.14 shows the history of salinity over the 32-day period near the mouth of the estuary. For the scenario that considered mainly advection ($D_f=0.05$), salinity seemed to nearly reach the equilibrium level (in the tidal average sense) at a concentration of 33 ppt at the end of 20 tidal days (500 hours). For $D_f=0.45$ salinity fluctuations over a tidal cycle are larger, with the result that a comparable level of steady state was only attained at the end of 32 days of simulation, converging to a somewhat lower mean of approximately 32.5 ppt. A similar plot shown for Branch 26 in Figure 3.15 indicates that it would take longer for concentrations at this location to reach an equilibrium state than for locations near or at the estuary mouth, as expected. Simulations using low dispersion showed slower convergence toward equilibrium at a mean of approximately 28 ppt after 32 days, as compared to 31 ppt for the case with $D_f=0.45$. This is attributed to the lesser domination of tidal influence in the case of low dispersion.

Figure 3.16 presents the history of salinity computed for Branch 22. For $D_f=0.05$, salinity reached a mean value of 23 ppt after 32 cycles, at which point the concentration was still rising. Figure 3.17 shows salinity over the 32-day period for Branch 10. For the scenario corresponding to the dispersion factor of 0.45, the salinity level (tidal mean) rose to 23 ppt after 32 tidal cycles, whereas in the case of advection dominant transport ($D_f=0.05$), it reached 14 ppt at the end of 32 tidal cycles. For these locations, salinity was still rising because they are closer to the upper boundaries through which fresh water inflows are conveyed.

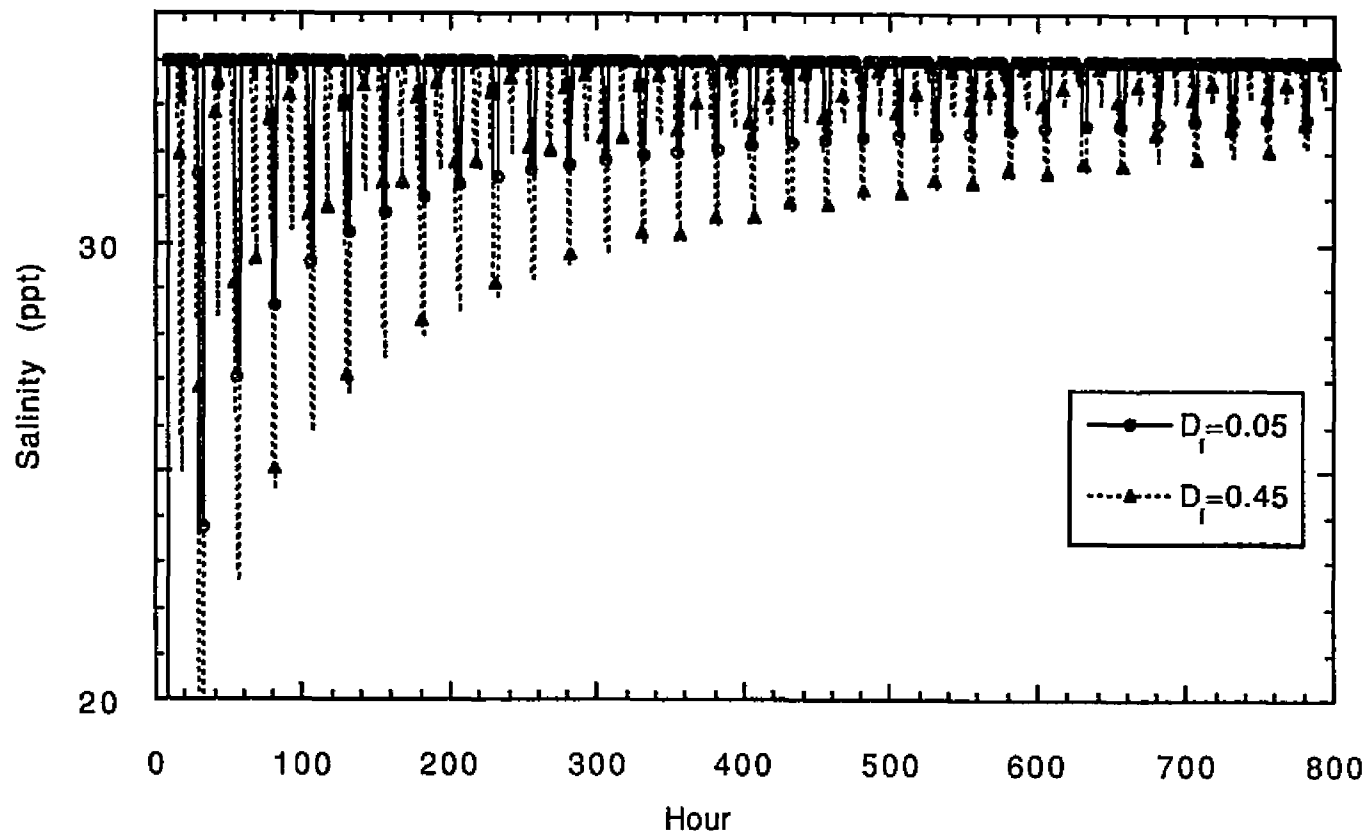


Figure 3.14 32-Day Salinity History (Computed) of Branch 28 (near Lower Boundary)

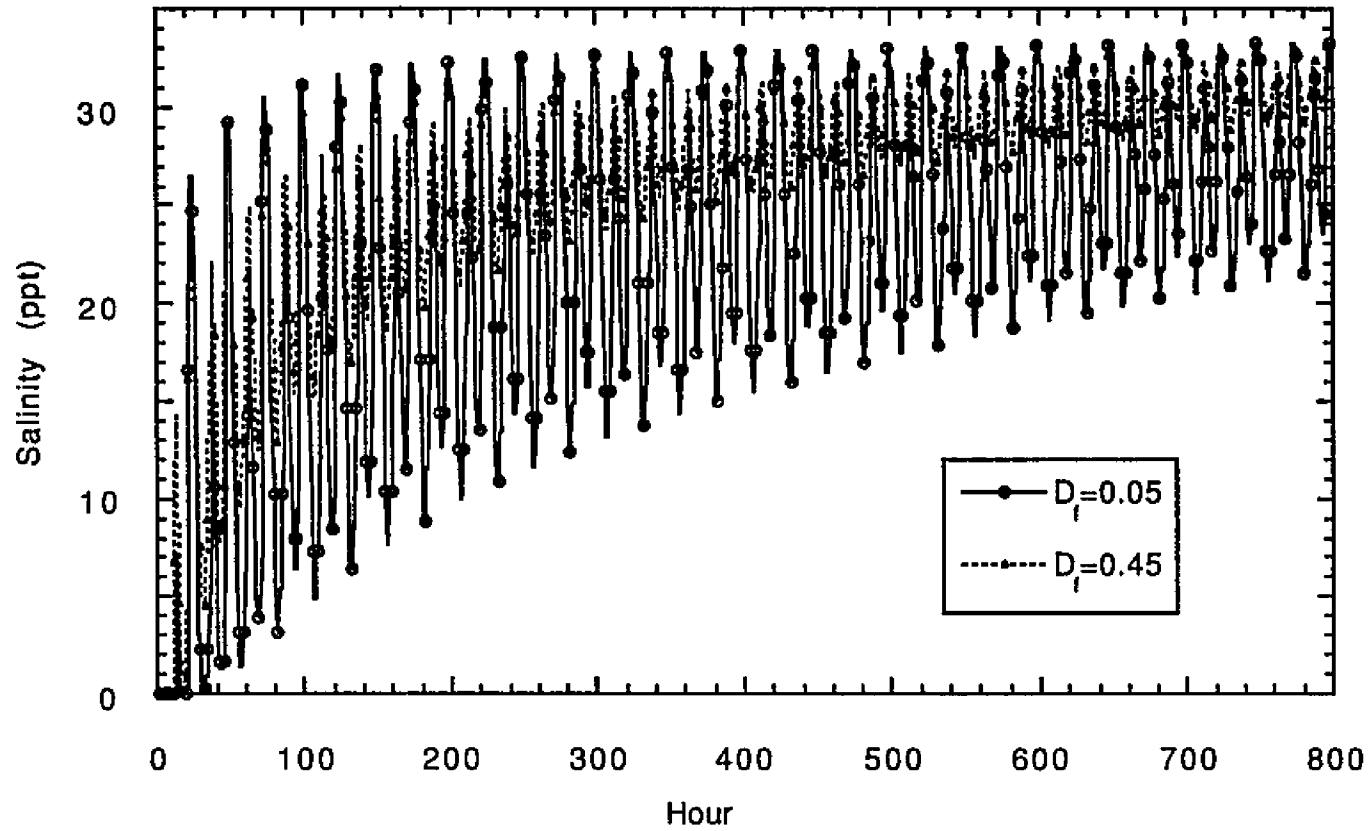


Figure 3.15 32-Day Salinity History (Computed) of Branch 26

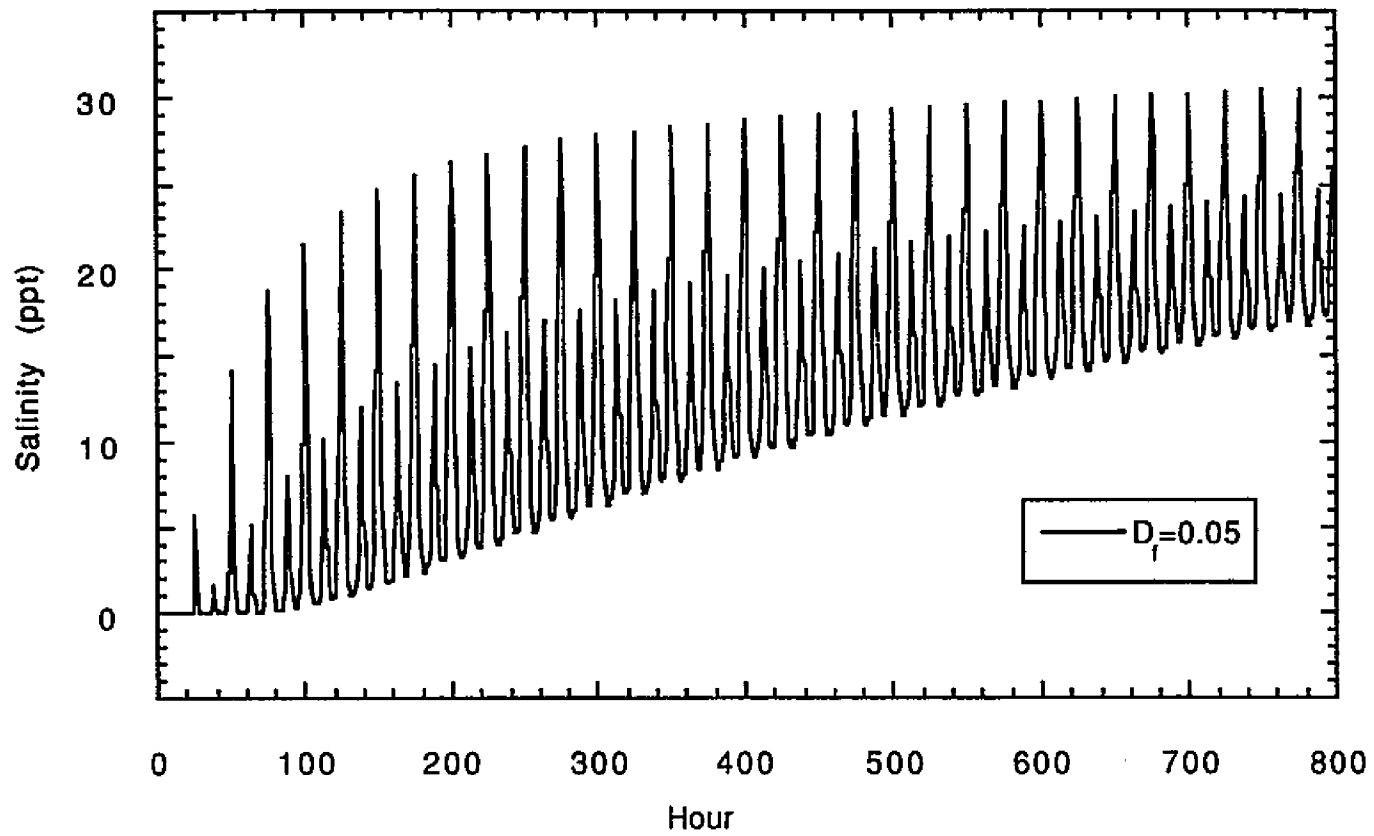


Figure 3.16 32-Day Salinity History (Computed) of Branch 22

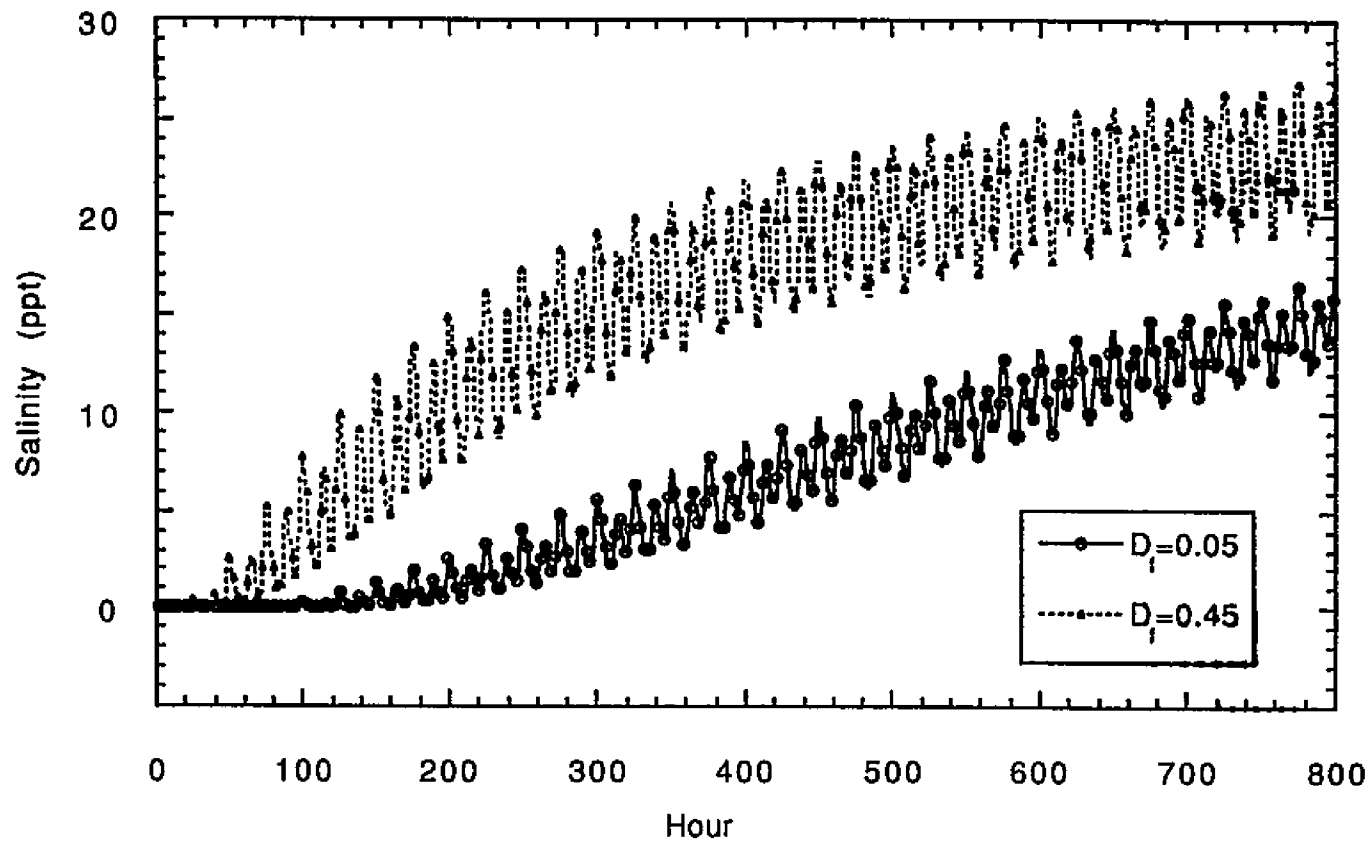


Figure 3.17 32-Day Salinity History (Computed) of Branch 10

3.4.7 Comparison with Field Data

The BLTM was run for a period of 32 days. The final results yield temporal descriptions of water quality parameters that characterize the system at various locations. Table 3.1 below compares the model results at locations B26, B22 and B10, also discussed earlier (see Figures 3.15 through 3.17), with the observed data in Newport Bay, available from the report "Sedimentation in Newport Bay" (Bishop et al., 1978). Locations selected for the model results are nearest to the stations reported below. The locations of the sampling stations at Newport Bay are provided in Figure IV-1 of the above report. Figures V-2 through V-5 of the report present observed salinity during the period from February 7 through 20 of 1978. The range shown for model results represents various dispersion factors used.

Table 3.1 Comparison of Field Data and Model Results

Salinity (parts per thousand)

Location	@ 8 day	@ 32 day	Field (Feb 20, 1978)
B26 (station 2)	25	28-31	27
B22 (station 9)	18	23-29	27
B10 (station 12)	10	14-23	18

Field data were chosen for February 20, the last day for which the observed data were available. Since an intense rainstorm occurred in the area in early February, lasting until February 15, it is expected that salinity would have been slightly higher on February 27, the date of observed freshwater input of 30 cfs that was used in the model, and thus would be a more reasonable base for comparison purposes.

Although the prototype data are so sparse that clear conclusions can not be made, it can be inferred from the above table that the model produced results that lie within a possible range actually observable in the field. It also shows that the model can replicate the variation in constituent concentrations induced by the tidal dynamics of the estuarine system. As noted in the report cited above, an analysis of field data showed that sea water salinity is the major water quality influence on lower Newport Bay when there is no rain, an observation confirmed by model results.

The use of zero initial conditions throughout the estuary and ocean salinity at the lower boundary also tested the model's capability to handle steep concentration gradients correctly. The successful model runs with very low dispersion factors demonstrated that the BLTM is able to model advection dominated transport of constituents. However, for modeling non-conservative constituents, it was determined from this investigation that new water quality routines should be developed for the purpose of the present study. This issue is explored in detail in the next chapter.

It is noted that the above exercise is not an attempt to calibrate the model for salinity; rather it was only for the purpose of examining the suitability of the model for application to a more complex estuary. Calibration of the new model, after integrating a modified version of BLTM with the new subroutines developed in this study for simulation of non-conservative constituents, will be described when the extended model is applied to the much more complex Sacramento-San Joaquin Delta System (see Chapter 5).

3.4.8 Comparison with the Link-Node Model Results (L-N)

The Link-Node Water Quality Model was also run using the identical hydraulic and salinity conditions used in BLTM simulations. Figure 3.18 shows salinity plots for a location near the estuary mouth over an 8 day period using both L-N and BLTM ($D_f=0.45$) results. It is noted that no dispersion coefficient is assigned for the Link-Node model. The Link-Node results compare better with the case with $D_f=0.45$ than with $D_f=0.05$ (see Figure 3.9), suggesting artificial dispersion-like effects are inherent in the model.

Figure 3.19 shows plots comparing BLTM results with Link-Node results at the upstream end of Branch 26. The Link-Node model results compared better with $D_f=0.45$, and they followed the trend shown by increasing dispersion factors. The L-N model seemed to indicate even higher mixing in the system than shown by the scenario corresponding to the dispersion factor of 0.45.

Another plot is shown in Figure 3.20 comparing L-N results with BLTM at the location near the upstream end of Branch 22. As

observed for the other locations, L-N results compared most favorably with those from the BLTM with a D_f of 0.45 (also see Figure 3.12). The mean salinity level was higher for the L-N results at the end of 8 tidal cycles for all four locations examined.

It should be noted that the numerical dispersion induced by the L-N model is dependent both on the degree of discretization of the channel system, i.e., the number of links (channels) and the time step used. With increased spatial detail numerical dispersion is retarded (as discussed in Section 3.1) while with shorter time intervals, i.e., more time steps per tidal cycle, it is enhanced. Therefore the comparisons with BLTM is specific to the L-N spatial and temporal scales selected.

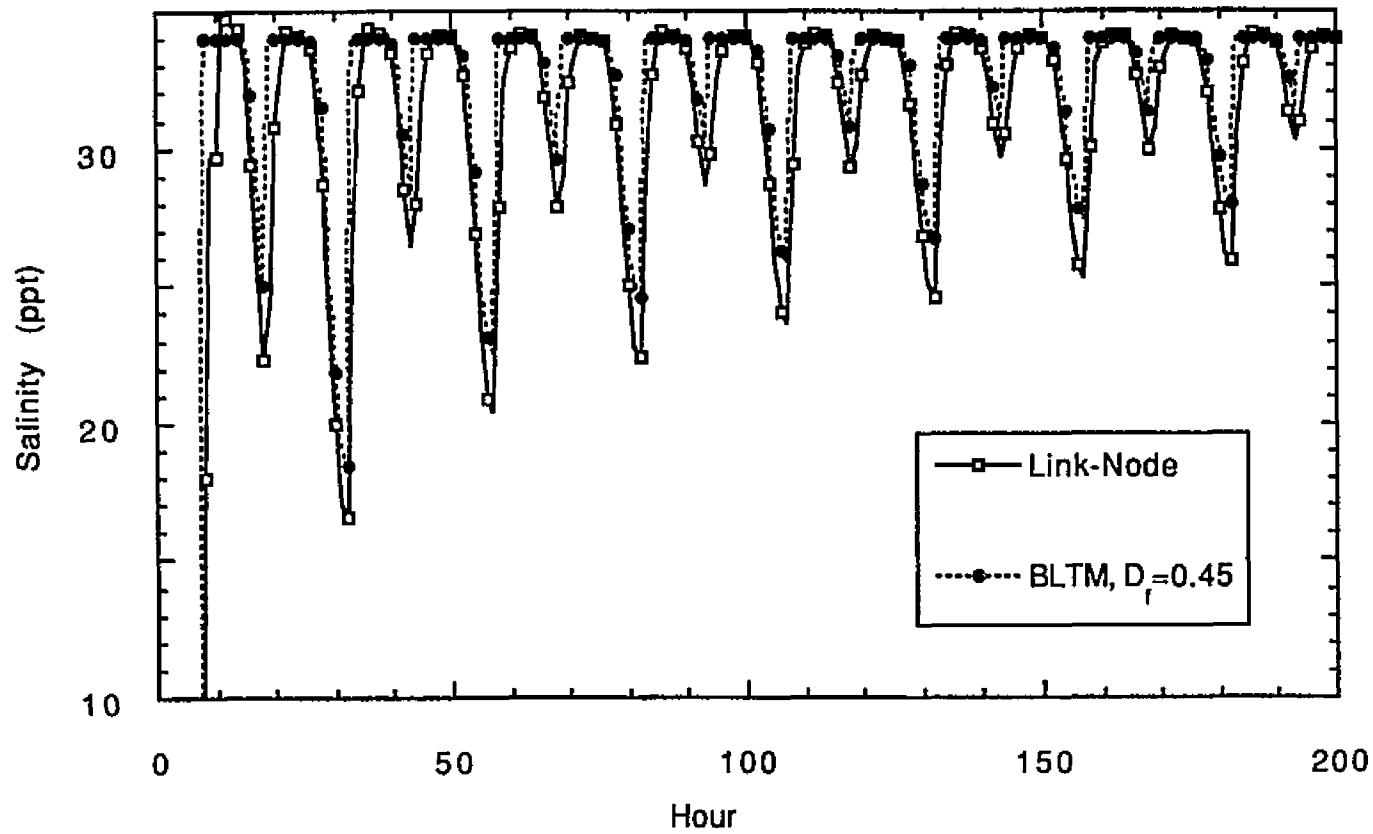


Figure 3.18 Salinity at Branch 28 (near Lower Boundary) using BLTM and Link-Node Models

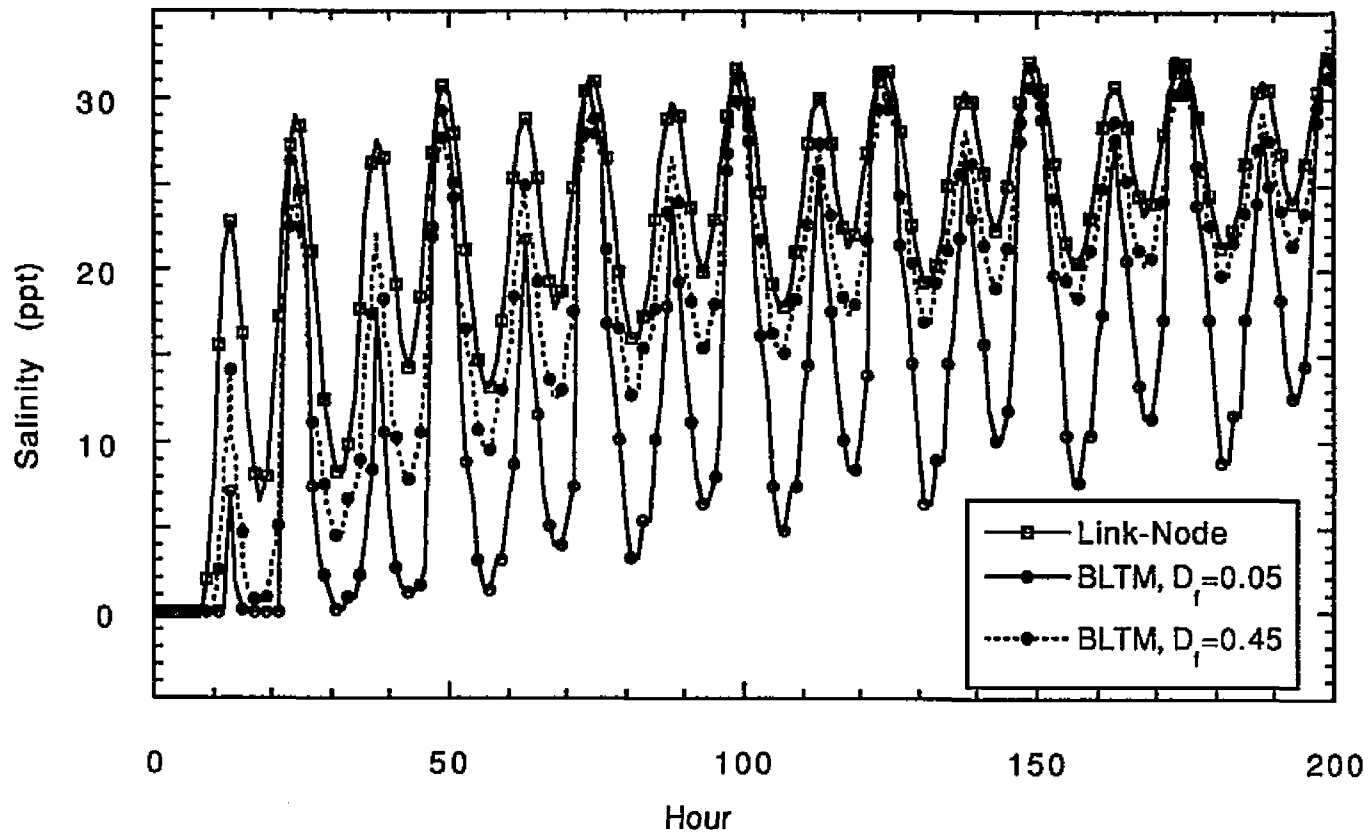


Figure 3.19 Salinity at Branch 26 using BLTM and Link-Node Models

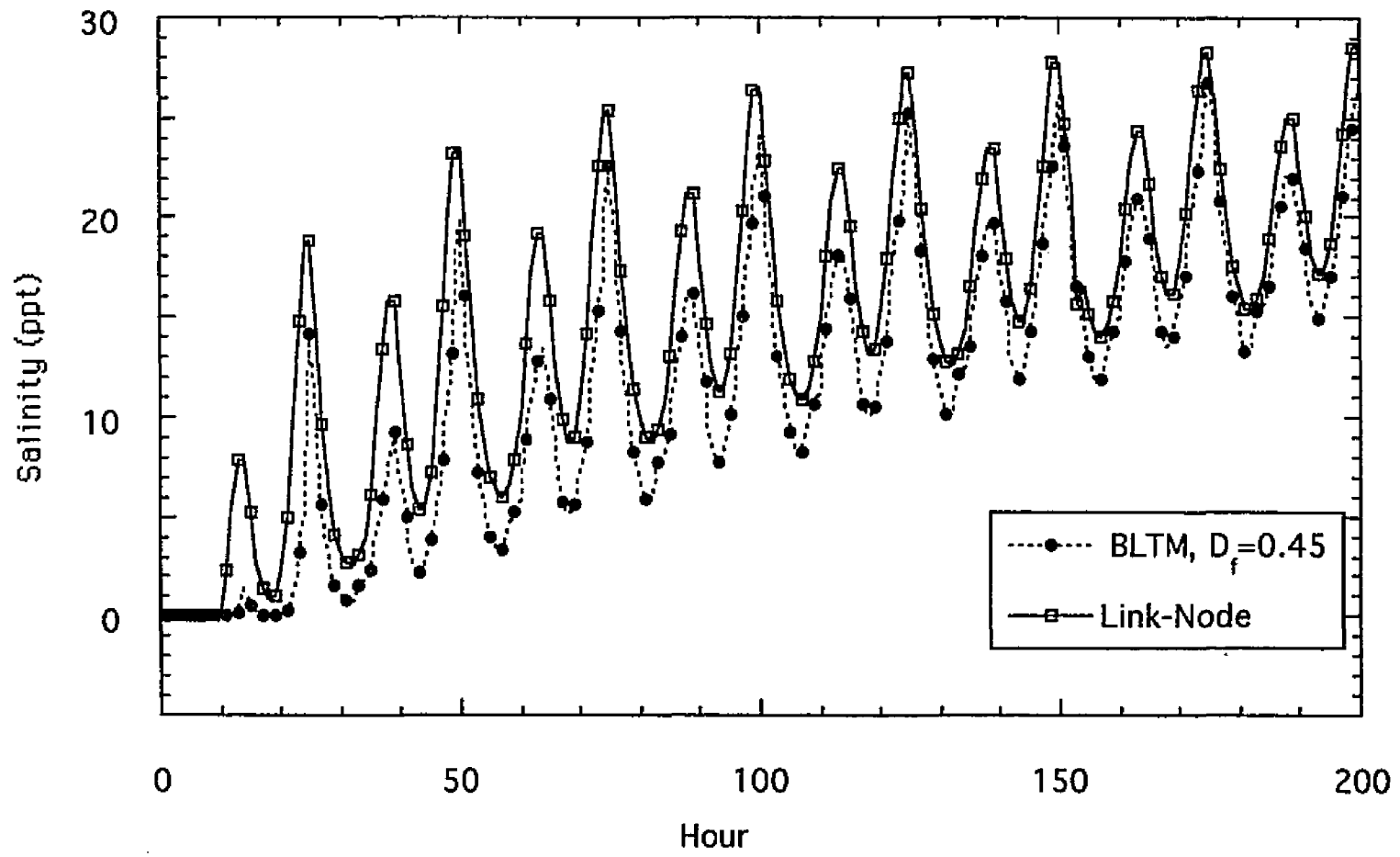


Figure 3.20 Salinity at Branch 22 using BLTM and Link-Node Models

4. MODEL DEVELOPMENT

4.1 Introduction

To describe the transport and fate of water quality variables in an estuary, it is necessary to include the important processes of advection, diffusion (dispersion) and kinetic interactions in the model. An outline of the steps involved in such an effort is presented in Figure 4.1.

Investigations discussed earlier showed that a Lagrangian approach is suitable in the present context, and that the transport modeling framework of the BLTM, described in Chapter 3, is an appropriate base for the development of this model. It is assumed that the system being modeled can be approximated spatially by a one-dimensional network of channel segments. Kinetic interactions among water quality variables represented in this model are based on relationships derived from the recent literature.

During the investigative phase of this research, and while conducting tests with the Newport Bay system described earlier, it was determined that major changes would be necessary in the existing subroutines, if one is to incorporate more comprehensive kinetic formulations in the model. In anticipation of modeling large and complex estuarine systems on a routine basis, it is highly desirable to have a computer program that is "transparent." That is, the program should be easy to understand and amenable to frequent extensions in the future, since modeling needs are likely to expand.

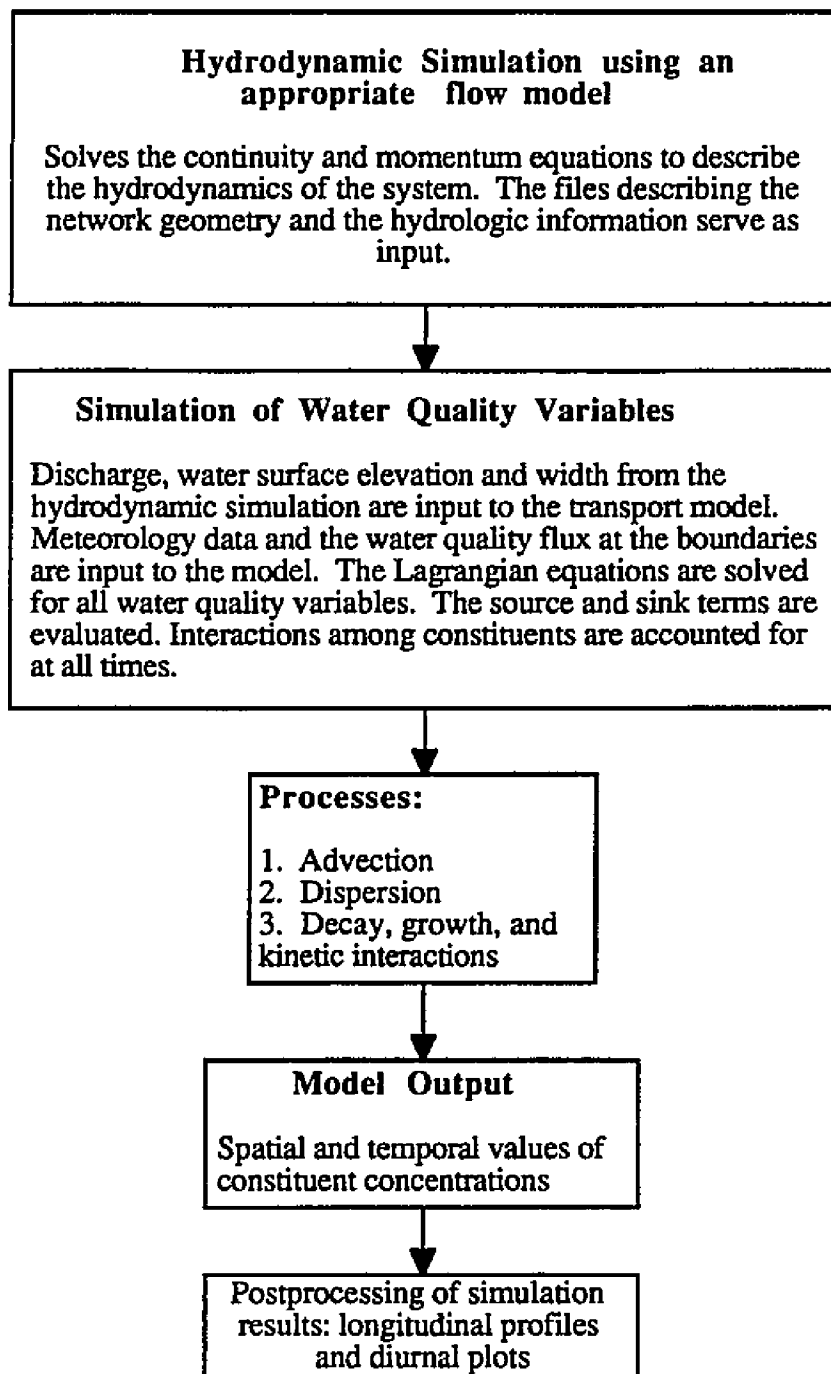


Figure 4.1 Flowchart for the Dynamic Simulation of Water Quality in an Aquatic System

Needs to debug the program will undoubtedly arise frequently as tests of new formulations under different combinations of physical circumstances are conducted, and as calibrations against the real systems are attempted.

Also, the existing kinetic coefficient routine (called FINK) in BLTM is tied to another subroutine (called DECAY) which calculates decay and interactions of the constituents (see Jobson and Schoellhamer, 1992). This routine needed modification too, for purposes of efficiency and improvement in the numerical algorithm, especially when simulating multiple constituents in a large estuary.

For these principal reasons, it was decided that for the purpose of this study the existing kinetics routines of BLTM should be removed, and a complete new set of water quality routines should be developed. The routines should include an algorithm that updates change in concentrations due to interactions among the constituents at each time step.

The development of a model cannot be considered complete until it is actually applied to a real system and model coefficients are calibrated against field data. The model should then be validated by applying it to the same system, but for a different set of boundary conditions. This important part of model development is achieved in the present instance by applying it to the complex estuarine system of the Sacramento-San Joaquin Delta in California. Features of the water quality model investigated and developed in this study are described in this chapter. A description of the Delta is included in Section 4.4.

4.2 Water Quality

Most water quality parameters can be broadly categorized as conservative or non-conservative. A conservative constituent is one that does not decay or change its state within the defined aquatic system. Its total mass within the system can only be changed due to advective and dispersive mass transport through the boundaries of the system. It is not affected by physical, chemical or biological changes in other constituents. Total dissolved solids or chlorides are typical examples of conservative variables in an aquatic system.

A non-conservative constituent, on the other hand, like dissolved oxygen may undergo a transformation of state, and its mass within the system may be changed by chemical, physical or biological processes. The rate of change of its concentration in water is usually a function of its concentration, environmental conditions, including temperature processes that increase or decrease mass, and concentrations of other constituents in the aquatic system that affect reactions. Reaction rates governing key processes that affect concentrations of a specific constituent are usually approximated by first order kinetics.

The distribution of water quality variables in space and time is computed by solving the following equation, in which non-conservative constituent relationships are considered to be governed by first order rates. Because the equation is considered in

a reference frame that moves with the mean velocity of water, the advection term i.e., $u \frac{\partial C}{\partial x}$ is implicitly included.

$$\frac{\partial C}{\partial t} = \frac{\partial}{\partial \xi} \left[E_x \frac{\partial C}{\partial \xi} \right] \pm k C + s \quad (4.1)$$

where

C = constituent concentration

E_x = longitudinal dispersion coefficient

k = first order rate constant

s = sources and sinks which are often functions of other constituent concentrations.

ξ = distance from the parcel, the Lagrangian distance coordinate.

$$\xi = x - x_0 - \int_{t_0}^t u \, d\tau \quad (4.2)$$

x_0 = location of the fluid parcel at time t_0 .

x = Eulerian distance coordinate

The newly developed water quality model has the capability to simulate eleven constituents which are:

1. Dissolved oxygen
2. Carbonaceous BOD
3. Phytoplankton
4. Organic nitrogen
5. Ammonia nitrogen

6. Nitrite nitrogen
7. Nitrate nitrogen
8. Organic phosphorus
9. Dissolved phosphorus
10. Arbitrary constituent
11. Temperature.

4.2.1 Formulation of Water Quality Equations

The interaction among the water quality parameters as represented in the new model is shown in Figure 4.2. For simplicity the processes of advection and diffusion, which are common to all the constituents are not shown in the figure. The conceptual and functional descriptions of constituent reactions represented in the new model are based generally on two of the most commonly used water quality models, QUAL2E (Brown and Barnwell, 1987) and WQRRS (Smith, 1978). Whenever necessary, relationships are derived directly from Bowie et al. (1985) or other related work, as noted.

Each reaction process, contributing in part to the total change, is represented mathematically according to kinetic principles (Chen and Orlob, 1975). A mass balance equation is written for each quality constituent and each parcel of water. A discussion of the important processes concerning water quality variables represented in the new model is provided in the next section.

Formulation for Oxygen Balance

Dissolved oxygen (DO) is the most widely used water quality parameter to indicate the general health of the aquatic ecosystem.

In an aquatic system, the sources of DO are:

- reaeration from the atmosphere
- photosynthesis during algal growth
- DO in incoming tributaries or effluents

Internal sinks of DO are:

- oxidation of carbonaceous organic matter
- oxidation of nitrogenous organic matter
- sediment oxygen demand
- oxygen use by aquatic plants

The mass (per unit volume) balance equation for dissolved oxygen is represented by:

$$\frac{\partial [O]}{\partial t} = \frac{\partial}{\partial \xi} \left[E_x \frac{\partial (O)}{\partial \xi} \right] - (k_1 + k_3) L + k_2 (O_s - [O]) - \alpha_5 k_n [NH_3]$$

Diffusion
CBOD
Reaeration
Ammonia oxidation

$$- \alpha_6 k_{ni} [NO_2] + \alpha_3 \mu [A] - \alpha_4 \rho [A] - K_4/d \quad (4.3)$$

Nitrite oxidation
Photosynthesis
Respiration
Benthic demand

See Appendix A for a definition of the variables. Similar equations of the form (eq. 4.3) are written for each state variable represented in the new model. They are presented in Appendix A.

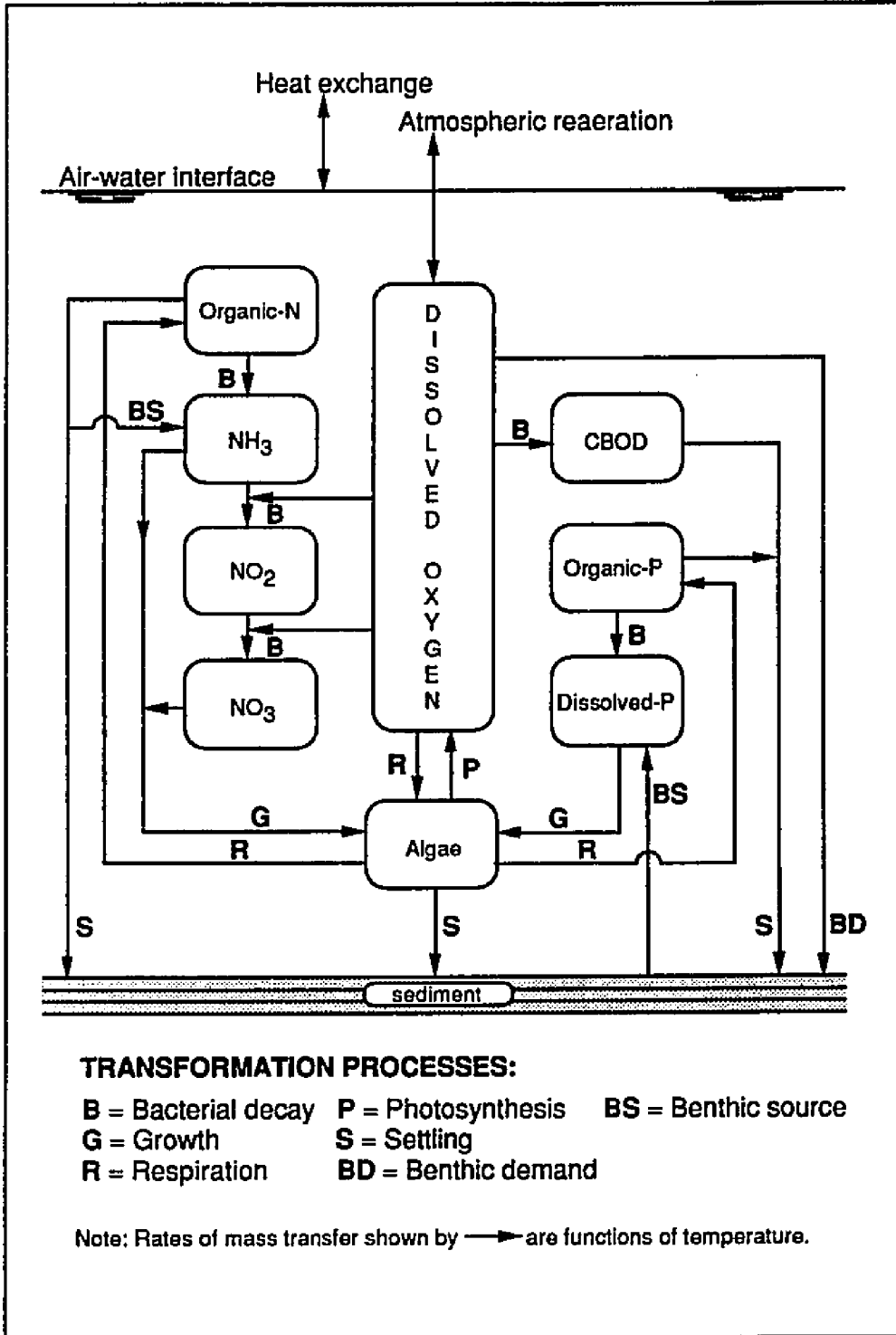


Figure 4.2 Interaction among Water Quality Constituents in the Model.

4.2.2 Water Quality Parameters and Related Processes

Dissolved Oxygen Saturation

The solubility of dissolved oxygen in water decreases with increasing temperature and salinity. Among about half a dozen or so expressions for DO saturation concentration as a function of temperature reported in the literature, the following algorithm recommended by American Public Health Association (APHA, 1985) and rated the best by Bowie et al. (1985), was adopted for the model:

$$\begin{aligned} \ln O_{sf} = & -139.34411 + (1.575701 \cdot 10^5)/T_k \\ & - (6.642308 \cdot 10^7)/T_k^2 + (1.243800 \cdot 10^{10})/T_k^3 \\ & - (8.621949 \cdot 10^{11})/T_k^4 \end{aligned} \quad (4.4)$$

where

$$\begin{aligned} O_{sf} &= \text{"freshwater" DO saturation concentration in} \\ &\quad \text{mg/l at 1 atm} \\ T_k &= \text{temperature in } ^\circ\text{K} \\ &= T (^{\circ}\text{C}) + 273.15 \end{aligned}$$

The effect of salinity on DO saturation is incorporated as shown below (APHA, 1985):

$$\ln O_{ss} = \ln O_{sf} - S [1.7674 \cdot 10^{-2} - (1.0754 \cdot 10^1)/T_k + (2.1407 \cdot 10^3)/T_k^2] \quad (4.5)$$

where

$$\begin{aligned} O_{ss} &= \text{"saline water" DO saturation concentration in} \\ &\quad \text{mg/l at 1 atm} \\ S &= \text{salinity in ppt} \end{aligned}$$

The effect of barometric pressure on DO saturation is to increase the saturation value and is expressed as:

$$O_s = O_{ss} P \left[\frac{[1 - (P_{wv}/P)](1 - \phi P)}{(1 - P_{wv})(1 - \phi)} \right] \quad (4.6)$$

where

O_s = DO saturation at pressure P, mg/l

P = nonstandard pressure in atm

P_{wv} = partial pressure of water vapor (atm)

calculated from:

$$\ln P_{wv} = 11.8571 - (3840.70/T_k) - (216961/T_k^2) \quad (4.7)$$

$$\phi = 0.000975 - (1.426 * 10^{-5} T_k) + (6.436 * 10^{-8} T_k^2) \quad (4.8)$$

T = temperature in °C = $T_k - 273.15$

Other terms are as defined previously.

Atmospheric Mass Transfer (Reaeration)

Reaeration, a process by which oxygen is exchanged between the atmosphere and a water body, is one of the main sources of oxygen in aquatic systems. The transfer rate of oxygen from air to water may be represented by:

$$\frac{d[O]}{dt} = k_2 (O_s - O) \quad (4.9)$$

where O_s and O are the oxygen concentrations at saturation and oxygen concentrations of the water body, respectively, and k_2 is the

reaeration coefficient. The oxygen transfer coefficient in natural waters depends on:

- temperature
- internal mixing and turbulence
- mixing due to wind
- waterfalls, dams, rapids
- surface active regents

(Thomann and Mueller, 1987 and Gromiec, 1989)

Numerous equations are available for predicting reaeration coefficients, giving a wide range of predicted values for specific hydraulic conditions (Rathbun, 1977). Reviews of predictive models for reaeration coefficient can be found in Bowie et al. (1985), Rathbun (1977) and Gromiec (1989). For purposes of illustration, a few of these models are discussed below.

O'Connor and Dobbins' (1956) equations were based on their analysis of reaeration mechanisms that considered the rate of surface renewal through internal turbulence. They recommended the following equation for the reaeration coefficient for moderately deep to deep channels (approximately between 1 ft to 30 ft. deep) and velocities between 0.5 ft/s and 1.6 ft/s:

$$k_2 (20^\circ\text{C}) = (D_m \bar{u})^{0.5} d^{-1.5} \quad (4.10)$$

where

$$D_m = \text{molecular diffusion coefficient} = 0.000081 \text{ ft}^2/\text{hour}$$

- \bar{u} = the mean velocity (ft/s)
- d = average stream depth (ft)

The above equation is often expressed as:

$$k_2 (20^\circ\text{C}) = 12.9 \bar{u}^{0.5} d^{-1.5} \quad (4.11)$$

Note that the units for k_2 have been transferred to per day.

O'Connor and Dobbins also developed a second formula for shallow streams, but O'Connor (1958) showed that the difference between the two formulas was insignificant, and proposed that the above formula should be generally used.

Churchill, Elmore and Buckingham (1962) investigated the reaeration mechanisms of several tributary streams in the upper Tennessee basin. They applied dimensional analysis and multiple regression techniques to analyze the data and derived nineteen expressions for the reaeration coefficient. Various combinations of the variables namely, mean velocity, mean depth, energy slope, resistance coefficient, fluid density, fluid viscosity, surface tension, molecular diffusion coefficient, and a vertical diffusion coefficient were examined in the study. The recommended equation was of the form:

$$k_2 (20^\circ\text{C}) = 11.6 \bar{u}^{0.969} d^{-1.673} \quad (4.12)$$

where

- K_2 = reaeration coefficient per day
- \bar{u} = the mean velocity (ft/s)
- d = average stream depth (ft)

Additional models of the reaeration coefficients were developed by several investigators using the data by Churchill et al. (1962). For example, Owens et al. (1964) combined their data with the data collected by Churchill et al. (1962) and Gameson et al. (1955) and using regression obtained the following equation:

$$k_2 (20^\circ\text{C}) = 23.3 \bar{u}^{0.73} d^{1.75} \quad (4.13)$$

Variables are as defined previously.

This formula is applicable for streams with depths of 0.4 to 11 ft. and velocities of 0.1 to 1.8 ft/s. (Bowie et al., 1985).

Another interesting study is by Langbein and Durum (1967) who, from their analysis of the field data of Churchill et al. (1962), data reported by O'Connor and Dobbins (1956), and the laboratory data of Streeter et al. (1936) and of Krenkel and Orlob (1962), obtained an equation of the form:

$$k_2 (20^\circ\text{C}) = 7.6 \bar{u} d^{-1.33} \quad (4.14)$$

Variables are as defined previously.

In summary, numerous equations are available for predicting the reaeration coefficients, and these equations give a wide range of predicted coefficients for a specific set of hydraulic conditions (Rathbun, 1977). It will be prudent to apply the predictive models for the reaeration coefficient in consistency with the conditions for which the models were derived. One should be aware that outside of the range of variables for which the model is developed,

significant errors may occur (Bowie et al., 1985). Since atmospheric reaeration is one of the main sources of oxygen in streams, the development of reliable methods for measuring and predicting the reaeration coefficient would contribute significantly to water quality modeling (Gromiec, 1989).

For tidal rivers and estuaries, one of the most widely applied models is the O'Connor-Dobbins equation (eq. 4.11) described above and has been adapted in the model.

The effect of temperature on the reaeration coefficient is represented by

$$k_2 (t^{\circ}\text{C}) = k_2 (20^{\circ}\text{C})(\phi)^{(t - 20)} \quad (4.15)$$

The numerical value of ϕ depends on the mixing conditions of the water body. Reported values range from 1.008 to 1.047 (Bowie et al., 1985). In practice a value of 1.024 is often used (Thomann and Mueller, 1987, Gromiec, 1989 etc.) and has been adopted for the present model.

Carbonaceous Biochemical Oxygen Demand (CBOD)

The dissolved oxygen content of a pure natural water body would tend towards saturation if it were not for processes that either produce or utilize oxygen. Among these the biochemical oxidation of dissolved or suspended organic matter is the most prominent. For the present study, carbonaceous biochemical oxygen demand (CBOD) is assumed to obey first order kinetics, implying that oxygen

uptake rate (BOD exertion) is only a function of the oxidizable organic matter remaining at any time.

Photosynthesis

Algae play an important role in the quality of natural water body. With the aid of solar energy, these microscopic plants (primary producers) assimilate nutrients and convert them to cell material. These organic materials are consumed by herbivorous animals such as zooplankton (secondary producers) which, in turn, are consumed by carnivores animals such as fish. The phytoplankton, thus, are the base of the food chain in natural waters.

Very large population of phytoplankton can have adverse effects in natural waters. For example, it may cause large diurnal variations in dissolved oxygen which can be fatal to fish.

The available information on phytoplankton is not sufficiently detailed to specify the growth kinetics for individual algal species in a natural environment (Ambrose et al., 1988). So, as in most modeling efforts, phytoplankton population will be characterized as a whole by a measurement of the phytoplankton biomass present rather than considering the problem of different species and their associated environmental and nutrient requirements. Chlorophyll-a is a parameter characteristic of all phytoplankton and hence is used to describe the ensemble phytoplankton population. It is directly proportional to the concentration of phytoplanktonic algal biomass. As in most conventional water quality models (for example, see Bowie et al., 1985) the nutrient compositions of the cells and the

resulting stoichiometric ratios are assumed constant. The following expression is used in the present formulation to convert algal biomass to chlorophyll-a.

$$\text{Chl-a} = \alpha_7[\text{A}] \quad (4.16)$$

where

α_7 = a conversion factor, $\mu\text{g Chl-a/mg [A]}$

chl-a = chlorophyll-a concentration, $\mu\text{g l}^{-1}$

Phytoplankton increase by growth and decrease by respiration and settling. The rate of growth is determined using an appropriate factor for light intensity and the limiting nutrient concept (either nitrogen or phosphorus). See equation A.4 in Appendix A. Although, in principle, a complete growth function should include carbon and silicon as well, these variables are not included in this model, because diatoms are not simulated as a separate algal group for reasons explained above and carbon is usually available in excess relative to nitrogen and phosphorus. Equations A.4 through A.8 (Appendix A) present processes related to algae.

Chemical Oxidation: Nitrogen Series

Nitrogenous compounds affect the quality of the natural body of water principally in two ways: oxidation of various forms of nitrogen by bacteria and the associated uptake of oxygen; and assimilation of the inorganic nitrogen by phytoplankton during growth and the release of organic nitrogen by phytoplankton during respiration. Depending upon the circumstances, either one of these conditions may dominate. For example the first process will

dominate in areas that receive waste water with little or partial treatment, whereas in the aquatic systems that receive mostly biologically treated effluents or agricultural drainage, the second process will dominate (O'Connor et al., 1973). Equations A.9 through A.13 (Appendix A) present the processes of nitrogen cycle represented in the model.

Phosphorus Transformation

Organic forms of phosphorus are generated by the death of algae. These get transformed to the dissolved inorganic state, where it is available to algae for primary production. In the model the processes governing phosphorus cycle are represented by equations A.14 and A.15 (Appendix A).

Benthic (sediment) Oxygen Demand

Oxygen demand by benthic sediments and organisms can represent a large fraction of oxygen consumption in surface waters (Bowie et al., 1985). Particulate organic sediment in waste water and dead vegetal matter that settle to the bottoms of channels contribute to this demand. In addition to the demand caused by decay of organic matter, resident invertebrates can generate significant oxygen demand through respiration. The process of exertion in oxygen demand is usually called sediment oxygen demand (SOD) apparently because it is typically measured by enclosing the sediments in a chamber. The change in dissolved oxygen mass inside the sediment is measured at regular intervals of time either in the laboratory or

in situ. The resulting SOD is measured as oxygen consumed per unit area and time ($\text{g/m}^2\text{-day}$).

Temperature

Water temperature has an important role in the overall balance of an aquatic ecosystem. From the water quality perspective temperature affects the quality of an aquatic system by either accelerating or retarding the processes of biological and chemical interactions among other important water quality variables. The effect of temperature on the reaction rate is represented by

$$k_t = k_{20} \phi^{(t-20)} \quad (4.17)$$

Rate at t °C Rate at 20 °C

The numerical value of temperature coefficient (ϕ) depends on the conditions of the system being modeled. Reported values in QUAL2E range from 1.02 to 1.083 and are listed in Table A.1 in Appendix A. In the present model, temperature coefficients are specified by the user. The formulation of temperature and the components of heat budget that describe the net energy flux (Q_n) across the air-water surface are presented in Appendix A.

4.3 Numerical Scheme for Updating Kinetic Interactions

In developing an appropriate numerical scheme to update concentrations due to decay, growth and biochemical transformations, criteria such as numerical characteristics of the transport scheme as well as simplicity of the proposed scheme were considered.

Lagrangian box models are most accurate when time steps are small enough to adequately define the important time variations of flow and concentration. Advantage can be taken of such small time steps by employing a Modified Euler method to update concentrations due to kinetic interactions. It is one of the most cost effective methods and achieves sufficient accuracy when time steps are relatively small, provided that there are no rapid changes in concentrations within the time step. The appropriate time steps for the BLTM are usually on the order of 15 minutes, or so, when applied to tidally driven systems such as that of the Sacramento-San Joaquin Delta. For example, if the dispersion coefficients are assumed to be in the range of 100-400 ft²/s*, and a representative velocity is about 1 ft/s, then application of eq. (3.6) gives time steps in the range of approximately 4 minutes to one hour. This corresponds to dispersion factors in 0.1-0.4 range, as suggested by Jobson and Schoellhamer (1986B) for greatest model stability.

In applying the water quality model, physical changes resulting from advection, diffusion and volume changes due to tributaries or agricultural drainage are first computed. These operations are executed in the BLTM routines (see Jobson and Schoellhamer, 1992). Following this operation, concentration updating will be done for growth and decay of each constituent for each parcel passing through a channel or an open water area. This updating will be done at least once in every time step, and more often, if the parcel in

* Fischer et al. (1979) gives a dispersion coefficient of 161 ft²/s for Sacramento River.

question has passed a grid point¹ before the entire duration of the current time step is accounted for. In the latter case, the reaction time step will be the time remaining to be accounted for, which will be less than the model time step. Therefore, time steps are usually small, and the choice of the proposed numerical scheme for rate updating is appropriate. The use of higher order Runge-Kutta schemes (such as those of the fourth order), which require more evaluations of f (see eq. 4.20) per time step directly increasing cost, is not necessary.

Since changes in concentration of any constituent affect the other constituents, either directly or indirectly, tests are included to check whether corrections are necessary in constituent concentrations. The flowchart presented in Figure 4.4, showing the sequence of these tests, will be explained later in this section.

A typical kinetic equation of first order

$$\frac{dC}{dt} = -kC \pm s \quad (4.18)$$

can be represented in discrete form by

$$C^* = C^n + f^n (\Delta t_r) \quad (4.19)$$

where

$$f = -kC \pm s \quad (4.20)$$

$$C^* = \text{Euler estimate of } C \text{ at time } = n+1$$

¹ grid refers to the Eulerian grid in the network of channels where flow and geometry information are stored.

(Δt_r) = reaction time step

See Figure 4.3 for an illustration of this scheme. Note that the rates of change in concentration are exaggerated for the purpose of illustration only. Typically rates are less than 0.05 per hour.

Equation (4.20) written for each constituent represents a source/sink matrix at time, n . For each constituent, f^n is computed by calling the subroutine CALSCSK where source/sink matrices of every constituent are formed (Figure 4.4). Next, using updated concentrations from equation (4.19), CALSCSK is called again, and the source/sink matrices are updated (f^*). The updated source/sink matrices are now used to get a better estimate of C^{n+1} as shown below.

$$C^{n+1} = C^n + 0.5 (f^n + f^*) \Delta t_r \quad (4.21)$$

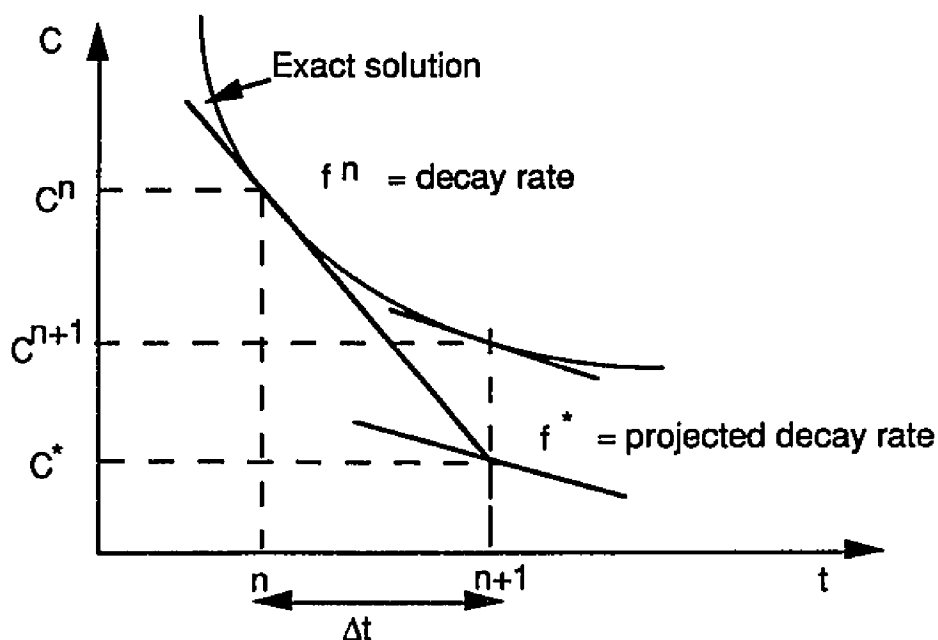


Figure 4.3 Numerical Scheme used in the Subroutine KINETICS

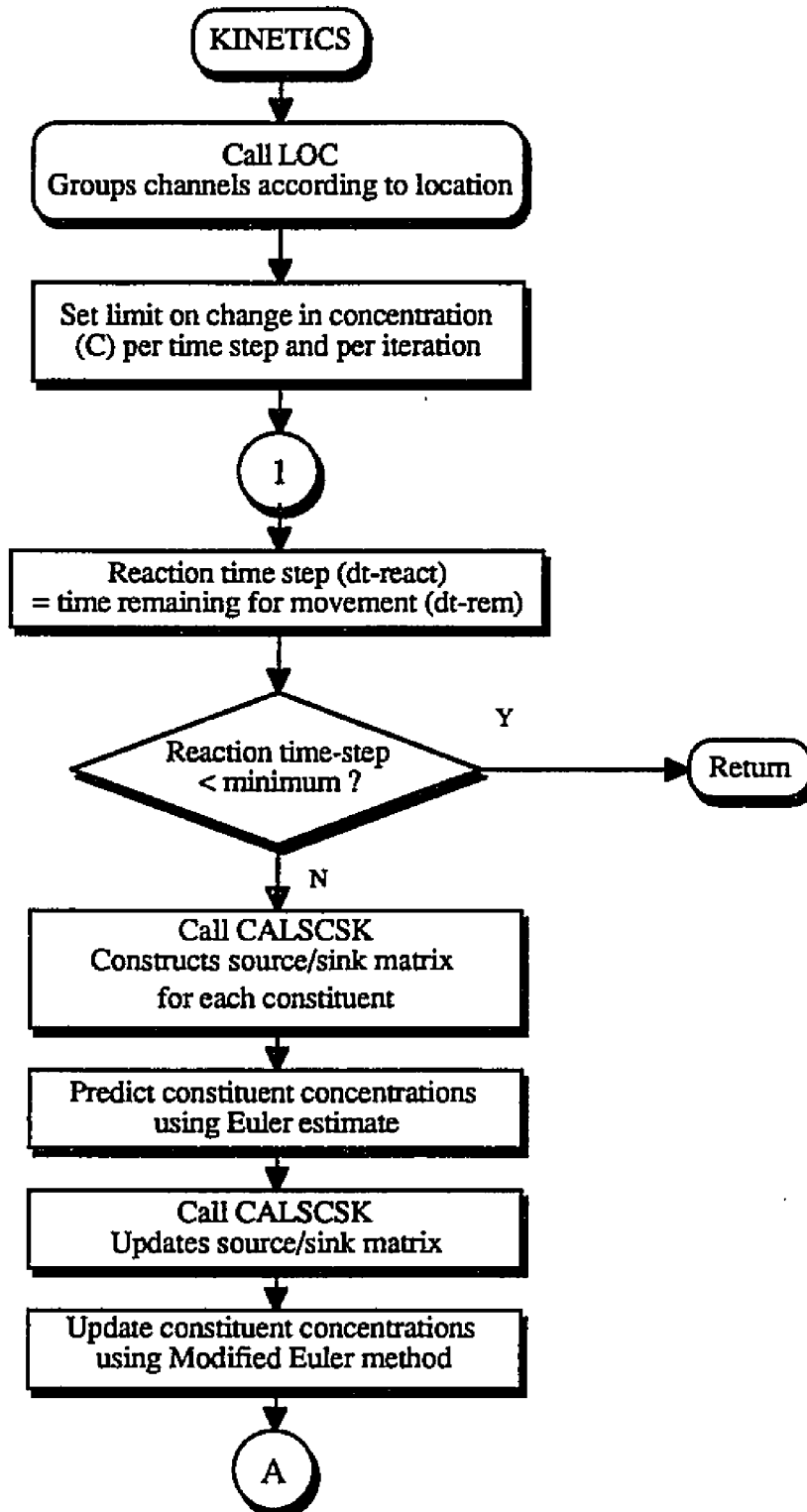


Figure 4.4 Flowchart for KINETICS (continued)

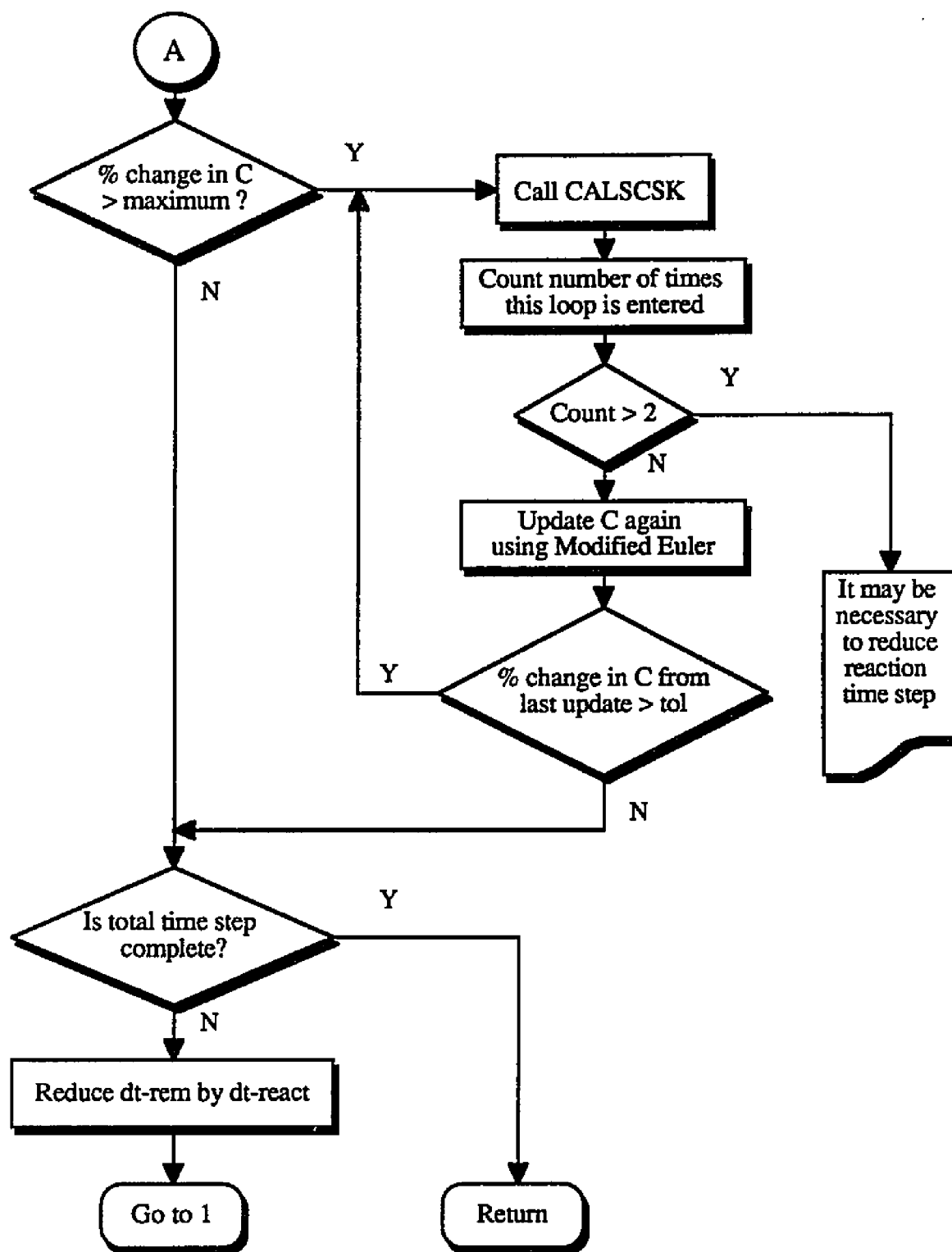


Figure 4.4 (continued) Flowchart for KINETICS

Equations (4.19) and (4.21) together represent the Modified Euler method which is a special case of the popular Runge-Kutta methods of second order (Gerald and Wheatley, 1985).

Tests for Update of Predicted Concentrations

If concentrations from equations (4.19) and (4.21) differ by ten percent or more, new corrections are computed and the test repeated (Figure 4.4). This ensures that if there is even a moderate change in concentration of any constituent within a time step, corrections are provided by repeatedly updating the concentration, or by reducing the time step as explained below.

CALSCSK is called to update the source/sink matrix once again. Using updated values of f^* new concentrations are calculated from equation (4.21). If the change in concentration from its previously predicted value is within a user-supplied tolerance limit (currently set at 5% of the previous value), updating of concentration for this time step (or part of this time step) is considered final. The procedure is then repeated for the next constituent. After concentrations for all the constituents are updated, the algorithm moves to the next point in time (or the remaining part of this time step).

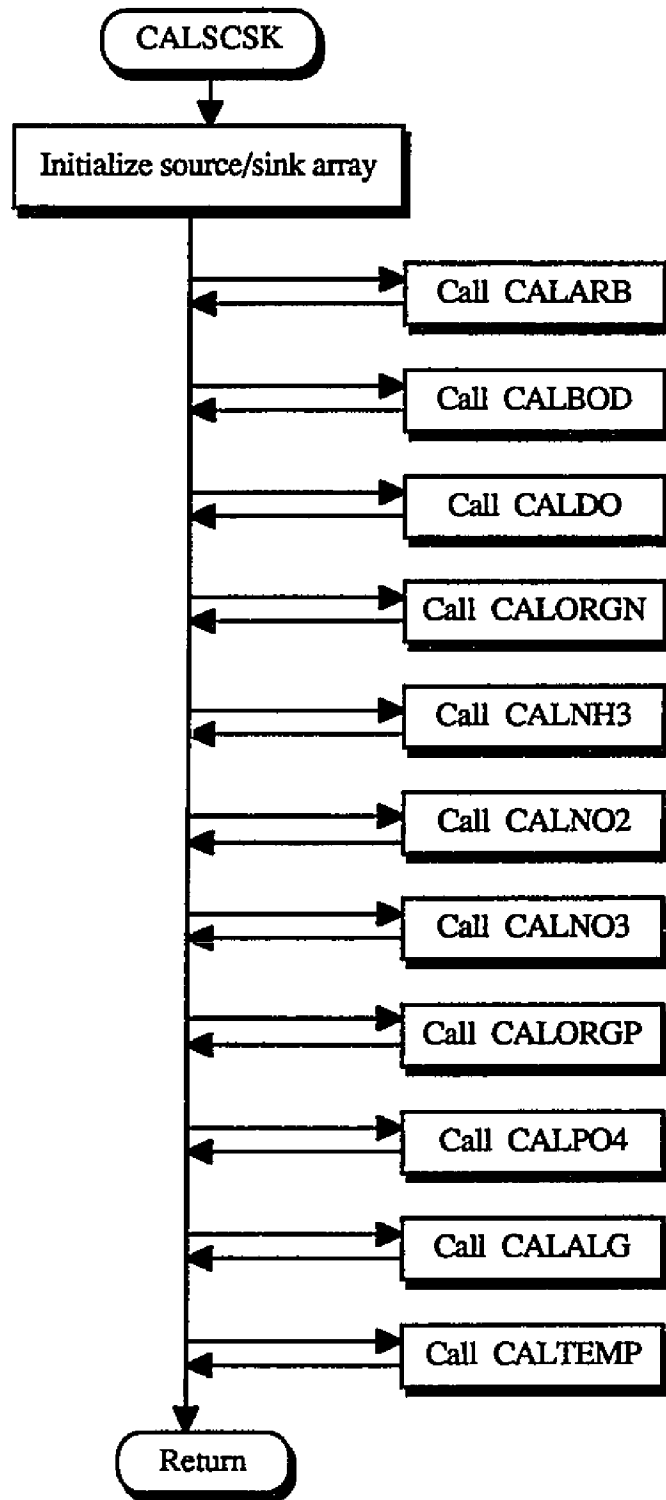


Figure 4.5 Flowchart for Subroutine CALSCSK

However, if the tolerance is not met, the process of updating f^{n+1} is repeated once again. In case the concentrations still differ by more than the tolerance limit, the model is instructed to reduce the reaction time step. Because this may indicate the case of a highly nonlinear rate of change in concentration, and a reduced time step will be more efficient to begin with (for example, see Gerald and Wheatley, 1985). This situation is less likely to occur and was not necessary in any of the application runs done in this study. Note that the tests compare ratios of change in concentration to previous concentration, and not simply changes in concentration. This ensures that the tests are not too restrictive for certain constituents while being too tolerant for the others. In order to avoid a possible division by zero when concentrations are extremely small or zero, the computer program is instructed to let $C = 0.000001$ if $C < 0.000001$.

4.4 Case Study: Sacramento-San Joaquin Delta

The Sacramento-San Joaquin Delta (Figure 4.6) is a part of the San Francisco Bay/Delta Estuary where the mix of fresh water from tributary rivers and salt water from the Pacific Ocean sustains a diverse population of flora and fauna. Also, the Delta is the heart of California's largest water delivery systems, the federal Central Valley Project (CVP) and the State Water Project (SWP), whose waters are vital for 20 million residents, the state's multibillion industry, and more than 4 million acres of productive farmland, primarily in the San Joaquin Valley (Sue McClurg, 1993). As a focal point for a wide variety of water related issues over the last decade, the fragile Delta system has experienced increased pressure and an upsurge in interest in solving Delta problems. Controlling factors in Delta water management include a steep decline in many fish species that live in or migrate through the Delta, laws and public pressure to protect the environment, and increases in water demand caused by a rapid population growth. These have been especially evident during the recent six years of drought (1987-1992).

4.4.1 Ecosystem

The Bay-Delta ecosystem is one of the most severely impacted among estuarine systems in the world, especially considering the number and kinds of changes which have occurred over recent years

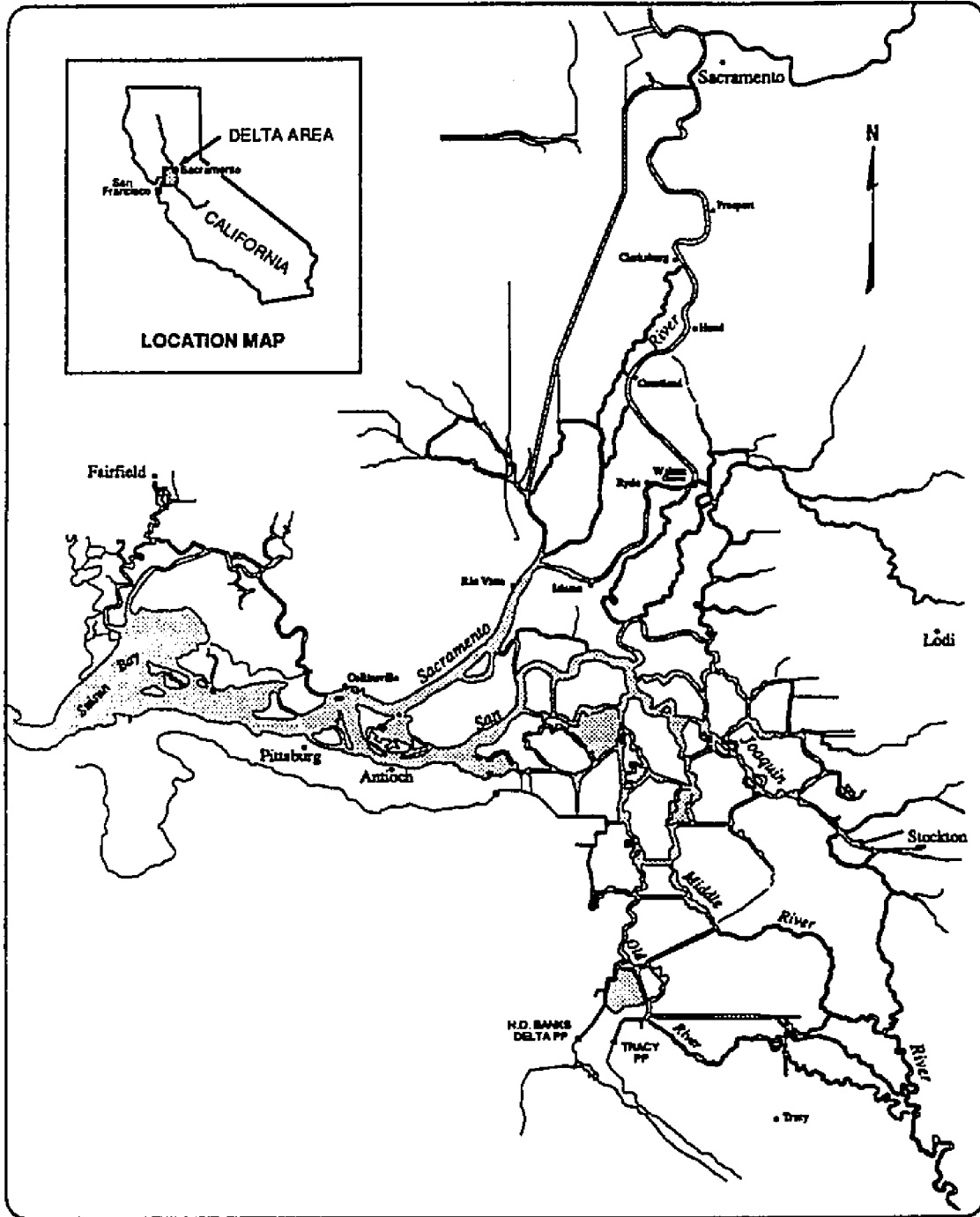


Figure 4.6 Sacramento-San Joaquin Delta

(Nichols et al., 1986). Further impacts on the ecosystem continue, and the situation threatens to worsen, even today. Potential impacts and threat to Delta resources include: loss of tidal marshes and wetlands as a result of agricultural and urban development, loss and injury to species caused by poisoning from waste discharges, decline in fish species and their number due to changes in flow patterns, increased harvesting of some fish species, by entrainment by pumping facilities, or by alternatives in the aquatic environment. As in other estuarine systems, the most important environmental factors that affect biological resources in the Delta, are fresh water inflows, circulation, temperature, and salinity and temporal and spacial variations in these.

Primary production in the Delta is dominated by phytoplankton, mainly diatoms. Most phytoplankton biomass is produced within the delta channels, although some is introduced from upstream sources together with essential nutrients. Production is dependent upon a combination of different factors including water residence time, nutrient concentrations, sunlight, consumption by predators and toxic substances (Herbold and Moyle, 1989). A diverse animal community ranging from microscopic zooplankton to large fish, birds and mammals is dependent upon the Delta's primary productivity.

4.4.2 Water Quality

Water quality within the Delta depends significantly on the quantity and quality of water flowing into the Delta from the Sacramento

and San Joaquin Rivers and other source streams, as well as on tidal intrusion of salt water from the ocean. The relative contribution of each source to the resulting quality depends on source amounts and on flow patterns within the Delta.

Sources of water differ in their characteristics, such as salinity and nutrient content, and upon the nature of pollutants they contain. As water from different sources mix, the quality of Delta waters changes. Water quality in the Delta is determined by a complicated mix of water flow and discharges into and through the Delta, the quality of source water, water use within the Delta and diversions which remove water from the delta or alter flow patterns (California State Lands Commission (CSLC),1991).

Among the major sources, the Sacramento River contributes about 85 percent of the inflow to the Delta. Water quality in the Sacramento River is generally good, however, in May and June agricultural drainage of lesser quality may constitute as much as 30 percent of the flow (Gunther, et al., 1987 as reported in CSLC, 1991). The San Joaquin River contributes only about 10 percent of the inflow to the Delta. The river is much more saline than the Sacramento River and carries higher concentrations of several constituents including nitrates, selenium, nickel, manganese and boron (California Regional Water Quality Control Board, 1991). During the period April through September, a large part of the flow in the San Joaquin River is made up of agricultural drainage. This water consists partly of excess irrigation runoff from fields and partly of flow from underground tile drainage systems in the valley

(DWR, 1987), although recently these systems have been shut down to control selenium accretions in drainage waters (San Joaquin Valley Drainage Program, 1990).

Delta inflows come largely from winter rains and spring runoff including snowmelt from Sierra streams. Regulated flows also come from reservoir releases in the summer and fall, some of these to meet the needs of migratory salmon. Delta flows are not only necessary for the needs of fish and wildlife, but are essential for repelling the intrusion of salt water from the ocean which would endanger agricultural uses. Reverse flows that occur in many Delta channels due to SWP and CVP pumping disorient migratory striped bass, salmon, and steelhead. Such reversals from normal circulation may further increase impacts on fish population by pulling the smaller fish from the western Delta nursery area into the pumping plants. During operational periods that cause reverse flows, more water than is needed for export must be released from project reservoirs to repel intruding sea water and to maintain required water quality in western Delta channels. The required amount of extra outflow, so-called "carriage water", is substantial (DWR, 1987).

Demands on Delta water supplies come from the Central Valley Project, the State Water Project, agricultural interests within the Delta, and urban and industrial water users. Human demands for high quality water, especially during dry climate periods, compete with fisheries and other Delta wildlife needs. Diversions within and upstream from the region also impact the Delta. About 1,800

localized agricultural diversions within the Delta collectively account for about 960,000 acre-feet of consumptive water use annually (CSLC, 1991).

Changes induced by diversions, both major and minor, include modification of water quality characteristics such as salinity, temperature, dissolved oxygen and nutrients. Also affected are the location of the so-called "null" zone, channel flow directions and velocities, and water residence time. These changes also affect the distribution and abundance of phytoplankton and zooplankton in the Delta, thus ultimately affecting fish species that depend on these sources of food. Young salmonids are sensitive to waters with low oxygen content and high temperatures, conditions that can occur on occasion in Delta channels.

4.4.3 Modeling Need

Both hydrodynamic and water quality changes in the Delta are of critical importance in the maintenance of a healthy ecosystem. A major goal in Delta water management is to find that combination of controllable operation factors that will assure an equitable balance between in-Delta needs, including water quality, and export requirements of the CVP and SWP.

Mathematical models have the potential to play important roles in aiding the Delta management in resolving such complex water management issues. Models can provide objective and quantifiable assessments for evaluating the effects of various management plans and alternatives. Most of the investigative tools that are

available to decision makers today are not adequate to describe the important dynamic variations in water quality that occur in complex estuaries like the Delta. A reliable tool that can describe these variations can contribute greatly to the overall goal of Delta water management, i.e. finding an equitable balance among the needs of a diverse group of Delta water users.

4.4.4 Spatial Discretization

The DWRDSM model grid of the Sacramento-San Joaquin Delta was chosen as the model geometry for the new water quality model. This is grid comprised of 496 channels, 416 junctions and 13 open water areas (see Figure 4.7).

It is noted that the original BLTM requires all internal junctions to be numbered first, followed by the external junctions. Branches and junctions should be numbered sequentially without skipping or repeating any number (Jobson and Schoellhamer, 1992). This requirement was accomplished by the use of a preprocessor routine that reads the geometry information assigned to the DWRDSM grid and reassigns it according to the BLTM numbering system.

4.4.5 Hydrodynamics Model

The DWRDSM hydrodynamics model was used to provide circulation information for the water quality model. The mathematical formulation of this model is based on the Fischer Delta Model (H. B. Fischer Inc., 1984) which utilizes the method of characteristics to solve a pair of Saint-Venant shallow water wave equations, one for

continuity and one for momentum. One-dimensional approximation of these equations is represented as:

$$\frac{\partial Q}{\partial x} + \frac{\partial A}{\partial t} = 0 \quad \text{Continuity} \quad (4.22)$$

$$-\frac{\partial y}{\partial x} + S_o - S_f = \frac{1}{g} \left(\frac{\partial u}{\partial t} + \frac{\partial u}{\partial x} \right) \quad \text{Momentum} \quad (4.23)$$

where

- Q = discharge rate,
- A = flow cross-sectional area,
- y = flow depth,
- S_o = channel bottom slope,
- S_f = friction slope,
- u = mean channel velocity,
- g = acceleration due to gravity,
- x = variable in space,
- t = variable in time.

The unknown dependent variables are flow depth y and velocity u.

The reader is referred to Rayej and Chung (1993) for further details on the DWRDSM Hydrodynamics Model.

For the purpose of the present study, the computed values of flows, widths and depths are stored in a binary file for input to a modified version of the BLTM (Nader, personal communication). These values

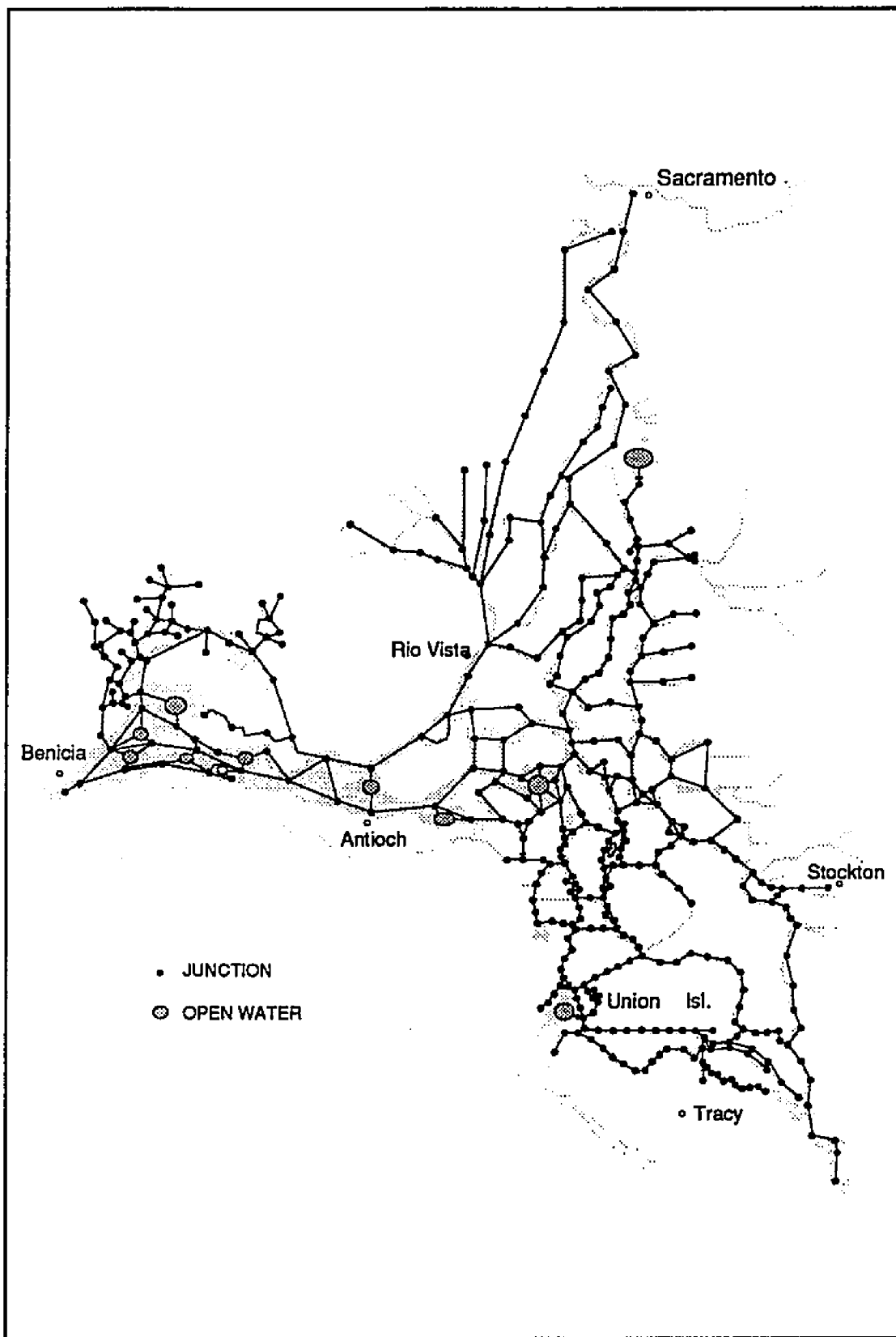


Figure 4.7 DWRDSM Delta Model Grid.

are averaged over the specified time interval, typically 15 minutes to a half hour, before storing them in the file.

4.4.6 Special Features for Simulation of Water Quality in the Delta

In the context of applying the new model to the Sacramento-San Joaquin Delta for its preliminary calibration and verification, modifications were made to include some features that are specifically applicable to the Delta.

Agricultural Diversions and Returns

BLTM, in its original form, has the option of assigning flows to any grid point within the channel. Flow estimates for agricultural drainage and diversions are currently provided to the hydrodynamic model at specified nodes. To make the water quality and the hydrodynamic models compatible with each other, BLTM was modified to allow this option (DWR, 1995B). An example is shown below to illustrate how the model accounts for this (see Figure 4.8).

$$C_2 = C_{div} = \frac{Q_1 C_1 + Q_{ag} C_{ag}}{Q_1 + Q_{ag}} \quad (4.24)$$

$$Q_2 = Q_1 + Q_{ag} - Q_{div} \quad (4.25)$$

where

Q_{ag} = agricultural drainage (return)

Q_{div} = agricultural diversion

Q_1 = flow rate entering the junction (node)

- Q_2 = flow rate leaving the junction
 C_1 = constituent concentration for entering flow
 C_2 = constituent concentration for flow leaving
 Δt = time step

Open Water Area

Open water areas in the Delta (reservoirs) are modeled as well-mixed tanks (DWR, 1995B). The concentration of a conservative constituent during a time step is assumed to be constant within the reservoir. During each time step, constituent mass is added to, or removed from, the reservoir with inflow or outflow (Figure 4.9). The concentration is then updated using the principle of conservation of mass as shown below.

$$V_{res}^{n+1} = V_{res}^n + Q_i \Delta t - Q_o \Delta t \quad (4.26)$$

$$C_{res}^{n+1} = \frac{V_{res}^n C_{res}^n + Q_i C_i \Delta t - Q_o C_o \Delta t}{V_{res}^{n+1}} \quad (4.27)$$

where

- V_{res} = volume of water in the reservoir
 C_{res} = constituent concentration in the reservoir
 n = integer denoting time level
 Q_i = rates of flows entering the reservoir
 Q_o = rates of flows leaving the reservoir
 C_i = Concentrations of flows entering the reservoir
 C_o = Concentrations of flows leaving the reservoir

For non-conservative constituents the change in constituent concentration due to decay and growth including mutual interactions is first determined during each time step. The procedure shown above is then followed for each constituent using this updated concentration as C_{res}^n in equation 4.27.

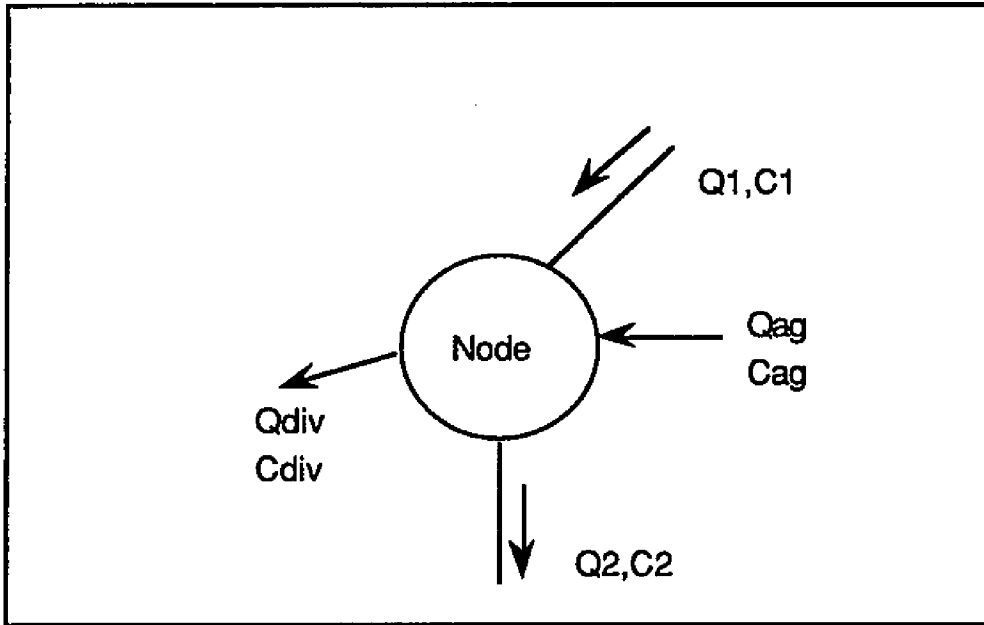


Figure 4.8 Node with Agricultural Drainage and Diversion

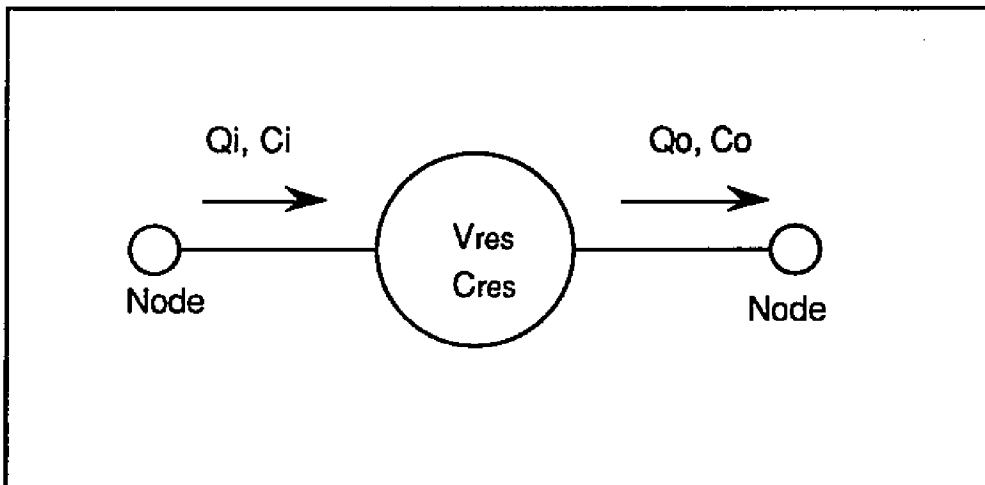


Figure 4.9 An Example of Open Water Area (Reservoir)

4.5 Description of New Subroutines

New subroutines have been developed for modeling non-conservative constituents in an aquatic system. These routines are structured in modular form so that they are easy to understand and can be extended to simulate additional conservative or non-conservative constituents with minimum change in existing routines, if such needs arise in the future. Flexibility has been built into the model so that any combination (one, a few, or all) of the variables can be modeled as suited to the needs of the user.

The model, in its present form, can simulate the eleven water quality variables described in the beginning of this chapter. The original BLTM routines for the basic transport part were somewhat modified in development of the new model for computational efficiency and for adapting to the new routines developed in this study. The integrated modeling package, comprising of the modified BLTM routines (basic transport part) and the new routines developed in this study for simulation of non-conservative constituents, will be referred to as DSM2-QUAL.

In the new subroutines generic variable names are used whenever appropriate, for convenience and flexibility to users, and for ease of documentation and programming. For example, rcoef (icon, j, loc) is used to denote all rate coefficients for all constituents. The variable "icon" will represent constituent name (1 to 11, in the present case), the middle cell is used to distinguish the type of rate coefficient (1 = rate of decay/growth, 2 = settling rate, 3 = benthic

source/demand rate etc.); 'loc' is used to have capability to vary rates as functions of location. A brief description of the subroutines is provided below. Figures are included for a few routines to illustrate the main processes.

KINETICS

The main function of this subroutine is to update constituent concentrations at each time step. KINETICS is called by the parcel tracking subroutine (ROUTE) for every parcel at each time step. The flowchart (Figure 4.4) shows the logic of this subroutine, explained in detail in Section 4.3. It has also been extended to simulate kinetic interactions in 'reservoirs', when the model is applied to the Sacramento-San Joaquin Delta.

CALSCSK

This subroutine builds a source/sink matrix for each constituent by calling each constituent subroutine. Individual constituent routines are listed in Figure 4.5. Flowcharts for three principal constituents (DO, algae, temperature) are presented in Figures 4.10 through 4.12 for illustrative purposes.

HEAT

Subroutine HEAT has been adapted from the QUAL2E model with some restructuring. This version computes the net short wave solar radiation and the long wave atmospheric radiation once every hour (Figure 4.13).

MET

A call statement to this subroutine (for every hour) was added to the subroutine BLTM (not shown here; see Jobson and Schoellhamer, 1992 for details on it). Meteorology data are read by MET, and are used in computation of heat components as shown in Figure 4.13.

RATE

Physical, chemical and biological rate coefficients are read in this subroutine. Some of these coefficients are constant throughout the system; some vary by location; and most are temperature-dependent. A list of these coefficients, including their ranges and calibrated values for this model, is provided in Tables 5.6 and 5.7. Temperature coefficients for reaction rates are presented in Table A.1 (Appendix A).

LOC

This subroutine groups channels by their number or location. The grouping allows the input of spatially varying rate coefficients in the model.

4.6 Additional Comments

As noted earlier, the original kinetic routines of the BLTM modeling package were not simply modified, but were replaced with new routines that provide the updated model with additional flexibility. More detailed explanation of these improvements that have resulted in the new model DSM2-QUAL is provided here.

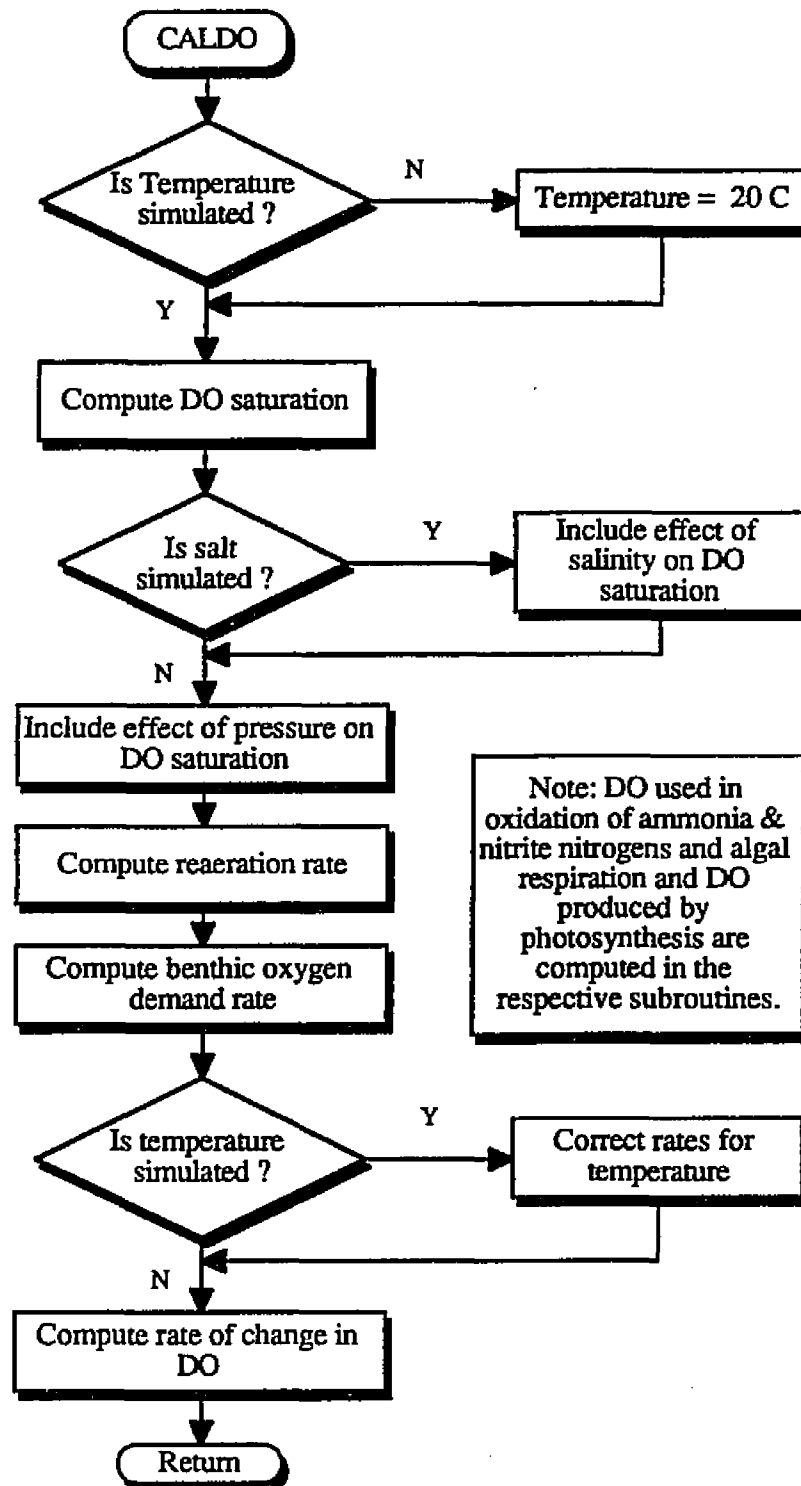


Figure 4.10 Flowchart for Subroutine CALDO (DO)

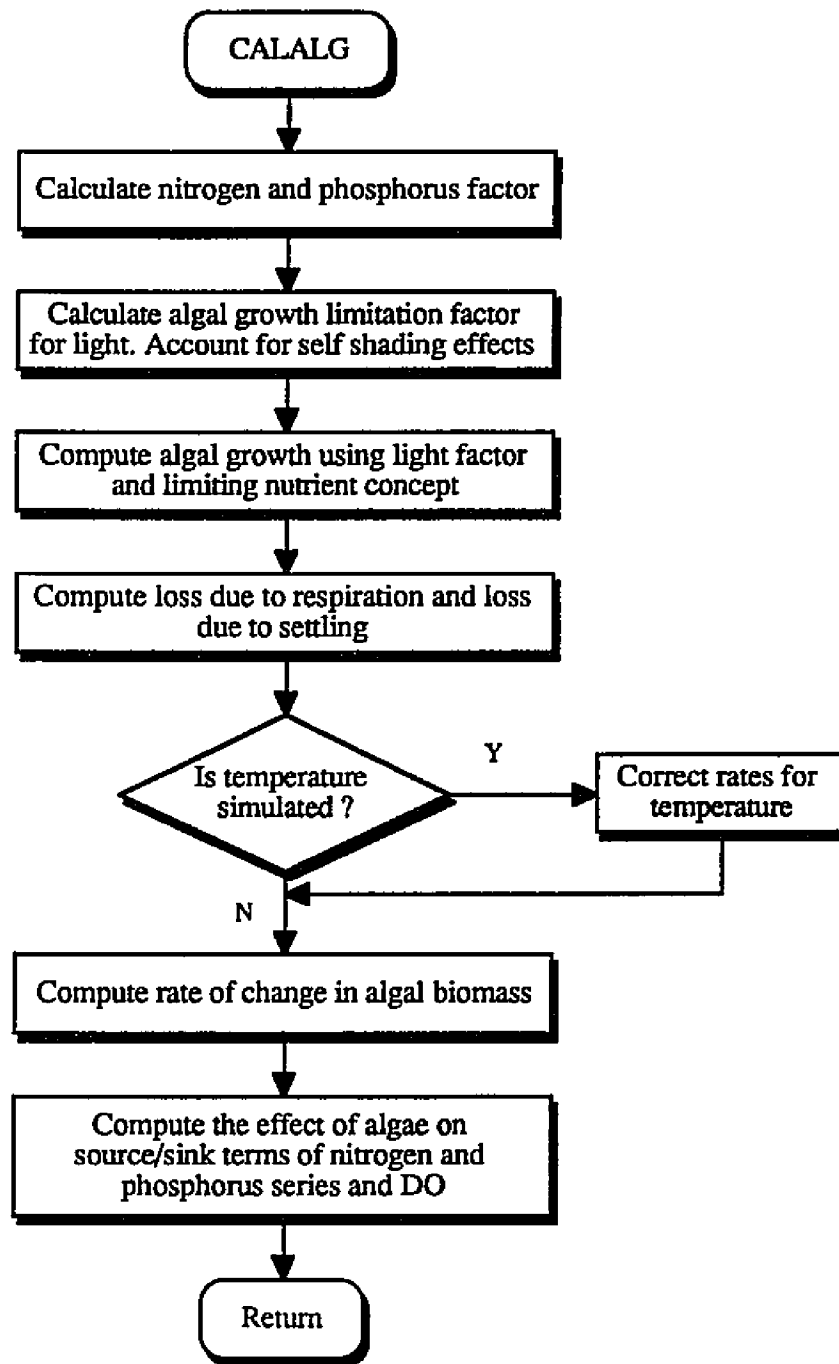


Figure 4.11 Flowchart for Subroutine CALALG (algae)

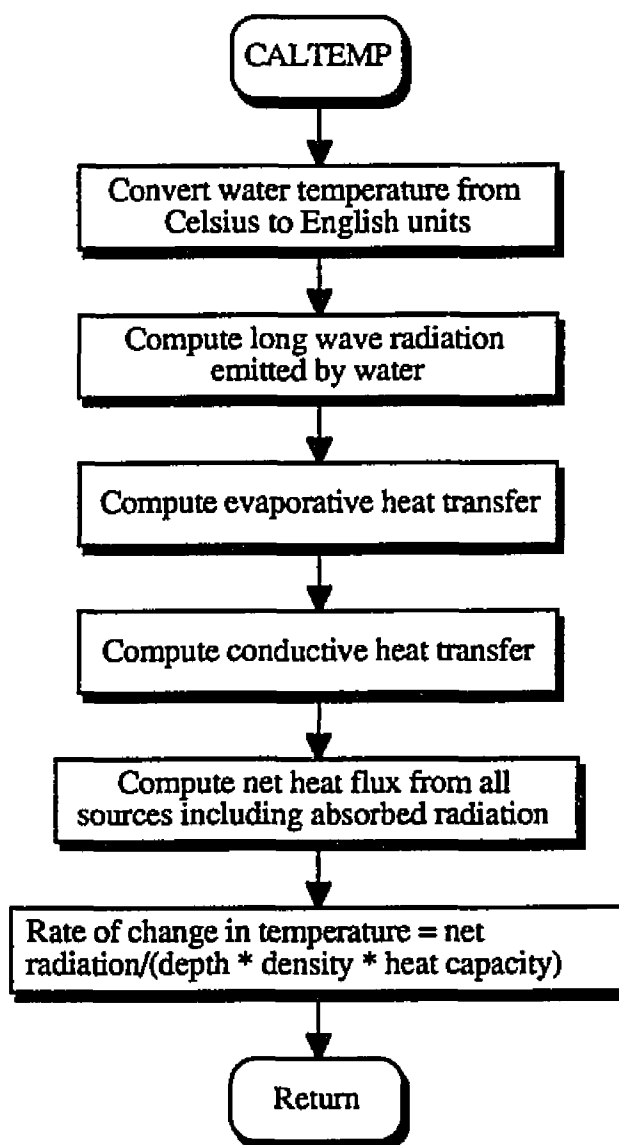


Figure 4.12 Flowchart for Subroutine CALTEMP (Temperature)

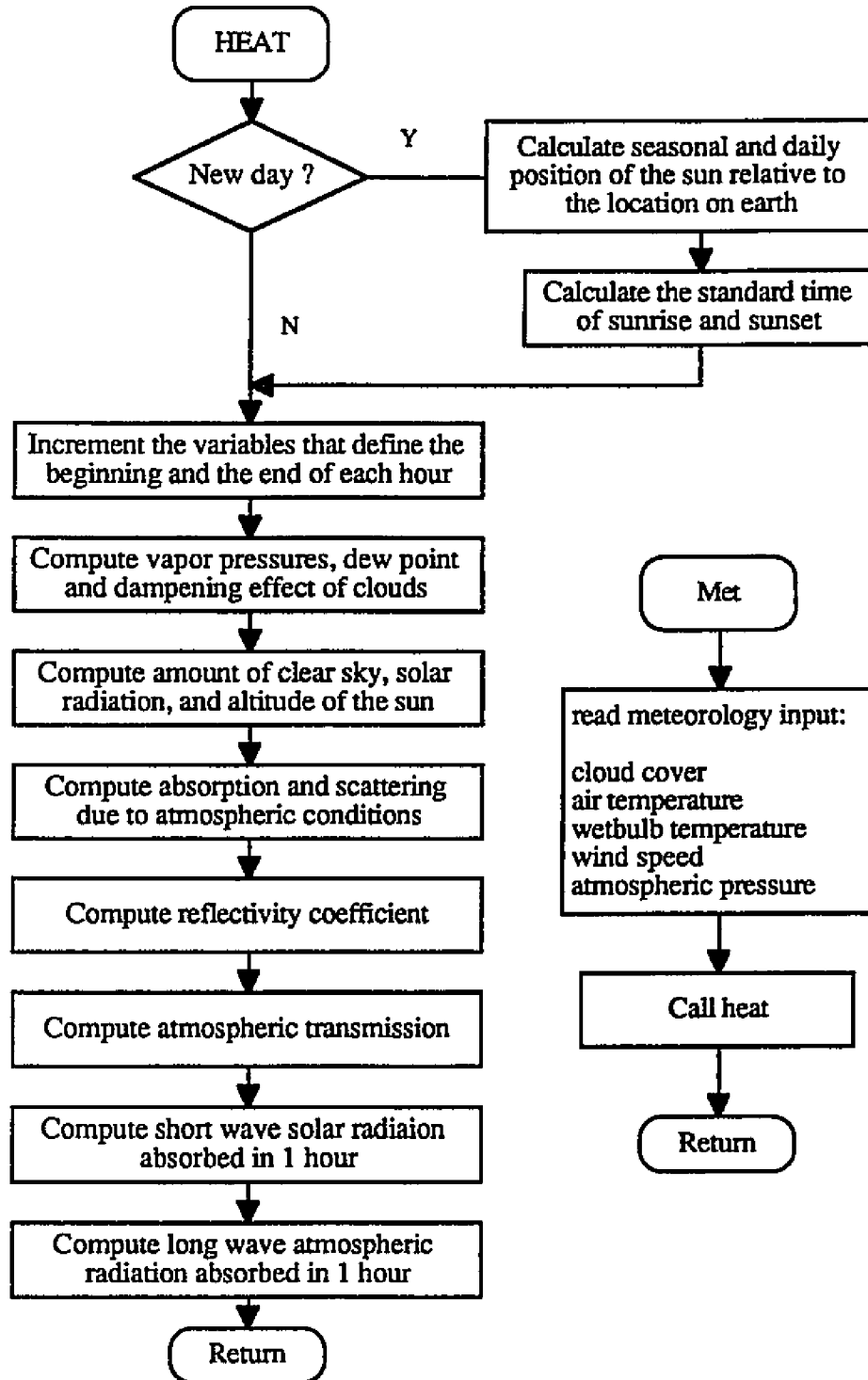


Figure 4.13 Flowcharts for Subroutines HEAT and MET

The subroutine FINK in the original BLTM model represents a simplified form of the kinetics, an early version of the QUAL2 model (Roesner et al., 1977A and 1977B). In DSM2-QUAL this subroutine has been replaced with CALSCSK with a subset of eleven subroutines, one for each of eleven constituents. It is noted that the original version of QUAL2 has undergone significant modification since 1977. In its present form, QUAL2E (Brown and Barnwell, 1987), it is a more versatile model, perhaps even beyond the specific needs for Delta simulation. For the present study only the most recent changes that are pertinent to Delta water quality have been included. The reader may refer to previous sections and Appendix A for detailed descriptions of the governing equations and parameters. The most significant changes are summarized as follows.

1. Interactions among algae, nitrogen, phosphorus and dissolved oxygen were improved by adding the variables organic nitrogen, and organic phosphorus, and an algal preference factor for utilization of ammonia as a nitrogen source.
2. Algal growth rate was made dependent upon both ammonia and nitrate concentrations;
3. Algal self-shading was incorporated in the algal growth equation.
4. Simulated solar radiation e.g., light availability for photosynthesis was linked directly to algal growth.

5. The DO saturation function was updated to correspond to that given in the 16th Edition of Standard Methods (APHA, 1985).
6. An arbitrary non-conservative constituent with first order kinetics was introduced to allow simulation of a degradable constituent, e.g. coliforms, toxics, etc.

In addition to the above enhancements, the new model, DSM2-QUAL, includes the following additional features that were not parts of the original BLTM kinetic package, but are presently included as options in QUAL2E.

1. Effect of pressure on DO saturation
2. Computation of reaeration coefficients that include the effects of hydraulic characteristics of the system, e.g., the O'Connor-Dobbins equations.

To extend the applicability of the model to estuaries where salinity intrusion may be significant, equation (4.5), the effect of salinity on DO saturation concentration has been included. In test simulations using the new model, where salinity was varied over a range of 5000 to 20,000 ppm, the changes in DO saturation could be as much as 15-20%. Salinity effects are not included in the QUAL2E model package.

The model BLTM (Jobson and Schoellhamer, 1992) represented a significant advance in treating problems of numerical dispersion in branched systems or networks of channels. However, for a system like that of the Delta with its many real or potential water quality

problems it was found to be limited in the sense of practical applications. The substantial modifications and extensions that have transformed BLTM to the improved model DSM2-QUAL now provide much of the flexibility required in simulation of water quality in the Delta. It is acknowledged that the conceptual framework set out by Jobson and Schoellhamer in their BLTM have made development of the new model, DSM2-QUAL, feasible.

4.7 Test Case for Verifying the Reaction Kinetics in the New Model

For the purpose of examining the consistency of reaction kinetics incorporated in the new model with the popular QUAL2E model, the following test case was undertaken.

The models QUAL2E and DSM2-QUAL were applied to a hypothetical channel, rectangular in shape, 20 Kilometers long, 100 meters wide and 2.067 meter deep. The channel was discretized into 8 reaches, each with 11 grid points, creating a total of 80 subreaches. Additionally, for QUAL2E, the channel was discretized with 80 computational elements. Note that in the case of DSM2-QUAL these grid points are required only for assigning the hydraulic information.

The following steady-state hydraulics data were assigned to the channel¹.

Flow	100 m ³ /s (3530 cfs)
Velocity	0.484 m/s (1.59 ft/s)

The system coefficients and the meteorology data were assigned at the following values for the entire simulation period.

Latitude	42.5 deg
Longitude	83.3 deg
Longitude of standard meridian	75 deg
First day of simulation	180
Cloudiness (fraction)	0.2
Air temperature	25° C (77° F)
Wet bulb temperature	20° C (68° F)
Atmospheric pressure	1012.5 mbars (30.27 in. Hg)
Wind speed	3 m/s (6.71 mph)

Initial conditions and the quality at the upstream boundary of the test channel are shown in Table 4.1. The reaction rate coefficients adopted for the test case are shown in Table 4.2. Climatologic coefficients required for heat exchange computations are presented

¹ Note that QUAL2E can not simulate unsteady flow hydraulics.

in Table 4.3. A dispersion coefficient of $0.6 \text{ m}^2/\text{s}$ ($6.5 \text{ ft}^2/\text{s}$) was assigned to both the models.

The models DSM2-QUAL and QUAL2E were run for 24 hours of dynamic simulation. Time steps of 15 minutes were used in both simulations. Computed results at the end of 24 hours are presented in Figures 4.14, 4.15 and 4.16 for chlorophyll-a, dissolved oxygen and the temperature, respectively. The values shown are for the downstream end of each reach, 250 m. (820 ft) long.

The results for all three constituents are almost identical, verifying that the new model DSM2-QUAL represents reaction kinetics that are consistent with those formulated in QUAL2E. It is noted that a zero salinity is assigned to the channel in this test case, because QUAL2E, unlike DSM2-QUAL, does not include the effect of salinity on dissolved oxygen. The very small differences in the computed results may have resulted from the differences in the numerical schemes of the two models for representation of the processes of advection and diffusion in the two models. Also the round-off errors in converting the reaction coefficients from metric to English units may have resulted in some differences.

Table 4.1 Initial Conditions and Water Quality at the Upstream Boundary for the Test Problem

	Initial Condition	Upstream Inflow
TDS	0.0	0.0
BOD	3.0	4.0
DO	7.7	8.0
Organic N	1.0	1.0
NH3-N	0.03	0.03
NO2	0.0	0.0
NO3	0.5	0.5
Organic P	0.2	0.2
Ortho-PO4	0.1	0.1
Chlorophyll-a $\mu\text{g/l}$	4.0	4.0
Temperature $^{\circ}\text{C}$	20	22

Table 4.2 Reaction Coefficients for the Test Problem

Global coefficients (with the FORTRAN variable names used in DSM2-QUAL) are listed below .

<u>Variable</u>		<u>Range</u>	<u>Test Problem</u>
alph(5)	oxygen used in conversion of ammonia to nitrite	3.0-4.0	3.50
alph(6)	oxygen used in conversion of nitrite to nitrate	1.0-1.14	1.20
prefn	algal preference factor for ammonia	0-1.0	0.90
alph(7)	chlorophyll-a ($\mu\text{g/l}$) to biomass (mg/l) ratio	10-100	50
alph(1)	fraction of algal biomass which is nitrogen	0.07-0.09	0.085
alph(2)	fraction of algal biomass which is phosphorus	0.01-0.02	0.012
alph(3)	oxygen produced in photosynthesis	1.4-4.8	1.6
alph(4)	oxygen consumed with respiration	1.6-2.3	2.0
klight_half	half saturation constant for light ($\text{BTU/ft}^2\text{-min}$)	0.02-0.1	0.111
knit_half	half saturation constant for nitrogen (mg/l)	0.01-0.30	0.30
kpho_half	half saturation constant for phosphorus (mg/l)	0.001-0.05	0.04
xlam0	non-algal light extinction coefficient (ft^{-1})	variable	0.116
xlam1	linear algal self shading coeff. $\text{ft}^{-1}(\mu\text{g-Chl}a/\text{l})^{-1}$	0.002-0.02	0.003
xlam2	nonlinear algal self shading coefficient $\text{ft}^{-1}(\mu\text{g-Chl}a/\text{l})^{-2/3}$	0.0165	0.0165

Note: rates are in units per day except when specified.

Table 4.2 (contd.) Reaction Coefficients for the Test Problem

<u>Variable</u>		<u>Range Test Problem</u>	
k 1	BOD decay rate	0.02-3.4	0.3
k 3	BOD settling rate	-0.36-0.36	0.0
k 4	benthic demand rate for DO (g/m ² /day)	variable	3.5
mumax	maximum algal growth rate	1.0-3.0	2.5
resp	algal respiration rate	0.05-0.5	0.1
s1	algal settling rate (ft/day)	0.5-6.0	0.49
kn-org	organic nitrogen decay rate	0.02-0.4	0.25
s4	organic nitrogen settling rate	0.001-0.1	0.1
kn	ammonia decay rate	0.1-1.0	0.15
s3	benthic source rate for ammonia(mg/m ² /day)	variable	4.0
kni	nitrite decay rate	0.2-2.0	1.0
kp-org	organic phosphorus decay rate	0.01-0.7	0.2
s5	organic phosphorus settling rate	0.001-0.1	0.1
s2	benthic source rate for dissolved P (mg/m ² /day)	variable	1.0

Note: rates are in units per day except when specified.

Table 4.3 Climatologic Coefficients used in the Test Problem

<u>Parameter</u>	<u>Test Problem</u>
'a' in ft/hr-in. of Hg.	0.00110
'b' in ft/hr-in. of Hg.-mph	0.00049
Dust Attenuation Coefficient	0.13

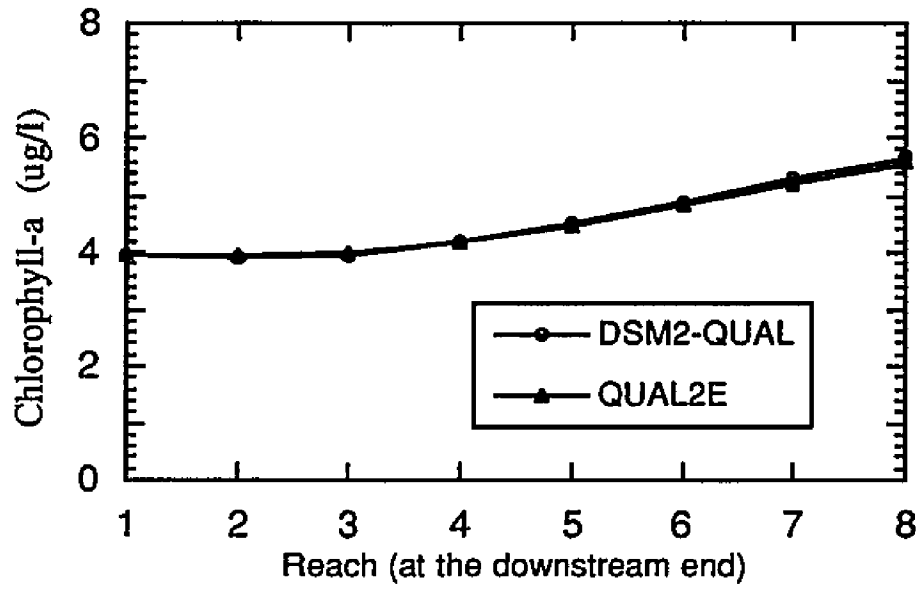


Figure 4.14 Computed Chlorophyll-a after 24 Hours

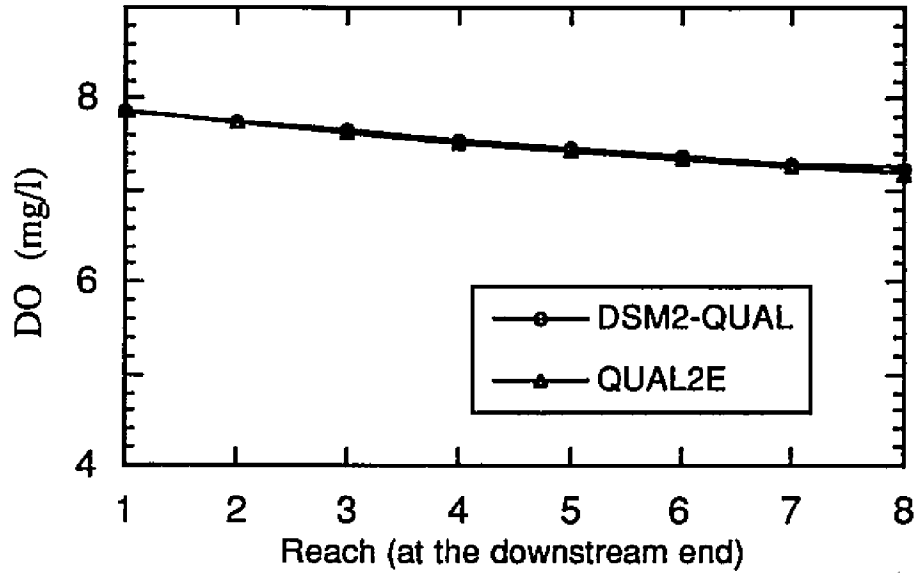


Figure 4.15 Computed Dissolved Oxygen after 24 Hours

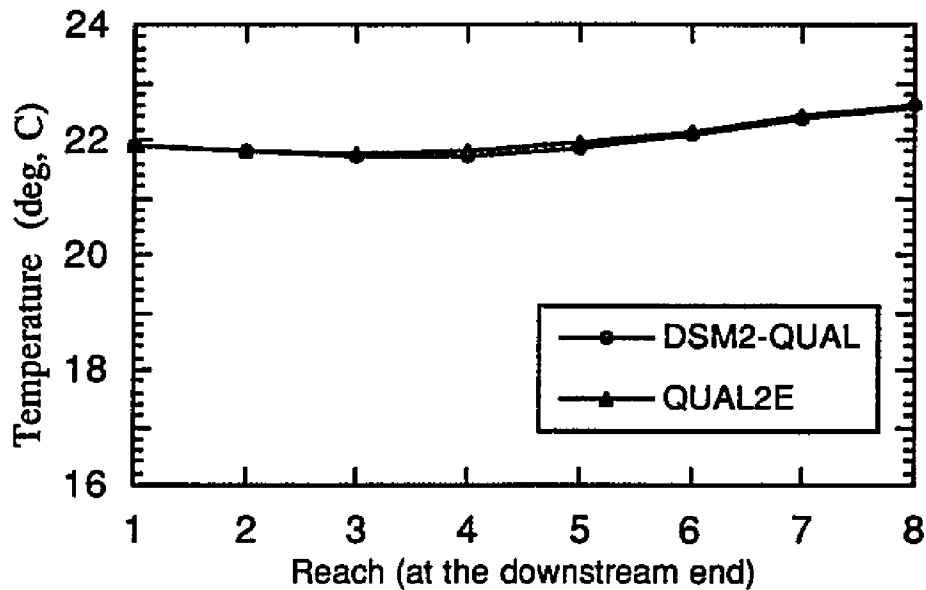


Figure 4.16 Computed Temperature after 24 Hours

4.8 Summary

A new model DSM2-QUAL for characterizing the spatial and temporal distribution of important quality variables in rivers and estuaries has been developed and incorporated into the structure of an existing transport model. New routines were developed for computation of decay, growth and the interaction among various water quality parameters. A cost-effective numerical scheme is employed to update constituent concentrations due to these kinetic processes at each time step. The reaction kinetics in the new model has been verified by applying it to a test problem and comparing the model results with those from QUAL2E. Specific features have been added, as an option, in order to simulate water

quality in the Sacramento-San Joaquin Delta, an estuarine system chosen for initial application of the new model. A manual for the users of DSM2-QUAL has been written (see Appendix C).

5. MODEL DEVELOPMENT PHASE 2: APPLICATION, PERFORMANCE AND ANALYSIS

A preliminary evaluation of DSM2-QUAL was conducted by applying the model to the Sacramento-San Joaquin Delta, California (see Chapter 4 for background). This chapter first describes preliminary calibration of the model, specifically in the region including the Stockton Ship Channel. Next, the model is verified for a new set of boundary conditions. Finally, the model is applied to examine the response of the estuary to changes in effluent discharge and climate conditions.

5.1 Conditions for Model Evaluation

In this study the year 1988 was chosen for model evaluation because extensive calibration and verification of DWRDSM model, which would provide the required hydrodynamics for water quality simulation was done by the California Department of Water Resources for that period. Calibration of DWRDSM was achieved by changing the values of Manning's coefficients (n) in each channel to minimize the differences between observed and computed stages. Verification of the model was achieved for selected months in 1988 and 1989 using stage data, and in some cases (May 1988) flow data (DWR, 1991). According to the report the model performed well in the majority of channels in the Delta. It captured well even small disturbances in water surface elevations of channels in the vicinity of Clifton Court Forebay and inside the forebay as induced by gate

operation. Details of the hydrodynamic study are not included here, but are available for review (DWR, 1991).

For purposes of calibration and verification of the water quality model it was decided to use data from a series of studies to evaluate the effects of the City of Stockton's waste water discharge on the San Joaquin River. Figure 5.1 shows the locations of water quality monitoring stations in the San Joaquin River in the vicinity of Stockton, both upstream and downstream of the City's waste water discharge. Specific survey periods of September 20, 1988 and October 12, 1988 were chosen for model calibration and verification, respectively, because of well documented hydrodynamic conditions prevailing in these periods and the availability of water quality data that provided good temporal and spatial coverage of the study area. The unique hydrodynamic conditions identified with these two dates were due in part to placement of a rock barrier at the head of Old River during the period September 22-28, after the first survey and before the second. The barrier caused increased flow downstream in the San Joaquin River toward Stockton, restricting flow into Old River toward Clifton Court. Modeling of these two scenarios provided an excellent opportunity to contrast the effects of local hydrology and distinctive hydraulic behavior. Additionally, it served the need for objective calibration and verification of the water quality model.

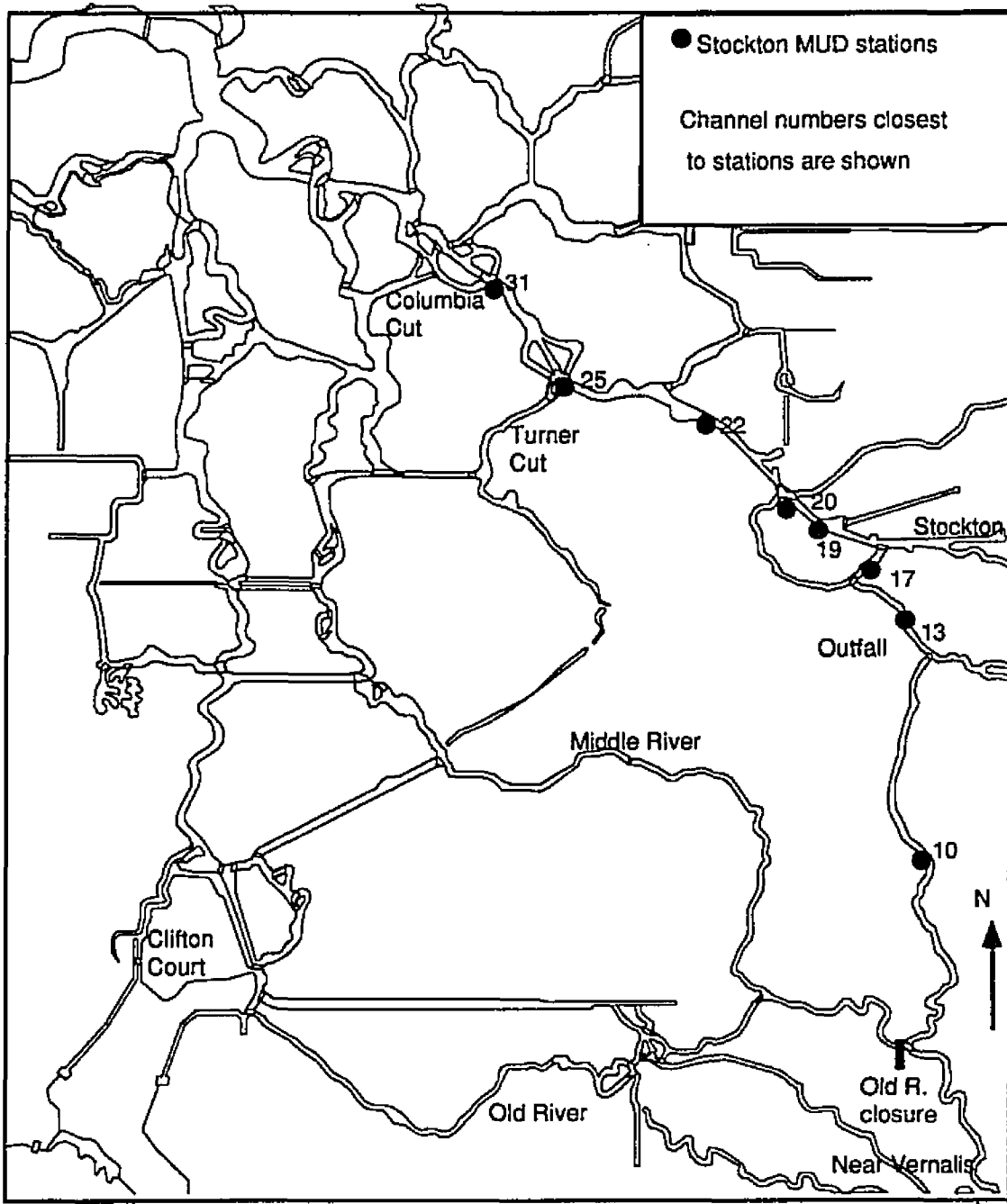


Figure 5.1 Monitoring Stations in San Joaquin River near Stockton

5.2 Model Input

Hydrologic Data

Average daily flows reported in DWR Dayflow Data Summary (DWR, 1988A) were used to specify boundary inflows for the San Joaquin, Sacramento and Mokelumne Rivers and withdrawals by the State Water Project (SWP), the Central Valley Project (CVP) and the Contra Costa Water District (CCWD). Effluent flows from the City of Stockton waste water treatment plant were obtained from the monthly laboratory data files of the Stockton Municipal Utilities District (Huber, personal comm., 1995). Clifton Court intake gate (opening and closing) schedules needed to operate DWRDSM were obtained from monthly operation reports (DWR, 1988B). Agricultural withdrawals and return flows, which are also input to the model, were based on the Department of Water Resources' monthly estimates (DWR, 1995A). Hydrologic and hydrodynamic data for both simulation periods are presented in Table 5.1.

Water Quality Data

Since water quality grab samples were collected only at frequencies of one or two samples per month near model boundaries in the San Joaquin and Sacramento Rivers, and at Martinez, observations made closest to the selected calibration and verification dates were used. These data were extracted from the "Water Quality Surveillance Program" report (DWR, 1990B). Water qualities for inflows at Freeport on the Sacramento River and for the Mokelumne River were derived from Water Resources Data (USGS, 1989, 1990). Stockton

effluent data, available at daily or weekly intervals, were also input to the model (Huber, personal comm., 1995). Chlorophyll-a and ortho-phosphate data for the months of September and October were only available from effluent monitoring on a monthly basis in 1989. These values were used as representative of the 1988 conditions simulated.

Table 5.1 Hydrology used in Model Calibration and Verification

Inflow/Export	<u>Calibration</u>		<u>Verification</u>	
	Discharge (Sep 20,1988) (cfs)	(m ³ /s)	Discharge (Oct 12,1988) (cfs)	(m ³ /s)
Sacramento River	11700	331	11100	314
San Joaquin River	1610	45.6	1050	29.7
Mokelumne River	29	0.8	30	0.8
State Water Project export	2383	67.5	4388	124
CVP export	4610	130	4407	125
Contra Costa Canal export	221	6.3	214	6.1
Stockton City Effluent	31.6	0.9	23.6	0.7
Consumptive Use	2048	58	1260	36
Net Delta Outflow (computed)	4108	116	1934	55

All input data, including some at selected monitoring sites in the Delta, are listed in Tables 5.2 through 5.5. Figure 5.2 shows the locations of these monitoring stations. Note that BOD values are not included in the assembled data set, because such observations were not made in any of the field surveys, reported in the references cited above. An overall background level of BOD at 1.5 mg/l was assumed for the Delta, based on experience with Delta water quality in

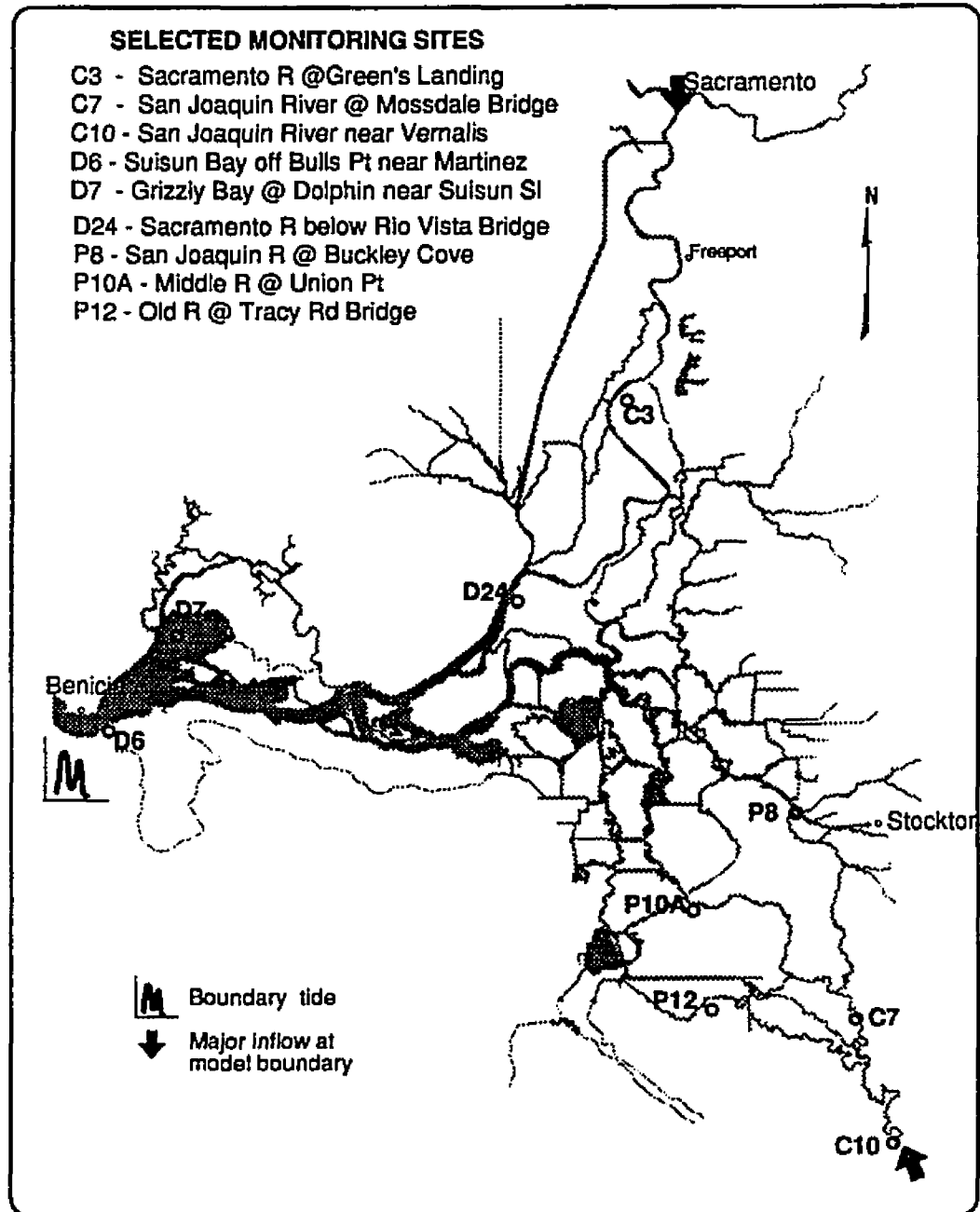


Figure 5.2 Selected Monitoring Stations in the Sacramento-San Joaquin Delta

Table 5.2 Water Quality (Field Data¹) at the Model Boundary
September 1988 Simulation

	Sacramento River at Green's L. (C3) or Freeport	San Joaquin River at Vernalis (C10) or Mossdale ² (C7)	Suisun Bay near Martinez (D6)	Mokelumne River at Woodbridge	Agricultural Return	Stockton City Effluent
Date/Time	Sep 15/0815 Sep 13/1130f	Sep16/0950	Sep21/1255	Sep 14/1120		
TDS	139 f	hourly (450-480)	hourly (16k-21k)	63	1030	900
DO	8.0 f	hourly (7-8)	7.9	8.7 (97% Sat)	5.1	5.3
Organic N	0.5 f	0.3	0.3	0.2	1.4	2.5
NH3-N	0.2	0.01	0.02	0.03	0.31	14.0
NO2+NO3	0.09	1.30	0.37	0.09		
NO2	0.01 e	0.13 e	0.04 e	0.01	0.02	1.46
NO3	0.08 e	1.17 e	0.33 e	0.08	1.3	1.19
Organic P (estimate)	0.03 b	0.11*	0.07 b	0.04	0.09	
Ortho-PO4	0.1 b	0.12*	0.15 b	0.02	0.40	0.66 a
Chlorophyll-a µg/l	0.3	19.1	0.2	0.3	10.0	14.0 a
Temperature °C	20	hourly (18-19)	hourly (18.5-19.5)	21.5	19.6	20.0
BOD					3.9	11.0
a	=	09/20/89				
b	=	09/01/88				
e	=	estimate				
f	=	Freeport 09/13/88				
*	=	09/02/88				

¹ Note: All units are in mg/l except when noted. Organic phosphorus was obtained by subtracting ortho-PO4 from total phosphorus. Dissolved nitrite and nitrate were obtained by subdividing their known total into 10 and 90 percent values. Hourly data are also shown by plots (Figures 5.3 through 5.11).

² Mossdale data were used as hourly data for the model boundary at Vernalis.

Table 5.3 Water Quality (Field Data¹) at the Model Boundary
October 1988 Simulation

	Sacramento River at Green's Landing (C3) or Freeport	San Joaquin River at Vernalis (C10) or Mossdale ² (C7)	Suisun Bay near Martinez (D6)	Agricultural Return	Stockton City Effluent
Date/Time	Oct 17/0955 Oct 18/1100f	Oct 18/1210	Oct 5/1300		
TDS	96 f	hourly (498-536)	hourly (14500-23800)	807	1004
DO	8.9 f (96% Sat)	hourly (7.2-8)	hourly (7.8-8.3)	5.3	6.2
Organic N	0.2	0.3	0.3	1.4	3.8
NH3-N	0.51	0.00	0.01	0.31	21.4
NO2+NO3	0.09	1.10	0.34		
NO2	0.01 e	0.10 e	0.03 e	0.02	0.26
NO3	0.08 e	1.0 e	0.31 e	1.3	0.7
Organic P	0.03	0.11	0.18	0.09	
Ortho-PO4	0.18	0.1	0.06	0.40	2.94 ^a
Chlorophyll-a µg/l	0.9	27.6	0.1	10.0	28 ^a
Temperature ° C	19	hourly (18.8-19.6)	hourly (17.7-18.7)	17.3	19.0
BOD				6.0	8.0

a = 10/25/89
e = estimate
f = Freeport

¹ Note: All units are in mg/l except when noted. Organic phosphorus was obtained by subtracting ortho-PO4 from total phosphorus. Dissolved nitrite and nitrate were obtained by subdividing their known total into 10 and 90 percent values. Hourly data are also shown by plots (Figures 5.3 through 5.11).

² Mossdale data were used as hourly data for the model boundary at Vernalis.

Table 5.4 Water Quality (Field Data¹) at Selected Delta Locations
September 1988 Simulation

	Old R. at Tracy Road Bridge (P12)	Middle R. at Union Point (P10A)	Sac R. below Rio Vista Bridge (D24)	Grizzly Bay at Dolphin (D7)
Date/Time	Sep 16/1135	Sep 15/1100	Sep 20/1420	Sep 20/1025
Tide	LH	LH	LH	LH
TDS	527*	257 b	178 (+)	13500 (+)
DO	8.6	7.7	8.3	8.1
Organic N	0.3	0.1	0.4	0.3
NH3-N	0.03	0.04	0.1	0.01
NO2 (estimate)	0.12	0.02	0.03	0.04
NO2+NO3	1.20	0.21	0.27	0.40
NO3 (estimate)	1.08	0.19	0.24	0.36
Organic P (estimate)	0.10*	0.03 b	0.03(+)	0.10
Ortho-PO4	0.14*	0.08 b	0.11(+)	0.18 (+)
Chlorophyll-a mg/l	26	2.4	2.1	1.2
Temperature ° C	20	21	20	18 °C
BOD				

b = 09/1/88 data
* = 09/2/88 data
(+) = 09/6/88 data

¹ Note: All units are in mg/l except when noted. Organic phosphorus was obtained by subtracting Ortho-PO4 from total phosphorus. Dissolved nitrite and nitrate were obtained by subdividing their known total into 10 and 90 percent values.

Table 5.5 Water Quality (Field Data¹) at Selected Delta Locations
October 1988 Simulation

	Old R. at Tracy Road Bridge (P12)	Middle R. at Union Point (P10A)	Sac R. below Rio Vista Bridge (D24)	Grizzly Bay at Dolphin (D7)
Date/Time	Oct 18/1435	Oct 17/1240	Oct 19/1325	Oct 19/1015
Tide	LH	LH	LH	LH
TDS	591 (+)	270 b	335 (+)	13200 (+)
DO	8.7	7.8	8.1	7.8
Organic N	0.4	0.2	0.1	0.2
NH3-N	0.00	0.07	0.07	0.00
NO2 (estimate)	0.09	0.03	0.02	0.04
NO2+NO3	0.93	0.32	0.22	0.43
NO3 (estimate)	0.84	0.29	0.20	0.39
Organic P (estimate)	0.09	0.03	0.06 (+)	0.14 (+)
Ortho-PO4	0.12	0.10	0.07 (+)	0.12 (+)
Chlorophyll-a, $\mu\text{g/l}$	39.2	1.4	2.5	0.8
Temperature °C	21	21	20	19
BOD				

b = 10/03/88
* = 10/03/88
(+) = 10/04/88

¹ Note: All units are in mg/l except when noted. Organic phosphorus was obtained by subtracting ortho-PO4 from total phosphorus. Dissolved nitrite and nitrate were obtained by subdividing their known total into 10 and 90 percent values.

general, and previous works by Smith (1988), and Chen and Orlob (1975).

To allow representation of diurnal values whenever possible, hourly averaged concentrations of dissolved oxygen, total dissolved solids and temperature were assigned for the boundary at Martinez. Since such detailed data were not available at Vernalis, hourly averaged values of DO, TDS, and temperature available from the nearby station at Mossdale were used to approximate these quantities for the boundary inflow at Vernalis. Hourly averaged data provided for the calibration and verification periods are shown in Figures 5.3 through 5.8. Figure 5.9 through 5.11 are included to show the trend of field data at Rough and Ready Island in the San Joaquin River near Stockton. Similar time series could not be made for the Sacramento River inflow, since there are no continuously monitored stations near this boundary.

In conducting water quality simulations the concentrations of all eleven key constituents were kept constant at the Sacramento River boundary for the simulation period (25 hours). At the other boundaries, the concentrations of eight constituents were kept constant for the period; while concentrations of DO, TDS, and temperature were allowed to vary over the period.

Water quality of agricultural returns at internal Delta locations was based on an estimate derived using 1964 data (DWR, 1967). Flow weighted averages of nitrogen and phosphorous concentrations were computed using data from thirteen sampling stations in the Delta.

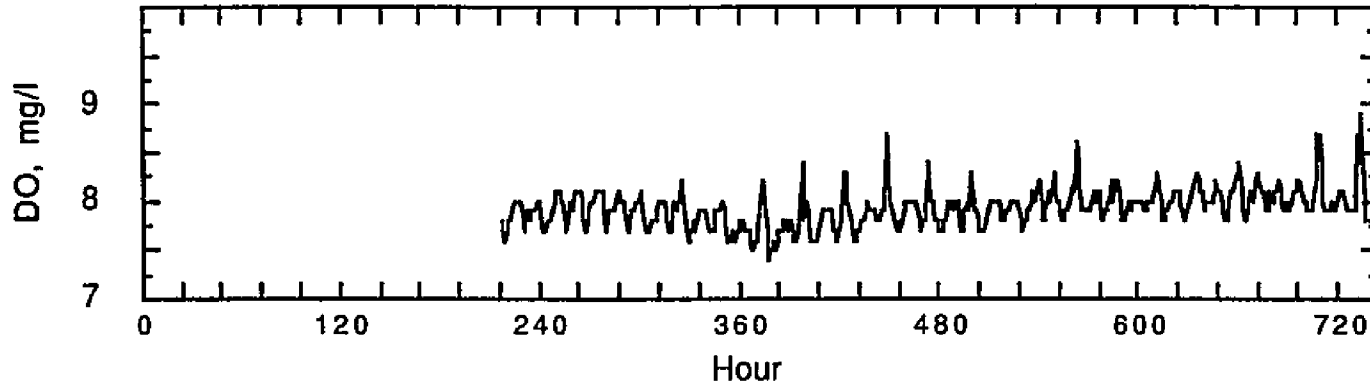


Figure 5.3 Dissolved Oxygen at Martinez (Sep 23 to Oct 15,1988)

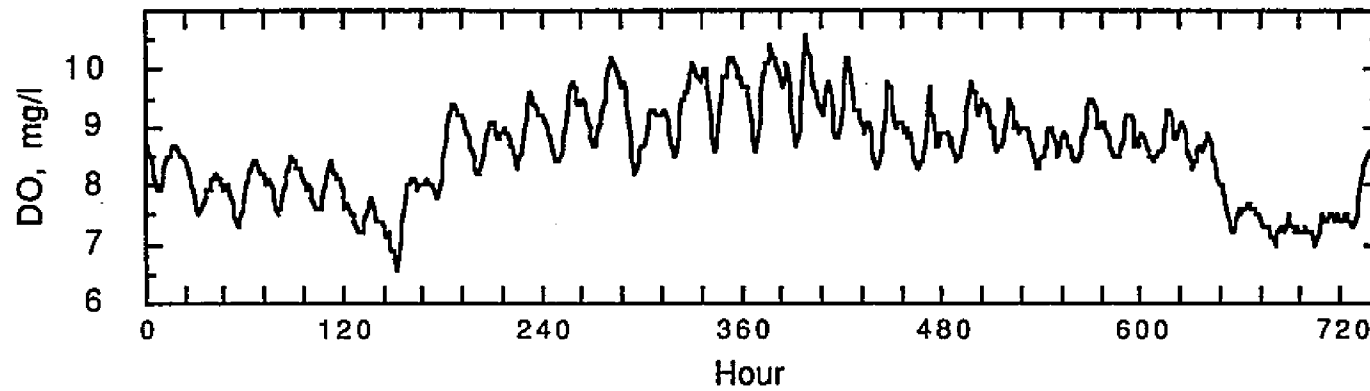


Figure 5.4 Dissolved Oxygen in the San Joaquin River at Mossdale (Sep 15 to Oct 15,1988)

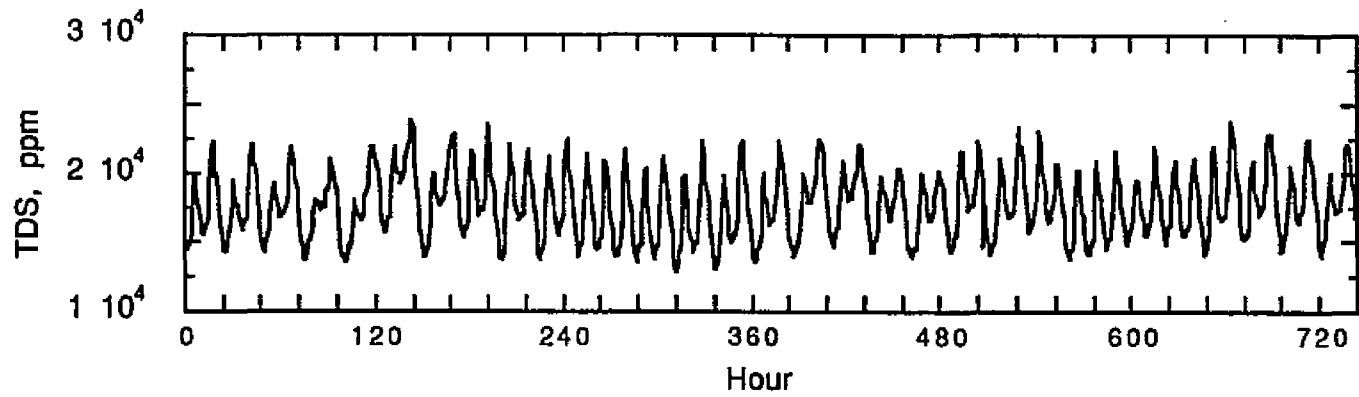


Figure 5.5 Total Dissolved Solids at Martinez (Sep 15 to Oct 15,1988)

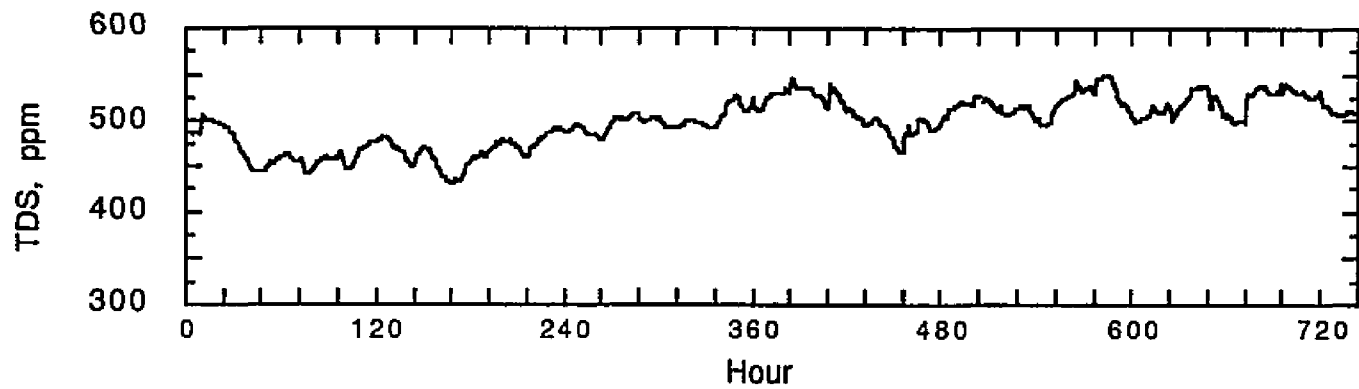


Figure 5.6 Total Dissolved Solids in the San Joaquin River at Mossdale (Sep 15 to Oct 15,1988)

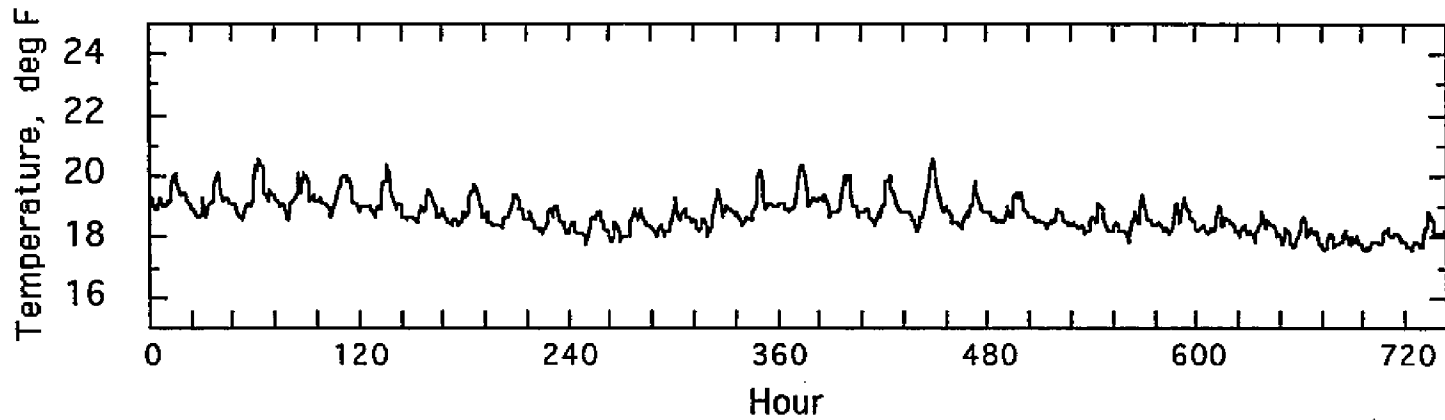


Figure 5.7 Temperature at Martinez (September 15 to October 15, 1988)

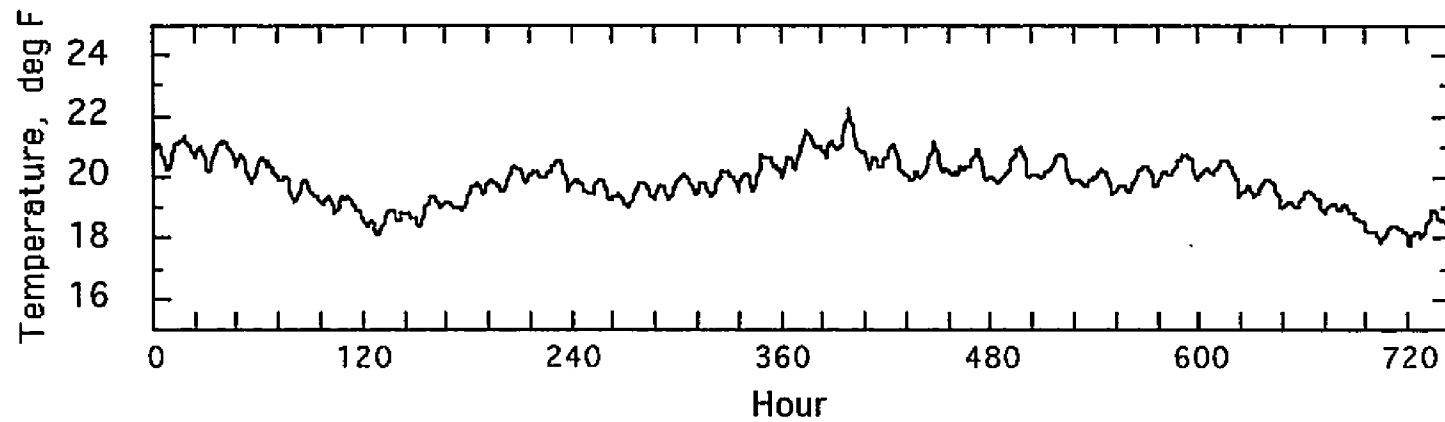


Figure 5.8 Temperature in the San Joaquin River at Mossdale (September 15 to October 15, 1988)

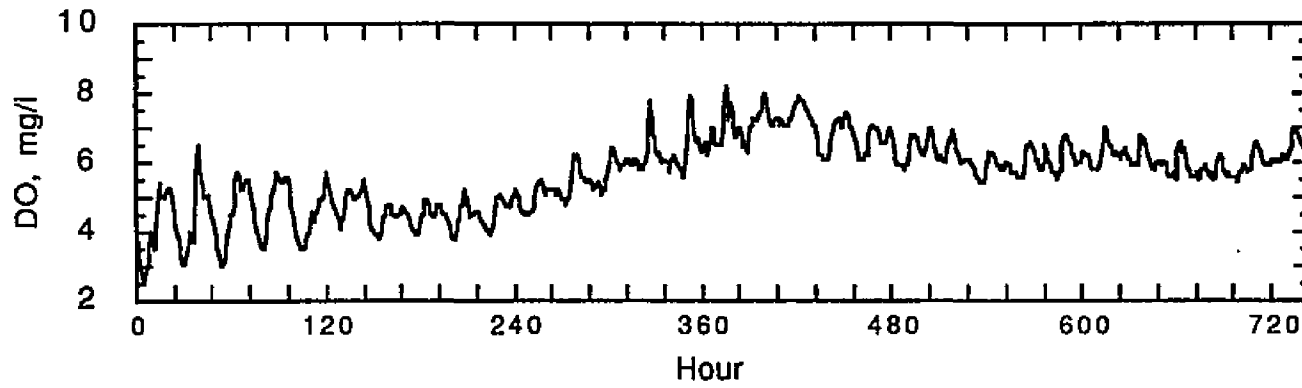


Figure 5.9 Dissolved Oxygen in the San Joaquin River at Stockton (Sep 15 to Oct 15,1988)

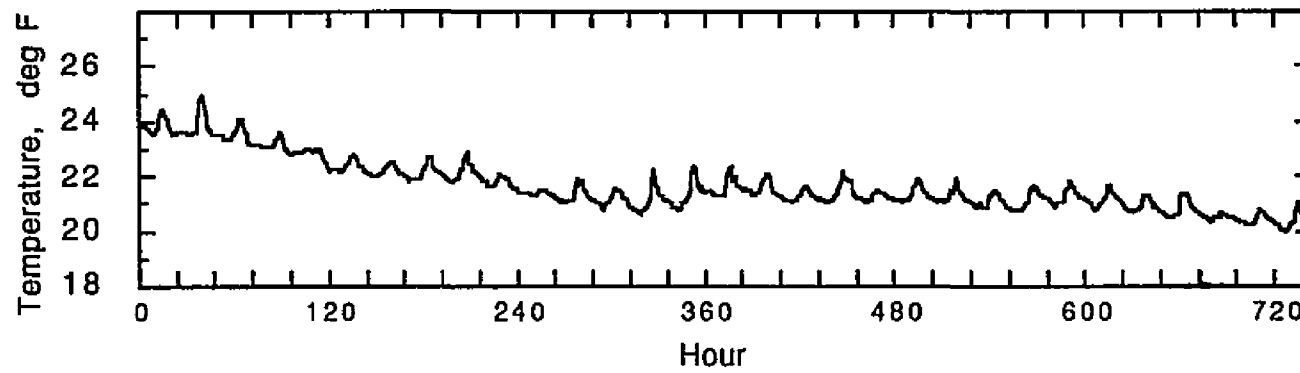


Figure 5.10 Temperature in the San Joaquin River at Stockton (Sep 15 to Oct 15,1988)

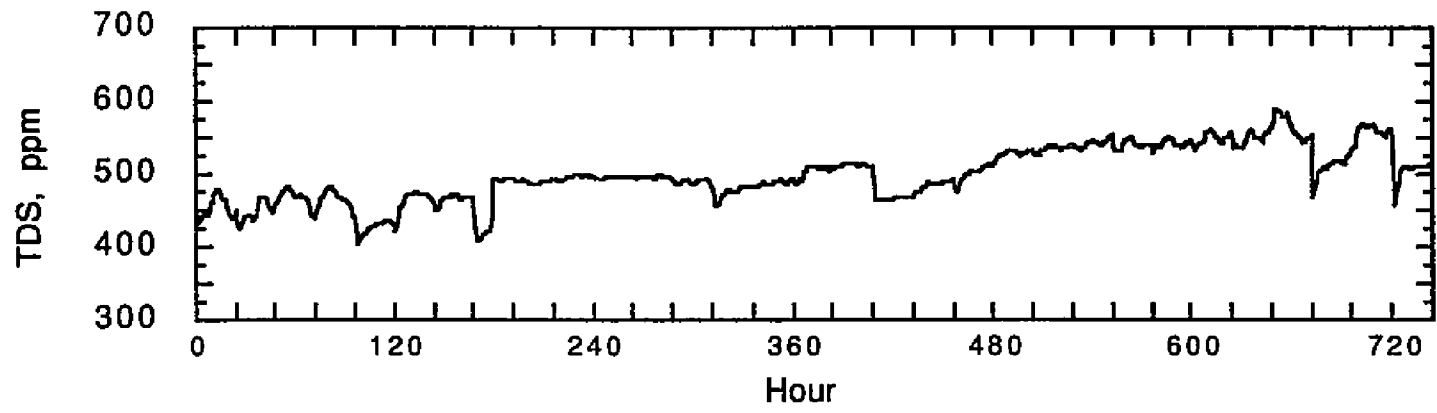


Figure 5.11 Total Dissolved Solids in the San Joaquin River at Stockton (Sep 15 to Oct 15,1988)

Estimates for DO, temperature and TDS concentrations for agricultural return flows were obtained by averaging the values corresponding to three sub-regions in the Delta for the particular months simulated (MWQI Data Request, 1995). These sub-regions were classified according to the distribution of dissolved organic carbon in the Delta. Since data on chlorophyll-a was not available at any stations for agricultural drainage within the Delta, it was set to a value corresponding to an average for the Sacramento and San Joaquin Rivers during the period of simulation. Although the new model allows specification of quality for agricultural drainage at each node (see "special features" in Chapter 4), only one set of data was used, irrespective of location, since no detailed data on drainage quality is available for the specified period. Data for agricultural quality are included in Tables 5.2 and 5.3 for September (calibration) and October (verification) simulations.

Hourly meteorological conditions for September 20 and October 12, 1988 were generated from climatological data at the Sacramento Executive Airport (NOAA, 1988). Plots of these data are shown in Figures 5.12 and 5.13 for September 20, 1988 to illustrate temporal variability.

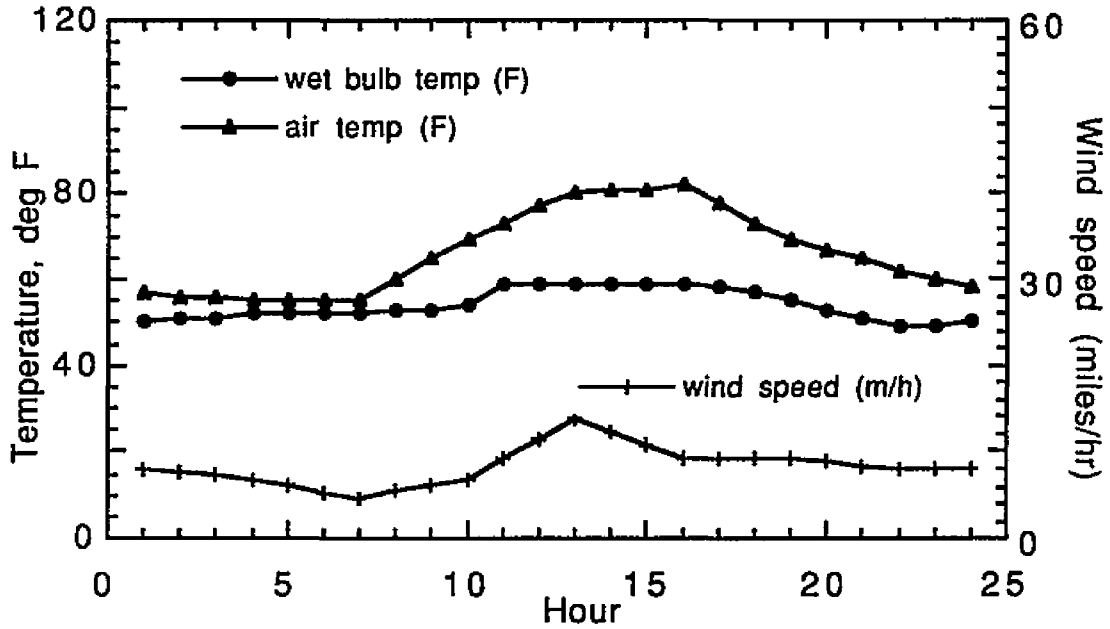


Figure 5.12 Weather Data, Sacramento (September 20, 1988)

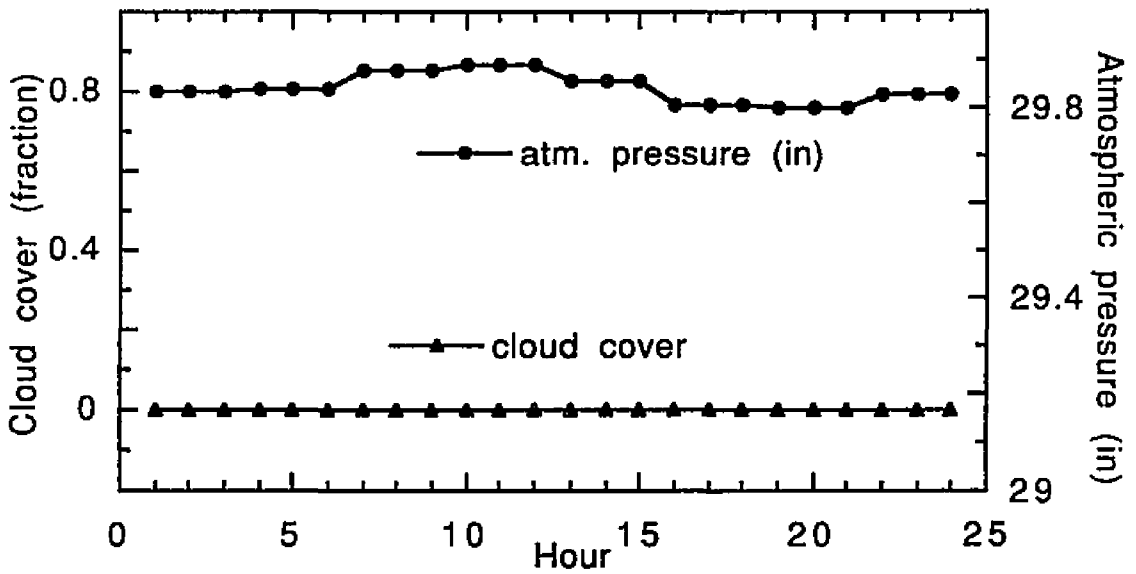


Figure 5.13 Cloud and Pressure Data, Sacramento (Sep 20, 1988)

5.3 Scenario 1: Calibration of the Model

Calibration of a numerical model refers to the process of adjustment so that model results reproduce actual system behavior. The extent to which this agreement may be achieved depends both upon the structure of the model and the amount of data available upon which to base calibration.

Hydrodynamics

This scenario represents conditions corresponding to September 20, 1988, when there was no barrier at the head of Old River. The actual tide at the Martinez boundary was adjusted so as to repeat each 25-hour period (Figure 5.14). With this tide imposed at the seaward boundary and using the freshwater inflows presented in Table 5.1, the DWRDSM Hydrodynamics Model was run until a state of dynamic equilibrium was achieved.

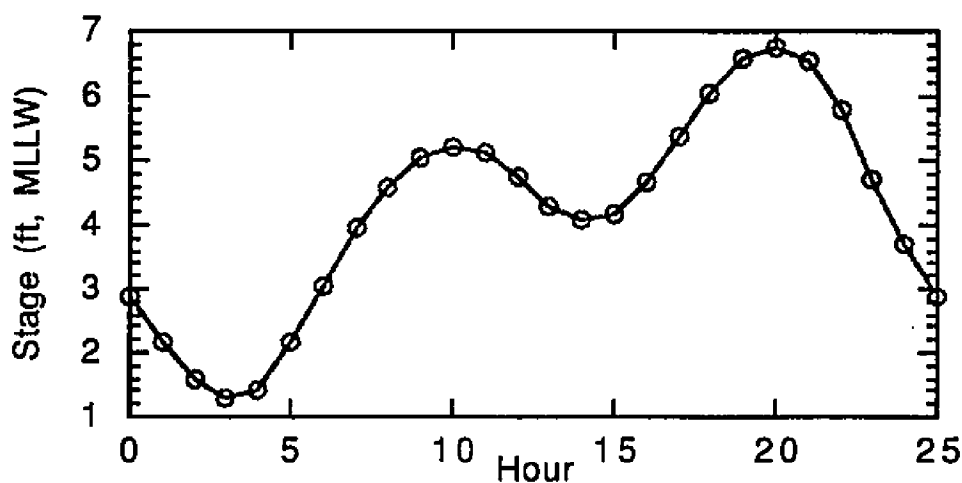


Figure 5.14 Tide at Martinez (Sep 20, 1988)

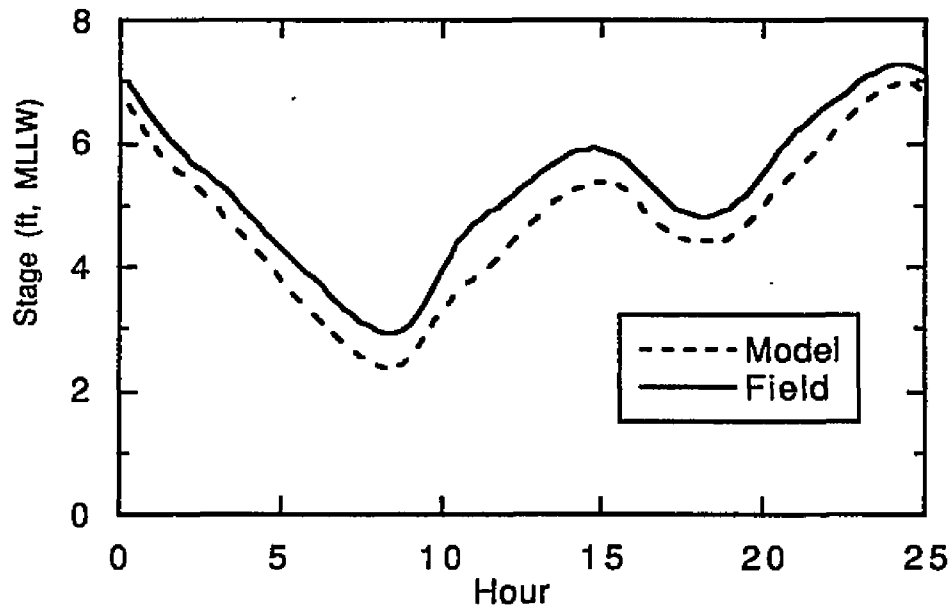


Figure 5.15 Comparison of Stage for Calibration Period (9/20/1988)
San Joaquin River near Stockton

Examination of simulation results at locations near Stockton indicated that the computed water stages compared well in phase with actual observations (Figure 5.15), but showed a consistently lower values in amplitude¹. Since the slopes matched well, it is believed that currents are accurately described by the model. The flow split (daily mean) at the head of Old River was simulated close to that actually observed during the time period simulated (see DWR, 1990A). Model results showed 83 percent of the flow entering Old

¹ This may be attributed in part to the neglect of baroclinic effects in the hydrodynamic model i.e. the influence of salinity at the seaward boundary will support the somewhat higher water elevation in the interior of the Delta indicated in Figure 5.15.

River, while only 17 percent (260 cfs) passed downstream in the San Joaquin River toward Stockton (Figure 5.16). Figures 5.17 and 5.18 are included to show the variation of channel widths and depths in the river. Channel depth is an important factor in the computation of mass transfer of oxygen by atmospheric reaeration, benthic oxygen demand as well as in the computation of light limitation factor for algal growth.

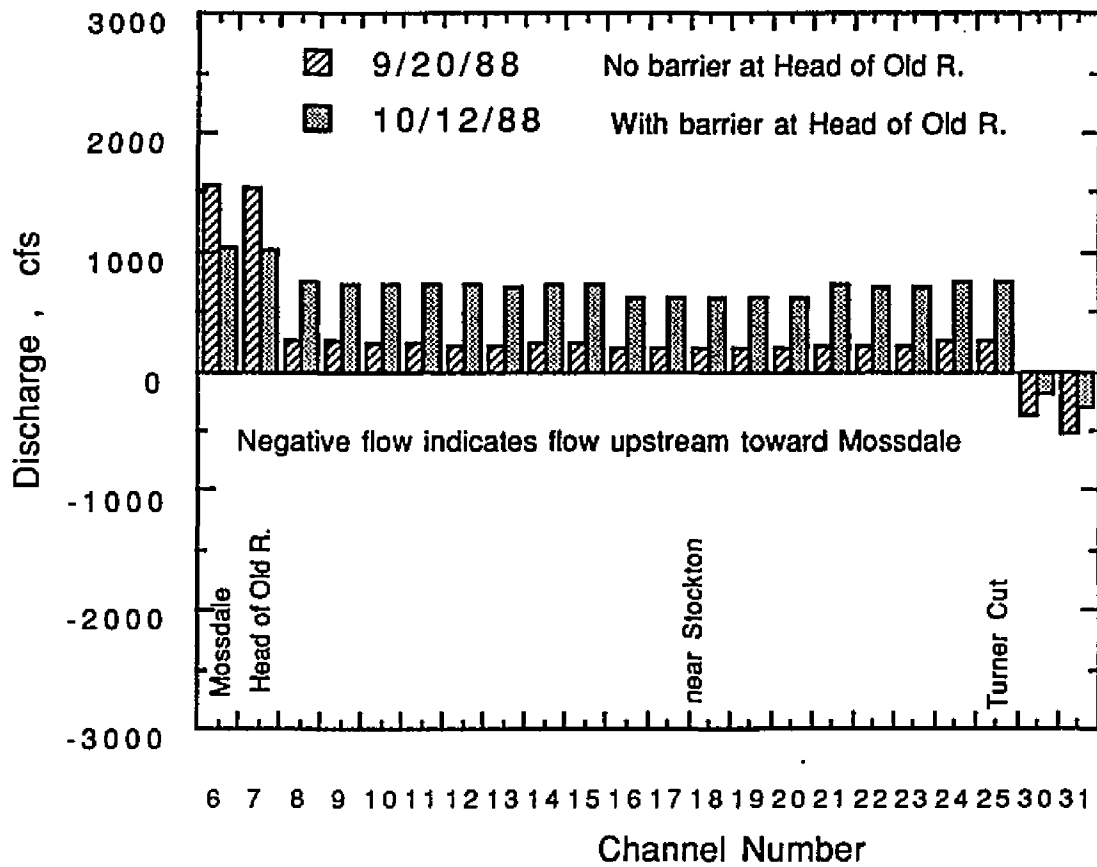


Figure 5.16 Tidal Day Average of Computed Flows (San Joaquin River)

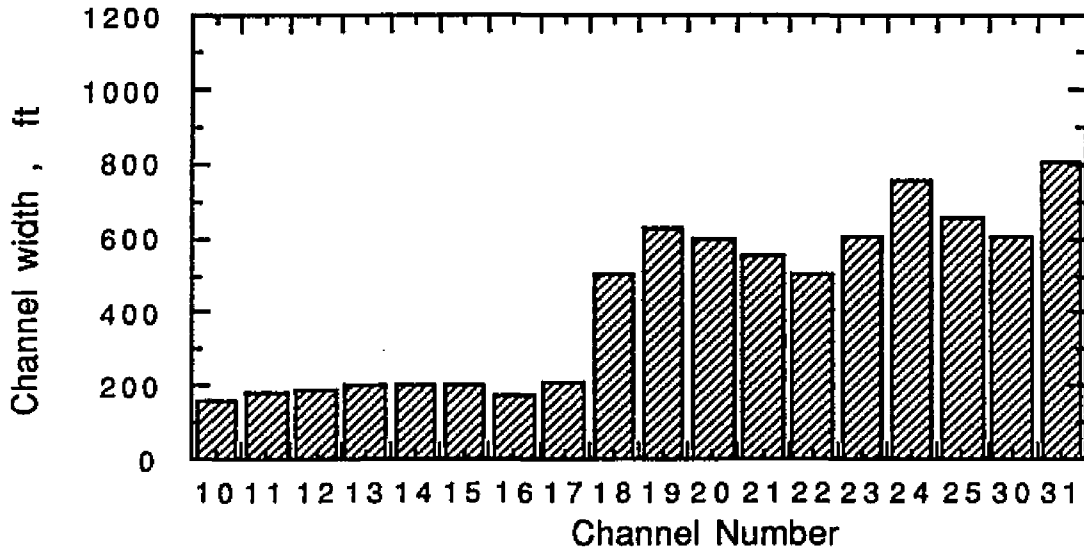


Figure 5.17 Variation of Channel Widths in the San Joaquin River

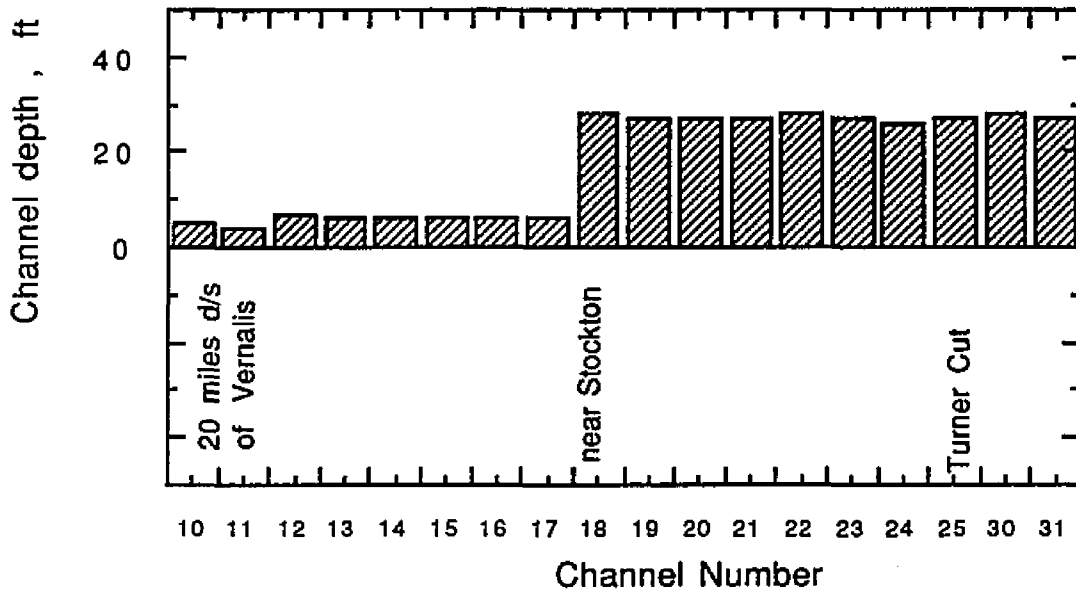


Figure 5.18 Variation of Channel Depths in the San Joaquin River

Water Quality

Site-specific calibration of the water quality model was focused on the region of San Joaquin River near the Stockton Ship Channel where relatively more water quality data were available. Using this region for model calibration also provided some unique opportunities to examine the local effects of Stockton's waste water effluent and the unique hydrodynamic conditions due to the placement of the Old River barrier. Initially, all rate coefficients were set either to intermediate values in the ranges suggested in the QUAL2E manual (Brown and Barnwell, 1987), or they were set based on previous modeling experiences in the Delta and other similar estuarine systems (Rajbhandari and Orlob, 1990, Smith, 1988, HydroQual, 1985). Detailed discussions on the sources of data, ranges and their reliabilities are given in Bowie et al. (1985). Table 5.6 shows the ranges of parameter values considered and the final calibrated values adopted for the model.

Temperature Calibration

Calibration started with comparison of diurnal variations of computed temperature against observed (hourly averaged) data at Rough and Ready Island near Stockton (Channel 20). Adjustments of dust attenuation and evaporation coefficients were made until reasonable agreement between the temperature patterns observed and simulated was obtained. These coefficients affect water temperatures by increasing or decreasing net short wave solar radiation input and heat energy losses due to evaporation, respectively. A comparison of simulated temperatures

Table 5.6 Typical Ranges and Assigned or Calibrated Values
for Reaction Coefficients

Global coefficients (with the FORTRAN variable names used in DSM2-QUAL) are listed below .

Variable		Range	Model
alph(5)	oxygen used in conversion of ammonia to nitrite	3.0-4.0	3.43
alph(6)	oxygen used in conversion of nitrite to nitrate	1.0-1.14	1.14
prefn	algal preference factor for ammonia	0-1.0	0.5
alph(7)	chlorophyll-a ($\mu\text{g/l}$) to biomass (mg/l) ratio	10-100	10
alph(1)	fraction of algal biomass which is nitrogen	0.07-0.09	0.08
alph(2)	fraction of algal biomass which is phosphorus	0.01-0.02	0.012
alph(3)	oxygen produced in photosynthesis	1.4-4.8	1.6
alph(4)	oxygen consumed with respiration	1.6-2.3	2.0
klght_half	half saturation constant for light ($\text{BTU}/\text{ft}^2\text{-min}$)	0.02-0.10	0.1
knit_half	half saturation constant for nitrogen (mg/l)	0.01-0.30	0.05
kpho_half	half saturation constant for phosphorus (mg/l)	0.001-0.05	0.003
xlam0	non-algal light extinction coefficient (ft^{-1})	variable	0.26
xlam1	linear algal self shading coefficient $\text{ft}^{-1}(\mu\text{g-Chl}a/\text{l})^{-1}$	0.002-0.02	0.003
xlam2	nonlinear algal self shading coefficient $\text{ft}^{-1}(\mu\text{g-Chl}a/\text{l})^{-2/3}$	0.0165	0.0165

Note: rates are in units per day except when specified.

Table 5.6 (contd.) Typical Ranges and Assigned or Calibrated Values for Reaction Coefficients

Location dependent coefficients are listed below with variable names used in the text (Chapter 4 and Appendix A). These coefficients are described by the array *rccoef* in the FORTRAN code.

Variable		Range	Model
k1	BOD decay rate	0.02-3.4	1.1
k3	BOD settling rate	-0.36-0.36	0.24
k4	benthic source rate for DO(g/m ² /day)	variable	see text
karb	decay rate for arbitrary non-cons. constituent	variable	
s6	settling rate for arbitrary non-cons. constituent	variable	
s7	benthic source rate for arbitrary non-cons. const.	variable	
mumax	maximum algal growth rate	1.0-3.0	1.5
resp	algal respiration rate	0.05-0.5	0.1
s1	algal settling rate	0.5-6.0	1.5
kn-org	organic nitrogen decay rate	0.02-0.4	0.1
s4	organic nitrogen settling rate	0.001-0.1	0.01
kn	ammonia decay rate	0.1-1.0	0.1
s3	benthic source rate for ammonia (mg/m ² /day)	variable	0.0
kni	nitrite decay rate	0.2-2.0	1.5
kp-org	organic phosphorus decay rate	0.01-0.7	0.1
s5	organic phosphorus settling rate	0.001-0.1	0.01
s2	benthic source rate for dissolved P(mg/m ² /day)	variable	0.0

Note: rates are in units per day except when specified.

against field observations is shown in Figure 5.19. The calibrated values (see Table 5.7) were within the range suggested in the literature (Brown and Barnwell, 1987; TVA, 1972). Note that 'a' and 'b' refer to coefficients in the Lake Hefner type relationship (equation A.26 in Appendix) used to calculate evaporation rate.

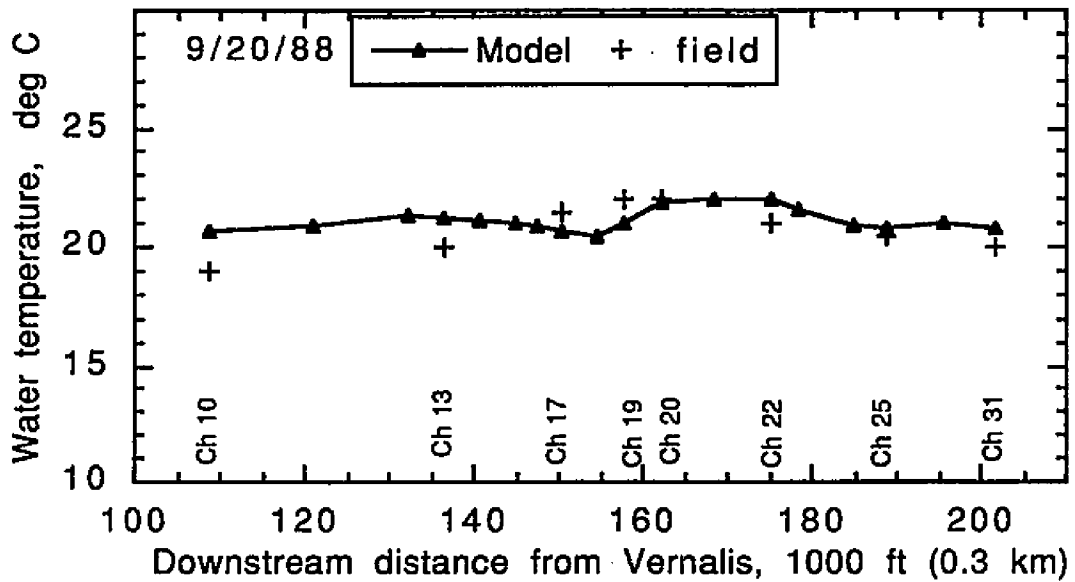


Figure 5.19 Calibration of Temperature

Table 5.7 Climatologic Coefficients used in Temperature Calibration

<u>Parameter</u>	<u>Acceptable Range</u>	<u>Calibrated Values</u>
'a' in ft/hr-in. of Hg.	0 - 0.00068	0.00021
'b' in ft/hr-in. of Hg.-mph	0 - 0.00027	0.00012
Dust Attenuation Coefficient	0 - 0.13	0.04

Dissolved Oxygen Calibration

Dissolved oxygen is the most important parameter of interest in the current study, consequently it was the primary subject of calibration. DO was generally observed to be at depressed levels, well below saturation, in the Stockton Ship Channel near the waste water outfall (DWR, 1990A), a condition that represented an excellent test for the model.

Calibration for DO often focuses on a trade off between the rates of reaeration and benthic oxygen demand (SOD), both of which have significant impacts on DO balance. Other processes such as photosynthetic oxygen production and chemical-biochemical oxidation also affect oxygen balance but have comparatively minor influences on DO balance in this case. Until the rates of reaeration or benthic demand can be explicitly measured or calculated either or both of the dominant processes (reaeration and benthic demand) are subject to adjustment to achieve acceptable calibration.

As noted earlier the O'Connor-Dobbins reaeration equation (eq. 4.11) was coded into the model. It computes a reaeration rate based on an instantaneous channel velocity and a depth of water derived from hydrodynamic simulation. In order to account for reaeration during very low velocity, slack tide conditions a minimum rate (as a function of depth) of $\frac{3.0}{d}$ per day, where d = average depth, ft., was adopted. This is based on the suggested minimum value in the literature (Hydroscience (1971) as reported by Thomann and Mueller, 1987)

In the calibration exercise there was generally more latitude for adjustment in DO by varying benthic demands, although these were only varied spatially, not temporally. In areas near the effluent outfall site, sediment oxygen demand is expected to be higher because deposits of settleable organic solids tend to build up over time, especially due to historically poor circulation of water in the area, most notable during extended droughts. The demand is likely to be further augmented due to the decaying of dead algae that settles out of the water column during algal blooms that normally occur in the area during this period. During the calibration process various values of the benthic oxygen demand were tried based on the suggested range of 2.0-10.0 g/m²-day (Thomann, 1972).

After more than a dozen or so simulations, adjustments of parameters, and examination of DO profiles from the downstream end of channel 10 (approximately 20 miles downstream of Vernalis) to channel 31 (approximately 38 miles downstream of Vernalis), model results were found to be in good agreement with field data. Computed dissolved oxygen concentrations, compared to field data, are presented in Figure 5.20; these are further discussed in the section "verification of the model." The fully calibrated model uses benthic oxygen demands of 1.6 g/m²-day for channels 1 through 9 and 4.9 g/m²-day from channels 10 through 20 (in the vicinity of the outfall). A uniform demand rate of 0.5 g/m²-day was assigned to the rest of the Delta.

Figure 5.21 shows the comparison of nitrate-nitrogen concentrations along the reach. Because the field data were

available only at weekly intervals, comparison of computed data was made with the monthly range for September, 1988. Nitrate is generally underestimated by the model due, most likely, to uncertainties in boundary values as well as agricultural drainage quality.

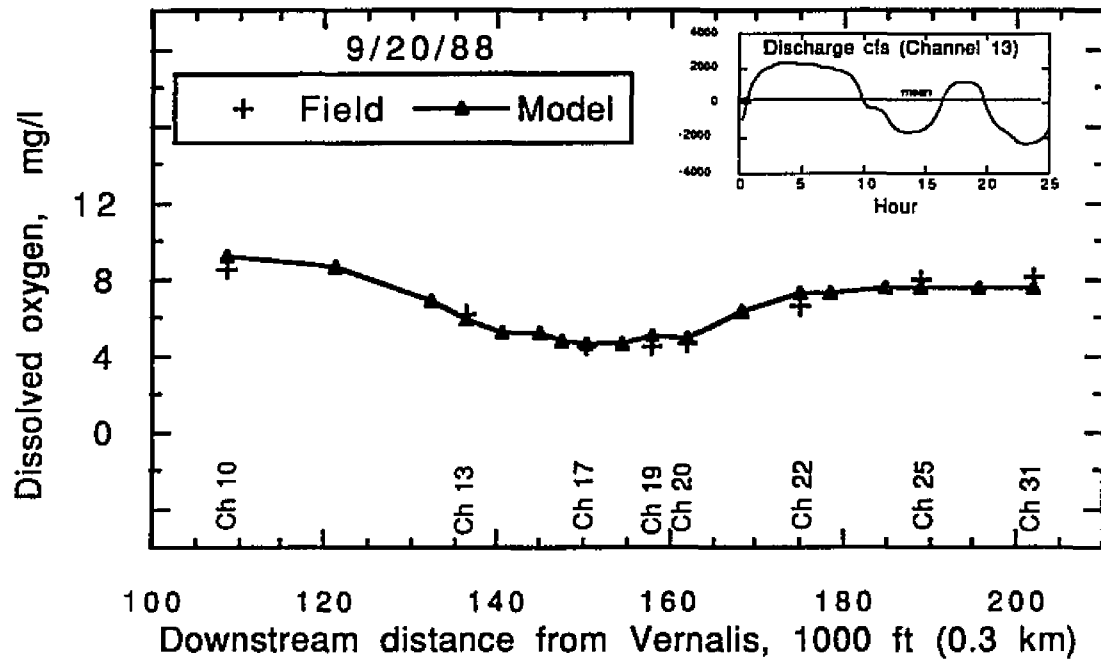


Figure 5.20 Calibration of Dissolved Oxygen

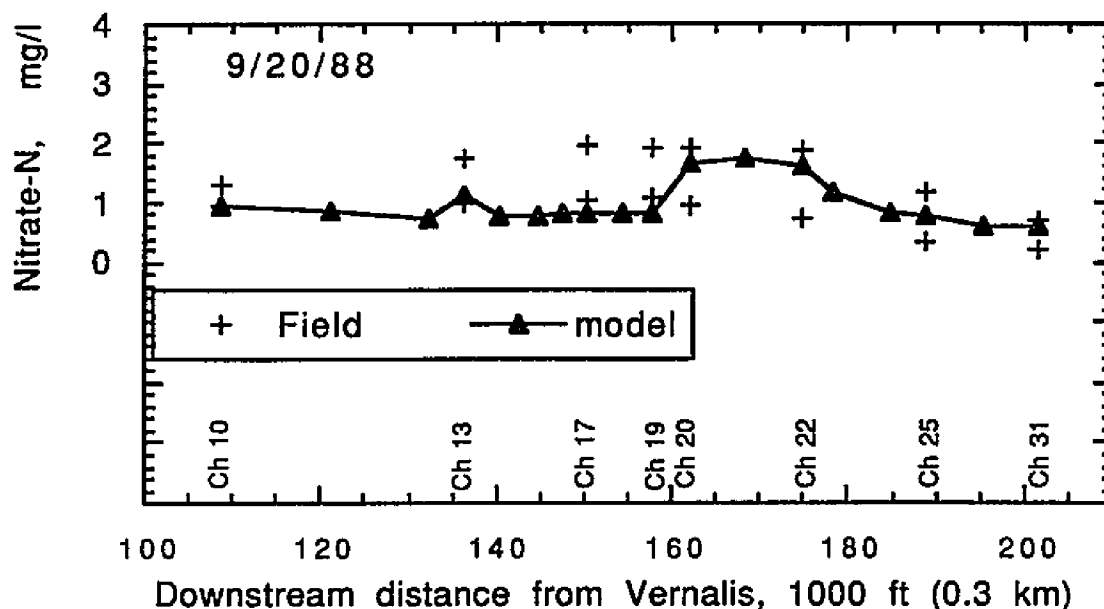


Figure 5.21 Observed and Simulated Nitrate-N (Sep 1988)

Additional coefficients used in calibration (which have not been previously mentioned) are maximum algal growth rate, algal settling rate, and dispersion factor. A somewhat smaller coefficient for maximum algal growth rate (1.5 per day, as shown in Table 5.6) seemed appropriate due to the fact that grazing by zooplankton is not considered in the formulation of algal growth equation. It could be a factor in reducing photosynthetic oxygen production, a possibility that remains to be examined in future investigations. Based on the limited available field data, several trial runs were made to match DO data with different dispersion factors. Application of a uniform dispersion factor of 0.1 in the San Joaquin River near Stockton produced most realistic results, and hence it

was adopted for the model. This is equivalent to a dispersion coefficient of 90 ft²/s when velocities are 1 ft/s.

Since data on phytoplankton biomass (chlorophyll-a) was poorly distributed both in time and space, algae biomass was not directly calibrated, although some adjustments were achieved indirectly while calibrating for DO. It seems pertinent here to explain how the rate for non-algal light extinction coefficient (λ_0) was derived.

The equation for the light extinction coefficient (equation A.8 in Appendix A) is reproduced here for ease of reference.

$$\lambda = \lambda_0 + \lambda_1 \alpha_7 [A] + \lambda_2 (\alpha_7 [A])^{2/3} \quad (\text{A.8})$$

Values for algal self-shading coefficients were assigned, according to the ranges suggested in QUAL2E manual (see Table 5.6), which are,

$$\begin{aligned} \lambda_1 &= 0.003 \text{ ft}^{-1} (\mu\text{g-Chl}a/l)^{-1} \\ \lambda_2 &= 0.0165 \text{ ft}^{-1} (\mu\text{g-Chl}a/l)^{-2/3} \end{aligned}$$

However, no specific value was available for λ_0 , apparently because it varies depending upon the system being modeled. An alternative approach is to estimate λ_0 using secchi disc observations. For this case secchi depth (z_s) of 5 ft. was assumed for the region of the Delta near Stockton (based on scattered readings, available in the report by DWR, 1990B). Thomann and Mueller (1987) estimate λ as a function of z_s as

$$\lambda = x/z_s$$

where $x = 1.7-1.9$

Assuming $x = 1.8$ and $z_s = 5$, we obtain

$$\lambda = 1.8/5 = 0.36 \text{ per ft.}$$

Assuming algal biomass [A] of 1 mg/l, chlorophyll to biomass ratio (α_7) of 10, and substituting values for λ , λ_1 and λ_2 in eq. 4.38, we obtain

$$\lambda_0 = 0.26 \text{ per ft.}$$

This value was used in the model. But note that λ itself (see equation A.8 in Appendix A) is not a constant. It varies both temporally and spatially dependent upon the instantaneous value of algal biomass determined by the model.

Figures 5.22 and 5.23 present computed profiles of chlorophyll-a and ortho-phosphate of the reach for the simulation period. In these plots, field data at only one station (P8, see Figure 5.2 for its location) were available for comparison, and hence, it is difficult to draw reasonable conclusions. However, good matching of both chlorophyll-a and ortho-phosphate data for the single site available is encouraging.

5.4 Scenario 2: Verification of the Model

In this simulation calibration coefficients previously established remain unaltered. This allows us to examine how well the model can simulate hydrodynamic and water quality conditions different

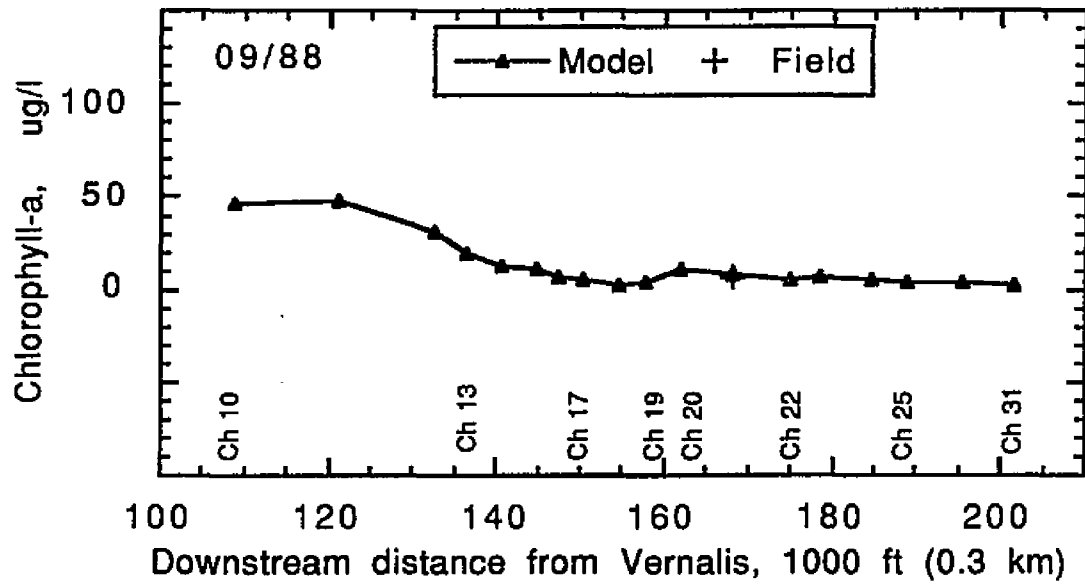


Figure 5.22 Observed and Simulated Chlorophyll-a (Sep 1988)

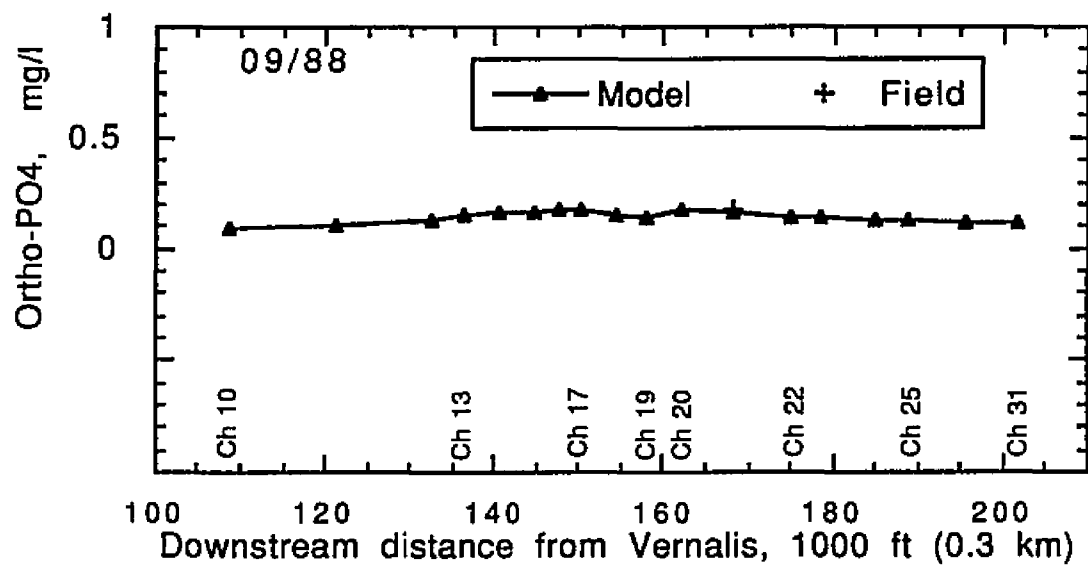


Figure 5.23 Observed and Simulated Ortho-phosphate (Sep 1988)

from those of the calibration period, a measure of the model's reliability as a simulation tool.

Hydrodynamics

Following calibration, the model was set up to simulate water quality for October 12, 1988. Prior to this date, a rock barrier was put in place at the head of Old River. As in the calibration run, the actual tide at the Martinez boundary for this date was adjusted so as to repeat after 25 hours. With this tide imposed at the seaward boundary (Figure 5.24) and using the freshwater inflows presented in Table 5.1, the DWRDSM Hydrodynamics Model was run until a state of dynamic equilibrium was achieved.

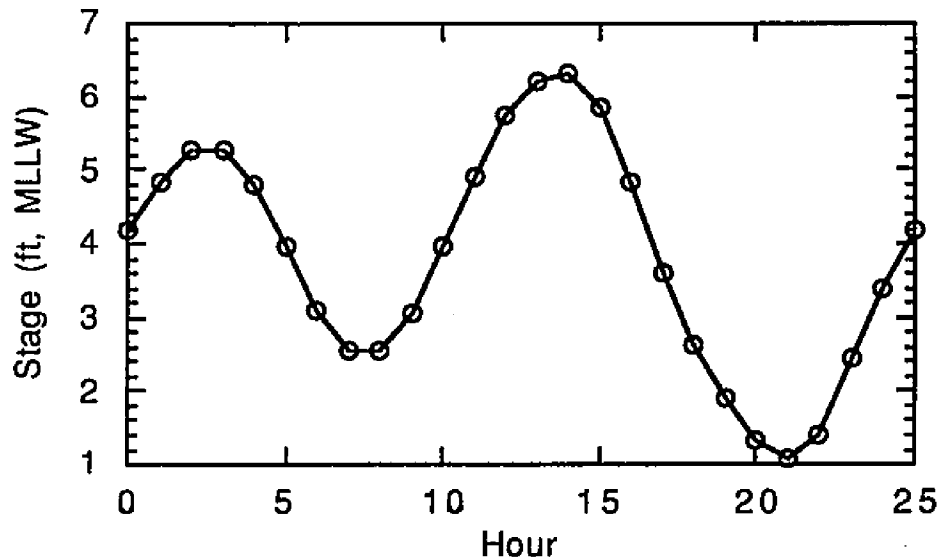


Figure 5.24 Tide at Martinez (Oct 12, 1988)

The flow split at the Old River Head computed by the model was found to be close to that actually observed during the same time period (see DWR, 1990A). Model results showed the flow split (daily mean) into Old River at its head to be 27 percent (280 cfs), with 73 percent (741 cfs) of the flow passing downstream in the San Joaquin River. This represents a nearly three-fold increase in the net downstream flow in the river over that of the September 20, 1988 calibration period (Figure 5.16). The comparison of computed stage with field data, shown for the San Joaquin River near Stockton, is good as shown in Figure 5.25. Because the slopes of water surface elevations for both field and model results match well, currents are considered accurately described by the model.

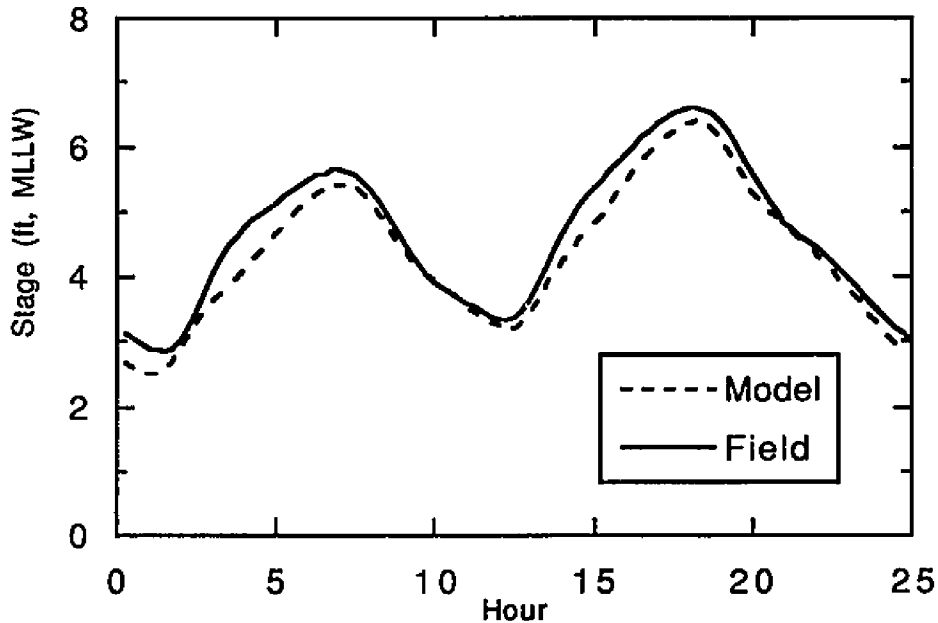


Figure 5.25 Comparison of Stage for Verification Period
San Joaquin River near Stockton

Water Quality Verification

A comparison of simulated temperature profiles against field observations is shown in Figure 5.26 for conditions representative of October 12, 1988. The comparison looks reasonable, considering the fact that two sets of climate data, one for calibration and one for verification period, were used for the entire simulated region. Note that data from the Sacramento Airport Station was used, due to lack of detailed data at Stockton Station, although the latter would have been more appropriate because of the focus on Stockton area in this evaluation.

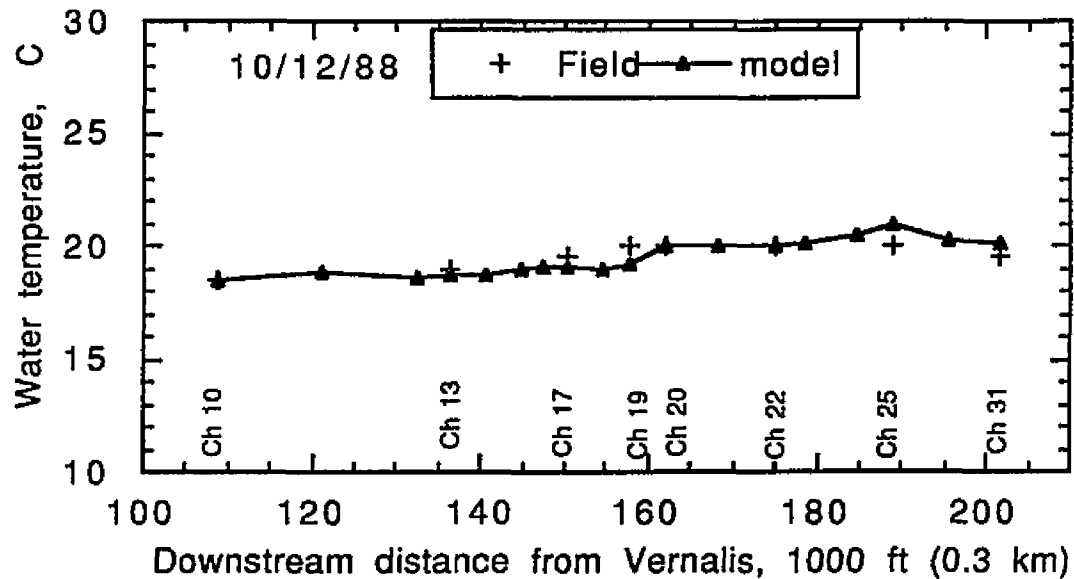


Figure 5.26 Verification of Temperature

Figure 5.27 represents the comparison of computed dissolved oxygen and field data for the verification runs. Model results agree very closely with field observations over the 18-mile (29-

Km) reach of the river, reproducing most features of the "oxygen sag" in both cases. Especially notable between the two runs is the displacement of the sag downstream due to the increase in net downstream flow (the verification case compared to the calibration case) and the increase in the DO sag minimum, due apparently to improved reaeration and dispersion along the channel.

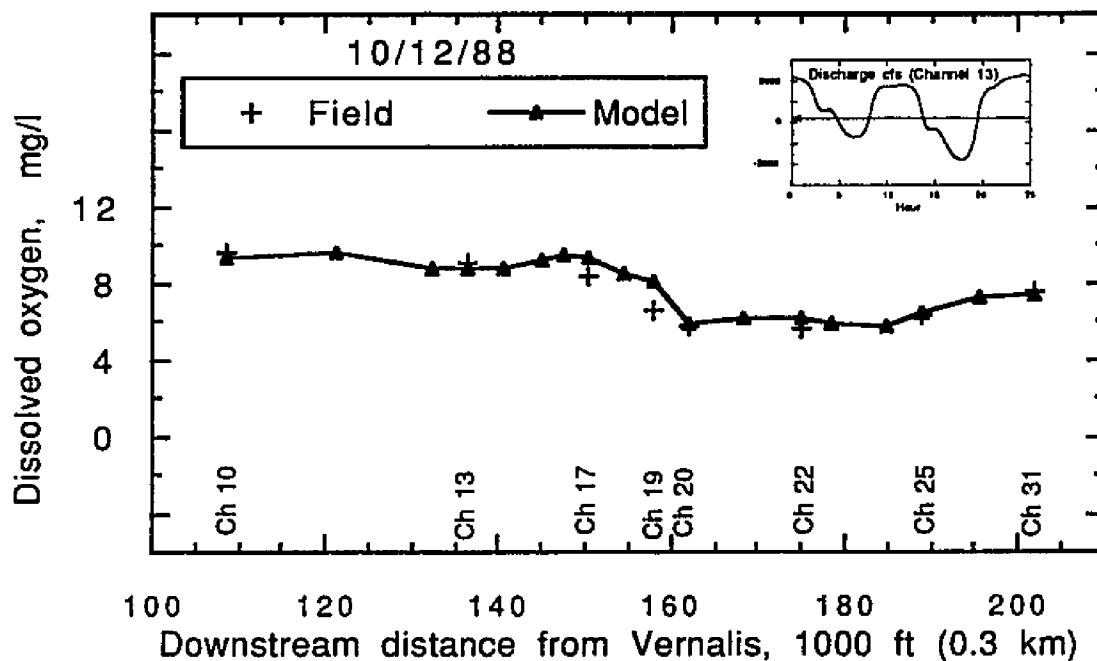


Figure 5.27 Verification of Dissolved Oxygen

Figure 5.28 shows the profiles of nitrate-nitrogen during the October simulation period. Ranges of observed data for the month of October, 1988 (measured at weekly intervals) are shown for comparison. Nitrate is somewhat better estimated by the model, in this case, compared to the calibration scenario. Future

modeling efforts, combined with improved database for calibration, are expected to improve nitrate simulation capability.

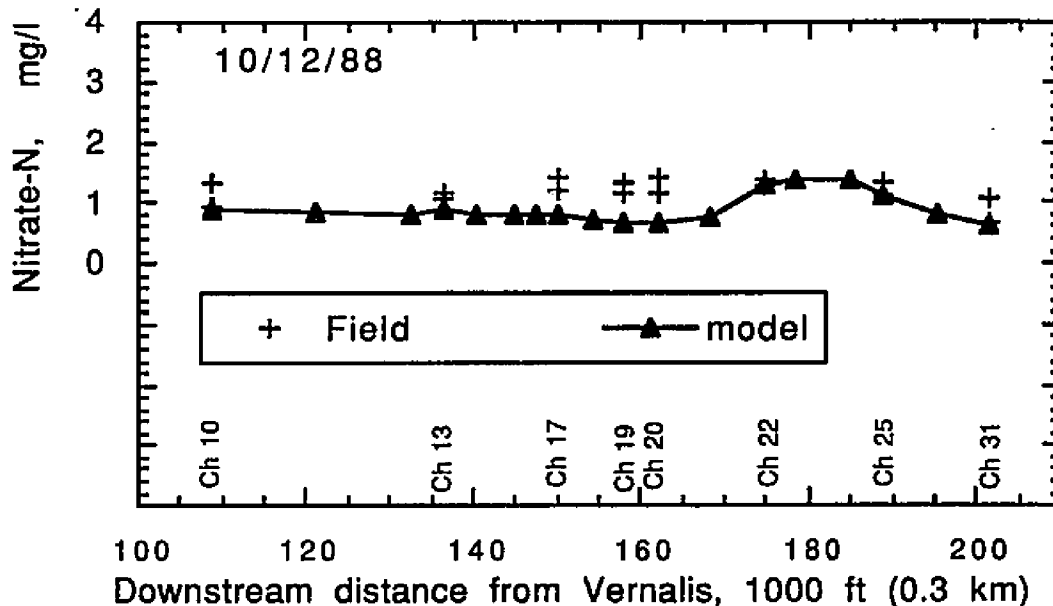


Figure 5.28 Observed and Simulated Nitrate Nitrogen (Oct 1988)

Figures 5.29 and 5.30 present computed profiles of chlorophyll-a and ortho-phosphate of the reach for the verification period. As in the calibration case, field data are sparse. For the site where data are available comparison for both the constituents seems reasonable.

Profile plots of ammonia, organic nitrogen, nitrite nitrogen, BOD and organic phosphorus are not included because of data inadequacy at boundaries (for model input) as well as at these sites.

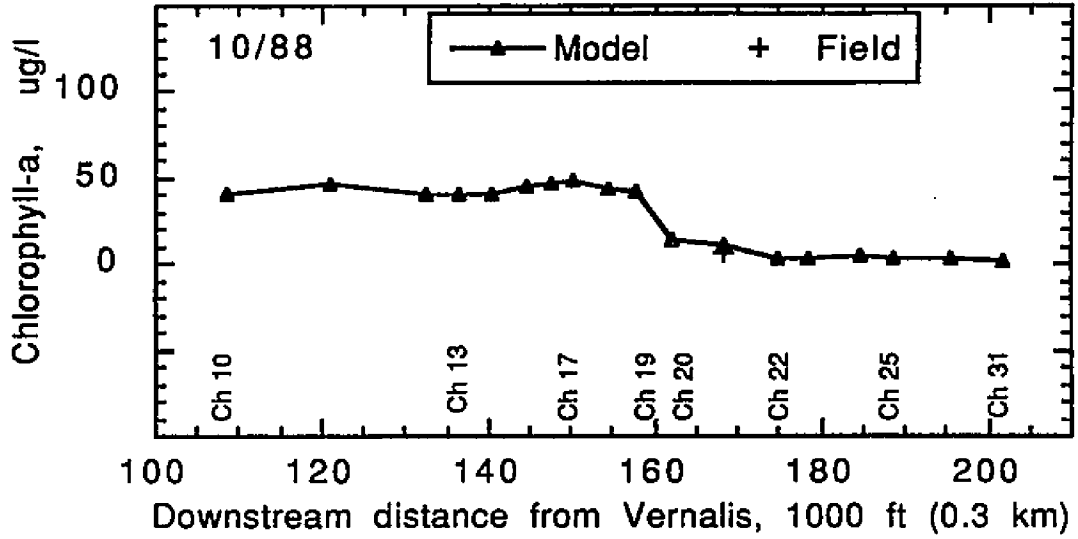


Figure 5.29 Observed and Simulated Chlorophyll-a (Oct 1988)

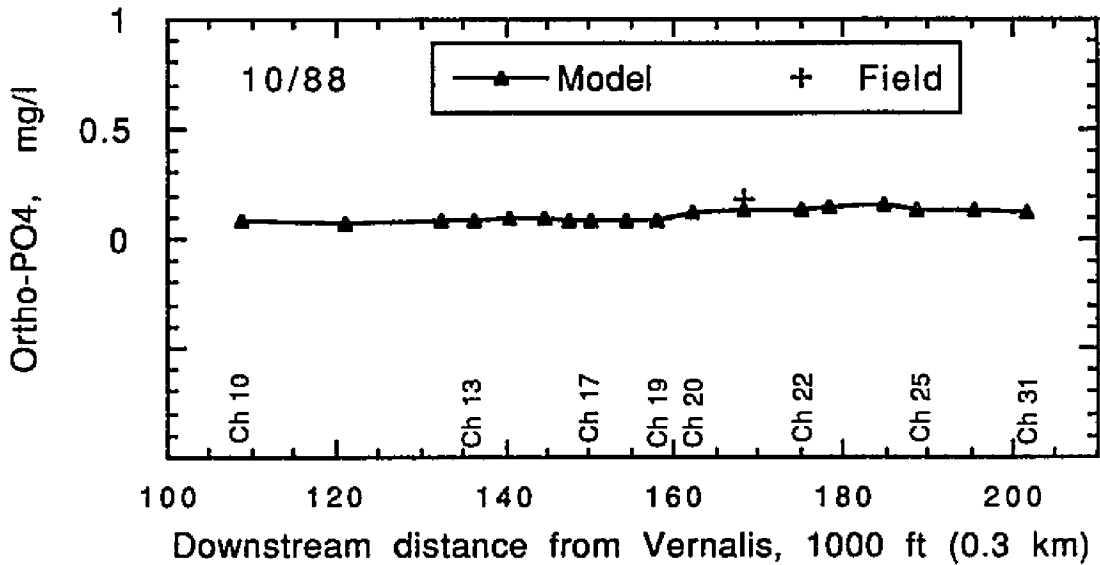


Figure 5.30 Observed and Simulated Ortho-phosphate (Oct1988)

5.5 Diurnal Variations in Water Quality

Diurnal variation of dissolved oxygen is important because it informs us about how low or how high DO levels can get during certain hours of the daily cycle. This variation can be particularly significant when algae biomass is present in high concentrations in the water. Figures 5.31 through 5.37 show diurnal variations of selected quality variables at a station near Stockton (Channel 17) for the September 1988 scenario.

The chlorophyll pattern shown in Figure 5.31 is typical of what would be expected on a clear day. The sinusoidal pattern seen for afternoon hours shows that the influence of solar radiation peaks during early afternoon (for an illustration of the diurnal pattern of short and long wave radiation, see Figure 5.38). DO concentrations, shown in Figure 5.32, exhibit a similar trend in concentration variations with elevated levels during the afternoon. This pattern reflects the effect of the increase in photosynthetic oxygen production during afternoon hours. Increased chlorophyll-a levels in the system also indicate elevated algae biomass that can rapidly deplete nutrients in the system which, in turn, could increase oxygen production in day time and reduce DO at night. Hourly variations of ammonia and nitrate nitrogen concentrations (see Figures 5.33 and 5.34) show gradual depression during the hours that correspond to rising chlorophyll-a levels, most likely resulting from the increased uptake rates of nitrogen to maintain cell growth. A similar trend is exhibited by the diurnal pattern of inorganic phosphorus (ortho-

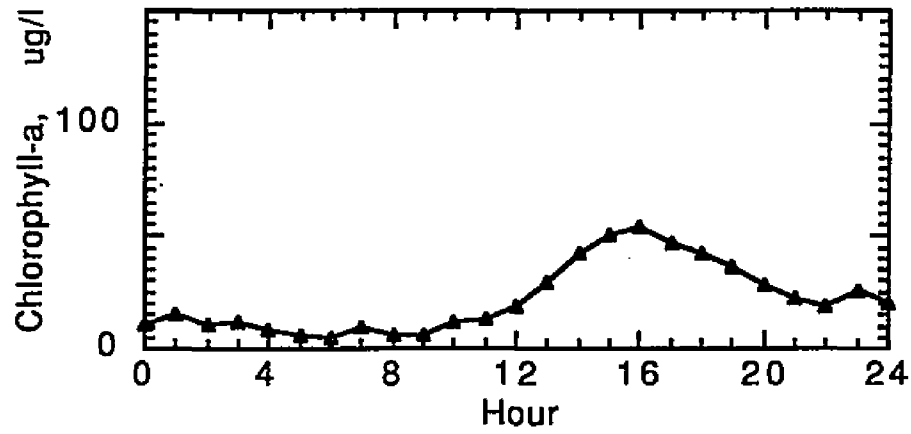


Figure 5.31 Computed Hourly Variation of Chlorophyll-a (Channel 17)

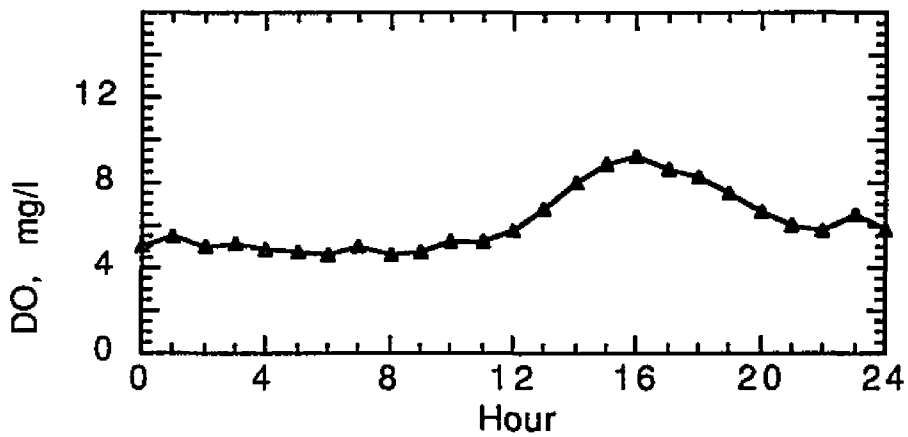


Figure 5.32 Computed Hourly Variation of Dissolved Oxygen (Channel 17)

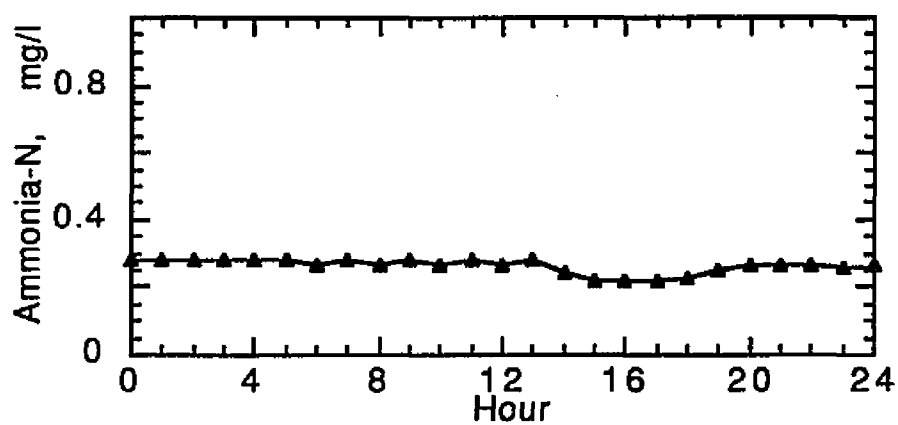


Figure 5.33 Computed Hourly Variation of Ammonia-N (Channel 17)

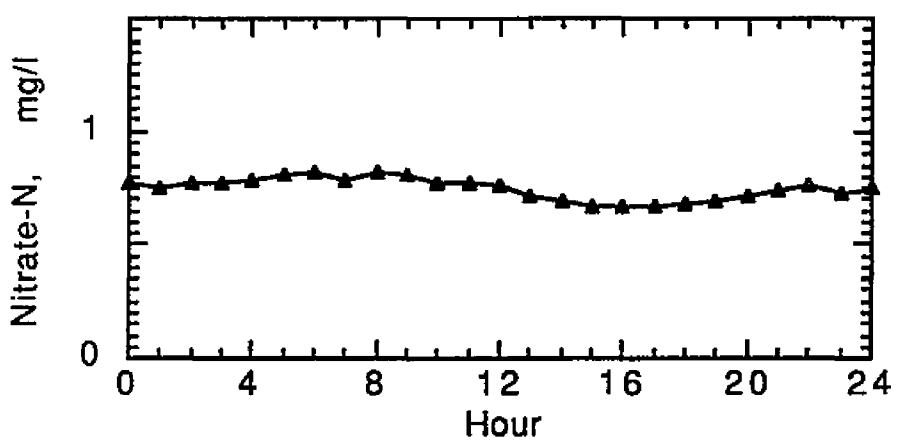


Figure 5.34 Computed Hourly Variation of Nitrate-N (Channel 17)

phosphate) as shown in Figure 5.35. The fall in phosphate concentrations results from the increased phosphorus uptake during growth.

Figure 5.36 shows computed organic nitrogen concentrations over a 24 hour period. The rise and fall pattern follows that of chlorophyll-a resulting from the increased release of algal cells during respiration. The hourly variation of computed temperature is shown in Figure 5.37. Note that all the mass transformation processes, described above, are dependent on temperature (represented by eq. 4.17), and hence implicitly include the effect of temperature variation.

In summary, the variation patterns of the constituents during the 24-hour cycle seem consistent with the model structure that represents their relationship (shown in Figure 4.2). This observation adds credibility to the capability of the new model in reproducing the dynamic variations of the modeled constituents. Overall, the results of calibration and verification runs lend support to the apparent capability of the model to represent the important water quality processes in a complex estuarine system like that of the Delta.

5.6 Sensitivity Analysis

It is important to recognize that the calibration and verification exercises include some uncertainties in the selection of specific coefficients and parameters, as well as boundary conditions. To

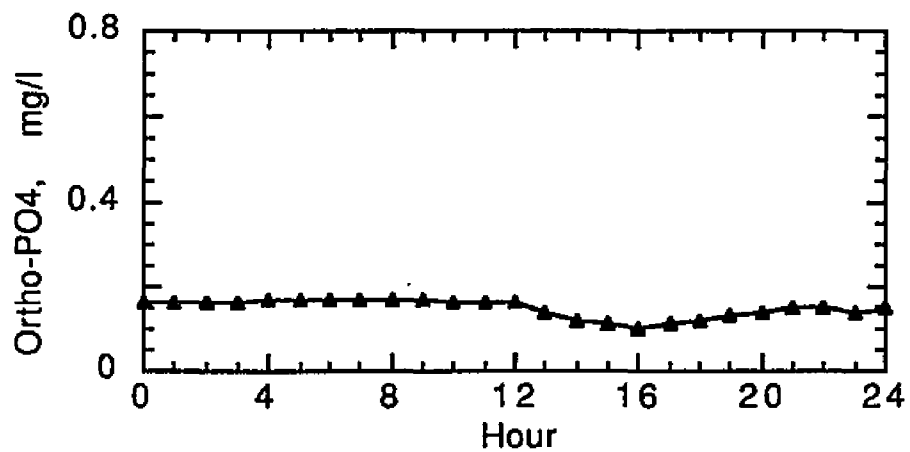


Figure 5.35 Computed Hourly Variation of Ortho-phosphate (Channel 17)

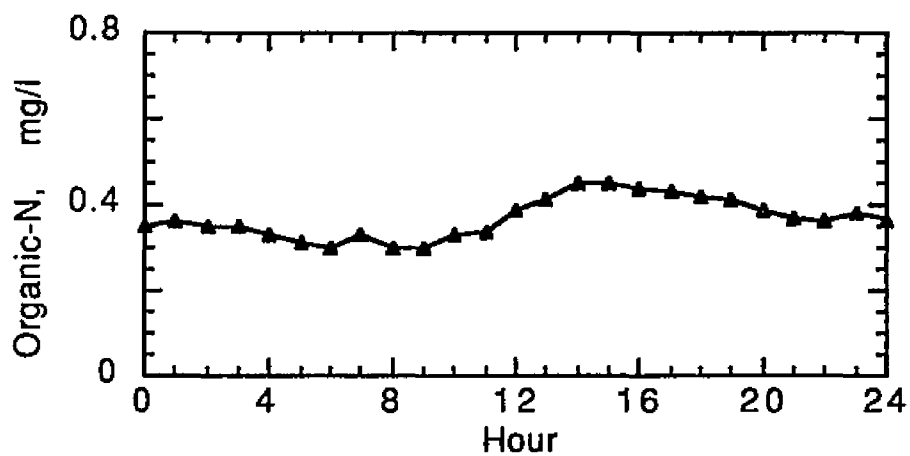


Figure 5.36 Computed Hourly Variation of Organic Nitrogen (Channel 17)

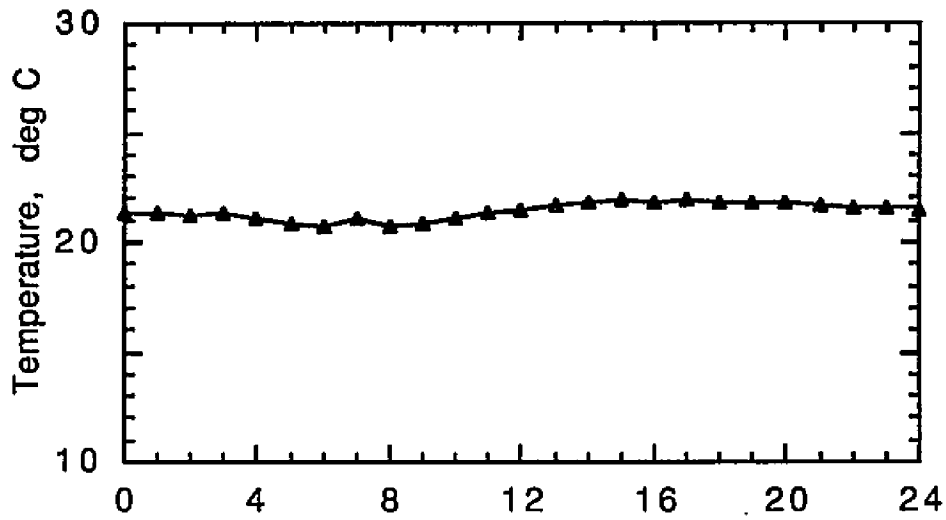


Figure 5.37 Computed Hourly Variation of Temperature (Channel 17)

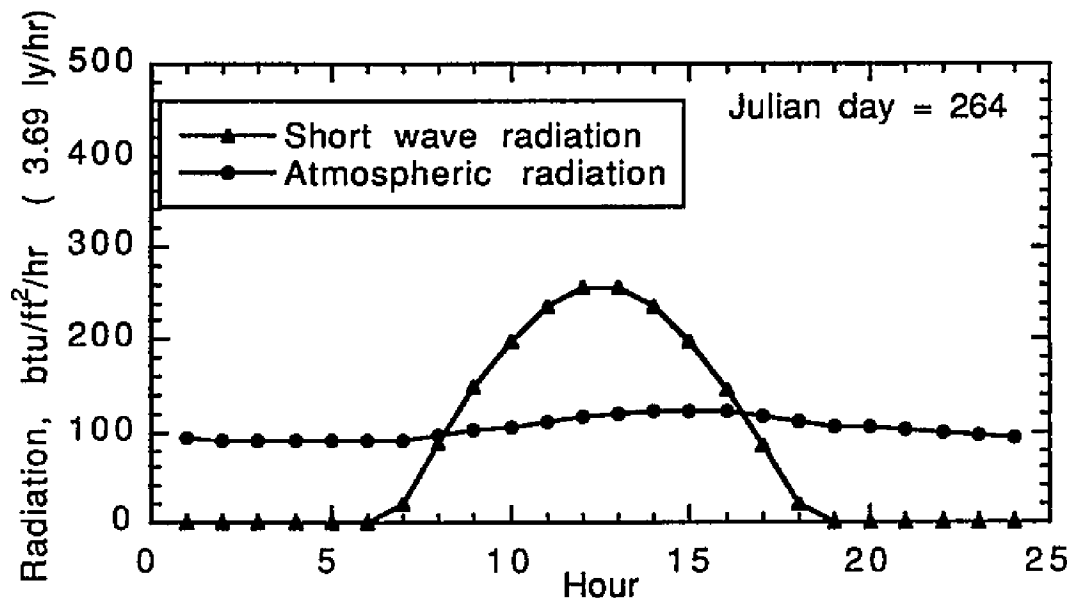


Figure 5.38 Computed Solar and Atmospheric Radiation (based on Sacramento weather data Sep 20, 1988)

assess the relative importance of certain variable quantities it is desirable to perform sensitivity analysis where changes in the primary response variables are related to changes in parameter and coefficients that must be elected by the model user. For this purpose series of simulation runs were made to examine response of San Joaquin River water quality to changes in effluent loading and climate conditions. As designed, these cases give some preliminary information on model sensitivity, as well as incremental effects induced by the changes between test cases, although they do not constitute comprehensive sensitivity testing in a formal sense. Such testing will be a subject for future investigation with the model, along with improved design of field data collection programs to support continued evaluation and updating of the model.

The following test cases were simulated:

1. Stockton effluent discharged at a rate of 20.4 million gallons per day (MGD), in September 1988. Water quality in the river set at that of September 20, when available; see Table 5.2. This run, identified as the "base" case in the plots that follow, is identical to the run used for calibration.
2. Stockton effluent discharge increased to 65 MGD (projected discharge estimate for ten years in the future, as proposed by the firm of Parsons ES, 1995). This run is identified as 'st4' in the plots.
3. Climate conditions changed to those of July 1988

(monthly average values at 3-hour intervals). Vernalis boundary temperature of 24°C corresponding to the average for July 1988. All other conditions (hydrodynamics and water quality) were kept the same as in the base case. This run is identified as 'st6'.

4. The final scenario 'st7' corresponds to a combination of cases 2 and 3 above, representing high temperature conditions and increased effluent loading.

In these simulations initial conditions were kept at the same level as in the case of the base scenario.

Figures 5.12 and 5.39 show the hourly variations of dry and wet bulb temperatures, and wind speed in Sacramento for September 20, 1988 and July 1988 conditions. These values were interpolated from the

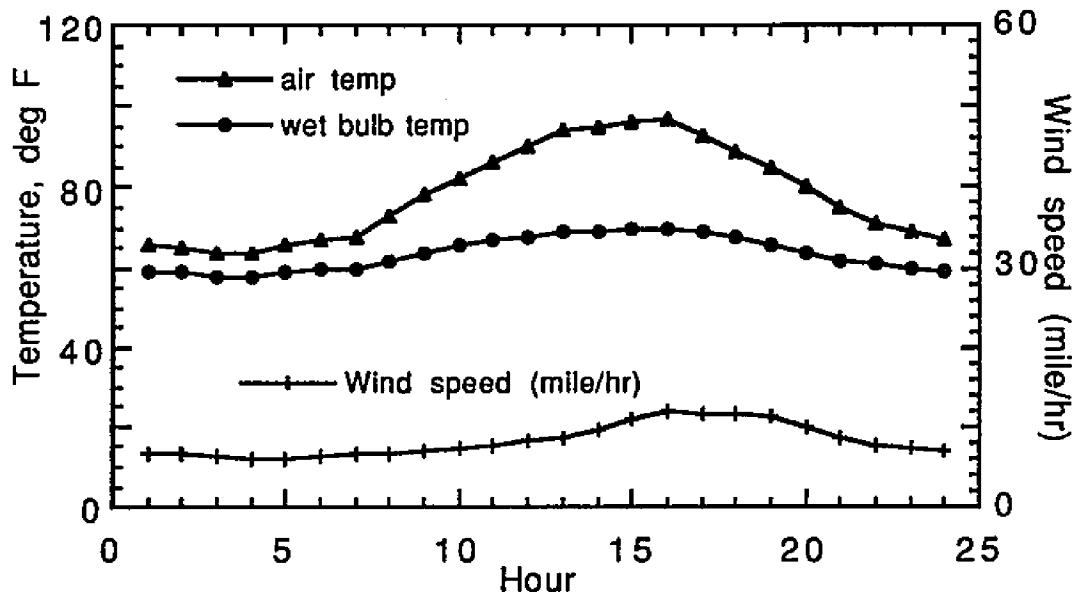


Figure 5.39 Weather Data, Sacramento
July 1988 (Monthly Average)

three-hourly values available for the Sacramento Executive Airport (NOAA, 1988). Plots showing distributions of cloud cover fractions and atmospheric pressures for these two periods of time are presented in Figures 5.13 and 5.40. Note that the plot for September 20 shows clear sky conditions. Using these climate data, the knowledge of the sun's position during these periods (based on the corresponding Julian dates), and the latitude and the longitude of the region, estimates for solar and atmospheric radiation are computed by the model. The plots of radiation based on these results are shown in Figures 5.38 and 5.41 for September 20 and July 1988 weather conditions respectively.

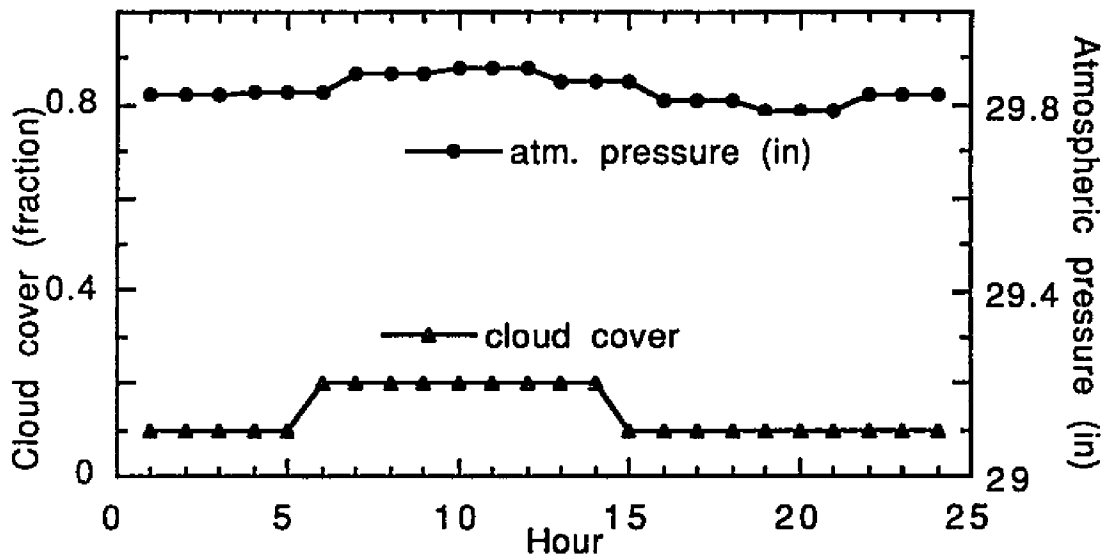


Figure 5.40 Cloud and Pressure Data, Sacramento July 1988 (Monthly Average)

Figures 5.42 through 5.44 represent a sample of results based on the four alternative scenarios described above. Simulation results indicate that within most of the eighteen-mile reach, dissolved

oxygen is brought down to lower concentrations by the higher effluent discharge (see Figure 5.42). This appears reasonable because the higher effluent discharge results in higher loadings of constituent masses in the river, including those of BOD and ammonia, both of which are major sinks of oxygen.

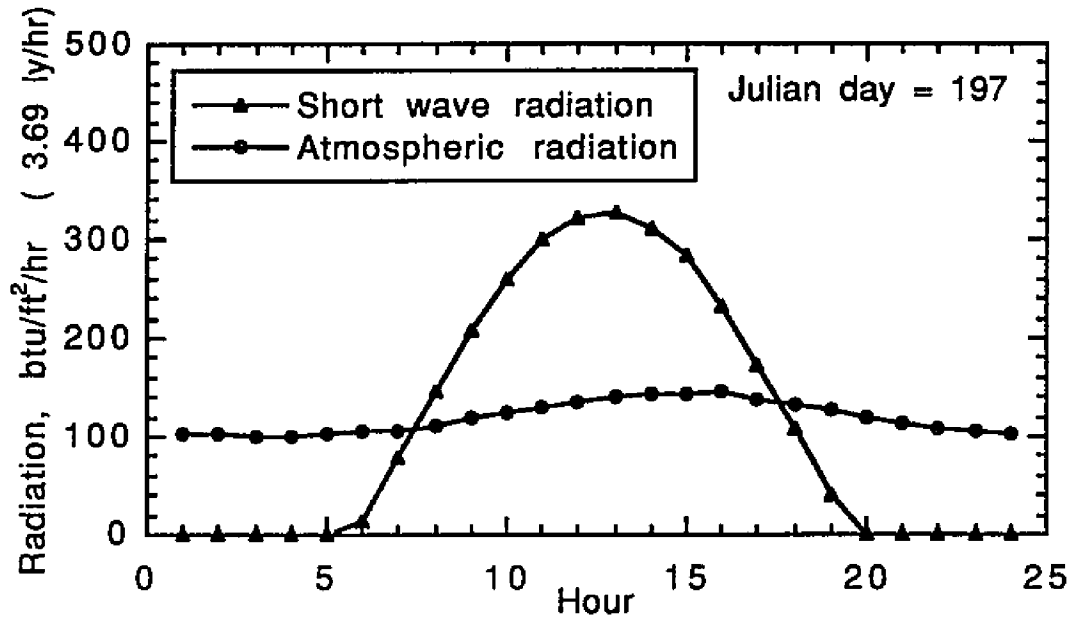


Figure 5.41 Computed Solar and Atmospheric Radiation based on Sacramento data, July (average) 1988

The effect of warmer climate on the DO profile (st6) is to increase DO in Channels 12, 13 and 14. It may be because of the increased production of photosynthetic oxygen in these locations marked by high algal productivity (see Figure 5.44). In contrast, along the San Joaquin River reach further downstream, which is characterized by the oxygen sag noted earlier, DO is brought down by the warmer reach conditions, as expected. Beyond Channel 20, however, the

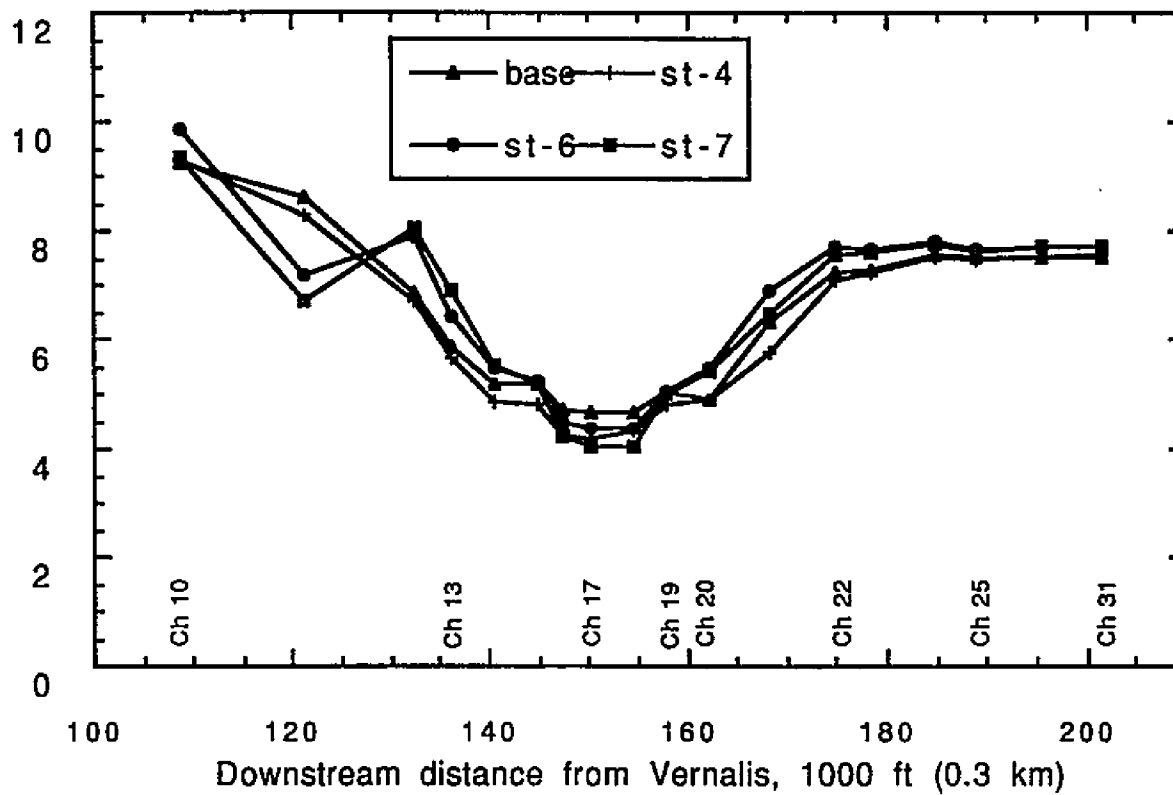


Figure 5.42 Response of River DO to Change in Climate and to Increase in Effluent Loading

effect is again to increase DO level apparently due, once again, to the influence of increased photosynthetic oxygen.

Figure 5.43 shows an overall increase in temperature of the river reach resulting from the change in weather conditions from fall to summer. There is no noticeable increase in the river temperature in the case of the increased effluent discharge (st4), because the effluent temperature (20°C) is comparable to the ambient water temperature (the difference is within a degree or two Celsius, as shown in Figure 5.19).

Similarly, there is an overall increase in primary production (represented by chlorophyll-a) of the river reach, induced by the change in weather to warmer conditions, as shown in Figure 5.44. Primary production is also higher along most of the reach for the case of higher effluent discharge.

Impact on Diurnal Variation of Water Quality

Figures 5.45 through 5.49 are presented to examine the effect of warmer conditions on diurnal variation in river water quality. Channel 17 near Stockton was chosen for illustration.

A rise in water temperature occurred throughout the daily cycle for July conditions, as expected (shown in Figure 5.45). The water temperature rise of 2.4°C to 3°C (that is, 4.3°F to 5.4°F) seems consistent with an air temperature difference ranging from 10 to 15 °F (see Figures 5.12 and 5.39) for the two time periods .

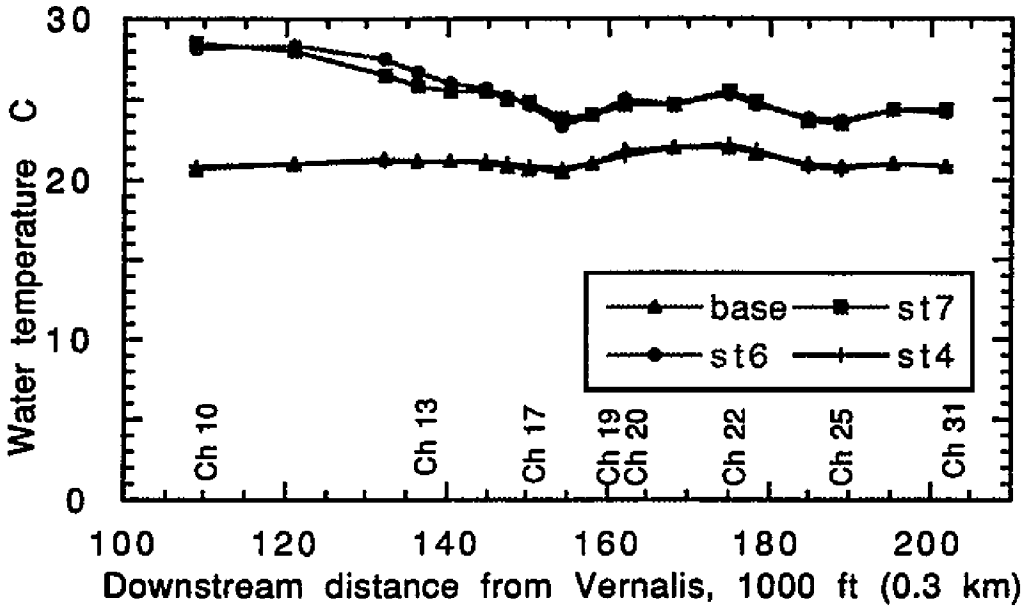


Figure 5.43 Response of River Temperature to Change in Climate and to Increase in Effluent Loading

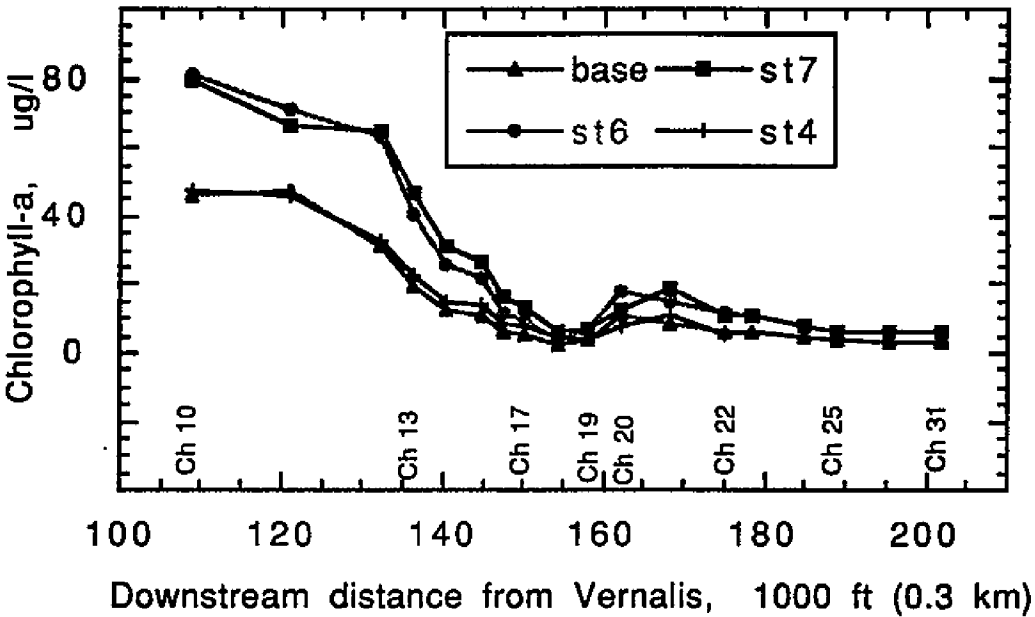


Figure 5.44 Response of River Chlorophyll-a to Change in Climate and to Increase in Effluent Loading

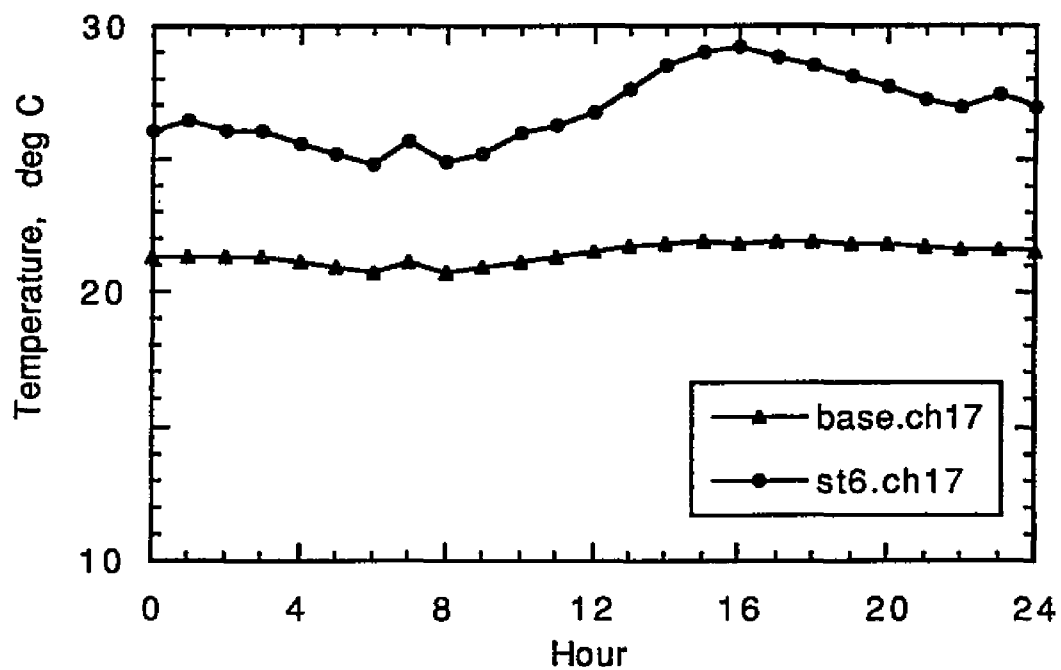


Figure 5.45 Computed Diurnal Temperature (Channel 17)
Two Climate Conditions

Comparison of diurnal patterns of chlorophyll-a (Figure 5.46) for July and September conditions reveals that the highest increase occurs during afternoon hours. Apparently, the increase in short wave solar radiation, which is a factor in the formulation of algal growth terms (see equation A.6 in Appendix A), contributes to this increase. This can be inferred from the plots of computed solar radiation shown in Figures 5.38 and 5.41. The effect of temperature on the rate coefficients (see eq. 4.17) of related constituents also contributes to this increase.

Computed levels of dissolved oxygen in a 24-hour period are shown in Figure 5.47. For the initial ten hours of simulation, representing the warmer climate conditions, DO tends to increase initially, but later it decreases to a value within about 0.5 mg/l of the September simulation results. This may be a result of a complex chain of effects which can be explained as due to the effect of increased temperature on rate coefficients, also affecting the decay/growth rates of all non-conservative constituents that are simulated. Since constituent concentrations vary in time, as does temperature as well, reaction rates will also vary in time. Consequently, due to the interdependent nature of constituent kinetics, concentrations may be affected differently at different points in time. At times, this leads to an overall increase and at other times to a net decrease.

The higher increase in DO levels during most of the afternoon hours, however, may have resulted from the dominant effect of a relatively

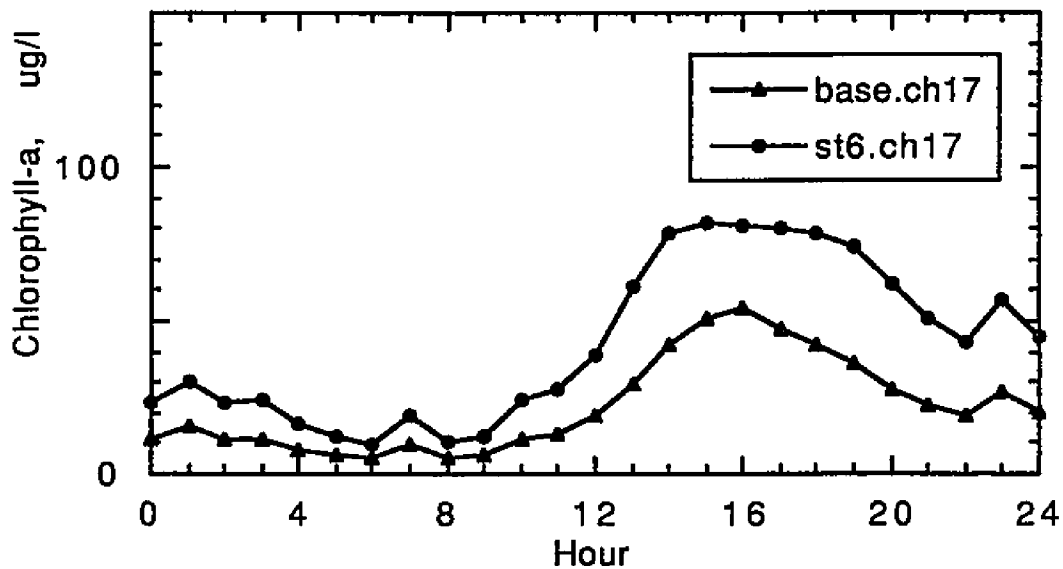


Figure 5.46 Computed Diurnal Chlorophyll-a (Channel 17)
Two Climate Conditions

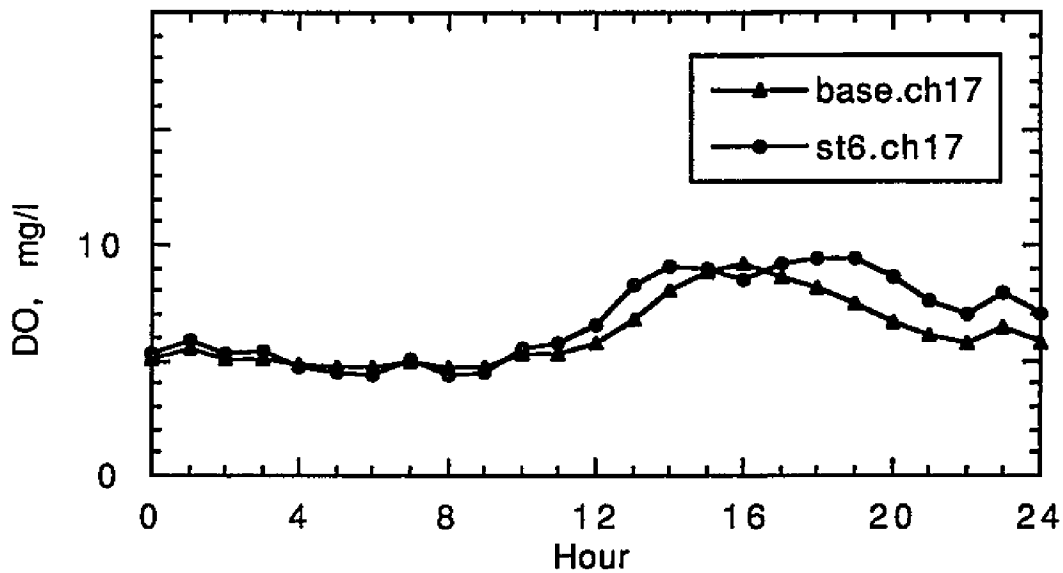


Figure 5.47 Computed Diurnal DO (Channel 17)
Two Climate Conditions

large increase in photosynthetic oxygen production during those hours for the July conditions of climate.

Figures 5.48 and 5.49 present a picture of nutrients in the specified location of the river, as they may vary during the day, for the two climatic scenarios. Concentrations of both nitrate and ammonia nitrogen are relatively depressed for the warmer scenario. While the smaller variations in concentration noted for the earlier hours of day can be explained in terms of the argument presented above for the case of dissolved oxygen, the relatively larger depression in nutrient levels for the later hours is apparently caused by the higher uptake rates of nutrients by algal biomass, greater for July conditions.

Simulated Water Quality in the Delta

Figures 5.50 through 5.54 present contour plots of selected constituents in the Delta for the September 20, 1988 scenario. Since this simulation was based on very sparsely available field data, except in the vicinity of Stockton, results are to be viewed mainly for illustrative purposes, and not to be considered quantitatively at locations remote from Stockton.

Contours of dissolved oxygen shown in Figure 5.50 include the oxygen sag near Stockton, while also showing spots of high DO at Old River near Tracy, apparently results of localized photosynthetic oxygen production (see Figure 5.52). Simulated DO concentrations in

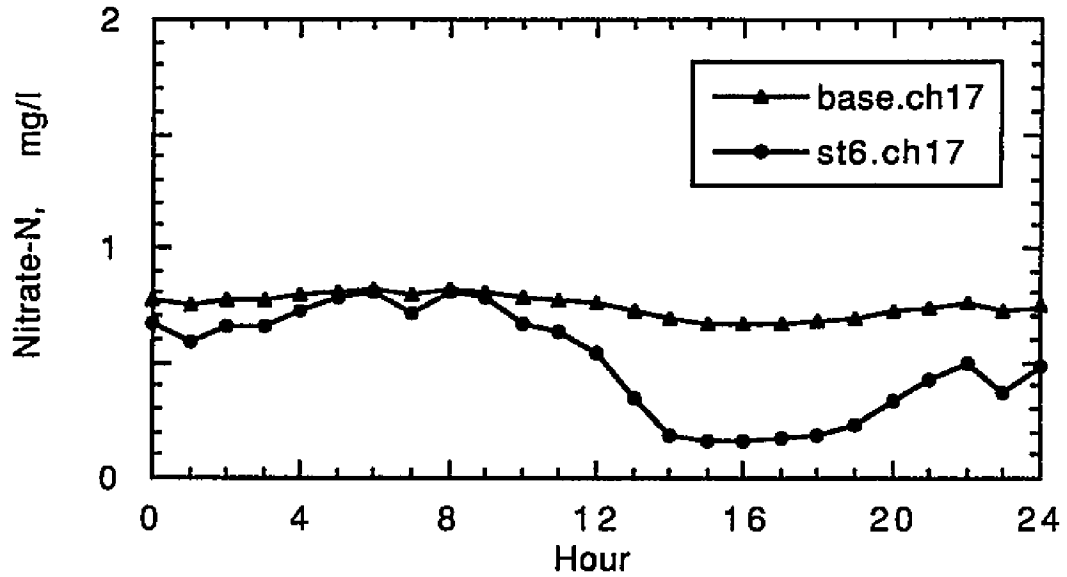


Figure 5.48 Computed Diurnal Nitrate-N (Channel 17)
Two Climate Conditions

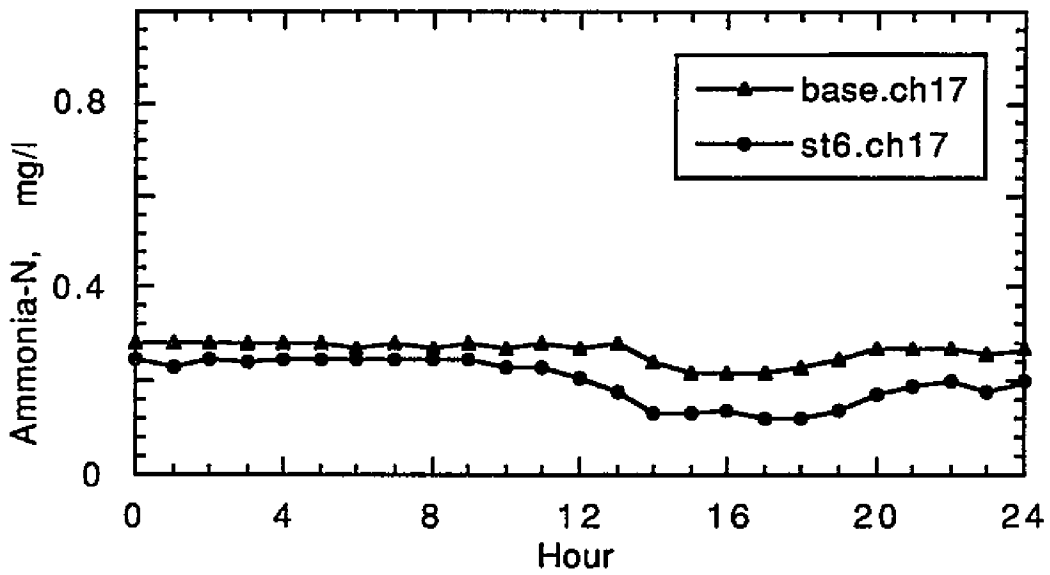


Figure 5.49 Computed Diurnal Ammonia-N (Channel 17)
Two Climate Conditions

most parts of the Delta seem reasonable, since they appear to be within the levels generally observed (for example, see Table 5.4).

Contour plots of temperature are shown in Figure 5.51.

Temperatures range from a low of 19 degrees near Benicia to a high of 22 degrees near Stockton for September 1988 conditions. A sample plot of chlorophyll-a (Figure 5.52) shows high algal primary productivity in regions of the South Delta, as has been actually observed during the late summer month (see Tables 5.2 and 5.4).

Sample contour plots of nitrate and total dissolved solids are also included for illustration (Figures 5.53 and 5.54), although corroborating data are very limited.

Computer Capabilities Needed

The Sacramento-San Joaquin Delta is probably one of the largest systems that will ever be simulated with such a model, hence it is important to consider the practical questions of simulation time and cost. Simulation of eight tidal days (200 hours) required about 1.5 hour of CPU time on a Sun SPARC-2 workstation (running at 40 MHz). The machines of this class perform at 28.5 MIPS (millions of instructions per second) or 22.8 SPECfp92 (floating point compute performance). Considering that a time step of 15 minutes was used, eleven constituents were simulated in nearly five hundred "channels" in the Delta, and each channel can have one to twenty-four water parcels moving at a time, the computation time seems reasonable. Assuming that an average of ten parcels exist in a channel at any

time, and reaction time step is of comparable size (it could be smaller, as explained in Chapter 4), a total of about four million computations are made for each constituent. With the experience of the past in advancing computational hardware it seems likely that the model will become an increasingly useful and flexible tool for water quality assessment in large, branched estuarine systems.

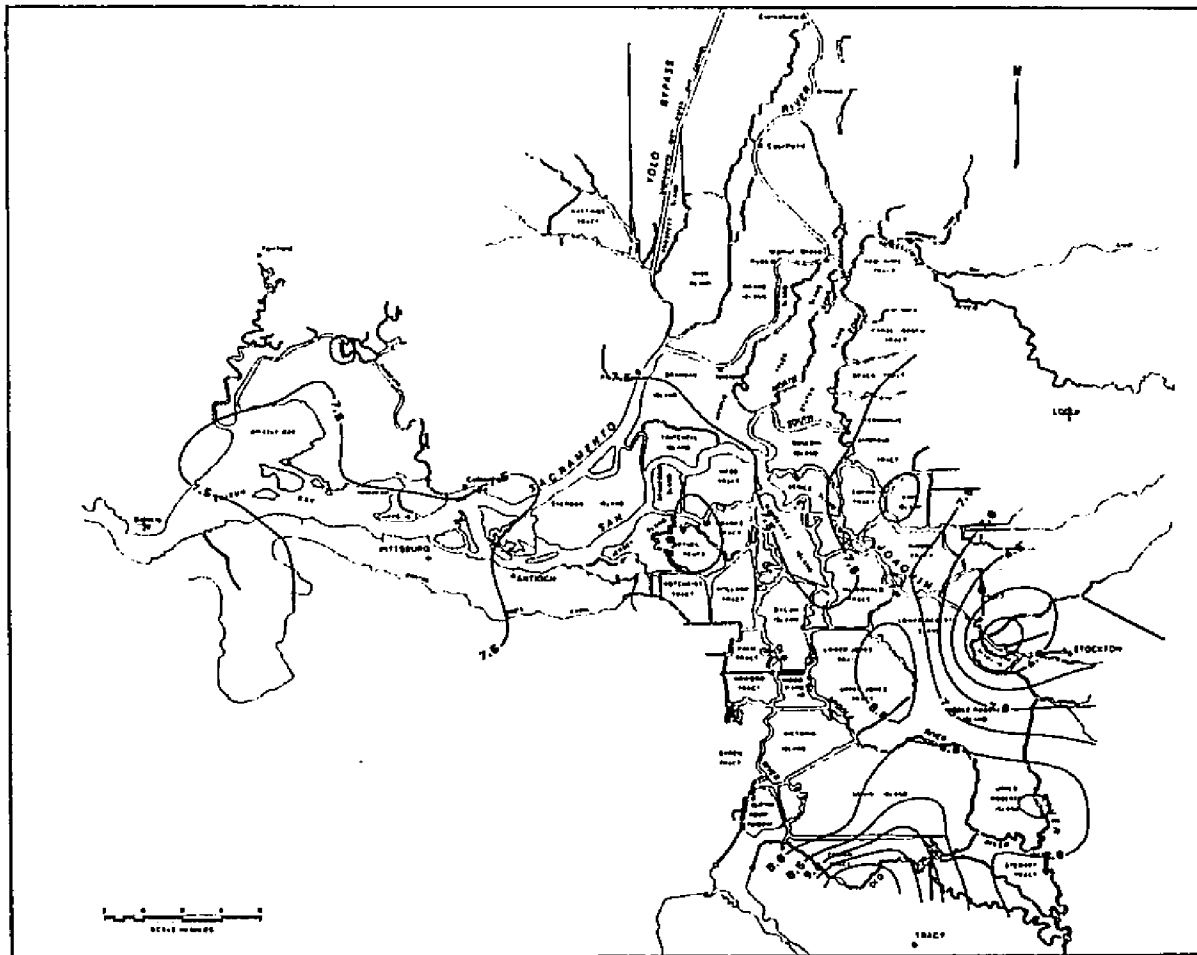


Figure 5.50 Simulated Dissolved Oxygen in the Delta (Sample Plot, Sep 20, 1988 Test Run)
 Contour Lines are for Concentrations of DO in mg/l

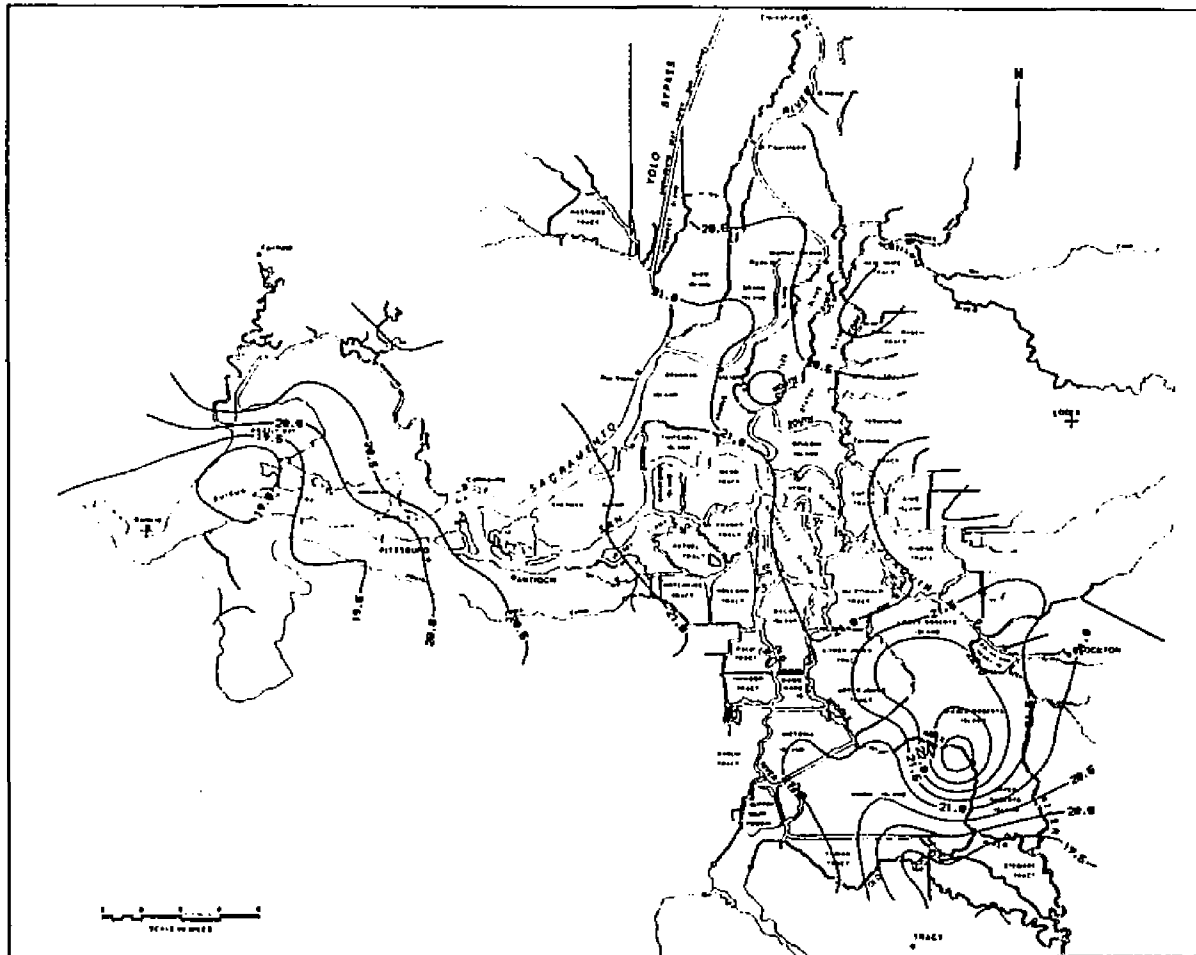


Figure 5.51 Simulated Temperature in the Delta (Sample Plot, Sep 20, 1988 Test Run)
 Contour Lines are for Temperature in degrees, Celsius

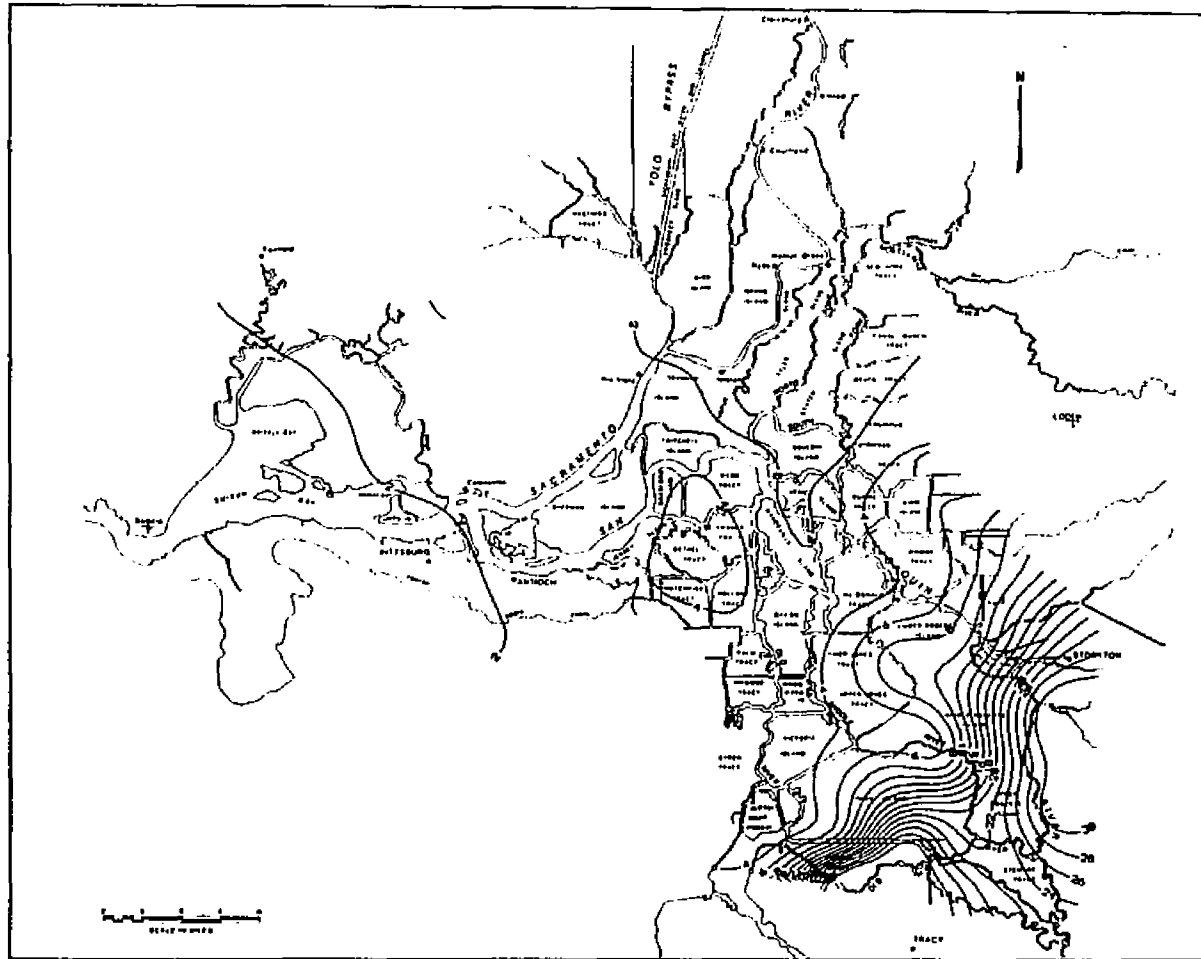


Figure 5.52 Simulated Chlorophyll-a in the Delta (Sample Plot, Sep 20, 1988 Test Run)
Contour Lines are for Chlorophyll-a in $\mu\text{g/l}$

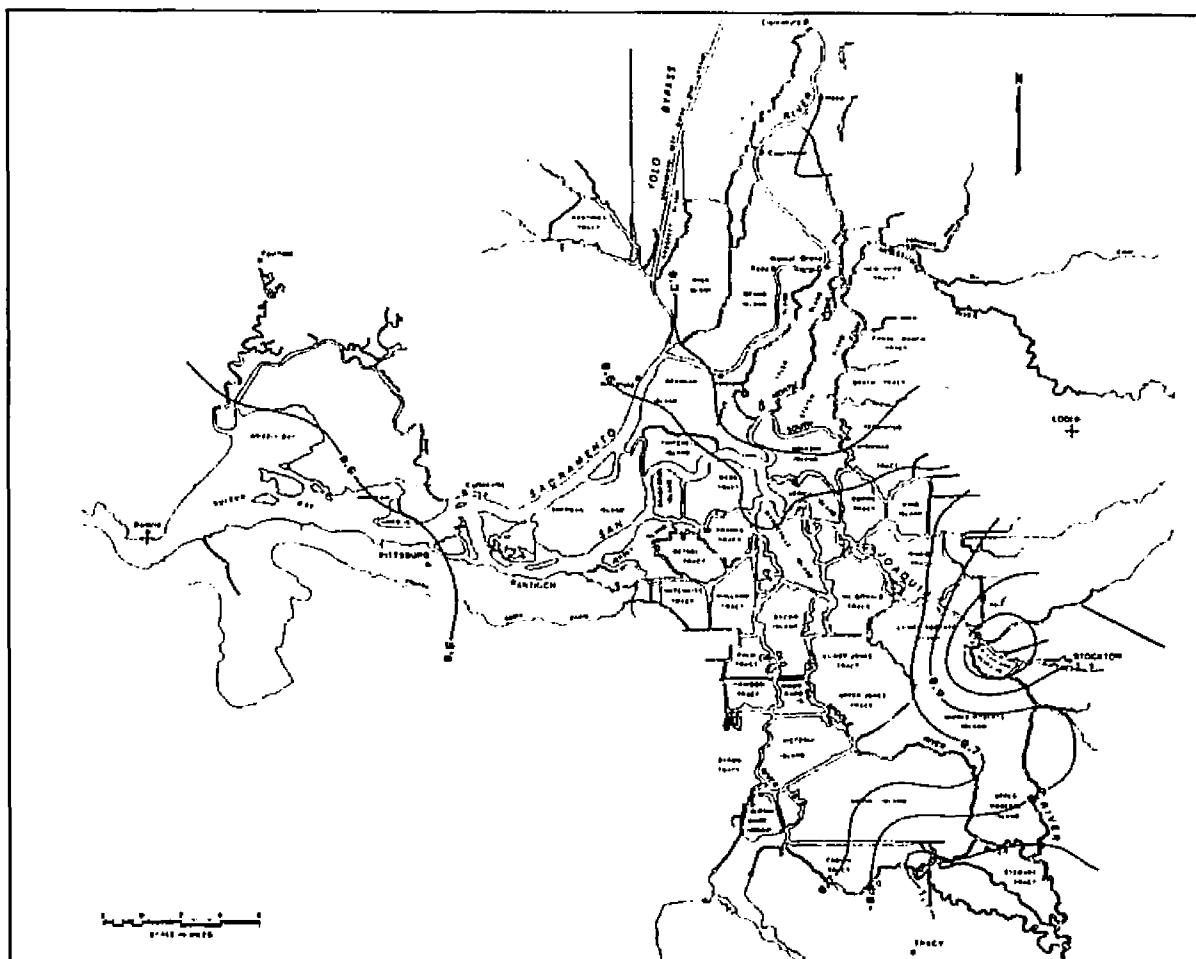


Figure 5.53 Simulated Nitrate-N in the Delta (Sample Plot, Sep 20, 1988 Test Run)
 Contour Lines are for Nitrate-N in mg/l

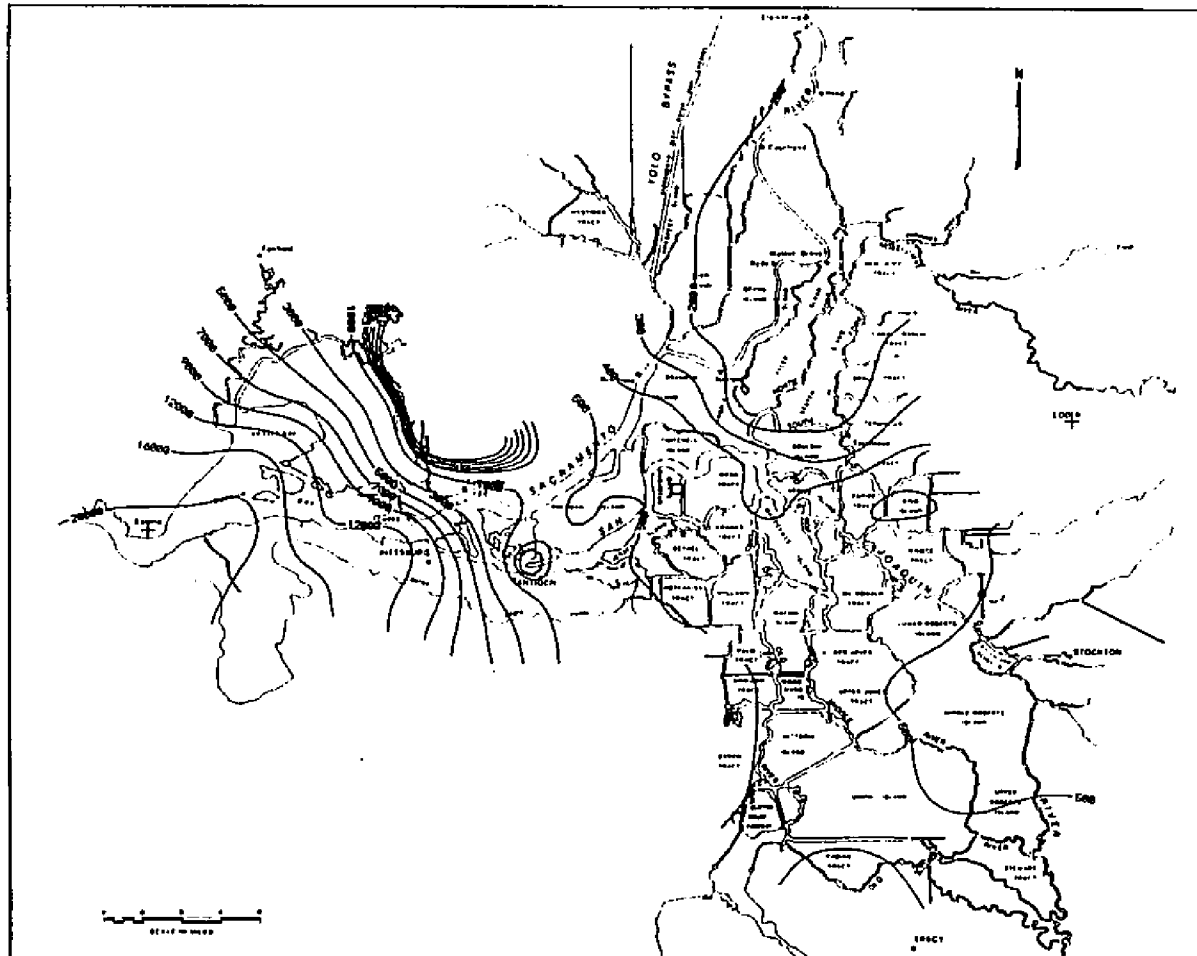


Figure 5.54 Simulated TDS in the Delta (Sample Plot, Sep 20,1988 Test Run)
Contour Lines are for Total Dissolved Solids in parts per million

6. CONCLUSIONS AND RECOMMENDATIONS

6.1 Summary and Conclusions

A mathematical tool, a computer model, has been developed in this research that can characterize the spatial and temporal distribution of important quality variables in rivers and estuaries. The capability of DSM2-QUAL to simulate water quality responses has been demonstrated on a portion of the Sacramento-San Joaquin Delta of Northern California. The processes of calibration and verification focused on the reach of the San Joaquin River near Stockton, California, for reasons of access to reliable field data and some unique conditions of hydrology, hydrodynamic and structural modification of some Delta channels (Chapter 5).

In general, the results of calibration and verification established the capability of the new model to represent the important water quality processes in a complex estuarine system like that of the Delta. The ability of the model to simulate moderately steep concentration gradients near Stockton (see Figure 5.20) is noteworthy. Considering the complexity of the estuary and the problems of obtaining reliable data for calibration, the test, even though somewhat limited by being constrained to a specific part of the Delta, was challenging enough.

Reaction kinetics incorporated in DSM2-QUAL have been verified by applying it to a hypothetical test problem and comparing the simulated results with those from QUAL2E. An important

characteristic of this model of not being tied to any particular hydrodynamic driver (except for the basic assumption of one-dimensionality) has also been verified in this research. The model, however, is best suited to cell-type hydrodynamic models i.e. those with flow defined over a cell. At different stages of this research, two different hydrodynamic models, with some modifications, were used to provide circulation information to the water quality model: the Link-Node Hydrodynamics Model in the initial investigative phase of this research, as applied to Newport Bay Estuary (see Chapter 3), and the DWRDSM Hydrodynamics Model in the later phases of this research when applied to the Delta. The new model has also been recently tested using circulation information generated from the modified version (DWR, 1995B) of the Four-Point (Hydrodynamics) Model (DeLong, 1995). They were found compatible (Nader, personal comm., 1995).

DSM2-QUAL was demonstrated as capable of capturing diurnal variations of important constituents, such as dissolved oxygen, phytoplankton, temperature and nutrients under the unsteady conditions of an estuarine environment. Variations were realistic, although lack of a large temporal variation in observed data, especially near the model boundaries, was somewhat of an impediment to testing the model's full capability to predict field conditions. The general trends shown by the 24-hour cycle patterns of constituents were judged consistent in terms of the inter-constituent relationships formulated in the model. This observation adds credibility to the potential of the new model to represent

short term temporal variations in modeled constituents, an ability not often found in models that are currently available. For example, in a previous study of Delta water quality using an eutrophication model (HydroQual, 1985), tidally averaged flows (i.e., net flows over a tidal cycle) generated by a hydrodynamic model were used.

Because the intratidal variation in flows were not accounted for, the effect of this important hydrodynamic component was not reflected in the concentrations of constituents computed by the eutrophication model. The velocity fluctuations within a tidal cycle can have significant effects on BOD and DO profiles, as demonstrated by Bella and Dobbins (1968).

Because of the dynamic nature of water quality in estuaries, even in studies where a model is used primarily in the analysis or prediction of long term trends, such as variations with temporal scales of days or even months, model results may be expected to improve when they take into account the short term intratidal variations of both hydrodynamics and water quality. Moreover, the ability to predict diurnal variations of major constituents is important because it can help in design of water quality protection measures by indicating how poor the water quality of a system may become during a daily cycle, possibly as a consequence of certain water management practices. For example, in situations where the average daily DO is satisfactory it may be that extremely low values of dissolved oxygen for a prolonged time during a daily cycle may threaten the survival of some fish species. Prediction of such events may be critical in the water quality management process.

From the perspective of the entire Sacramento-San Joaquin Delta, the new model now has the capacity to produce credible descriptions of most of the traditional variables of concern to water quality managers. Although it is ready for practical use, it is still necessary to strengthen the model's reliability in certain geographic areas by providing an improved database.

Tests of the model's capability to distinguish between alternatives in terms of incremental changes in water quality were encouraging. DSM2-QUAL has great potential for use as a practical tool for analysis of the impacts of water management alternatives. These may include examining the responses of the system being modeled to changes in waste water discharge characteristics, evaluating the effects of channel dredging on dissolved oxygen characteristics of the system, and, in some cases, indicating the more subtle causes of water quality problems, existing or potential. In such cases, initial evaluation of project impacts on water quality using models like DSM2-QUAL may save thousands of dollars of capital cost in construction of remedial facilities. An example could be the cost saving of upgrading waste water treatment with the objective of improving DO in the channel waters. Application of the model may reveal a different cause of the low DO problem, such as increased oxygen demand caused by years of deposit of decayed materials in benthic sediments. It may suggest a less costly alternative to correct the problem.

The Lagrangian algorithm embodied in the newly developed DSM2-QUAL, and the improved description of water quality variables in

the model, have resulted in a much enhanced capability to evaluate water quality management alternatives. Such a capability has not been available until now for the Sacramento-San Joaquin Delta, nor for that matter for similar large and complex estuarine networks, i.e., those that can be represented by systems of one-dimensional channels. This new tool, when used in conjunction with an improved database, will contribute substantially to our understanding of the complex mechanisms that affect water quality in the Delta and other estuaries. This should lead to improved measures to protect and enhance water quality, a potential that can only be realized by putting the model to work.

6.2 Recommendations and Future Directions

Demonstration of DSM2-QUAL's capability to simulate dynamic water quality changes in complex estuarine environments has been achieved within the scope of the present study. However, it was not possible in this investigation to complete all the procedures of calibration and verification for the entire Delta, due primarily to the lack of comprehensive observations from the field. Nor was it possible in this investigation to anticipate all future needs of water quality modeling in the Delta using DSM2-QUAL. Some tasks for future improvement in the model, including recommendations for future applications of the model, are described below.

1. *Develop an improved water quality database.*

a. *Expand spatial and temporal monitoring in the Delta.*

Because of the complexity of the constituent relationships that are built into the model, there is still a need to provide a much more comprehensive database of direct field observation. During the course of investigating the availability of field data needed for the purpose of model evaluation (using previous studies by federal, state, city and private agencies), it was determined that data for some constituents were relatively poorly distributed in both time and space. Considering the region near the City of Stockton's waste water treatment plant, data on organic phosphorus, ortho-phosphate and chlorophyll-a were found to have the poorest temporal and spatial distributions among the variables treated in the model. In the Delta, dissolved oxygen, temperature and TDS are relatively better described in both temporal and spatial distributions of data, although the data generally did not coincide with the model boundaries. Available data are still not adequate for a comprehensive exercise of calibration and verification of model application to the Delta as a whole.

A program to supplement the existing monitoring program and develop the needed database for future model calibration is desirable. The design of such a program is recommended. Monitoring coverage of the Delta should be expanded both spatially and temporally.

b. Extend monitoring of agricultural drainage quality and quantity.

Another area of database development that can be very beneficial for model improvement concerns the quality and quantity of agricultural drainage water. At the present time these data are poorly distributed both in space and time. In future modeling efforts, as more reliable data become available, a better spatial variation in the quality of agricultural drainage can be accommodated in the model, utilizing a capability already represented in the model grid structure and solution algorithm. Also, extension of model capability to represent dynamic variations in the quality of agricultural drainage (which is likely to be a function of the nature of irrigation practices and soil characteristics) should be investigated in order to possibly improve the model's performance.

c. Coordinate field monitoring with model needs. Sampling procedure should be consistent with model assumptions.

One major obstacle to the improvement of predictive water quality models, in general, is the lack of coordination between data needs for model calibration and verification and the data actually obtained in field surveys. To improve the model DSM2-QUAL there is a need to put the model to actual use and to refine it where necessary, as better data and more knowledge of water quality in the Delta become available. A minimum data collection program in support of the DSM2-QUAL should include both spatial and temporal characterization of the primary quality constituents, e.g., dissolved

oxygen, temperature, salinity, chlorophyll-a, and nitrogen species, under at least two distinct hydrologic and hydrodynamic conditions.

An important assumption in DSM2-QUAL is that complete mixing occurs within channel cross-sections. A better model calibration is possible if field data used for calibration correspond to this assumption. In other words, samples collected for model calibration should represent the cross-sectional average concentration at that location. This can be ensured by taking grab samples at locations where mixing across the full cross section is apparent.

2. Perform sensitivity analysis for fine tuning model and selecting appropriate time steps.

Sensitivity analysis should be performed to determine the relative influence of rate coefficients on model response. This process can guide in establishing priorities among rate coefficients for finer 'tuning' and provide additional information related to monitoring needs and laboratory experiments. Additional effort should be exerted to refine calibrated values of the rate coefficients which are most sensitive. Scenarios should also be designed to identify data gaps (spatial and temporal), and define the nature and frequency of future sampling surveys.

A series of model experiments should be performed to assess the sensitivity of model results to time step under a set of different scenarios. Such an analysis will be useful in establishing general

guidelines for model users in choosing optimal time steps, with considerations based both on accuracy and economy.

3. Apply the model to verify basic assumptions.

It is important that users of the water quality model understand the basic structure of the model in order to judge the validity of the basic assumptions in the context of the scenarios examined. This is a learning process that should be a part of future integration of DSM2-QUAL into the modeling framework for Delta water management. Additional recommendations pertinent to future modeling efforts in the Delta are presented below.

4. Extend model application to simulate long term events.

Future efforts to model Delta water quality should include simulations that are long term, i.e. with durations of a year or more, in order to capture seasonal variations in water quality. For example, the calibrated model can be used to predict seasonal algal blooms. Until a more detailed distribution of data is available, monthly or biweekly data, currently available at the twenty-five monitoring stations within the Delta (see DWR 1990B), can be used for calibration and verification of the model. These can be supplemented with time series data of dissolved oxygen, electrical conductivity (EC) and water temperatures available at the present time at six continuously monitored stations.

It is acknowledged that the computer time requirements of such runs will be substantial, and hence may not be practical without

resorting to somewhat coarser resolution in time. However, considering the rapid rate at which computer capabilities are advancing, it should not be long before such studies are feasible, possibly, with the next generation of workstations.

5. Test model ability to simulate extreme water quality episodes.

Once the model is calibrated for the Delta, extreme water quality conditions such as those observed in 1992 (see DWR, 1994A), could provide excellent test scenarios to examine the robustness of the new model and its ability to predict extreme variations in water quality that may have resulted from a complex combination of changes in environmental conditions. According to the DWR (1994A), the severity of the 1992 critically dry year, in combination with the accumulated effects of the 6-year drought, resulted in some of the highest nutrient concentrations and water temperatures in the Delta since 1986, and some of the lowest DO concentrations in the Stockton Ship Channel.

6. Benefit from future advances in hydrodynamics and salinity modeling.

The dependent nature of any water quality model on an adequate hydrodynamic information makes it important to have an equitable refinement of the hydrodynamic models. Recent efforts, organized among multiple levels of the government--local, state and federal, to measure flows and velocities on a continuous time frame at several key locations in the Delta, will contribute to improved hydrodynamic modeling of the Delta.

In a tidal estuary, salinity data provide useful information on dispersive processes. This information is often used in calibrating the dispersion coefficients in models. The coefficients obtained this way are usually adopted for other water quality constituents. As was demonstrated in this research (see Chapter 3), the choice of the dispersion factor, D_f , is important in many cases. Therefore, the accurate estimation of dispersion coefficients from salt transport is crucial for successful water quality modeling. It is expected that future advances in hydrodynamics and salinity modeling will greatly benefit the water quality simulation.

7. Conduct field sampling of benthic deposits.

Benthic sources of the nutrients as ammonia and phosphate and benthic oxygen demand can be specified in the model, as spatially varying parameters. A survey should be conducted of sediment deposits along the Delta channels, especially, the upper reaches of San Joaquin River, including the region near Stockton, to determine spatial variations in benthic oxygen demand, and the nitrogen and phosphorus content in the sediments. Such a survey should identify channels where benthic source or demand values need to be modified to improve calibration of the model.

8. Extend model to include higher trophic levels.

Subject to a consistent expansion of the database, future extensions in the model to add additional variables, such as zooplankton and benthic algae, are also likely to result in improvement in model performance. Extensions could also include

the ability to simulate additional species of algae and silica¹, if data availability and specific needs so indicate.

9. Interface DSM2-QUAL with particle tracking algorithms.

Additional uses of the model would be in providing the spatial and temporal distributions of water quality variables to a Particle Tracking Model with a random walk component, so that biological species can be more accurately modeled. In random walk particle tracking models the transport and fate of individual particles are simulated. The fate of particles can be determined probabilistically as a function of certain water quality parameters (Smith, personal comm., 1995). For example, a higher mortality rate for fish will occur if DO levels become too low, or water temperatures fall outside a certain range. Spawning and development rates of eggs and yolk-sac larvae may also be functions of temperature, a capability accommodated in an "individual-based model" of population dynamics of young striped bass (see Rose and Cowan, 1993). DSM2-QUAL, combined with a particle tracking model that includes dynamics of fish behavior, can become a useful tool for understanding the fate of an important fishing resource in a changing environment, such as that of the Sacramento-San Joaquin Delta.

¹ It is essential to include silica in the model if diatoms are simulated as a separate algal group.

10. *Interface DSM2-QUAL with trihalomethane (THM) module.*

The model should be expanded to include subroutines representing THM kinetics, so that THM formation potential can also be simulated, interactively using information on ammonia, temperature and other related constituents, as needed. The reader is referred to DWR (1994B, 1995B) and Hutton and Chung (1992) for details on the modeling of THM formation potential in the Delta.

11. *Test the model's ability to simulate dissolved organic carbon.*

Dissolved organic compounds are important constituents in the Delta. They contribute to the formation of THMs and other disinfection by-products in treated drinking water. Ability to simulate DOCs is also likely to improve the estimation of drainage quality in the Delta (see 1b above), because agricultural drainage is thought to be the dominant source of organics in the Delta (for example, see DWR, 1994B).

REFERENCES

1. Ambrose, R. B., Jr., T. A. Wool, J. P. Connolly and R. W. Schanz (1988) "WASP4, A Hydrodynamic and Water Quality Model-Model Theory, User's Manual and Programmer's Guide." EPA/600/3-87/039, Env. Research Laboratory, US EPA, Athens, Georgia.
2. American Public Health Association (APHA, 1985) Standard Methods for the Examination of Water and Waste Water. 16th Edition, Washington DC, 874.
3. Australian Water and Coastal Studies Pty Ltd. (1995) "Salt Pan Creek Stormwater Quality Management Strategy." Draft Report 95/09
4. Baptista, A. E. deM., E. E. Adams and K. D. Stolzenbach (1984) "Eulerian-Lagrangian Analysis of Pollutant Transport in Shallow Water." Report No. 296, Department of Civil Eng., MIT, Cambridge, Massachusetts.
5. Barrett, M. J. and B. M. Mollowney (1972) "Pollution Problems in Relation to the Thames Barrier." Philosophical Transactions, Royal Society, Vol. A272, London, England.
6. Bella, D. A. and W. J. Grenney (1970) "Finite-Difference Convection Errors." Journal of Env. Eng., ASCE¹, Vol. 96, No. SA6, 1361-1375.
7. Bella, D. A. and W. E. Dobbins (1968) "Difference Modeling of Stream Pollution." Journal of Sanitary Eng., ASCE, Vol. 94, No. SA5, Proc. Paper 6192, 995-1016.
8. Bishop, S. E., G. S. Conley, J. G. Crawford, J. A. Economides, T. L. Epperson, D. J. Gladen, K. L. Groom, L. S. Hartman and J. D. Springer (1978) "Sedimentation in Newport Bay." School of Engineering, University of California, Irvine.
9. Book, D. L., J. P. Boris and K. Hain (1975) "Flux-Corrected Transport II: Generalization of the Method." Journal of Computational Physics, Vol. 18, 248-283.

¹ ASCE abbreviated for American Society of Civil Engineers

10. Boris, J. P. and D. L. Book (1973) "Flux-Corrected Transport. I. SHASTA, A Fluid Transport Algorithm that Works." *Journal of Computational Physics*, Vol. 11, 38-69.
11. Bowden, K. F. (1984) "Mixing and Turbulence in Estuaries." In Estuary as a Filter, ed. V. S. Kennedy, Academic Press.
12. Bowie, G. L., W. B. Mills, D. B. Porcella, C. L. Campbell, J. R. Pagenkopt, G. L. Rupp, K. M. Johnson, P. W. H. Chan, and S. A. Gherini (1985) "Rates, Constants and Kinetics Formulations in Surface Water Quality Modeling." 2nd Edition, US EPA, Athens, Georgia, EPA 600/3-85/040.
13. Brown, L. C. and T. O. Barnwell (1987) "The Enhanced Stream Water Quality Models QUAL2E and QUAL2E-UNCAS: Documentation and Users Manual." US EPA, Athens, Georgia, EPA 600/3-87/007.
14. California Department of Water Resources (1995A) "Estimation of Delta Island Diversions and Return Flow." Division of Planning.
15. California Dept. of Water Resources (1995B) "Methodology for Flow and Salinity Estimates in the Sacramento-San Joaquin Delta and Suisun Marsh." 16th Annual Progress Report to the State of Water Res. Control Board in Accord. with Water Right Decision 1485.
16. California Department of Water Resources (1994A) "Water Quality Conditions in the Sacramento-San Joaquin Delta during 1992." Environmental Services Office.
17. California Department of Water Resources (1994B) "Methodology for Flow and Salinity Estimates in the Sacramento-San Joaquin Delta and Suisun Marsh." 15th Annual Progress Report to the State Water Resources Control Board.
18. California Department of Water Resources (1992) "Methodology for Flow and Salinity Estimates in the Sacramento-San Joaquin Delta and Suisun Marsh." 13th Annual Progress Report to the State of Water Resources Control Board.
19. California Department of Water Resources (1991) "Methodology for Flow and Salinity Estimates in the Sacramento-San Joaquin Delta and Suisun Marsh." 12th Annual Progress Report to the State Water Resources Control Board.

20. California Department of Water Resources (1990A) "Water Quality Conditions in the Sacramento-San Joaquin Delta during 1988." Division of Local Assistance.
21. California Department of Water Resources (1990B) "Sacramento-San Joaquin Delta Water Quality Surveillance Program-1988." Division of Local Assistance, Vol. 1.
22. California Department of Water Resources (1988A) "Dayflow Data Summary."
23. California Department of Water Resources (1988B) "State Water Project Operations Data: Monthly reports."
24. California Department of Water Resources (1987) "California Water Looking to the Future." Bulletin 160-87.
25. California Department of Water Resources (1967) "Delta and Suisun Marsh Water Quality Investigation." Bulletin 123.
26. California State Lands Commission (1991) "Delta-Estuary: California's Inland Coast, a Public Trust Report."
27. California Regional Water Quality Control Board, Central Valley Region (1991) "Water Quality of the Lower San Joaquin River: Lander Avenue to Vernalis." October 1989 to September 1990.
28. Chaudhari, N. M. (1971) "An Improved Numerical Technique for Solving Multidimensional Miscible Displacement Equations." *Society of Petroleum Engineers Journal*, 277-284.
29. Chen, C. W. and G. T. Orlob (1975) "Ecologic Simulation of Aquatic Environments." In Systems Analysis and Simulation in Ecology, ed. B. Patten, Academic Press, New York, NY, 475-528.
30. Churchill, M. A., H. L. Elmore and R. A. Buckingham (1962) "The Prediction of Stream Reaeration Rates." *Journal of the Sanitary Engineering Division, ASCE*, 88, SA4, 1-46.

31. DeLong, L. L., D. B. Thompson and J. K. Lee (1995) "Computer Program FourPT, a Model for Simulating One-Dimensional, Unsteady, Open-Channel Flow." US Geological Survey, Water Resources Investigations Report (Draft).
32. Elder, J. W. (1959) "The Dispersion of Marked Fluid in Turbulent Shear Flow." *Journal of Fluid Mechanics*, Vol. 5, 544-560.
33. El-Hadi, N., A. Harrington, I. Hill, Y. I. Lau and B. G. Krishnappan (1984) "River Mixing - a State of the Art Report." *Canadian Journal of Civil Eng.*, Vol. 11, 585-609.
34. Fischer, H. B., E. J. List, R. C. Y. Koh, J. Imberger and N. H. Brooks (1979). "Mixing in Inland and Coastal Waters." Academic Press, Inc.
35. Fischer, H. B. (1976) "Mixing and Dispersion in Estuaries." *Annual Reviews in Fluid Mechanics*, Vol. 8, 107-133.
36. Fischer, H. B. (1972) "A Lagrangian Method for Predicting Pollutant Dispersion in Bolinas Lagoon, Marin County, California." US Geological Survey Professional Paper (582-B).
37. Fischer, H. B. (1968) "Dispersion Predictions in Natural Streams." *Journal of the Sanitary Eng. Division, ASCE*, No. SA5, 927-943.
38. Fischer, H. B. (1967) "The Mechanics of Dispersion in Natural Streams." *Journal of Hydraulics Division, ASCE*, Vol. 93, No. HY6, 187-216.
39. Gameson, A. L. H., G. A. Trusdale and A. L. Downing (1955) "Reaeration Studies in a Lakeland Beck." *Journal of the Institution of Water Engineers*, 9, 7, 571-594.
40. Gerald, C. F. and P. O. Wheatley (1985) "Applied Numerical Analysis." Third Edition, Addison-Wesley Pub. Co.
41. Goodwin, C. R. (1991) "Simulation of the Effects of Proposed Tide Gates on Circulation, Flushing, and Water Quality in Residential Canals, Cape Coral, Florida." US Geological Survey, Open-File Report 91-237.

42. Gray, W. G. and G. F. Pinder (1976) "An Analysis of the Numerical Solution of the Transport Equation." *Water Resources Research*, Vol. 12, No. 1, 547-555.
43. Gresho, P. M. and R. L. Lee. (1981) "Don't Suppress the Wiggles---They're Telling You Something." *Computers and Fluids*, Vol. 9, No. 2.
44. Gromiec, M. J. (1989) "Reaeration." Ch.3 in: "Mathematical Submodels in Water Quality Systems." Ed. S. E. Jorgensen and M. J. Gromiec, Elsevier Pub.
45. Gunther, A. J., J. A. Davis and D. J. H. Phillips (1987) "An Assessment of the Loading of Toxic Contaminants to the San Francisco Bay Delta." Aquatic Habitat Institute Report, Richmond, California.
46. H. B. Fischer, Inc. (1984) "Fischer Delta Model Volume 2: Reference Manual." Prepared for the United States Bureau of Reclamation and the California Department of Water Resources.
47. Heinrich, J. and O. C. Zienkiewicz (1979) "Finite Element Method and "Upwinding" Techniques in the Numerical Solution of Convection Dominated Flow Problems." In Finite Element Methods for Convection Dominated Flows, ed. T. J. R. Hughes. American Society of Mechanical Engineers, New York, NY, Vol. 34, 105-136.
48. Herbold, B. and P. B. Moyle (1989) "The Ecology of the Sacramento-San Joaquin Delta: a Community Profile." US Dept. of the Interior, Fish and Wildlife Service, Research and Development, National Wetlands Research Center, Washington DC.
49. Holly, F. M. and J. M. Usseglio-Polatera (1984) "Dispersion Simulation in Two-Dimensional Tidal Flow." *Journal of Hydraulic Eng., ASCE*, Vol. 110, No. 7, 905-926.
50. Holly, F. M. Jr. and A. Preissmann (1977) "Accurate Calculation of Transport in Two-Dimensions." *Journal of Hydraulics Division, Proc. of ASCE*, Vol. 103, No. HY11, 1259-1277.
51. Huber, L. (1995) "Personal Communication and Fax." Department of Municipal Utilities, City of Stockton, California.

52. Hughes, T. J. R. and A. Brooks. (1979) "A Multi-Dimensional Upwind Scheme with No Crosswind Diffusion." In Finite Element Methods for Convection Dominated Flows, ed. T. J. R. Hughes, American Society of Mechanical Engineers, New York, NY, Vol. 34, 19-35.
53. Hutton, P. H., and Chung, F. I. (1992) "Simulating THM Formation Potential in Sacramento Delta. Part II." *Journal of Water Resources Planning and Management*, ASCE, Vol. 118, No. 5, 530-542.
54. HydroQual (1985) "Central Delta Eutrophication Model-Multiple Algal Species." Prepared for the Department of Water Resources, California. HydroQual, Inc., Mahwah, NJ 07430.
55. Hydrosience, Inc. (1971) "Simplified Mathematical Modeling of Water Quality." Prepared for the Mitre Corporation and the US EPA, Water Programs, Washington DC.
56. Jensen, O. K. and B. A. Finlayson (1980) "Solution of the Transport Equations using a Moving Coordinate System." *Advances in Water Resources*, Vol. 3, 9-15.
57. Jobson, H. E. and D. H. Schoellhamer (1992) "Users Manual for a Branched Lagrangian Transport Model." US Geological Survey, Water Resources Investigations Report, 87-4163.
58. Jobson, H. E. (1987A) "Estimation of Dispersion and First Order Rate Coefficients by Numerical Routing." *Water Resources Research*, Vol. 23, No. 1, 169-180.
59. Jobson, H. E. (1987B) "Lagrangian Model of Nitrogen Kinetics in the Chattahoochee River." *Journal of Environmental Eng., ASCE*, Vol. 113, No. 2, 223-242.
60. Jobson, H. E. (1985) "Simulating Unsteady Transport of Nitrogen, Biochemical Oxygen Demand, and Dissolved Oxygen in the Chattahoochee River Downstream from Atlanta, Georgia." US Geological Survey, Water-Supply Paper, Paper No. 2264.

61. Jobson, H. E. (1981) "Temperature and Solute-Transport Simulation in Streamflow using a Lagrangian Reference Frame." US Geological Survey, Water Resources Investigations, 81-2, 165.
62. Jobson, H. E. (1980) "Comment on A New Collocation Method for the Solution of the Convection-Dominated Transport Equation." By G. F. Pinder, and A. Shapiro, 1979, (in Water Res. Research, Vol. 15, No. 5, 1177-1182): Water Resources Research, Vol. 16, No. 6, 1135-1136.
63. King, I. P. and J. F. DeGeorge (1994) "RMA4Q: A Two-Dimensional Finite Element Model for Water Quality in Estuaries and Streams." Vers. 1.0.
64. King, I. P. (1993) "RMA2: A Two-Dimensional Finite Element Model for Flow in Estuaries and Streams." Version 4.4.
65. King, I. P. (1990) "RMA4: A Two-Dimensional Finite Element Water Quality Model." Version 3.1.
66. Krenkel, P. A. and G. T. Orlob (1962) "Turbulent Diffusion and the Reaeration Coefficient." Journal of the Sanitary Engineering Division, ASCE, Vol. 88, No. SA2, 53-83.
67. Lam, D. C. L. (1976) "Comparison of Finite Element and Finite Difference Methods for Nearshore Advection-Diffusion Transport Models." In Finite Elements in Water Resources, ed. W. G. Gray, G. F. Pinder and C. A. Brebbia, Pentech Press, London, Plymouth, 1.115-1.130.
68. Langbein, W. B. and W. H. Durum (1967) "The Reaeration Capacity of Streams." US Geological Survey Circular No. 542, Reston, Virginia.
69. Lee, J. H. W., R. S. S. WU, Y. K. Cheung and P. P. S. Wong (1991) "Dissolved Oxygen Variations in Marine Fish Culture Zone." Journal of Environmental Eng., Vol. 117, No. 6, 799-815.
70. Leith, C. E. (1965) "Numerical Simulation of the Earth's Atmosphere." Methods in Computational Physics, Vol. 4, 1-28.

71. Leonard, B. P. (1979A) "A Stable and Accurate Convection Modeling Procedure based on Quadratic Upstream Interpolation." *Computer Methods in Applied Mechanics and Eng.*, Vol. 19, 59-98.
72. Leonard, B. P. (1979B) "A Survey of Finite Differences of Opinion on Numerical Muddling of the Incomprehensible Defective Confusion Equation." In Finite Element Methods of Convection Dominated Flows, ed. T. J. R. Hughes, American Society of Mechanical Engineers, New York, NY, Vol. 34, 1-17.
73. McBride, G. B. and J. C. Rutherford (1984) "Accurate Modeling of River Pollutant Transport." *Journal of Environmental Eng., ASCE*, Vol. 10, No. 4, 808-827.
74. McClurg, S. (1993) "Lay Person's Guide to the Delta." Water Education Foundation, Sacramento, California.
75. Municipal Water Quality Investigation Data Request (MWQI, 1995) "Internal California Dept. of Water Resources Memorandum to P. Hutton from R. Woodard, February 1 and 15."
76. Nader, P. (1995) Personal Communication. California Department of Water Resources, Division of Planning.
77. National Oceanic and Atmospheric Administration (NOAA, 1988) "Local Climatological Data."
78. Neuman, S. P. (1981) "A Eulerian-Lagrangian Numerical Scheme for the Dispersion Convection Equation using Conjugate Space-Time Grids." *Journal of Computational Physics*, 41, 270-294.
79. New South Wales Department of Public Works and Services (1995) "Assessment of Impacts of Releasing Effluent to the Schoalhaven River." Draft Rept. MHL 735.
80. Nichols, F. R., J. E. Cloern, S. N. Luoma and D. H. Peterson (1986) "The Modification of an Estuary." *Science* 231, 525-648.
81. Noye, J. B. (1987A) "Numerical Methods for Solving the Transport Equation." In Numerical Modeling: Applications to Marine Systems, ed. B. J. Noye, Elsevier Pub., 195-229.

82. Noye, J. B. (1987B) "Finite Difference Methods for Solving the One-Dimensional Transport Equation." In Numerical Modeling: Applications to Marine Systems, ed. B. J. Noye, Elsevier Pub., 231-256.
83. O'Connor, D. J., R. V. Thomann, and D. M. Di Toro (1973) "Dynamic Water Quality Forecasting and Management." Manhattan College, New York, US EPA, Washington DC, EPA 660/3-73/009 NTIS Doc. PB 225-048/8ST.
84. O'Connor, D. J. (1958) "Measurement and Calculation of Stream Reaeration Ratio." Seminar on Oxygen Relationships in Streams, US Public Health Service, Robert A. Taft Sanitary Eng. Center, Report W 58-2, 35-45, Cincinnati.
85. O'Connor, D. J. and W. E. Dobbins (1956) "Mechanism of Reaeration in Natural Streams." Journal of the Sanitary Eng. Division, ASCE, Vol. 82, No. SA6, 1-30.
86. O'Neill, K. (1981) "Highly Efficient, Oscillation-Free Solution of the Transport Equation over Long Times and Large Spaces." Water Resources Research, Vol. 17, No. 6, 1665-1675.
87. Onyejekwe, O. O. (1983) "A Galerkin Finite Element Model for Solution of Nonconservative Water Quality Transport in an Estuarine System." Ph.D. Dissertation, University of California, Davis.
88. Orlob, G. T., A. E. Bale, H. Rajbhandari and M. Malagoli (1991) "Modeling Effects of Tidal Barrier Closure of Venice Lagoon." Water Science and Technology, Vol. 24, No. 6, 149-155.
89. Orlob, G. T. and N. Marjanovic (1989) "Heat Exchange." Ch. 5 in: Mathematical Submodels in Water Quality Systems." Ed. S. E. Jorgensen and M. J. Gromiec, Elsevier Pub.
90. Orlob, G. T., editor (1983) Mathematical Modeling of Water Quality: Streams, Lakes, and Reservoirs." John Wiley and Sons, Wiley-Interscience, NY.
91. Orlob, G. T., R. P. Shubinsky and K. D. Feigner (1967) "Mathematical Modeling of Water Quality in Estuarine Systems." Proc. of Symposium on Est. Pollution, Sanitary Eng. Division, ASCE, Stanford University.

92. Orlob, G. T. (1959) "Eddy Diffusion in Homogeneous Turbulence." *Journal of Hydraulics Division, ASCE*, Vol. 85, No. HY9, 75-101.
93. Orlob, G. T. (1958) "Eddy Diffusion in Open Channel Flow." Ph.D. Dissertation (Stanford University), and Contribution No. 19, Water Resources Center, University of California, Berkeley.
94. Owens, M., R. W. Edwards and J. W. Gibbs (1964) "Some Reaeration Studies in Streams." *International Journal of Air and Water Pollution* 8, 469-486.
95. Parsons ES (1995) "Stockton Plant on Fast Track Schedule" in the Spring Newsletter. P. Gallemore, Editor, Parsons Engineering Science, Inc., Pasadena, California.
96. Price, H. S., R. S. Varga and J. E. Warren (1966) "Applications of Oscillation Matrices for Diffusion-Convection Equations." *Journal of Mathematics and Physics*, Vol. 45, 301-311.
97. Rajbhandari, H. L. (1990) "Comparison of Finite Element Methods using Linear Elements, Quadratic and Cubic Upwinding, and Hermitian Cubics in Solving the 1-D Advection-Diffusion Equation." Class Project in the Course: Finite Elements, Application in Fluids (Instructor: I. P. King), University of California, Davis.
98. Rajbhandari, H. L. and G. T. Orlob (1990) "Evaluation/Development of Water Quality Models for Wasteload Allocation in Estuarine Environments." Prep. for Calif. State Water Resources Control Board and Calif. Regional Water Quality Control Board, San Francisco Bay Region, Dept. of Civil and Env. Eng., Univ. of California, Davis.
99. Rathbun, R. E. (1977) "Reaeration Coefficients of Streams, State-of-the-Art." *ASCE, Journal of Hydraulics Division*, Vol. 103, No. HY4, 409-424.
100. Rayej, M. and F. I. Chung (1993) "Mathematical Modeling of the Sacramento-San Joaquin Delta." *Proceedings of ASCE Hydraulics Conference*, San Francisco.
101. Roache, P. J. (1972) "Computational Fluid Dynamics." Hermosa Pub., Albuquerque, New Mexico.

102. Roesner, L. A., P. R. Giguere and D. C. Evenson (1977A) "Computer Program Documentation for the Stream Quality Model QUAL-II." Prep. by Water Resources Engineers Inc., Walnut Creek, California, for Southeast Michigan Council of Governments, Detroit, Michigan.
103. Roesner, L. A. , P. R. Giguere and D. C. Evenson (1977B) "Users Manual for the Stream Quality Model QUAL-II." Prep. by Water Resources Engineers Inc., Walnut Creek, California, for Southeast Michigan Council of Governments, Detroit, Michigan.
104. Rose, K. A. and J. H. Cowan, Jr. (1993) "Individual-Based Model of Young-of-the-Year Striped Bass Population Dynamics. I. Model Description and Baseline Simulations." Transactions of the American Fisheries Society, 122:415-438.
105. Rutherford J. C. (1994) "River Mixing." John Wiley and Sons Ltd.
106. San Joaquin Valley Drainage Program (1990) "A management Plan for Agricultural Subsurface Drainage and Related Problems on the Westside San Joaquin Valley: Final Report." (September).
107. Saviz, C. M., J. F. DeGeorge, G. T. Orlob and I. P. King (1995) "Modeling the Fate of Metam Sodium and MitC in the Upper Sacramento River: The Cantara-Southern Pacific Spill." Center for Env. and Water Resources Eng., Dept. of Civil and Env. Eng., University of California, Davis.
108. Sayre, W. W. (1969) "Dispersion of Silt Particles in Open Channel Flow." Journal of Hydraulics Division, ASCE, Vol. 95, No. HY3, 1009-1038.
109. Schaffranek, R. W., R. A. Baltzer, and D. E. Goldberg (1981) "A Model for Simulation of Flow in Singular and Interconnected Channels." US Geological Survey Techniques of Water Resources Investigations, Book 7, Chapter C3, 110.
110. Schoellhamer, D. H. (1988) "Lagrangian Transport Modeling with Qual II Kinetics." Journal of Env. Eng., Vol. 114, No. 2, ASCE, 368-381.
111. Schoellhamer, D. H., and H. E. Jobson (1986A) "Users Manual for a One-Dimensional Lagrangian Transport Model." US Geological Survey, Water-Resources Investigation, (4145).

112. Schoellhamer, D. H. and H. E. Jobson (1986B) "Programmers Manual for a One-Dimensional Lagrangian Transport Model." US Geological Survey, Water Resources Investigation, (4144), 101.
113. Schoellhamer, D. H. (1985) "Discussion of Numerical Alternatives in Transient Stream Response." By Sobey, R. J., 1984, in *Journal of Hydraulic Eng.*, ASCE, Vol. 110, No. 6, 749-772.
114. Schohl, G. A. and F. M. Holly (1991) "Cubic-Spline Interpolation in Lagrangian Advection Computation." *Journal of Hydraulics Eng.*, ASCE, Vol. 117, No. 2, 248-255.
115. Smith, D. J. (1988) "Effects of the Stockton Ship Channel Deepening on the Dissolved Oxygen of Water Near the Port of Stockton, California (Phase II)." Resource Management Associates, Inc., Lafayette, California.
116. Smith, D. J. and L. C. Roig (1986) "Users Guide for the Stockton Ship Channel Project, Link-Node Hydrodynamic and Water Quality Models." Resource Management Associates, Inc.
117. Smith, D. J. (1978) "Water Quality Simulation for River Reservoir Systems." US Army Corps of Engineers, Hydrologic Engineering Center.
118. Smith, I. M. (1977) "Integration in Time of Diffusion and Diffusion-Convection Equations." In Finite Elements in Water Resources, ed. W. G. Gray, G. F. Pinder and C. A. Brebbia, Pentech Press, 1.3-1.20.
119. Smith, T. A. (1995) Personal Communication. California Dept. of Water Resources, Division of Planning.
120. Sobey, R. J. (1984) "Numerical Alternatives in Transient Stream Response." *Journal of the Hydraulic Eng.*, Vol. 110, No. 6, ASCE, 749-772.
121. Sobey, R. J. (1983) "Fractional Step Algorithm for Estuarine Mass Transport." *International Journal for Numerical Methods in Fluids*, Vol. 3, 567-581.
122. Sobey, R. J. (1982) "Hermitian Space-Time Finite Elements for Estuarine Mass Transport." *International Journal for Numerical Methods in Fluids*, Vol. 2, 277-298.

123. Streeter, H. W., C. T. Wriugh and R. W. Kehr (1936) "Measures of Natural Oxidation in Polluted Streams, Part III." An Experimental Study of Atmospheric Reaeration under Stream-Flow Conditions, Sewage Works Journal 8, 2, 282-316.
124. Taylor, G. I. (1954) "The Dispersion of Matter in Turbulent Flow through a Pipe." Proc. Royal Soc., London Ser. A, 223, 446-468.
125. Taylor, G. I. (1953) "Dispersion of Soluble Matter in Solvent Flowing Slowly through a Tube." Proc. Royal Soc., London, Ser. A, 219, 186-203.
126. Taylor, G. I. (1921) "Diffusion by Continuous Movements." Proc. London Math. Soc., Ser. 2, 20, 196-212.
127. Water Surface and the Atmosphere." Engineering Lab Report No. 14, Norris, Tennessee.
128. Thomann, R. V. and J. A. Mueller (1987) "Principles of Surface Water Quality Modeling and Control." Harper and Row, New York.
129. Thomann, R. V. (1972) "Systems Analysis and Water Quality Management." McGraw-Hill, Inc., New York.
130. Thomson, N. R., J. F. Sykes and W. C. Lennox (1984) "A Lagrangian Porous Media Mass Transport Model." Water Resources Research, Vol. 20, No. 3, 391-399.
131. US Geological Survey (1990) "Water Resources Data, California, Water Year 1989." Vol. 3 and 4.
132. US Geological Survey (1989) "Water Resources Data, California, Water Year 1988." Vol. 3 and 4.
133. van Genuchten, M. Th. and W. G. Gray (1978) "Analysis of Some Dispersion Corrected Numerical Schemes for Solution of the Transport Equation." International Journal for Numerical Methods in Eng., Vol. 12, 387-404.
134. van Genuchten, M. Th. (1977) "On the Accuracy and Efficiency of Several Numerical Schemes for Solving the Convective-Dispersion Equation." In Finite Elements in Water Resources, ed. W. G. Gray, G. F. Pinder and C. A. Brebbia, Pentech Press, 1.71-1.90.

135. Varoglu, E. and W. D. L. Finn (1980) "Finite Elements Incorporating Characteristics for One-Dimensional Diffusion-Convection Equation." *Journal of Computational Physics*, Vol. 34, No. 3, 371-389.
136. Walton, R. and M. Webb (1994) "QUAL2E Simulations of Pulse Loads." *Journal of Environmental Eng., ASCE*, Vol. 120, No. 5, 1017-1031.
137. Water Resources Engineers (1965) "A Water Quality Model of the Sacramento-San Joaquin Delta."
138. Water Resources Engineers (1973) "Newport Bay: Recommended Water Quality Management Plan." Walnut Creek, California.

Appendix A

A.1. Governing Equations for Water Quality Parameters

This section lists the equations for each constituent written in a Lagrangian reference frame that moves with the cross-sectional mean velocity. Consequently, the advection term does not appear in these equations.

Dissolved Oxygen

The rate of change in DO concentration is given by:

$$\frac{\partial [O]}{\partial t} = \frac{\partial}{\partial \xi} \left[E_x \frac{\partial (O)}{\partial \xi} \right] - (k_1 + k_3) L + k_2 (O_s - [O]) - \alpha_5 k_n [NH_3]$$

Diffusion
CBOD
Reaeration
Ammonia oxidation

$$- \alpha_6 k_{ni} [NO_2] + \alpha_3 \mu [A] - \alpha_4 \rho [A] - K_4/d \quad (A.1)$$

Nitrite oxidation
Photosynthesis
Respiration
Benthic demand

where

- [O] = dissolved oxygen concentration, mg/l or, g/m³,
- k₁ = CBOD decay rate at the ambient temperature, day⁻¹,
- k₃ = rate of loss of CBOD due to settling at the ambient temperature, day⁻¹,
- L = CBOD concentration, mg/l,
- k₂ = reaeration coefficient, day⁻¹,
- O_s = dissolved oxygen concentration at saturation, mg/l,

- k_n = ammonia decay rate at the ambient temperature, day⁻¹,
 $[NH_3]$ = ammonia concentration as N, mg/l,
 α_5 = amount of oxygen consumed in conversion of ammonia to nitrite,
 α_6 = amount of oxygen consumed in conversion of nitrite to nitrate,
 k_{ni} = nitrite decay rate at the ambient temperature, day⁻¹,
 $[NO_2]$ = nitrite concentration as N, mg/l,
 α_3 = amount of oxygen produced per unit of algal photosynthesis,
 μ = phytoplankton growth rate at the ambient temperature, day⁻¹,
 α_4 = amount of oxygen consumed per unit of algae respired,
 ρ = phytoplankton respiration rate at the ambient temperature, day⁻¹,
 $[A]$ = phytoplankton concentration, mg/l,
 K_4 = benthic oxygen demand, g/m² day⁻¹,
 d = mean channel depth, ft (0.30m),
 ξ = distance from the parcel, the Lagrangian distance coordinate.

$$\xi = x - x_0 - \int_{t_0}^t u \, d\tau \quad (A.2)$$

x_0 = location of the fluid parcel at time t_0 ,

x = Eulerian distance coordinate.

Carbonaceous Biochemical Oxygen Demand (CBOD)

Accounting also for the removal of CBOD that may be due to settling of organic particles, the rate of change of CBOD due to both biochemical oxidation and settling can be expressed as:

$$\frac{\partial L}{\partial t} = \frac{\partial}{\partial \xi} \left[E_x \frac{\partial L}{\partial \xi} \right] - (k_1 + k_3) L \quad (\text{A.3})$$

Terms are as defined previously.

Algae (Phytoplankton)

The rate of increase in algal biomass is computed by:

$$\frac{\partial [A]}{\partial t} = \frac{\partial}{\partial \xi} \left[E_x \frac{\partial [A]}{\partial \xi} \right] + [A] (\mu - \rho) - \sigma_1 \frac{[A]}{d} \quad (\text{A.4})$$

σ_1 = phytoplankton settling rate at ambient temperature,
ft/day,

$[A]$ = phytoplankton concentration, mg/l.

$$\mu = \mu_{\max} (FL) \text{ Min} \left(\frac{N}{K_N + N}, \frac{P}{K_P + P} \right) \quad (\text{A.5})$$

μ_{\max} = maximum algal growth rate at the ambient
temperature, day⁻¹,

N = inorganic nitrogen concentration (NO₃ + NH₃), mg/l,

K_N = nitrogen half saturation constant, mg/l,

K_P = phosphorus half saturation constant, mg/l,

K_L = half saturation constant for light, $\text{Kcal.m}^{-2}.\text{s}^{-1}$ or $\text{Btu/ft}^2 \text{-hr}$ (light intensity at which phytoplankton grows at half the maximum rate),

FL = algal growth limitation factor for light.

$$FL = \left(\frac{1}{\lambda d}\right) \ln \left[\frac{K_L + I}{K_L + I e^{-\lambda d}} \right] \quad (\text{A.6})$$

Equation (A.6) is obtained when the variation of light intensity with depth represented by the relationship shown below is substituted in the Monod expression for light and integrated over the depth of flow.

$$I_z = I \exp (- \lambda z) \quad (\text{A.7})$$

where

I = light intensity at the surface, $\text{Kcal.m}^{-2}.\text{s}^{-1}$ or $\text{Btu/ft}^2 \text{-hr}$,

I_z = light intensity at a given depth (z), $\text{Kcal.m}^{-2}.\text{s}^{-1}$ or $\text{Btu/ft}^2 \text{-hr}$,

z = depth variable, ft,

λ = light extinction coefficient, ft^{-1} .

The light extinction coefficient is usually defined as the linear sum of several extinction coefficients representing each component of light absorption (Bowie et al., 1985). The light extinction coefficient (λ) will be computed using the expression:

$$\lambda = \lambda_0 + \lambda_1 \alpha_7[A] + \lambda_2 (\alpha_7[A])^{2/3} \quad (\text{A.8})$$

where

λ_0 = non-algal portion of the light extinction coefficient, ft^{-1} ,

λ_1 = linear algal self shading coefficient, $\text{ft}^{-1}(\mu\text{g-Chla/l})^{-1}$,

λ_2 = nonlinear algal self shading coefficient, $\text{ft}^{-1}(\mu\text{g-Chla/l})^{-2/3}$,

α_7 = conversion factor, $(\mu\text{g-Chla/mg [A]})$.

Other terms are as previously defined.

The reader is referred to the manual on QUAL2E (Brown and Barnwell, 1987) for other possible options for modeling algal growth rate and relationship of algae with light. These options will be included, if deemed necessary, in the future versions of the model.

Chemical Oxidation: Nitrogen Series

The differential equations representing transformations of organic nitrogen to ammonia, ammonia to nitrite, and nitrite to nitrate are presented below.

Organic Nitrogen

$$\frac{\partial[\text{N-org}]}{\partial t} = \frac{\partial}{\partial \xi} \left[E_x \frac{\partial[\text{N-org}]}{\partial \xi} \right] + \alpha_1 \rho[\text{A}] - k_{\text{n-org}} [\text{N-org}] - \sigma_4 [\text{N-org}] \quad (\text{A.9})$$

where

$[\text{N-org}]$ = concentration of organic nitrogen, day^{-1} ,

$k_{n\text{-org}}$ = rate constant for hydrolysis of organic nitrogen to ammonia nitrogen at the ambient temperature, day⁻¹,

α_1 = fraction of algal biomass, which is nitrogen,

σ_4 = organic nitrogen settling rate at the ambient temperature, day⁻¹.

Ammonia Nitrogen

$$\frac{\partial[\text{NH}_3]}{\partial t} = \frac{\partial}{\partial \xi} \left[E_x \frac{\partial[\text{NH}_3]}{\partial \xi} \right] + k_{n\text{-org}} [\text{N-org}] - k_n[\text{NH}_3] + \frac{\sigma_3}{d} - f\alpha_1\mu[\text{A}] \quad (\text{A.10})$$

where

σ_3 = benthic release rate for ammonia nitrogen at the ambient temperature, mg/m²day⁻¹,

f = fraction of algal uptake of nitrogen which is ammonia.

$$f = \frac{p[\text{NH}_3]}{P[\text{NH}_3] + (1-p)[\text{NO}_3]} \quad (\text{A.11})$$

p = preference factor for ammonia nitrogen (0 to 1.0).

Nitrite Nitrogen

$$\frac{\partial[\text{NO}_2]}{\partial t} = \frac{\partial}{\partial \xi} \left[E_x \frac{\partial[\text{NO}_2]}{\partial \xi} \right] + k_n [\text{NH}_3] - k_{ni} [\text{NO}_2] \quad (\text{A.12})$$

Nitrate Nitrogen

$$\frac{\partial[\text{NO}_3]}{\partial t} = \frac{\partial}{\partial \xi} \left[E_x \frac{\partial[\text{NO}_3]}{\partial \xi} \right] + k_{ni} [\text{NO}_2] - (1-f) \alpha_1 \mu[A] \quad (\text{A.13})$$

Phosphorus Transformation

Organic Phosphorus

$$\frac{\partial[\text{p-org}]}{\partial t} = \frac{\partial}{\partial \xi} \left[E_x \frac{\partial[\text{p-org}]}{\partial \xi} \right] + \alpha_2 \rho[A] - k_{\text{p-org}} [\text{p-org}] - \sigma_5 [\text{p-org}] \quad (\text{A.14})$$

where

- [p-org] = concentration of organic phosphorus, mg/l,
- α_2 = fraction of algal biomass which is phosphorus,
- $k_{\text{p-org}}$ = organic phosphorus decay rate at the ambient temperature, day^{-1} ,
- σ_5 = organic phosphorus settling rate at the ambient temperature, day^{-1} .

Dissolved Phosphorus

$$\frac{\partial[\text{PO}_4]}{\partial t} = \frac{\partial}{\partial \xi} \left[E_x \frac{\partial[\text{PO}_4]}{\partial \xi} \right] + k_{\text{p-org}} [\text{PO}_4] - \alpha_2 \mu[A] + \frac{\sigma_2}{d} \quad (\text{A.15})$$

where

- [PO₄] = concentration of inorganic or dissolved phosphorus, mg/l,

σ_2 = benthic release rate for dissolved phosphorus at the ambient temperature, $\text{mg}/\text{m}^2 \text{ day}^{-1}$.

Arbitrary Non-Conservative Constituent

Any additional constituent can be added to the model. Below is given a typical expression for the growth and decay of such a constituent.

$$\frac{\partial[\text{arb}]}{\partial t} = \frac{\partial}{\partial \xi} \left[E_x \frac{\partial[\text{arb}]}{\partial \xi} \right] - k_{\text{arb}} [\text{arb}] - \sigma_6 [\text{arb}] + \frac{\sigma_7}{d} \quad (\text{A.16})$$

where

$[\text{arb}]$ = concentration for the arbitrary constituent, mg/l ,

σ_6 = constituent settling rate at the ambient temperature, day^{-1} ,

σ_7 = benthic source for constituent at the ambient temperature, $\text{mg}/\text{m}^2 \text{ day}^{-1}$.

Eq. (A.16) will work for a conservative constituent if each term in the right side is made zero.

Temperature

The transport equation shown in equation 4.1 written for heat as the constituent is:

$$\frac{\partial C_h}{\partial t} = \frac{\partial}{\partial \xi} \left(E_x \frac{\partial C_h}{\partial \xi} \right) + s \quad (\text{A.17})$$

Where

C_h = concentration of heat (HL^{-3})

which can be represented as

$$C_h = CPT \quad (\text{A.18})$$

where

C = specific heat of water (1 btu/lb-°F or 1 cal/g-°C),

ρ = density of water, 62.4 lb/ft³ or 1g/cm³,

T = water temperature, (deg C).

Other terms are as defined previously.

The source/sink term (s) accounts for heat exchanged through the air-water interface. Substituting equation (A.18) into equation (A.17) and representing s in the form of the net energy flux (Q_n) into the water surface finally leads to:

$$\frac{\partial T}{\partial t} = \frac{\partial}{\partial \xi} \left(E_x \frac{\partial T}{\partial \xi} \right) + \frac{Q_n}{\rho c d} \quad (\text{A.19})$$

where

d = hydraulic depth of the water body.

Table A.1 Temperature Coefficients For Reaction Rates

Constituent	Reaction type	Temperature coefficient	Variable (FORTRAN)
BOD	decay	1.047	thet(1)
	settling	1.024	thet(2)
DO	reaeration	1.024	thet(3)
	SOD	1.060	thet(4)
ORGANIC-N	decay	1.047	thet(5)
	settling	1.024	thet(6)
AMMONIA-N	decay	1.083	thet(7)
	benthic source	1.074	thet(8)
NITRITE-N	decay	1.047	thet(9)
ORGANIC-P	decay	1.047	thet(10)
	settling	1.024	thet(11)
DISSOLVED-P	benthic source	1.074	thet(12)
ALGAE	growth	1.047	thet(13)
	respiration	1.047	thet(14)
	settling	1.024	thet(15)

A.2 Components of Heat Exchange at the Air-Water Interface

Heat exchanges through the air-water interface depend upon both the internal hydromechanical behavior of the water body and the physics of its interaction with the overlying air mass.

Meteorological factors such as solar radiation, wind, humidity, pressure, and cloudiness figure prominently in the many physical processes involved (Orlob, 1983). Accounting for the most

important of these processes the rate of energy transfer is computed as:

$$Q_n = Q_{sn} + Q_{at} - Q_{ws} - Q_e - Q_h \quad (A.20)$$

where

Q_n = net heat energy transfer across the air-water interface,

Q_{sn} = net short wave solar radiation flux,

Q_{at} = net long wave atmospheric radiation flux,

Q_{ws} = water surface back radiation flux,

Q_e = evaporative heat flux,

Q_h = sensible heat flux.

All the above terms are in units such as Btu/ft²-day or cal/cm²-day. A table (Table A.2) on unit conversion of various terms appearing on this section is provided at the end of this section. The remainder of this section describes how each of the heat components is represented in the model.

Net Short Wave Solar Radiation, Q_{sn}

The net incoming solar radiation is short wave radiation which passes directly from the sun to the earth's surface. The attenuating effects of the absorption and scattering of the light in the atmosphere due to cloud cover and the reflection from the water surface must be considered in the computation of the solar radiation that penetrates the water surface. It may be represented by:

$$Q_{sn} = Q_o a_t (1 - 0.65 C^2)(1 - R_s) \quad (\text{A.21})$$

where

- Q_o = solar radiation intensity at the top of the atmosphere,
a function of location and time,
 a_t = atmospheric transmissivity term,
 C = cloud cover in tenths of sky covered, from 0.0 to 1.0,
 R_s = reflectivity of the water surface, a function of the
solar altitude of the form:

$$R_s = A\alpha^B \quad (\text{A.22})$$

where

α is the solar altitude in degrees and A and B are functions of cloudiness. Values for A and B are shown below (as reported in the QUAL2E manual).

Cloudiness C	0		0.1-0.5		0.6-0.9		1.0	
	Clear		Scattered		Broken		overcast	
Coefficient	A	B	A	B	A	B	A	B
		1.18	-0.77	2.20	-0.97	0.95	-0.75	0.35

The reader is referred to the QUAL2E manual (Brown and Barnwell, 1987) for details on the representation of the atmospheric transmission term (a_t) and Q_o .

Net Atmospheric Radiation. Q_{at}

Some short-wave radiation from the sun plus radiation emitted by the ground or water surfaces enters the earth's atmosphere and is partly absorbed by water vapor, carbon dioxide, ozone and other atmospheric gases. These constituents, in turn, emit long wave

radiation back to the ground and water surfaces, and outward to space. Such radiation is called atmospheric radiation. It is a function of absolute air temperature, cloudiness and water surface reflectivity (Orlob and Marjanovic, 1989) and is expressed as:

$$Q_{at} = C_{at} \sigma (T_a + 460)^6 (1 + 0.17 C^2)(1 - R_a) \quad (A.23)$$

where

C_{at} = Swinbank's coefficient approximately equal to
 $2.89 * 10^{-6} \text{ } ^\circ\text{R}^{-2}$,

σ = Stefan-Boltzman constant = $1.73 * 10^{-9} \text{ Btu/ft}^2/\text{hr/}^\circ\text{Rankine}^4$,

T_a = temperature of the radiating air mass, $^\circ\text{F}$,

R_a = water surface reflectivity of long wave radiation =
 0.03.

Water Surface Back Radiation. Q_{ws}

The loss of energy from a water body by long wave radiation is expressed by the Stefan-Boltzman Fourth Power Radiation Law for a black body as:

$$q_{ws} = \epsilon \sigma (T_s + 460)^4 \quad (A.24)$$

where

ϵ = emissivity of the water surface, i.e., ratio of an
 actual radiation to that of a black body = 0.97,

T_s = water surface temperature, $^\circ\text{F}$.

Evaporative Heat Flux, Q_e

The evaporative heat loss occurs due to water changing a liquid state to a gas state (vapor) and the heat loss associated with the latent heat of vaporization.

$$Q_e = \gamma L_v E \quad (\text{A.25})$$

where

γ = specific weight of water, lb/ft³,

L_v = latent heat of vaporization, Btu/lb,

E = evaporation rate, ft/hr, often expressed as

$$(a+bW) (e_s - e_a) \quad (\text{A.26})$$

where

a, b = constants (see Table 5.7 for the calibrated values),

W = wind speed, miles/hr, measured 6 ft. above the water surface,

e_s = saturation vapor pressure of the air (in. of Hg) at the temperature of the water surface, as given by

$$e_s = 0.1001 \exp (0.03T_s) - 0.0837$$

e_a = water vapor pressure (in. of Hg) at a height of 6 feet above the water surface, given as

$$e_a = e_{wb} - 0.000367 P_a (T_a - T_{wb})$$

Other terms are as defined earlier.

e_{wb} = saturation vapor pressure (in. of Hg) at the wet bulb temperature,

T_{wb} = wet bulb temperature °F,

P_a = local barometric pressure, in. of Hg.

Sensible Heat Flux, Q_h

Sensible heat is transferred between air and water by conduction and transferred away from the air-water interface by the same mechanisms as for evaporation. It is convenient to relate sensible and evaporative heat fluxes using Bowen's ratio in the form:

$$Q_h = Bq_e$$

where

$$B = \text{Bowen's ratio} = 0.01 \frac{T_s - T_a}{e_s - e_a} \frac{P_a}{29.92} \quad (\text{A.27})$$

Table A.2 Unit Conversion Related to Heat Equations
(adopted from Bowie et al., 1985)

1 BTU/ft ² /day	0.131 watt/m ²	0.271 Ly/day	0.113 kcal/m ² /hr
Ly/day	0.483 watt/m ²	3.69 BTU/ft ² /day	0.42 kcal/m ² /hr
kcal/m ² /hr	1.16 watt/m ²	2.40 Ly/day	8.85 BTU/ft ² /day
1 mb	0.1 kp	0.769 mm Hg	0.03 in Hg
1 mm Hg	1.3 mb	0.13 kp	0.039 in Hg
1 in Hg	33.0 mb	25.4 mm Hg	3.3 kp

Dispersion Factor

Schoellhamer and Jobson (1986B) derived a relationship between the dispersion factor D_f and the Peclet number as shown below.

The net contribution to mass per unit volume of parcel k in Figure 3.4 (see Chapter 3) is

$$\Delta C = \Delta t [DQ_k C_{k-1} - DQ_k C_k + DQ_{k+1} C_{k+1} - DQ_{k+1} C_k] \frac{1}{V_k} \quad (\text{B.1})$$

where

ΔC = change in parcel concentration

Δt = time step

V_k = parcel volume

The coefficient D_f can be defined in terms of model and physical parameters by considering the Lagrangian transport equation

$$\frac{\partial c}{\partial t} = \frac{\partial}{\partial x} \left(E_x \frac{\partial c}{\partial x} \right) \quad (\text{B.2})$$

Using an explicit finite difference form and integrating,

$$\int^{\Delta t} \frac{\partial c}{\partial t} = \int^{\Delta t} \frac{\left(E_x \frac{\partial c}{\partial x} \right)_k - \left(E_x \frac{\partial c}{\partial x} \right)_{k+1}}{\Delta x} dt \quad (\text{B.3})$$

where

Δx = parcel length

k = upstream boundary of parcel k

$k+1$ = upstream boundary of parcel $k+1$

Using finite difference forms and assuming that Δt is small, we obtain

$$\Delta c = \Delta t \left[E_{x,k} (c_{k-1} - c_k) + E_{x,k+1} (c_{k+1} - c_k) \right] \frac{1}{\Delta x^2} \quad (\text{B.4})$$

Multiplying both numerator and denominator by $Q = au$, we get

$$\Delta c = \Delta t Q \left[E_{x,k} (c_{k-1} - c_k) + E_{x,k+1} (c_{k+1} - c_k) \right] \frac{1}{V_k u \Delta x} \quad (\text{B.5})$$

Comparing equations B.1 and B.5 gives the definition

$$DQ = Q \frac{E_x}{u \Delta x}$$

But $D_f = \frac{DQ}{Q}$ (see equation 3.4)

Hence, $D_f = \frac{E_x}{u \Delta x} = \frac{1}{Pe}$

in which Pe is the Peclet number.

APPENDIX C
C.1 User's Manual: Part 1. Transport Input File: BLTM.IN

This part of the manual describes the transport input file format. It has been somewhat modified from the original format written by Jobson and Schoelhamer (1992). New variables have been added to extend model capability to include reservoir and agricultural drainage simulations. However, changes in the structure of the input file have been kept to the minimum.

Card Type 1. Simulation Title

Field	Variable	Format	Description
1	Title	20a4	Title of simulation

Card Type 2. Simulation Control Parameters

Field	Variable	Format	Description
0		10X	Card identifying characters ¹
1	nbrch		Number of branches to be simulated (Maximum = 510)
2	njnct	I7	Number of interior junctions (Maximum = 450)
3	nhr	I7	Number of time steps to be modeled
4	neq	I7	Number of constituents to be modeled (Maximum = 11)
5	jts	I7	Number of time steps between midnight and the start of the model
6	jgo	I7	Number of time steps between printouts in bltm.out
7	jpo	I7	Number of time step between printouts in parcel.out

¹ Card identifying characters are labels for the user convenience. They are not interpreted by the program.

8	itdds	I7	Code indicating use of flow file: 0 = use flow file in an original BLTM format, 3 = use binary flow file)
9	ieng	I7	Input units (0 = metric (length unit is meters except for river miles), 1 = English (length unit is feet except river miles), default = 0)

Card Type 3. More Control Variables

Field	Variable	Format	Description
0		10X	Card identifying characters
1	dt	F7.0	Time step size in hours
2	dqv	F7.0	Minimum dispersive velocity in ft/s or m/s

Card Type 4. Constituent Labels

Field	Variable	Format	Description
0		10X	Card identifying characters
1	1	17	Constituent number
2	label(1)	3X,A5	Name of constituent (5 characters maximum)

Repeat one constituent label card for each constituent. (Cards must be in order from constituent 1 to neq).

Card Type 5. Branch Information

Repeat card 2 for each grid in branch n. Repeat cards 1 and 2 for each branch. Branches must be input in sequence starting with branch 1.

(Card 1 of 2 - header)

Field	Variable	Format	Description
0		10X	Card label for branch n
1	nxsec(n)	I7	Number of grids in branch n
2	dqq(n)	F7.0	Dispersion factor for branch n (unitless)
3	jncu(n)	I7	Junction number at upstream end of branch n
4	jncd(n)	I7	Junction number at downstream end of branch n
5	inpr(n)	I7	Initial number of parcels per reach in branch n (default = 1)
6	b(n)	F10.0	Width of the channel, ft

Card 2 of 2. Grid Data for Branch n and Initial Conditions (quality)

Field	Variable	Format	Description
0		10X	Card label for grid i of branch n
1	x(n,i)	F7.3	Distance of grid i from upstream end of branch n (jncu (n)) in miles.
2	iout(n,i)	I7	Outflag (equal 1 if output in bltm.out is desired for this grid, 0 otherwise).
3	gpt(n,i,1)	F7.3	Initial concentration of constituent 1 between grid i and i+1 (omit for i = nxsec (n))
•	•	F6.2	
•	•	•	
13(max)	gpt (n,i,neq)	F6.2	Initial concentration of last constituent between grid i and i+1 (omit for i = nxsec (n))

Card Type 6. Inflow Quality at Interior Junctions (Agricultural returns or effluents)

Field	Variable	Format	Description
0		24X	Card identifying characters
1	cadg(1)	F7.3	Initial concentration of constituent 1
.	.	.	
.	.	.	
.	.	.	
11(neq)	cadg(neq)	F7.3	Initial concentration of last constituent

Include a separate card for effluent data.

Card Type 7. Initial Conditions (quality) Reservoirs

Field	Variable	Format	Description
0		24X	Card identifying characters
1	salst (1)	F7.3	Initial concentration of constituent 1, mg/l
.	.	.	
.	.	.	
11(max)	salst (neq)	F7.3	Initial concentration of last constituent, mg/l

Card Type 8. Boundary Quality Specifications

Card 1 of 2

Field	Variable	Format	Description
0		10X	Card label identifying time step
1	nbc		Number of boundary conditions that change during current time step

Card 2 of 2

Field	Variable	Format	Description
0		2X	Label
1	n	I3	Branch n where boundary condition changes
2		3X	Label
3	i	I2	Grid i (location of boundary condition) for branch n
4	gtrib (n,l,i)	F7.3	Initial concentration of constituent 1, mg/l
.	.	.	
.	.	.	
14(max)		F7.3	Initial concentration of last constituent, mg/l

Repeat card 2 nbc times and card 1 for every time step, upto the total number of time steps (nhr).

C.2 User's Manual: Part 2. Kinetic Rate Coefficients File (QUALITY.IN)

Part 2 describes the input file format for the physical, chemical and biological rate coefficients. Table 5.6 and 5.7 present the recommended ranges of these coefficients. Refer to Table A.1 for temperature coefficients (i.e., correction for rate coefficients).

Card 1. Title

Field	Variable	Format	Description
1	qtitle	A80	Input title line

Card 2. Number of Constituents

Field	Variable	Format	Description
1	nqual	I3	Total number of constituents that can be simulated
2	neq	I3	Number of constituents simulated in this run

Card 3. Constituent I.D.

Field	Variable	Format	Description
0		10X	Card identifying characters
1	iconst(1)	I5	1 = Arbitrary Non-Conservative
2	iconst(2)	I5	2 = BOD
3	iconst(3)	I5	3 = DO
4	iconst(4)	I5	4 = Organic-N
5	iconst(5)	I5	5 = Ammonia-N
6	iconst(6)	I5	6 = Nitrite-N
7	iconst(7)	I5	7 = Nitrate-N
8	iconst(8)	I5	8 = Organic-P
9	iconst(9)	I5	9 = Phosphate-P
10	iconst(10)	I5	10 = Algae
11	iconst(11)	I5	11 = Temperature

Cards 4 through 11 shown below represent the global rate coefficients. These variables remain constant for the entire channel system.

Card 4. Type of Coefficients

Field	Variable	Format	Description
1	coef-g	A80	Label (Global model parameters)

Card 5. Physical Coefficients

Field	Variable	Format	Description
0		8X	Card identifying characters
1	elev	F8.4	Basin elevation, ft (MSL)
2	lat	F8.4	Latitude, degrees
3	long	F8.4	Longitude, degrees
4	lsm	F8.4	Longitude of standard meridian, degrees
5	dayofy	F8.4	First day of simulation, Julian day
6	stime	F8.4	Time at which simulation begins, hour
7	dust	F8.4	Dust attenuation coefficient (Table 5.7)
8	ae	F8.4	Evaporation coefficient, ft/hr-in Hg (Table 5.7)
9	be	F8.4	Evaporation coefficient, ft/hr-in Hg-mph (Table 5.7)

Card 6. Temperature Correction for Arbitrary Constituent Rate Coefficients

Field	Variable	Format	Description
0		8X	Card identifying characters
1	thet(16)	F8.4	Temperature correction for arbitrary constituent decay rate
2	thet(17)	F8.4	Temperature correction for arbitrary constituent settling rate
3	thet(18)	F8.4	Temperature correction for arbitrary constituent benthic rate

Card 7. Temperature Correction for BOD and DO Rate Coefficients

Field	Variable	Format	Description
0		8X	Card identifying characters
1	thet(1)	F8.4	Temperature correction for BOD decay rate
2	thet(2)	F8.4	Temperature correction for BOD settling rate
3	thet(3)	F8.4	Temperature correction for reaeration rate
4	thet(4)	F8.4	Temperature correction for benthic oxygen uptake rate

Card 8. Rate and Temperature Coefficients for Nitrogen Series

Field	Variable	Format	Description
0		8X	Card identifying characters
1	alph(5)	F8.4	Oxygen used in conversion of ammonia to nitrite, mg-O/mg-N
2	alph(6)	F8.4	Oxygen used in conversion of nitrite to nitrate, mg-O/mg-N
3	thet(5)	F8.4	Temperature correction for organic nitrogen decay rate
4	thet(6)	F8.4	Temperature correction for organic nitrogen settling rate
5	thet(7)	F8.4	Temperature correction for ammonia oxidation rate
6	thet(8)	F8.4	Temperature correction for benthic source rate for ammonia
7	thet(9)	F8.4	Temperature correction for nitrite oxidation rate

Card 9. Temperature Coefficients for Phosphorus Series

Field	Variable	Format	Description
0		8X	Card identifying characters
1	thet(10)	F8.4	Temperature correction for organic phosphorus decay rate
2	thet(11)	F8.4	Temperature correction for organic phosphorus settling rate
3	thet(12)	F8.4	Temperature correction for benthic source rate for dissolved phosphorus

Card 10. Rate and Temperature Coefficients for Algae

Field	Variable	Format	Description
0		8X	Card identifying characters
1	prefn	F8.4	Algal preference factor for ammonia
2	alph(7)	F8.4	Ratio of chlorophyll-a to algal biomass $\mu\text{g/l-chl-a} / \text{mg/l-A}$
3	alph(1)	F8.4	Fraction of algal biomass which is nitrogen
4	alph(2)	F8.4	Fraction of algal biomass which is phosphorus
5	alph(3)	F8.4	Oxygen production per unit of algal growth, mg-O/mg-A
6	alph(4)	F8.4	Oxygen consumed per unit of algal respiration, mg-O/mg-A
7	thet(13)	F8.4	Temperature correction for algal growth rate
8	thet(14)	F8.4	Temperature correction for algal respiration
9	thet(15)	F8.4	Temperature correction for algal settling rate

Card 11. Additional Rate Coefficients for Algae

Field	Variable	Format	Description
0		8X	Card identifying characters
1	klght-half	F8.4	Half saturation constant for light, Btu/ft ² -min
2	knit-half	F8.4	Half saturation constant for nitrogen, mg-N/l
3	kpho-half	F8.4	Half saturation constant for phosphorus, mg-P/l
4	xlam0	F8.4	Non-algal light extinction coefficient, per ft.
5	xlam1	F8.4	Linear algal self shading coefficient, per ft-mg/l
6	xlam2	F8.4	Nonlinear algal self shading coefficient, per ft-(mg/l) ^{2/3}

Card 12. Type of Coefficients

Field	Variable	Format	Description
0		8X	Card identifying characters
1	coef-r	A72	Label (Spatially varying parameters)

Card 13. Type of Region

Field	Variable	Format	Description
0		8X	Card identifying characters
1	coef-vr	A72	Label (Region type)

Cards 14 through 23 represent location variable parameters. These can be varied by location (channel or region).

Card 14. Rates for Arbitrary constituent

Field	Variable	Format	Description
0		8X	Card identifying characters
1	rcoef(1,1,1)	F8.4	Arbitrary constituent decay rate, per day. Write zero if conservative constituent is simulated.
2	rcoef(1,2,1)	F8.4	Arbitrary constituent settling rate, per day. Write zero if conservative constituent is simulated.
3	rcoef(1,3,1)	F8.4	Arbitrary constituent benthic source rate, mg/m ² -day. Write zero if conservative constituent is simulated.

Card 15. Rates for BOD

Field	Variable	Format	Description
0		8X	Card identifying characters
1	rcoef(2,1,1)	F8.4	BOD decay rate, per day
2	rcoef(2,2,1)	F8.4	Rate of loss of BOD due to settling, per day

Card 16. Rates for DO

Field	Variable	Format	Description
0		8X	Card identifying characters
1	rcoef(3,1,1)	F8.4	Benthic demand rate for DO, g/m ² -day

Card 17. Rates for Organic-N

Field	Variable	Format	Description
0		8X	Card identifying characters
1	rcoef(4,1,1)	F8.4	Organic nitrogen decay rate, per day
2	rcoef(4,2,1)	F8.4	Organic nitrogen settling rate, per day

Card 18. Rates for Ammonia-N

Field	Variable	Format	Description
0		8X	Card identifying characters
1	rcoef(5,1,1)	F8.4	Ammonia nitrogen decay rate, per day
2	rcoef(5,2,1)	F8.4	Ammonia nitrogen benthic rate, mg/m ² per day

Card 19. Rates for Nitrite-N

Field	Variable	Format	Description
0		8X	Card identifying characters
1	rcoef(6,1,1)	F8.4	Nitrite nitrogen decay rate, per day

Card 20. Rates for Nitrate-N

It has no dependency on its own rate or concentration.

Field	Variable	Format	Description
0		8X	Card identifying characters

Card 21. Rates for Organic Phosphorus

Field	Variable	Format	Description
0		8X	Card identifying characters
1	rcoef(8,1,1)	F8.4	Organic phosphorus decay rate, per day
2	rcoef(8,2,1)	F8.4	Organic phosphorus settling rate, per day

Card 22. Rates for Dissolved Phosphorus

Field	Variable	Format	Description
0		8X	Card identifying characters
1	rcoef(9,1,1)	F8.4	Benthic source rate for dissolved P, mg/m ² -day

Card 23. Rates for Algae

Field	Variable	Format	Description
0		8X	Card identifying characters
1	rcoef(10,1,1)	F8.4	Maximum algal growth rate, per day
2	rcoef(10,2,1)	F8.4	Algal respiration rate, per day
3	rcoef(10,3,1)	F8.4	Algal settling rate, ft/day

Repeat Cards 14 through 23 for each location.

C.3 User's Manual: Part 3. Meteorological Data Input File (MET.IN)

This part of the manual describes the input file format for the meteorological data required for heat exchange calculations. Meteorological data are input at hourly intervals for the period of simulation and should represent an average condition during the hour.

Field	Variable	Format	Description
1	ihour	I5	Hour of the day.
2	dryblb	F7.0	Cloud cover fraction.
3	dryblb	F7.0	Dry bulb temperature, degrees F
4	wetblb	F7.0	Wet bulb temperature, degrees F
5	wind	F7.0	Wind speed, miles/hr.
6	atmpr	F7.3	Atmospheric pressure, in. of Hg
7	iyear	I10	Year
8	imonth	I5	Month
9	iday	I5	Day